NOISE SOURCE IDENTIFICATION ON LARGE GENERATOR UNITS

RICHARD G.D. WILLIAMS

A THESIS SUBMITTED FOR THE DEGREE OF DOCTOR OF PHILOSOPHY, HERIOT-WATT UNIVERSITY, DEPARTMENT OF COMPUTING AND ELECTRICAL ENGINEERING

NOVEMBER 1992

CONTENTS

ACKNOWLEDGEMENTS

The author would like to express his indebtedness to G.E.C. Alsthom Turbine Generators Ltd and Heriot Watt University for organising the research program. The work was also supported by the Science and Engineering Research Council of the United Kingdom.

Personal gratitude is conveyed to Dr. S.J. Yang for his continual guidance, advice and enthusiasm for the research undertaken. Thanks is extended to the personnel at G.E.C. Alsthom Turbine Generators, in particular to the Development Department personnel for their practical assistance with experimental work and Mr. S.G. Houldcroft, Mr. R.M. Booth and Mr. R.B. Bennett for their support.

The author also extends his appreciation to Professor F.J. Fahy, Institute of Sound and Vibration Research, Southampton, for many stimulating discussions on the sound intensity technique and Professor F. Jacobsen, Technical University of Denmark, for valuable comments on the sound pressure particle velocity coherence technique.

Special thanks go to Mrs. C. Chapman for converting the scribbled manuscript into a credible form, all over and above her normal duties.

ABSTRACT

Power station acoustic noise assessment has recently experienced increased environmental awareness and subsequently more stringent legislation. Despite this, comparatively little is known of the generator and it's excitation system's noise characteristics, principally due to the inability of traditional sound pressure techniques to isolate sources. This thesis describes the application of digital measurement and analysis techniques including sound intensity and coherence to identify noise sources on large generator units.

Generator unit components have been extensively investigated at site and during factory testing. Components have been ranked in order of sound power levels determined with acceptable, quantifiable accuracy from sound intensity measurements in a manner not hitherto possible. This technique is currently being developed into a standard and these measurements have contributed to this process. The site sound pressure level was fully explained in terms of the various influences and the major noise source mechanisms identified. The sound pressure particle velocity coherence technique has been used in an industrial application to classify sound fields.

A theoretical model for the predominant noise source, the pilot exciter, relates the siren tone levels to machine geometries and the aerodynamic behaviour that create them. Noise levels were accurately predicted using an equivalent acoustic circuit, standard fluid mechanics with assumed quasi-static behaviour and a radiation model. A test rig experimentally validated the model and novel in-duct measurements facilitated further source identification.

This thesis has presented a clear, correlated new level of insight into generator unit noise emission. The means to enact noise control measures including pilot exciter design changes to reduce siren tones has been presented.

1. INTRODUCTION

This thesis presents the research work undertaken by the author as part of an industrial sponsorship from GEC Alsthom Turbine Generators Ltd in conjunction with the Department of Computing and Electrical Engineering at Heriot-Watt University. The majority of the research was conducted at GEC Alsthom Turbine Generators Ltd in Stafford and covers the application of digital measurement and analysis techniques to quantify noise levels and identify the major noise source mechanisms on large generator units. A theoretical model was then developed for the predominant noise source. This model, in conjunction with a detailed experimental study, yields the necessary insight to enact noise control measures at source.

Considerable interest has been directed to the assessment and control of airborne noise in modern power plants for a number of years. This is as a result of increased awareness of the environment and subsequently more stringent legislation. Despite this most of the published work on electrical machinery noise emission concentrates on electrical motors. There are a number of intrinsic differences in electrical and mechanical design, which cause the noise characteristics of motors and generators to vary significantly. The generator unit contains extra excitation system components such as the exciter, pilot exciter and rotating rectifier, about which little is known of their acoustic characteristics.

The principal reason for this lack of knowledge is that traditional measurement techniques based upon sound pressure measurement have been found to be inadequate for analysing noise sources from large turbine generator units. Sound pressure is seldom simply related to adjacent machinery in industrial spaces such as a turbine hall. More commonly the sound pressure is created by a complex interaction of plant

radiation characteristics, reverberation and interference fields from many items of co-functioning equipment. The multitude of co-functioning equipment is illustrated in Fig.4.21, in Chapter 4, with four turbines driving each generator and many auxiliary pumps, valves, steam-lines and condensers. The noise output from these items can be appreciably greater than that from the generator itself. Sound pressure levels, S.P.L.'s, in the vicinity of the boiler feed pumps are between 100-110 dB(A) and valve noise can sometimes be in excess of 110 dB(A). The S.P.L. beside the generator is commonly around 90 dB(A). The background noise influences sound pressure beside the generator due to that transmitted directly and also it's contribution to the general reverberant "bath" of sound. This makes pinpointing of noise sources on the generator unit difficult.

The innovation of digital signal processing and subsequent sophisticated measurement techniques have provided an extra stimulus to noise assessment enabling even complex sound fields to be characterised. Extensive investigations using a variety of digital measurement and analysis techniques have been conducted on generators and their excitation system components at site and during factory testing.

In the remainder of chapter 1 the performance and construction of large generators and the components comprising their excitation systems are discussed. Sound intensity, which is the main measurement tool used during this research to assess generator unit noise source mechanisms is also introduced. The chapter concludes by summarising the main objectives of the research presented in this thesis.

The detailed literature survey is presented in chapter 2. This chapter summarises

published work on generator unit noise assessment. Various techniques for noise source identification are reviewed generally. Intensity methods and applications are critically reviewed. The ISO standard for sound power determination using sound intensity is also discussed in detail.

Chapter 3 outlines the measurement system developed for this investigation and accredits it's performance characteristics. Background theory, on the experimental technique and results analysis, is presented.

The results of the extensive investigations conducted at site and during factory testing are presented in chapter 4. As a first step to reduce noise emission it is necessary to identify the part of the plant which causes the predominant noise output. Sound intensity has enabled sound power determination within acceptable, quantifiable accuracy limits for each component in a manner not possible from traditional techniques despite the presence of the strong background noise and high levels of reverberation. The constituent generator unit components have been placed in rank order of sound power emission highlighting the most significant noise sources.

The main source mechanisms identified during the detailed experimental program are discussed in chapter 5. Some of the conclusions drawn are supplemented by theoretical studies into the generator magnetic forcing and the transmission loss of the wrapper of a hydrogen cooled generator. Measurement accuracy was of paramount importance when applying the sound intensity technique to the complex multi-source, reverberant environments encountered. During the investigation the field indicators used to quantify accuracy were accredited and a variety of conclusions drawn. Different techniques to assess accuracy and classify the acoustic environment were applied for the first time in

industrial environments. These results are also presented in chapter 5.

After identifying the worst noise source the 2nd stage of the thesis is to produce a theoretical model, which relates the machine geometries to the aerodynamic phenomenon creating the noise. This is a prerequisite of implementing design changes to reduce noise levels at source. Chapter 6 outlines the calculation of the siren tones produced by the pilot exciter, which was the major noise source for a 660MW generator unit.

In conjunction with the siren tone calculation a full scale test rig was manufactured to enable assessment of the main modelling assumptions, yield parameters which could not be predicted and facilitate a detailed measurement program using novel techniques to investigate other noise generation mechanisms. These results are presented in chapter 7.

1.1 LARGE GENERATOR UNITS : PERFORMANCE AND CONSTRUCTION

Large a.c. power networks operating at constant frequency, 50 Hz in the United Kingdom, rely almost exclusively on synchronous generators for the provision of electrical energy. Private, standby and peak-load plant with diesel or gas-turbine prime-movers also have synchronous generators. Non-land-based synchronous plant is found on oil rigs (upwards of 50 MVA), large aircraft (with hydraulically driven generators working at 400 Hz) and on ships for variable-frequency supply to synchronous propeller motors.

The speed n_s (in r/s) of a synchronous machine is related to the frequency F_1 and the number of pole pairs p by $n_s = F_1/p$. With a 2 pole construction this means 3000 r/min for 50 Hz. The use of rotating d.c. fields is almost universal as it permits the a.c. windings to be placed in the stator where they are more readily braced against electro magnetic force and insulated for high voltage. The rotor field construction may be with salient poles, or cylindrical with no polar protuberances.

The prime-mover speed has a profound influence on the constructional form of the generator. On all large units the limiting feature is the centrifugal force on the rotor. Steam-turbines driven machines using oil, coal, gas or nuclear fuels to produce steam must run at high speed and have either 2 or 4 pole rotors of solid forged steel, with diameters limited to about 1.3m and of axial length of several metres. Generators driven by water power or diesel engines are built for a wide range of comparatively low turbine speeds, and are axially short, but have large diameters to accommodate the many salient poles.[1]

This thesis concentrates on the noise characteristics of hydrogen cooled generators, 350-1000MW, and air cooled generators producing 110MW. The research is generally applicable to all cylindrical rotor generators driven by high speed steam turbines, which constitute 98% of the power generation in the U.K. Since the C.E.G.B. privatisation in 1991 the number of private suppliers has increased. Many of these have built combined cycle power stations using gas turbines in conjunction with steam turbines because of the better overall efficiency of 52% as opposed to 40% for steam turbine plant. The trend will continue. The gas turbines use either large air cooled generators up to 200MW or hydrogen cooled generators up to 250MW.

The operation of modern interconnected a.c. systems is a very complex phenomena. A few basic concepts behind the control of generator units within the system will be mentioned to explain the function of the various components. Despite the complexity any one turbine generator is controlled as a function of only two variables, steam flow to the turbines and d.c. excitation level to the generator. The design characteristics of the generator, regulator and excitation system, plus the characteristics of the transmission and distribution system determine the overall performance.

The steam flow and governing system control the load angle, which is the electrical angle between the rotor and the output voltage, and the active power component supplied by the generator. The rotor current controls the power factor, which normally is expressed as the cosine of the angle between the voltage and current vectors. An example which demonstrates the loss of effectiveness in a power circuit with a large phase angle, is when a sailboat is operating up-wind, tacking, with a large angle between the wind and the motion. The concept is the same for active and reactive sound intensity with sound pressure and particle velocity analogous to voltage and current respectively.

The generator unit operates within stability levels for stator voltage and active and reactive power. The limits are imposed by rotor and stator temperature rise and the inability of the unit to develop a balancing electromagnetic torque to the mechanical load being applied resulting in the unit pulling out of synchronism.

The d.c. excitation supply must perform the following functions (i) to control the generated voltage within stability limits (ii) to regulate the voltage under fault conditions (iii) to facilitate reactive power load sharing between generators operating in parallel.

In order to control this wide range of conditions the excitation must vary quickly with an operating voltage range of the order of 4/1 over that required for nominal stator voltage on no load. The excitation current for a 1000MW generator is 5000A and the normal operating voltage range is between 200 and 800V.

There are a large variety of excitation systems. For large generator units these all use solid state rectifiers due to the development of high rating diodes, thyristors and fuses. A static excitation system obtains d.c. excitation by means of a rectifier and a suitable a.c. supply. The d.c. is fed to the generator rotor by means of sliprings and brushgear. Brushless excitation systems have the permanent magnet hub of a pilot exciter, rotating rectifier unit and main a.c. exciter all mounted on the main shaft, Fig.1.1. The pilot exciter stator outputs high frequency a.c., which is rectified by a thyristor bridge controlled by the automatic voltage regulator. This d.c. energises the main exciter field and the rotating poly-phase winding produces a.c., which is converted to d.c. by means of shaft mounted rectifiers and fed directly to the main rotor winding, no sliprings or brushgear being needed.

Both static and brushless systems have good responses. The brushless system is predominant for large generator units as it requires little general maintenance.

The sectional arrangement for a 660MW, 2 pole, hydrogen cooled generator is given in Fig.1.2. The electric and magnetic loadings are exceptionally high in all large generator units. The 660MW rotor shaft has a maximum diameter of 1.14m and an overall length of approximately 13.4m between coupling faces. The rotors are commonly machined from single ingot forgings and the 660MW rotor weighs 75 tonnes. The slots are milled axially to receive concentric coil windings.

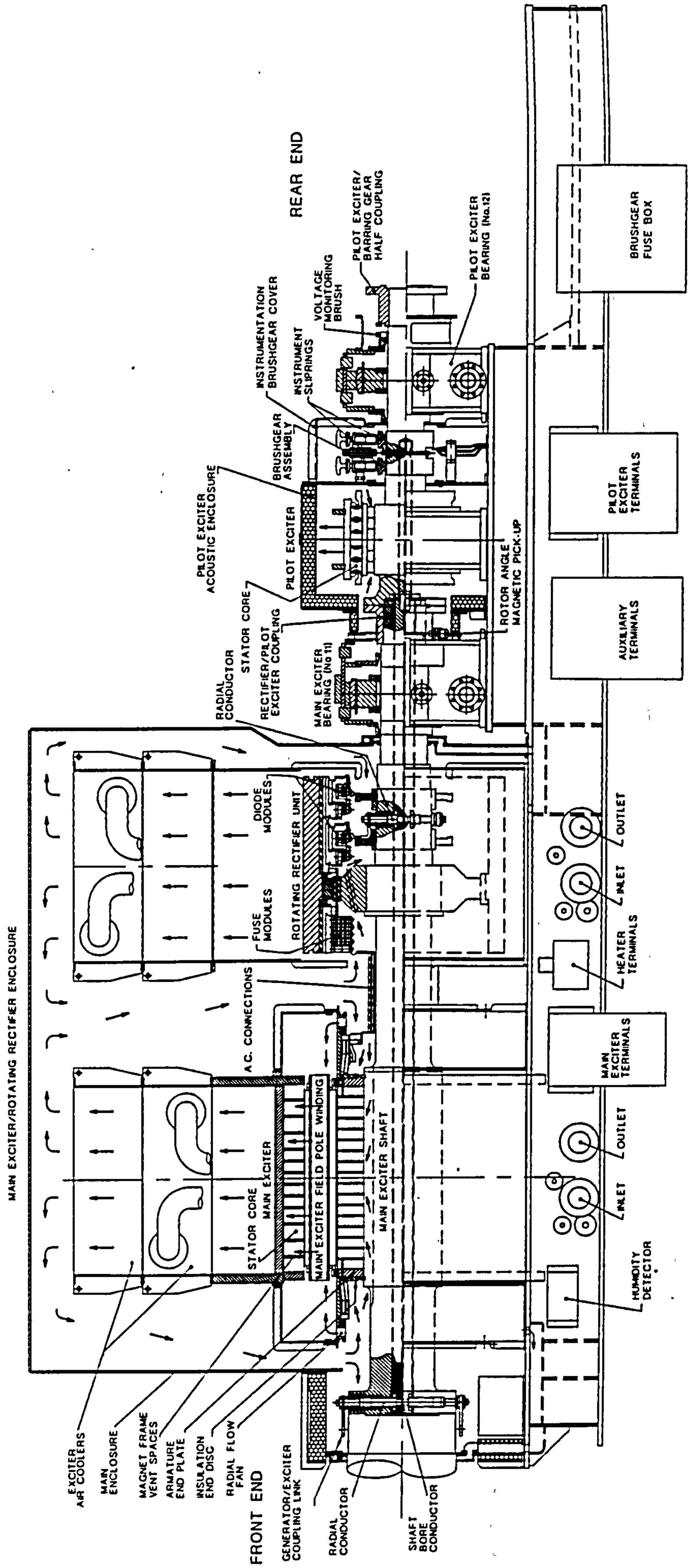

Fig.1.1 Sectional arrangement of exciter set

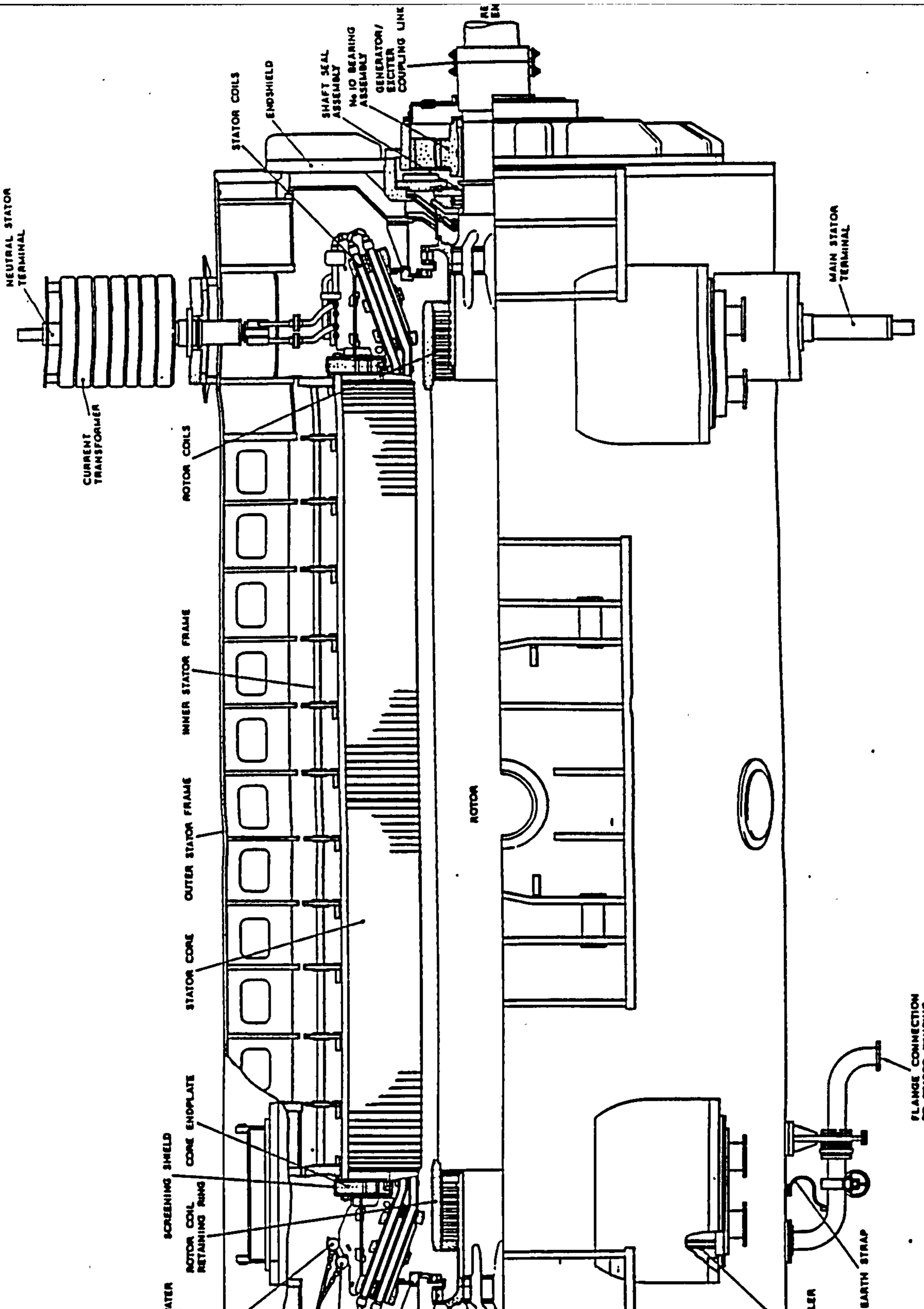

Fig.1.2 Sectional arrangement of generator set

The active length of the coils is retained in milled slots by wedges, but the coil ends are contained by endbells with an ultimate strength of 1150 MN/m². The windings are directly cooled via hollow conductors. All large rotors run in sleeve oil film journal bearings.

The stator core is built up of grain oriented steel. For the 660MW generator the inner core diameter is 1.42m and the back of the core diameter is 2.63m. The active core length must be of the order of 10mm per MVA. For generators between 100 and 200MVA ratings the terminal voltage is 15kV and for larger sets between 25 and 30kV. Even so the current per phase can reach 20kA. The stator windings are directly cooled by water for hydrogen cooled generators above 300MW. Lower ratings are cooled by gas passing radially over the coils. The core is built up on axial bars, which are welded to an inner stator frame. For ease of construction and to enable vibration isolation the inner frame is connected to the outer frame by flat plate spring mountings. These provide vertical and tangential support, while allowing the radial vibrational movement of the inner stator and restricting the transmission of the movement to the outer stator to reduce noise and vibration.

The gas cooling medium, air or hydrogen, is circulated through the rotor and stator core before being cooled itself by water cooled heat exchangers. The 660MW has two large radial fans, which circulate 10.2m³/s of gas. The hydrogen is retained by a complex oil film seal, which restricts gas leakage by maintaining a constant gas to oil differential pressure. The outer casing of the generator has a thickness of 20-25mm to contain the 3-5 barg hydrogen pressure even in the extremely unlikely event of an internal explosion.

The 110MW air cooled generator illustrated in Fig.4.47 has in general many similar design features to the 660MW unit previously discussed. The heat transfer properties of air are substantially inferior to hydrogen so the size of the air cooled generator, with a cover 8m long, is disproportionally large for the generated power. To counterbalance this air cooled generators have simpler auxiliaries requiring no hydrogen and stator winding water systems and far simpler frame constructions. Currently air cooled units constitute an increasing important market share due to the thermal efficiency of combined cycle station driven by gas turbines. Air cooled generators are currently being developed up to 230MW.

A typical sectional arrangement for a 660MW generator brushless excitation system is illustrated in Fig.1.1. The pilot exciter has 16 permanent magnet poles mounted on the exciter rotor shaft. The pilot exciter stator consists of a steel frame with laminated core with axial slots for insulated copper coils, which give a balanced 3 phase output. The construction is described fully in section 6.1.2 as the unit constituted a major noise problem, the detailed study of which represents a major part of the research presented in this thesis. The pilot exciter output is rectified by a thyristor bridge which is controlled by the automatic voltage regulator, A.V.R. The A.V.R. is a complex electronic controller which determines the excitation level to maintain nominal operating voltage even during fault conditions, and controls power factor. The rectified d.c. current is fed to the main exciter stator, which comprises of a fabricated and laminated steel frame with 8 laminated steel poles carrying an insulated copper coil bolted on the inside. The coils are connected to give alternative north and south polarity round the frame. The main exciter armature has a laminated core with axial slots carrying insulated copper coils connected to form a 3 phase 200 Hz output winding. Insulated wedges retain the coils in the slots and non-magnetic forged steel retaining rings restrain

the coil outside the slot. The 3 phase A.C. connections are connected to the rectifier which comprises of 2 separate diode wheels, one for each polarity. The diode wheels are mounted on heat sinks and are surrounded by a fabricated steel cover. The D.C. output is taken from the diode wheel via radial copper studs to insulated copper leads. These run down the exciter rotor shaft to the front end exciter coupling, where insulated radial studs in the coupling flange connect the leads to similar studs in the generator rotor via external copper alloy links bolted to the outer ends of the studs.

The main exciter and rotating rectifier are cooled by air circulated through water cooled heat exchangers. The pilot exciter is open vented. In Fig.1.1 the pilot exciter and rear end generator/front end exciter coupling are treated acoustically. This was enacted as a consequence of the findings of this research work. The overall length of the main exciter and rotating rectifier enclosure is 3.5m.

The construction if not the principal of operation is very different to that of the overhung exciter illustrated in Fig.4.47. The overhung is appreciably more compact having an overall length of 1m. The pilot exciter, main exciter armature and rotating rectifier are all on the same hub, which is bolted to the end of the generator rotor. The diode modules are mounted radially inside the armature. This compact design can be used for all sizes of exciter except that for larger designs hydrogen is used as the cooling medium.

1.2 SOUND INTENSITY

The traditional, and still most prevalent means today, to quantify acoustic output, is in terms of sound pressure. To some extent the use of sound pressure measurement to quantity sound source strength is like trying to rate the heat output from an electric fire

in terms of the temperature produced at some point around it. While sound pressure may be easiest quantity to measure, it is not very useful for diagnosing the precise cause of the noise. It is a scalar quantity with no direction. At any point in space the sound pressure field contains the contribution from many different sources. The presence of sound reflecting surfaces such as walls, floors and other machinery further complicates the sound pressure field, making it extremely difficult to pinpoint the main source of noise, an obvious prerequisite for any effective noise control measures.

The rate and direction of flow of sound energy is a more revealing and discriminatory measure of the distribution and strength of sound sources. This quantity is sound intensity, which is defined as the rate at which sound energy is transmitted through a unit area, the elemental area being so oriented that it lies perpendicular to the instantaneous particle velocity. Sound intensity is a vector quantity and, by definition, is directly linked to the noise source strength or sound power.

Sound power determination involves measuring the sound intensity at a large number of points around it. Multiplying the intensities by the areas over which they act and adding together the products gives the result. An alternative procedure to point sampling of the normal intensity distribution is to scan the probe over the measurement surface by means of a continuous sweeping motion. Only the sound power of the source within the enclosed region contributes to the scan. The sound intensity at any point is the resultant of the source under measurement and other external sources, but after the source being investigated is completely enclosed the accumulative effect of the external sources is zero.

Previously sound power determination could only be performed in special acoustic laboratories in which simple relationships exist between the measurable quantity, sound pressure, and quantity sought, sound power. Sound power could also sometimes be determined using sound pressure, in situ for an item, which can be operated in isolation, in a fairly open environment, in which reverberation is of minor importance. The sound intensity technique offers not only an obvious financial benefit reducing the need for special purpose acoustic test rooms, but also new technical opportunities to investigate the noise emission from components, which due to size or inability to be separated from essential co-functioning equipment, cannot be tested in special rooms.

Despite the obvious advantages afforded by the measurement of intensity the development of measuring instruments took many years. The sound intensity at a point in space is the product of the sound pressure and particle velocity of the oscillating air particles at that point. In the 1930's Olsen patented a sound intensity meter which used a piezoelectric crystal to measure sound pressure and a thin metal strip vibrating in a magnetic field to generate a fluctuating voltage proportional to the pressure gradient and hence the particle velocity[2]. The device was not reliable over a wide range of frequency and atmospheric conditions. The system had a further shortcoming, that was to severely hamper the development of later systems, and still represents one of major errors for contemporary systems, the phase responses of the two transducers did not match precisely. This small phase error swamped the real phase difference between the two recordings.

It was not until 1975 that the first practical instrument was produced by B.G. van Zyl[3], who utilised advances in solid state electronics and manufacturing technology to produce

a device, which worked over a broad range of frequencies. The device used two "identical" sound pressure microphones to infer particle velocity and calculate sound intensity. Between 1975 and 1980 more compact and sensitive instruments were developed in parallel with the growth of integrated circuit devices. In analogue circuitry the introduction of switched capacitor devices solved the problem of filter phase mismatch. Digital filters did not have any such problem except when anti-aliasing front end filters are present. The most commercially successful device was developed by Brüel and Kjaer at the start of the 1980's. The instrument used digital circuitry and allowed measurements to be taken up to 8 kHz. This system uses two condenser microphones 12mm apart. The microphones have undergone special development to minimise any phase mismatch. The sound intensity is derived from sound pressure signals, which yield the pressure gradient.

An alternative approach was published in 1977 by Fahy[4] which calculated the sound intensity using the imaginary part of the cross-spectrum of the signals from two closely placed microphones. The cross-spectrum is a quantity that is easily measured using presently available dual-channel Fast Fourier Transform (FFT) analysers.

In 1982 Norwegian Electronics introduced an intensity probe that works using an ultrasonic beam to determine the particle velocity and a conventional pressure microphone to measure the sound pressure. Other intensity techniques are discussed in section 2.2 and the relative merits of the aforementioned main commercial techniques discussed in section 3.1 outlining the reasons behind the selection of the measurement system adopted for this study.

The sound intensity measuring instrumentation has many varied applications. The

sound power outputs of sources of all kinds can now be calculated in situ.

Sources of noise can be placed in rank order of importance. Design changes to reduce noise can be quantified. In January 1991 an international standard was introduced with guidelines for sound power determination from point sound intensity measurement[5]. The sufficient number of measurement points, adequate geometrical distribution of these and the sound power determination accuracy are obtained by an iterative process of measurement, calculation of measurement indicators and measurement refinement. The standard and the sound field indicators are discussed fully in section 2.2. The companion standard covering the scanning technique for sound power determination has not been completed yet due to the added complexity associated with error prediction for non time stationary signals. There is however, every indication that both sampling techniques yield similar accuracy with the scanning technique resulting in considerable time savings for large applications.

Vector mapping of sound intensity can be used to pinpoint specific noise sources. Direct measurements can be made of sound insulation performance of partitions and weaknesses in seals and closures may be rapidly detected. The principal path of noise transmission in buildings can be identified including flanking transmission. The transmission loss of materials is conventionally determined by inserting the sample in a opening between two reverberant chambers. Alternatively it can be determined using one reverberant chamber containing a broadband noise and sound intensity measurement to measure the transmitted power. The incident power is inferred from the space-average mean square sound pressure in the source room. This technique requires only one special acoustic room and allows the presence of particularly transmissive elements in a partition to be identified.

The sound absorption coefficient of a material can be determined either in situ or in a reverberation chamber. For instance, the energy absorbed by a seat in an auditorium has been evaluated by integrating the intensity over an enveloping surface. In practice attempts to supplement traditional techniques with the intensity method has proved disappointing due to high uncertainty.

1.3 OBJECTIVES

The general approach to this research has been introduced in a preceding section. The specific aims are as follows.

Despite the increased interest in environmental awareness comparatively little is known of the generator and it's excitation system's noise characteristics, principally due to the inability of traditional sound pressure techniques to isolate sources. The first aim was therefore to determine sound power levels with acceptable, quantifiable accuracy from sound intensity measurements. This enables the main sources of noise to be placed in rank order. The site sound pressure level has been explained in terms of the contribution from the adjacent plant, the reverberant background noise and the direct background noise. This has yielded a clear, correlated new level of insight into the noise emission from generator units.

Much previously unpublished information about the main noise source mechanisms has been presented. It is outside the scope of the thesis to fully quantify each noise mechanism for each component of the generator unit. Interpretation of the experimental data is broadly discussed with the relative importance of each mechanism for each component given. For a hydrogen cooled generator magnetically induced vibration, mainly at twice the supply frequency, and aerodynamic sources each contribute about

50% of the overall level. The large generator casing transmission loss has been shown to limit the aerodynamic noise and explain the relatively low levels. The pilot exciter was the major noise source, creating siren tones at magnet pole passing frequencies and also broadband aerodynamic noise.

The sound intensity technique affords many advantages but error assessment is complex. Sound power determination using the point technique has been recently standardised and the companion standard for the scanning technique is at the proposal stage. It has therefore been necessary to identify the best means to assess accuracy under the wide range of conditions encountered. The accuracy is commonly assessed from field indicators. There is still discrepancy in the literature as to which field indicators are applicable and not everything is well understood. The choice of F_2 or F_3 to quantify phase error requires assessment. The belief that the spatial sampling error indicator can overestimate the point measurement error and is inappropriate for the scanned measurements has been investigated.

The sound pressure particle velocity coherence and the relationship between real and reactive intensity has been used in an industrial application to classify sound fields, which has important implications for industrial sound intensity measurements.

The final stage of the thesis was to conduct a detailed theoretical modelling investigation into the major noise source identified. This was the pilot exciter.

To implement design changes to reduce noise levels at source a theoretical model was developed, which relates the siren tone levels to the machine geometries and the aerodynamic behaviour that creates them. The technique has been applied by one author, Talaat[68], for an induction motor. The basic approach adopted for this model

is similar, but a number of underlying assumptions and techniques used by Talaat have been found to be incorrect. This model incorporates a number of significant improvements such as accounting for influence of the phase relationship between ducts on radiated sound power. Higher order harmonics, which can, as in this case, be more significant than the fundamental, have also been calculated for the first time.

Furthermore a full scale pilot exciter test rig was used to validate the modelling process and facilitate other noise source identification. In general, good agreement between predicted and measured sound power levels has been found for the first 4 harmonics for two operational speeds, commonly to within 3 dB. Novel sound pressure measurements in ventilation ducts using miniature microphones have yielded unique insight into the noise generation mechanisms. In addition pressure coherence measurements, and detailed sound intensity vector measurements have identified the main sources of broadband noise to be the magnet pole tips at the ends of the machine and the corebars. As a result of this work a relationship between noise emission and the machine geometries, which create the noise has been afforded representing a vital tool at the design stage to control noise at source.

2. LITERATURE SURVEY

To become familiar with relevant work and to gain an appreciation of the problems involved, a literature survey was conducted at the start of this investigation. This survey initially concentrated on two principal aspects, generator unit noise assessment and noise source identification techniques. Generator unit noise assessment information was limited so it was supplemented with the appreciably greater amount of available electric motor data. To develop a measurement system and practice, a detailed investigation was conducted into advanced noise source identification techniques. Special attention was given to the problems associated with the use of sound intensity in regions of high background noise. For the study into the pilot exciter siren mechanisms further review of fluid mechanics, duct acoustics and acoustic radiation was necessary at a later stage.

The various parts are considered in more detail in the following sections.

2.1 GENERATOR UNIT NOISE ASSESSMENT

Airborne noise has been assessed in power stations for a number of years and details of sound pressure measurement have been published for the last two decades. Sound pressure level is important as it is the basis for environmental accredition and factory safety regulations. Sound pressure is highly dependant on its measurement position, surroundings and the presence of interfering sources. It is therefore of limited value for diagnosing the precise cause of noise. Only in recent years have measurement techniques been developed, which can accurately quantify source strength independent of its location, identifying the main noise sources and also providing a new level of insight into the fundamental noise generation mechanisms.

Schwarzenbach[6] discussed the subjective effects of noise and sound pressure levels in two power stations on a general level. A more detailed account of sound pressure levels for large steam turbines with ratings from 100MW - 700MW was presented by Bannister[7]. 1m from an indoor turbine generator unit the S.P.L. was commonly between 90 to 99 dB(A). Levels in the vicinity of the boiler feed pumps were between 100 and 110 dB(A) and valve noise was sometimes in excess of 110 dB(A). It was claimed, albeit without substantiation, that the main generator noise source mechanism was magnetically induced vibration. The generator however did not make the major contribution to the S.P.L. beside it. The exciter ventilation noise is more significant. Pailly[8] provides similar suggestions claiming that the S.P.L. from a 700MW generator unit alone should be less than 85 dB(A).

The limitations of sound pressure measurement to quantify source strength and determine sound power level was illustrated by Grabkowski's detailed study[9]. The influence of background sources, reverberation and distributed source effects were too significant. Major noise sources can sometimes be identified from sound pressure, as indicated by further work by Grabkowski[10] in a turbine hall, although sound pressure is seldom simply related to adjacent machinery.

The sound intensity technique was applied to a 300MW steam turbine generator unit by Pleeck[11]. Inadequate measurement points were used for accurate sound power determination, however interesting observations were made. The rear end generator coupling was the major source creating an S.P.L. of 99 dB(A) with a radial intensity of 96 dB(A), whereas the S.P.L. beside the generator was 88 dB(A) and the radial intensity between 76.5 and 80.5 dB(A). The sound intensity scanning technique was more successfully applied by Reiniche[12] on a turbine generator to determine the sound power

for its various components. The sound pressure level and spectral composition was fairly constant beside all plant, whereas the sound intensity levels and spectra vary markedly. The paper discusses factors causing a difference in sound pressure level and average sound intensity, as well as sound power error limits. Specific source location is limited. Under extreme conditions such as those experienced by Taillifet[13] in a hydro power plant, despite it's advantages sound intensity may prove inadequate for source identification.

Hong[14] outlines an attempt to use fuzzy relationship classification to identify common characteristics from a group of seven turbine generator units, although at this stage this provides little new insight into noise problems. Goldfracht[15] predicted the sound pressure inside a power plant using assumed radiation patterns from manufacturers sound power data. The direct noise is supplemented by the first two reflections and barrier influences are considered. The analysis yielded surprisingly accurate results considering the complexity of industrial workspace noise transmission and the questionable accuracy of the assumed sound powers.

Much attention has been directed to the predictions of sound power emission from electric motors. These predictions are often a combination of analytical and empirical determinations of magnetically induced vibrations, mechanically induced vibration and aerodynamic noise[16, 17]. Due to the differing nature in equipment between motors and generator units and associated extra complexities little information of this nature has been published for generator units. Useful trends in vibration with load and power factor can be predicted using finite element analysis[18]. Actual levels of magnetically induced vibration cannot be accurately predicted for a generator due to its considerable variability with position and its high dependence on the detailed outer frame

construction and it's foundations. Due to difficulties in predicting vibration distributions and the complex radiation characteristics of the generator casing sound power emission cannot be predicted. For many years complex core spring mounting arrangements have been employed to reduce transmission of this vibration[19].

Motor aerodynamic noise generation empirical prediction schemes[20, 21] require further refinement and investigation before they can be applied to predicting generator noise. Large generators differ from motors as they have closed circuit cooling systems and solid as opposed to laminated rotors. The aerodynamic noise is substantially reduced by the thick generator casing adopted for hydrogen cooled generators, which has a transmission loss that can be calculated using statistical energy analysis[22].

2.2 NOISE SOURCE IDENTIFICATION TECHNIQUES

In order to reduce generator unit noise levels to within international regulations it is necessary to identify the parts of the plant and the source mechanisms, which constituent the major noise problems. The benefit of design changes needs to be quantitatively assessed. Caution should be exercised as the source of the troublesome agent, sound pressure, and the source as defined in terms of generation of sound power may not correspond at all closely. Only when this knowledge is obtained is it possible to make engineering changes to reduce the strength of the different source mechanisms or interfere with the noise propogation path.

Crocker[23] discusses traditional and more modern techniques for source identification. The oldest method that of subjective assessment, can prove valuable, but has the limitation of not being quantitative. Selective operation of complex machinery, if

physically possible, can indicate contributions from different parts provided the machine performance is not significantly altered. Selective wrapping of a machine with a high density material, such as lead, is widespread, but has the disadvantages of being time consuming, expensive, dependant on special test facilities and ineffective at low frequency due to poor transmission loss. Frequency analysis of sound spectra can relate pure tones to their causes. Near field sound pressure measurements can indicate sources for large machines, although this practice is restricted due to near field reactivity, contamination of microphone signals by adjacent sources and directivity effects. Sound power can be estimated by measuring a sufficiently representative mean squared normal surface velocity and assuming a radiation efficiency of one, or in other words the vibrating surface generates sound power effectively.

Identification of tonal sources on small motors can be accomplished using spectral resolution, r.p.m.. mapping and selective operation[24]. For generating plant operating in difficult multi-source, reverberant acoustical environments these simple approaches are inadequate. The generator cannot operate in isolation from its co-functioning plant or in a special test facility so selective operation, lead wrapping techniques and conventional sound power determination by sound pressure measurement are impractical. The failure to determine in situ sound power by sound pressure measurement for a generator unit due to reverberation and background noise was illustrated by Grabkowski[9]. Generator surface vibration is too complex to estimate sound power from.

Since the mid 1970's digital signal processing and subsequent sophisticated measurement techniques, including intensity and coherence, have yielded good results

even in complex acoustical environments. In parallel with the development of sound intensity measurement, introduced in chapter 1, alternative intensity techniques have been developed. Surface intensity measurements have been used to investigate the radiation characteristics of vibrating surfaces using a pressure microphone and a surface vibration transducer, most commonly an accelerometer. The microphone is placed in close proximity to the point of vibration and the normal intensity is determined using similar processing techniques to sound intensity.

The main advantage of this technique is that it is less susceptible to inaccuracies caused by high extraneous noise than airborne intensity measurements. The method has been successfully applied to a variety of sources including building structures[25] and diesel engines[26]. The technique does however have a number of disadvantages, which make it less suitable for application to large generator units. It is very awkward to transverse large structures and as vibration fields are less uniform than sound fields they are more difficult to sample. Leaks in partitions and uncovered rotating components cannot be investigated using surface techniques. Near field measurements in areas of recirculating acoustic energy are not ideal, but cannot be avoided irrespective of the measurement technique used in cases of extreme background noise.

Noise sources can also be studied using the spatial transformation of sound fields method. The Helmholtz Integral Equation states that from a knowledge of the sound pressure and particle velocity distribution over a enclosed surface surrounding a sound source the pressure can be predicted at any point outside the surface. Alternatively by suitably choosing the Green's functions in the Helmholtz Integral Equation the external sound field can be calculated from either the sound pressure or particle velocity distribution over an infinite plane. Commonly a two-dimensional scan over a plan close

to the test object is made with the cross-spectra being calculated from each scan point to each of a set of reference points[27]. Far field sound pressure, reactive and active sound intensity and sound power can all be predicted. The technique has been most commonly used in the automotive industry and can be used to simulate the effect of source attenuation on far field noise radiation. Nearfield acoustic holography[28] can provide valuable sound source characterisation. In general in multi-source, reverberant environments the particle velocity distribution is distorted by the background noise leading to confusing results. The technique can best be applied to sources which can be isolated.

The most reliable, under a wide range of adverse conditions, of the intensity methods and subsequently the most widespread is the measurement of direct sound intensity using the two microphone technique. The historical development of the sound intensity technique, the measurement principles and instrumentation have been introduced in chapter 1. Fahy summarises and references a good cross-section of this material[2]. There are basically two types of sound intensity analyser. The first type of analyser finds intensity using eqn.(3.2). The filters are either digital or analogue, and are placed either before or after the sum and difference circuits of the two sound pressure signals[29]. The other type of analyser is the dual-channel FFT analyser in which the intensity is calculated using Fahy's[4] eqn.(3.3). The narrow-band spectra can be synthesized into 1/3 octaves with the disadvantage of longer averaging times to have enough spectral lines at low frequencies. Complex mixtures of positive and negative frequency components can make quick assessment of measurements difficult. Tichy[30] illustrated that for a 10mm thick undamped steel plate the percentage of negative intensity in each third octave varied from 25% at 200 Hz to 5% at 1 kHz for a measurement distance of 100mm. The percentage of negative intensity increases for thinner steel plates and also

with smaller measurement distances. In reverberant enclosures measurement accuracy of pure tones can be dependant upon bandwidth making F.F.T. measurement potentially inaccurate if spectral resolution is inadequate[31]. The narrowband spectra can be related to a specific source mechanism proving a useful tool for source identification. F.F.T. analysers make coherence data readily available, which is useful in assessing random errors. FFT analysers can provide other quantities such as reactive intensity, sound pressure particle velocity coherence and be used for vibration measurement.

Despite the advantages afforded by the sound intensity measurement techniques there are a number of errors within the technique which impose restrictions on the measurement range and in severe cases invalidate results. A systematic error is inherent in the approximation of the pressure gradient by a finite pressure difference. The finite pressure difference is severe at high frequencies. The error can be calculated for idealised sources[2] resulting in an underestimation of less than 1 dB at 5 kHz for a 12mm microphone pair spacing. The phase mismatch between the two microphones and the channels of instrumentation gives rise to an error. The phase mismatch can be critical for small values of microphone spacings at low frequency. The importance of phase mismatch to measurement areas is reflected in literature[2, 32, 33, 34] and the standardisation[5]. One fundamental indicator the local pressure-intensity index, $\delta_{p|I|}$, the logarithmic difference between the sound pressure and true absolute sound intensity reflects measurement accuracy. As it is in terms of the true intensity the estimation of the indicator from a measurement is subject to the same phase mismatch error. It is claimed that it cannot therefore be used to predict measurement accuracy[2]. Jacobsen[33] has subsequently outlined how the indicator determined from the measured intensity can give a strict prediction of the phase mismatch error. Expressions for the random error in sound intensity has been presented by Pascal[35] in terms of the coherence between the

two pressure signals, the number of independent averages and the phase difference between the two pressure signals. This formulation has the limitation that the error in coherence estimate is not normally known, the phase difference may be inadequately resolved by the analyser and the underlying analysis is based on Gaussian noise excluding tonal sources. Jacobsen[36] provided an alternative expression for the random error in a frequency band, which is invariant of the spectral resolution of the frequency analyser. Jacobsen and Pascal error prediction is similar in less complex acoustic conditions such as plane wave propogation, but in reverberant fields and reactive nearfields of vibrating plates Pascal's formulation can underestimate the error.

Sound intensity measurement has been used in a wide range of applications including sound power determination, noise source location, measurement of sound absorption, specific acoustic impedance, transmission loss of partitions and radiation efficiency. Sound intensity can identify noise sources by source ranking and intensity mapping. In source ranking, the sound power radiated by different components of a machine is compared. Johns[37] successfully illustrated the value of this method to identify, quantify and rank order the noise sources in an industrial compressor plant installation. This resulted in optimal noise control measures being proposed. Very similar results were obtained for sound power emission from the constituent parts of a diesel engine[38] using sound intensity and lead mapping with great cost and time advantages for the intensity technique. In principle sound power can be obtained under any ambient conditions using the intensity technique. This can be accomplished in situ in the presence of background noise provided that it is constant and there is no absorption within the enclosing surface. Stirnemann[39] indicated practical limits of suppression are 14-18 dB. This represents an upper limit to suppression, defined as the logarithmic difference between the sound pressure integrated over a closed surface and the intensity integrated

over the same surface. This is known as the field indicator F_3 which is defined in Appendix D.

Bockhoff[40] claimed that provided a suitably small measurement distance was used, 5-10cm, the sound power determination was repeatable to within 1 dB when directly incident background caused the average sound pressure to increase by 10-15 dB. For a diffuse field Bockhoff presents similar levels of repeatability even with an increase in sound pressure of 20 dB. Pettersen[41] conducted an extensive round robin study of a test arrangement comprising of a motor, turbine, gearbox and two compressors. The study concluded that measurement accuracy of 2 dB could be guaranteed with a logarithmic difference between sound pressure and integrated sound intensity of 10 dB. These 3 surveys indicate quite different levels of suppression of background noise. This is to be expected as measurement accuracy is a function of the measurement principle, the acoustic field characteristics, the orientation of the probe within the field and the characteristics of the individual measurement system being used. These problems have been addressed by the standard's committee.

The vector property of intensity can be used to provide a detailed picture of the sound field distribution of a source. One notable application was by Pepin[42] who measured the 2D and 3D intensity distribution of a spinning beam. For such complex mechanical systems the interpretation of results is not straightforward. Pepin used numerical simulations of the observed sources to relate them to the measured intensity pattern. Astrup[43] measured the vector intensity distribution and partial sound power from a chain saw. The partial sound power gave a clear indication of the relative importance of the various components and the vector distribution highlighted the predominant source regions. In enclosed spaces such as vehicles the vector intensity behaviour can be very

difficult to interpret. In one example a floor was installed in an idealised aircraft cabin[44]. At frequencies above about half the ring frequency of the structural cylinder the acoustic pressure distributions were greatly altered by the floor, but the wall surface intensity distributions and radiated power were not significantly affected.

Sound intensity measurement at a point cannot discriminate between the component from one machine in the presence of background noise with that from another. This suppression can only be accomplished by employing the Gaussian integral over a completely enclosed surface. To distinguish between various uncorrelated sources selective intensity has been under development. The method uses reference transducers, which strongly represent the various sources in a system. These represent inputs to a multiple-input two-output system with the outputs being the two microphone signals comprising an intensity probe. The frequency response functions are found by a least squares approximation procedure, which permits the cross spectrum associated with the individual source to be estimated. Under certain circumstances these methods have proven successful. Tetherway[45] distinguished the intensity component due to mechanically induced vibration and aerodynamic origin in a small drill. The success of this technique is heavily dependent on obtaining representative, sufficiently incoherent input transducer signals.

Simpler coherence techniques have been previously applied using sound pressure and vibration input signals to relate the various contributions to sound pressure at a position of interest. One notable application was by Ying[46] in a power plant. The sources were definitely incoherent as the transducers were on different machines.

The standard ISO 9614-1[5] "The determination of sound power levels of sources by sound intensity measurement at discrete points" was accepted as a full standard in 1990. The standard aims to be applicable to a wide variety of sources operating in situ. The sufficient number of measurement points, adequate geometrical distribution of these and the sound power determination accuracy are obtained by an iterative process of measurement, calculation of measurement indicators and measurement refinement. The field indicators are defined in appendix D. There is still much discrepancy in the literature as to which indicators should be used.

The phase mismatch error is calculated from the global indicator, F_2, eqn. (D.1), which is the difference between the average sound pressure and the average unsigned sound intensity. If inaccuracy is too great due to the phase mismatch the measurement grid can be redefined or action must be taken to minimise background effects. There is some discrepancy in the literature if F_2 should be used to predict the error in sound power determination due to phase mismatch. In the ISO standard[5] and other work[2,32] F_2 is used. It has been demonstrated[33,34] practically and theoretically that it is the indicator, F_3, involving the integration of the signed intensity over the measurement surface, eqn. (D.2), that is really related to phase error. This is illustrated in appendix A. Further support is provided for sound measurements conducted on a motor with varying levels of background noise[47]. For cases of extremely large background noise there will be strong positive and negative intensity with a low F_2 indicator. However the overall sound power accuracy may be subject to an error. To some extent the condition that F_3-F_2 <3dB in ISO 9614-1 eliminates this possibility.

The standard outlines an acceptance criteria for phase mismatch error, if this is not acceptable corrective action is necessary. If the acceptance criteria is met the random

error associated with the discrete point sampling of the spatially continuous normal intensity field on the measurement surface is determined using the field indicator, F_4, eqn. (D.3). Assessment of the random error is based on the assumption that the distribution is Gaussian, which can be determined from the probability density. Irrespective of the actual distribution if the measurement definition is repeated randomly the averages of I_n will be normally distributed due to the central limit theorem. Therefore provided the number of measurements is sufficiently large for the sample variance to be a reasonable approximation of the actual variance of the continuously distributed normal intensity, error limits can be predicted for given confidence limits in terms of variance coefficient, F_4, using eqn. D.5.

The value of F_4 will be large i.e., above 2, where strong extraneous noise creates negatives intensities or where the majority of the source's total power is through relatively small areas. It is suggested by Hübner[48,49] that the overestimation of measurement points implied from F_4 and eqn. (D.5) can be obviated by determining the standard deviation for a smaller sub-grouping of measurements incorporating regions of high and low emission. The standard takes account of 'hot spots' by increasing the measurement density on these areas only rather than uniformly. This minimises extra measurement effort. The standard only permits this approach when F_3-$F_2 \leq$ 1dB. Hübner illustrates that this criteria is unnecessarily stringent.

The temporal variability of the total field in terms of the normalised standard deviation of the intensity at a 'control' position is calculated using the indicator F_5, eqn. (D.4). The steadiness of the total field is essential for application of Gauss's Integral Theory to globally suppress background noise. A number of investigations have demonstrated that the use of F_5 is not the best means to assess the overall steadiness as the result is

highly dependant upon the choice of control position. Gade[50] demonstrated for a sound source in a reverberation chamber that the value of F_5 was extremely variable with position and despite the sound field being stationary the acceptance criteria in the standard was exceeded in all cases. Gade suggests that pressure rather than intensity measurements should be used for calculation of temporal variability. It is felt that this may prove to be correct but further proof is necessary. In cases of high direct and reverberant background noise there is the potential for pressure not to be sensitive enough unless the acceptance criteria for variability is reduced in such cases. A table of F_5 limits based upon the nature of the acoustic environment described by F_2, F_3 and F_3-F_2 may prove the best approach.

The alternative to point sampling is to traverse the measurement probe over the source sections in a continuous scanning motion. This technique is quicker and more convenient than the fixed point measurement in many industrial situations. The number of discrete measurements necessary to suppress high levels of background noise can be prohibitive for a large structure such as a generator. The scanned probe produces non time stationary signals and much of the standard time series analysis theory is not strictly valid. Because of this the international scanning standard has not been finalised, but there have been many different detailed studies, which have illustrated that the scanning method produces results of a similar level of accuracy to those from point sampling. Many of the indicators from the point standard are not strictly applicable for the scanning technique such as F_2 due to added uncertainties. It is felt that this may be too conservative and Jacobsen's detailed analysis of random errors[51] supports this.

For theoretical and practical measurement considerations F_3 indicator is the parameter used for error quantification of measurements using the scanned technique. It is

suggested[41] that for $F_3 \leq 10$ dB, $10 \leq F_3 \leq 15$ dB and $F_3 > 15$ dB the grades of accuracy, as defined in the ISO 3740 series, are engineering, survey and not classified. Results corresponding to the engineering grade of accuracy have the following standard deviations of 3 dB (125 Hz), 2 dB (250 Hz), 1.5 dB (500-4000 Hz) and 3 dB (8000 Hz) for $F_3 \leq 5$ dB, and 5 dB (125 Hz), 3 dB (250 Hz), 2 dB (500-4000 Hz) and 3 dB (8000 Hz) for $5 < F_3 \leq 10$ dB. The A weighted power is commonly dictated by the 500-4000 Hz region. This correlation between F_3 and standard deviation was derived by a round robin test program on an industrial compressor application. Random errors are included in this.

In theory the scanning technique covers the entire measurement surface obviating the need to assess the random spacial sampling error. In practice to some extent the continuous intensity distribution is still sampled and needs to be assessed. Estimation of the error can still be achieved from the indicator F_4.

The applicability of the central limit theorem can be ascertained by repeating every n th measurement n times, for example 4. If the space averaged intensity error tends to that for the total measurement population the distribution is normal and the random errors can be calculated. The distribution of the intensity distribution can be further evaluated from a probability density or relative occurrence chart[12]. For a given frequency range the relative magnitude of the intensities to the mean can be evaluated as a fraction of the total number of measurements. The distribution of a relative occurrence chart cannot strictly be examined for a true Gaussian pattern as the data is plotted in logarithmic scales. It does however serve as a broad indication if the measurement sample has a random nature.

It is believed that the error may be more appropriately calculated from eqn. (D.5) using the n repeated averages provided different assessment paths are scanned.

3. EXPERIMENTAL TECHNIQUE AND BACKGROUND THEORY

3.1 REQUIREMENTS FOR MEASUREMENT SYSTEM

The preceding chapter outlines the value of sound intensity and coherence techniques. This section explains in more detail the requirements of the measurement system.

In recent years the availability of accurate, reliable instrumentation for the measurement of sound intensity allows sound power determination of noise sources in their normal operating environments. This in conjunction with vector intensity mapping assists source identification. The measurement system must therefore be capable of accurate sound power determination from large sources in the presence of high background noise. Fundamental to all measurement schemes employing two nominally identical pressure transducers is an optimally phase matched microphone pair. One measurement scheme employs direct digital or analogue filtering and electronic circuitry to calculate the necessary summation, integration and multiplication to evaluate the intensity. Alternatively the intensity can be calculated indirectly using an F.F.T. analyser.

The F.F.T. approach has the disadvantage that it requires longer averaging times for enough spectral lines to synthesis low frequency 1/3 octaves. The complex mixtures of positive and negative frequency components can make quick assessment of measurements difficult. Pure tone measurement accuracy in reverberant enclosures can be dependent on bandwidth making F.F.T. measurement potentially inaccurate if spectral resolution is inadequate. For purely dB(A) sound power determination direct filter systems are preferable. However for assessment of random errors, for example, inter

-channel coherence is necessary. F.F.T. analysers make coherence data available. More importantly for noise source identification other processing functions and extra flexibility are necessary. F.F.T. analysers can readily measure these. These other functions include reactive intensity and sound pressure particle velocity coherence, which can be calculated simultaneously with real intensity. · Vibration spectra and the coherence of this with sound pressure can also be measured by F.F.T. analysers.

To identify not only the major sources of noise, but also the relevant source mechanisms measurements have to be narrowband. This can indicate the presence of tones, which can be correlated with the source mechanism such as fan blade passing frequencies, magnetically induced vibration or structural resonance especially if excitation and speed can be varied.

Complementary software was written in parallel to implement the sound intensity algorithms, calculate sound power, process measurement spectra and synthesis into 1/3 octaves, etc. To maintain flexibility all software for post processing was written in house as opposed to adopting commercially available software[52, 53]. Despite the quality of this software the complexity of incorporating statistical analysis, measurement indicators and coherence function computation was deemed more troublesome than writing and verifying the necessary software.

In short, the F.F.T. approach was adopted to obtain a flexible, general purpose system capable of many other measurements and indepth validation of results necessary to yield insight into the complex source mechanisms.

3.2 SOUND PRESSURE

Noise causes annoyance, makes communication difficult and can damage hearing. It is sound pressure squared that damages the ear, so legislation for permissible noise exposure commonly refers to sound pressure level with the A-weighting, to model the ear's performance, and exposure duration. Until recently the recommended maximum noise dosage was 90 dB(A) for an 8 hour working day although in 1991 the European Commission have recommended this should be 85 dB(A).

For all measurement investigations the sound pressure level was measured at 1m from the machine under study at a height of 1.2m above floor level. A Brüel and Kjaer integrating sound level meter, type 2230, supported on a tripod was used in compliance with BS5969.

3.3 SOUND INTENSITY MEASUREMENT PRINCIPLES AND INSTRUMENTATION

For sound intensity measurement careful assessment of the error limits are of paramount importance due to the many potential systematic and random errors associated with the technique. These errors are not only dependent upon the nature of the sound field in which the measurements are conducted, but also the transduction principle utilised and the quality of the individual measurement system used. It is therefore necessary to relate the measurement principle and the instrumentation to the measurement errors.

3.3.1 Principle of sound intensity measurement

Sound intensity is defined as the rate at which sound energy is transmitted through a unit area, the elemental area being so oriented that it lies perpendicular to the

instantaneous particle velocity vector. The average sound intensity is computed as the vector quantity equal to the time averaged product of the instantaneous sound pressure and the associated instantaneous particle velocity vector. The component of intensity in the r direction I_r is given by

$$I_r = \langle p(t)v_r(t) \rangle \qquad 3.1$$

where p(t) is the sound pressure, $v_r(t)$ is the particle velocity and the symbol $\langle\ \rangle$ implies a time average.

The particle velocity can be obtained directly using an ultrasonic probe, but the most common transduction principle synthesises it indirectly from the Euler momentum equation, using two nominally identical microphones with pressures p_1 and p_2 separated by a small distance Δr.

If the instantaneous sound pressure, p, is taken as the mean of the two microphones' signals the sound intensity in the r direction is :

$$I_r = \frac{-1}{2\rho\Delta r} \langle (p_1 + p_2) \int (p_2 - p_1)\, dt \rangle \qquad 3.2$$

where ρ is the fluid mass density. The frequency distribution may be determined using the time averaged form of eqn. (3.2) by passing the two signals through identical filters, either before or after performing the sum, difference and integration operations, and then performing the time-average operation on the product of the filtered outputs. This is 'direct' frequency analysis.

'Indirect' frequency analysis procedures are based upon Fourier analysis of the two probe signals. This formulation is derived[4] via the correlation function and eqn. (3.2). The real intensity, I_r, and the imaginary intensity, Q_r, can be calculated as

$$I_r(\omega) = -(1/\rho\omega\Delta r)\ \mathrm{Im}\ \{G_{p1p2}(\omega)\} \quad 3.3$$

$$Q_r(\omega) = (1/2\rho\omega\Delta r)\ [G_{p1p1}(\omega) - G_{p2p2}(\omega)] \quad 3.4$$

where Im $\{G_{p1p2}(\omega)\}$ is the imaginary part of the cross spectrum between the two microphone signals and G_{p1p1} and G_{p2p2} are the autospectra of both microphones. Eqns. (3.3) and (3.4) can be implemented by feeding the outputs of two well matched microphones directly into an F.F.T. analyser. A block diagram for the signal processing associated with the indirect method is given in Fig.3.1.

3.3.2 **Instrumentation**

A photograph of the measurement system hardware is given in Fig.3.2. The B & K 3519 sound intensity probe was used, which contains the best commercially available phase matched 1/2" microphone pair, B & K 4181. The microphone polarisation voltage is supplied by the B & K 2807 power supply. The microphones have greatly improved low pass filter characteristics minimising interchannel phase mismatch, the importance of which is discussed in the following section on systematic errors. The microphones are mounted in a face to face configuration, minimising diffraction effects and using a solid plug to control the acoustical separation. With a conventional windscreen measurements can be conducted in airflow speeds up to about $5ms^{-1}$.

The signal processing was conducted by the F.F.T. analyser, Hewlett Packard 3562A. The analyser samples the two microphones simultaneously at 256 kHz and converts the analog sample to a 14-bit digital word. This results in an 80 dB dynamic range, which is maintained using auto ranging features. The data is re-sampled commonly using a 5 kHz frequency span and 6.25 Hz line bandwidth. The data is weighted with the required windowing function, fast Fourier transformed and averaged. The

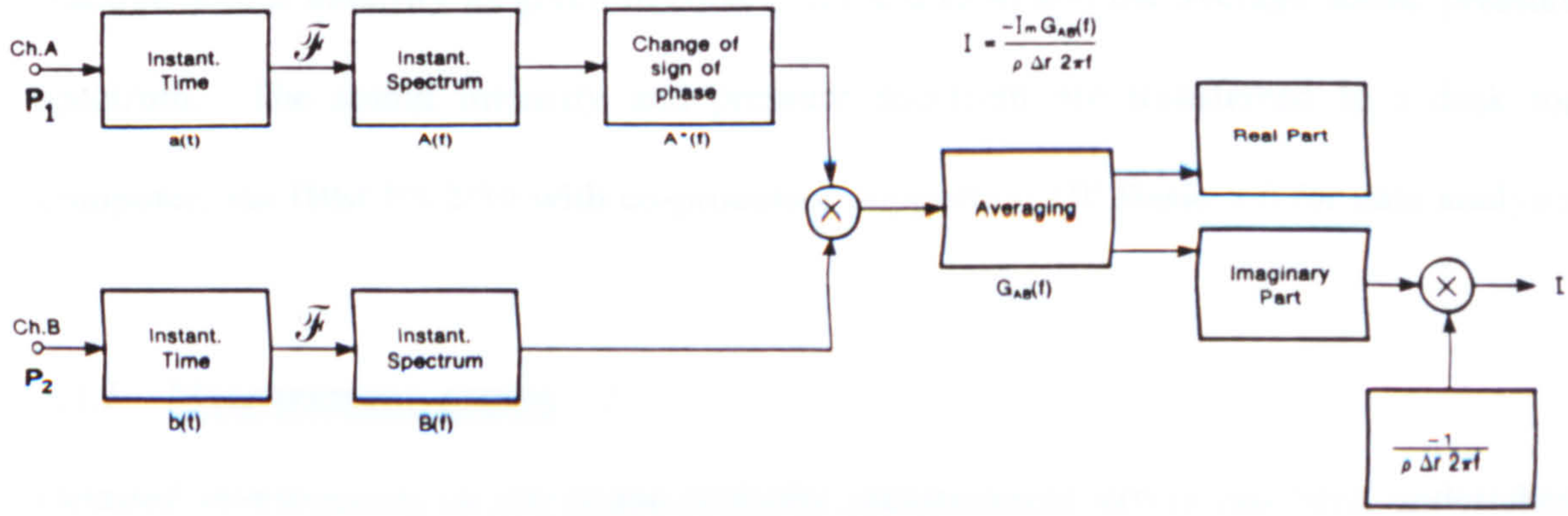

Fig.3.1 Block diagram of FFT analysis for p-p systems[2]

Fig.3.2 Sound intensity measurement system hardware

analyser is programmed to process the cross and auto spectra to calculate the real and reactive sound intensity as given in eqns. (3.3) and (3.4) and the average sound pressure spectrum. The sound intensity and pressure spectrum are transferred to a desk top computer, the IBM PS 2/30 with co-processor supporting HP Basic 5.0 for data analysis.

3.3.3 Measurement errors

Detailed investigation of the sound intensity measurement errors has been undertaken by several investigators. The errors associated with intensity measurement are discussed as follows and those related to sound power determination will be discussed in a later section.

i) The finite difference approximation error is inherent in the approximation of pressure gradient by a finite pressure difference. The error restricts the high frequency capability of the instrument. This error is dependant upon the type of field under investigation and as this is seldom known in advance the error cannot be predicted precisely. Except in sound near fields the error associated with a plane wave propogating along the probe axis is a conservative estimate of the actual error. The ratio of measured, $\hat{I}_r$, to true intensity, I_r, can be shown to be[2]

$$\frac{\hat{I}_r}{I_r} = \frac{\sin(k\Delta r)}{k\Delta r} \qquad 3.5$$

where k is the wavenumber and Δr is the distance between the microphones. For a 12mm spacing the error is an underestimation of less than 1 dB at 5 kHz.

ii) The phase mismatch between the two microphones and channels of instrumentation gives rise to an error. The effect of this error is dependant

upon the interchannel phase mismatch and the actual phase difference of the sound pressures at the transducers, which is dependant upon the nature of the sound field, measurement position and probe orientation.

iii) Statistical or random errors occur when continuous, periodic, time-stationary signals are approximated by finite duration samples. The error is a function of the coherence between the two pressure signals γ^2_{12}, the number of independent averages N and the phase difference between the two pressure signals $\emptyset_{21}$. Pascal's[35] expression for the error e_r in terms of these parameters is

$$e_r(\omega_n) = (1/2N)^{1/2} [(1 + \gamma_{12}^{-2}) + \cot^2 (\emptyset_{21}) (\gamma_{12}^{-2}-1)]^{1/2} \qquad 3.6$$

The equation has the limitations that the error at a narrowband frequency inthe estimate of coherence is not normally known, $\emptyset_{21}$ when small may be insufficiently resolved by the analyser and the analysis is based on Gaussian random noise, which excludes application of the analysis to tonal sources.

Villot[54] suggested computing the random error for a band by adding the variances of the frequency components within the band, calculated from eqn. (3.6). This may be liable to an error as the assumption that the frequency components are uncorrelated is not strictly true. The finite duration of the time records in the frequency analysis means that frequency components are somewhat correlated. An alternative expression is presented by Jacobsen[36] for the random error in a band as

$$\varepsilon_r\{\hat{i}(\omega_o, \Delta\omega)\} \approx \frac{(\int [(S_{11}(\omega)\, S_{22}(\omega) - C_{12}^2(\omega)+Q_{12}^2(\omega))/\omega^2]d\omega\ \ \pi/T)^{1/2}}{|\int (Q_{12}(\omega)/\omega)d\omega|} \qquad 3.7$$

where S_{11} and S_{22} are the power spectra of each pressure signal, C_{12} is the real part and Q_{12} is the imaginary part of the cross spectrum of the two pressure signals, T is the integration time and the integration limits are the limits of each band. The normalised random error will be large when the sound pressure particle velocity coherence discussed in section 3.7 is low. It can be shown that eqn. (3.7) is identical to eqn. (3.6) if the bandwidth is so narrow that the integrals are independent of the frequency. This needs to be determined as it is not necessarily the case for one-third octaves. Jacobsen concludes that the random error is invariant of spectral resolution of the frequency analyser. It can be large in reverberant fields, in source nearfields when sound pressure and particle velocity are nearly in quadrature and when coherence is less than unity due to extraneous electronic noise.

This random error analysis is not strictly applicable for scan measurements, only measurements at a fixed point. The error cannot be predicted precisely for non-stationary signals, but Jacobsen[51] illustrated that for slow scanning, $<0.2ms^{-1}$, the error from a point measurement is a good indication of that from a scan. This error will also be further assessed in conjunction with measurement repeatability and spatial sampling errors.

3.3.4 Calibration and evaluation of measurement system performance

Errors are dependant upon the nature of the measurement sound field, but it is impractical to monitor the intensity probe performance in the full range of these. Instead the measurement system performance can only be assessed from investigations in controlled conditions.

3.3.4.1 Calibration in anechoic chamber

Intensive probe diffraction tests were not carried out as the anechoic chamber available was not sufficiently anechoic for intensity calibration of high accuracy. Instead the relationship between intensity and sound pressure normal to a plane progressive wave was approximately investigated in an anechoic chamber with a cut off frequency of 150 Hz. A loudspeaker with broadband excitation was used as the source. The sound pressure of a separate microphone at the centre of the probe represents the free field intensity. The difference between this value and measured intensity is plotted in Fig.3.3a from 50 Hz to 10050 Hz. For comparison the error in intensity expected due to the finite difference approximation for a spherical wave calculated from eqn. (3.5) is plotted in Fig.3.3b. The general measurement discrepancy increases with frequency in correlation with that expected due to the finite difference approximation error. The discrepancy of ±1 dB at lower frequencies was mainly due to the inadequacy of the anechoic chamber. Subsequent sound pressure measurements illustrated in reality the chamber exhibited low levels of reflections not only below the supposed cut off frequency of 150 Hz, but also up to approximately 250 Hz.

3.3.4.2 Calibration in acoustic cavity

The residual pressure intensity index, $\delta_{po|Io|}$, is the logarithmic difference between sound pressure and intensity when both microphones are subjected to identical pressure. This represents the dynamic capability of the system and its ability to perform under adverse conditions. Ideally the pressure gradient and subsequentially sound intensity is zero. The residual index should tend to infinity. In practice due to the interchannel phase mismatch the pressure gradient is never zero and some

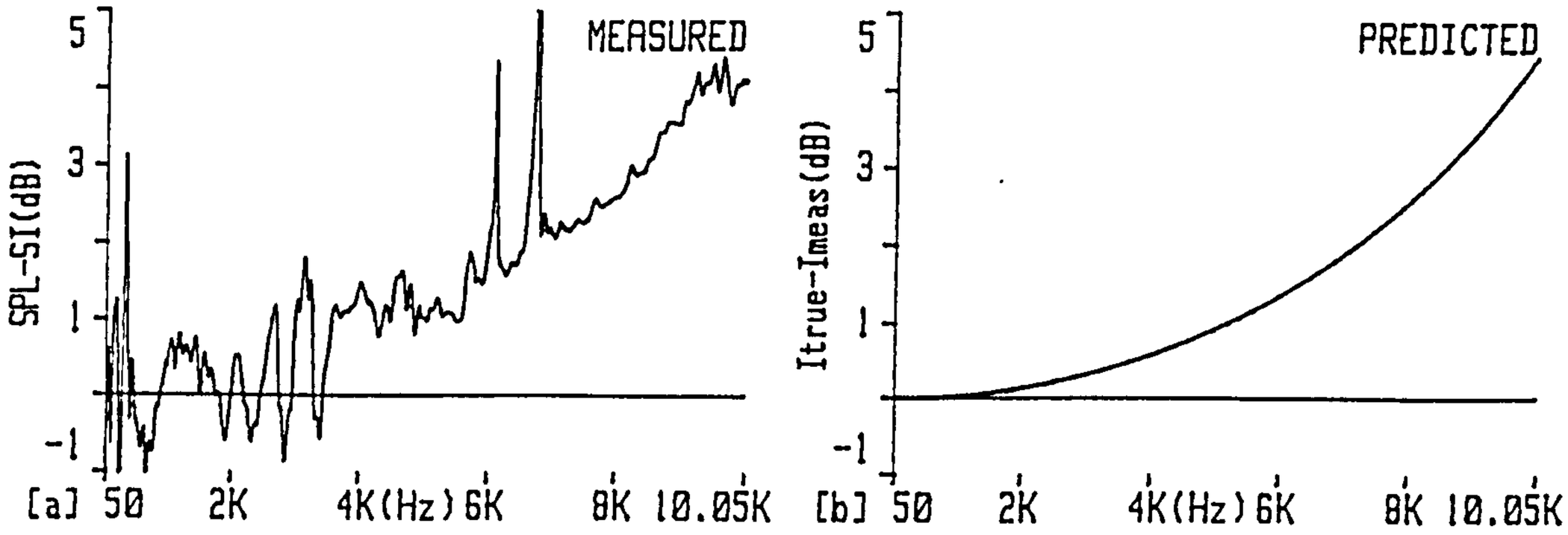

Fig.3.3 Logarithmic difference between a) measured sound pressure and sound intensity in free field b) true and measured sound intensity from eqn (3.5)

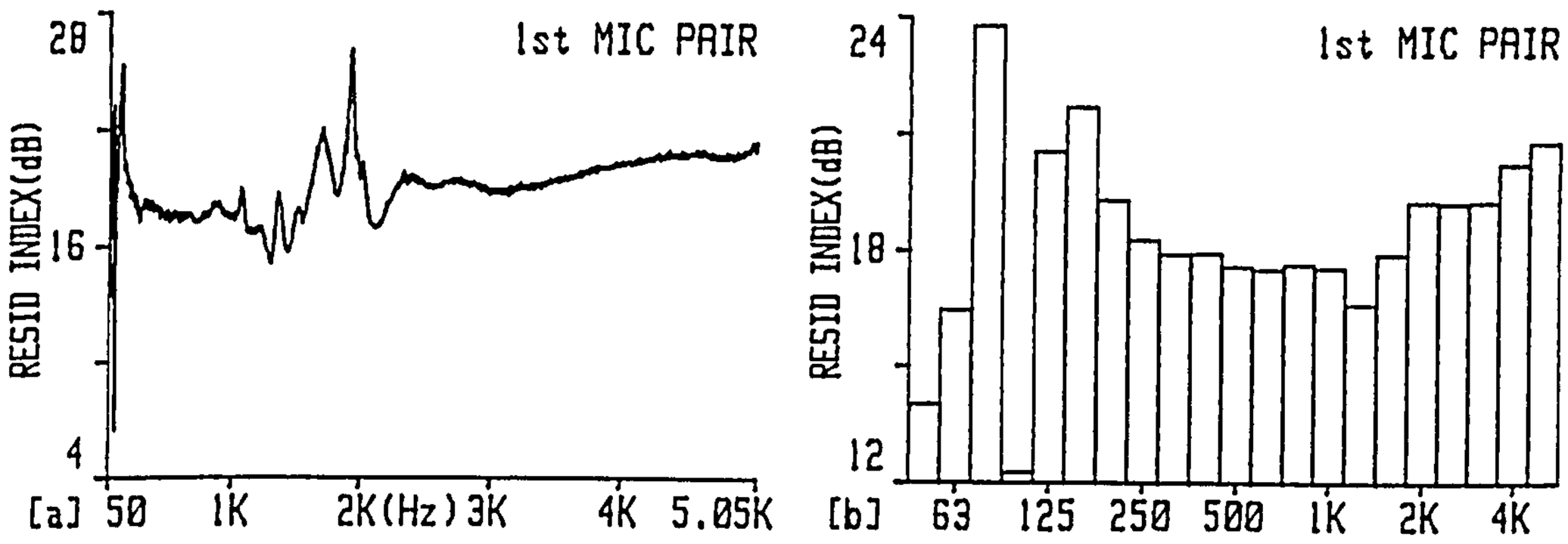

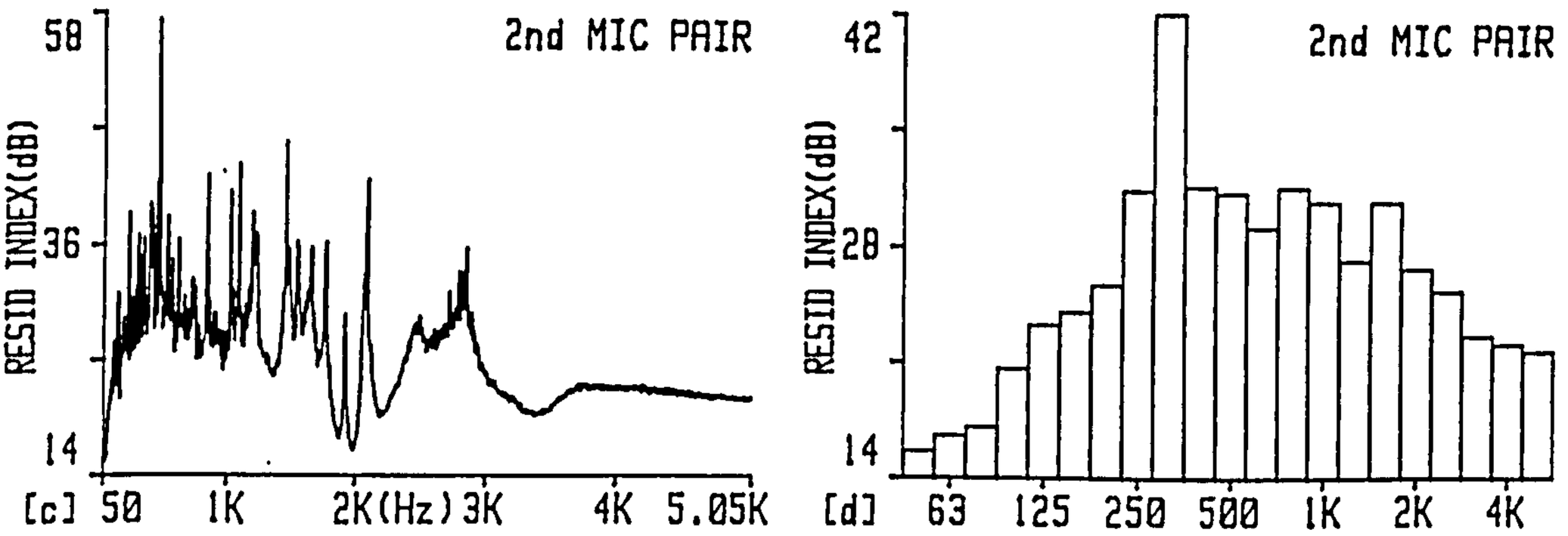

Fig.3.4 Residual sound pressure intensity index for microphone pair 1 a) narrowband b) 1/3 octaves and for microphone pair 2 c) narrowband d) 1/3 octaves

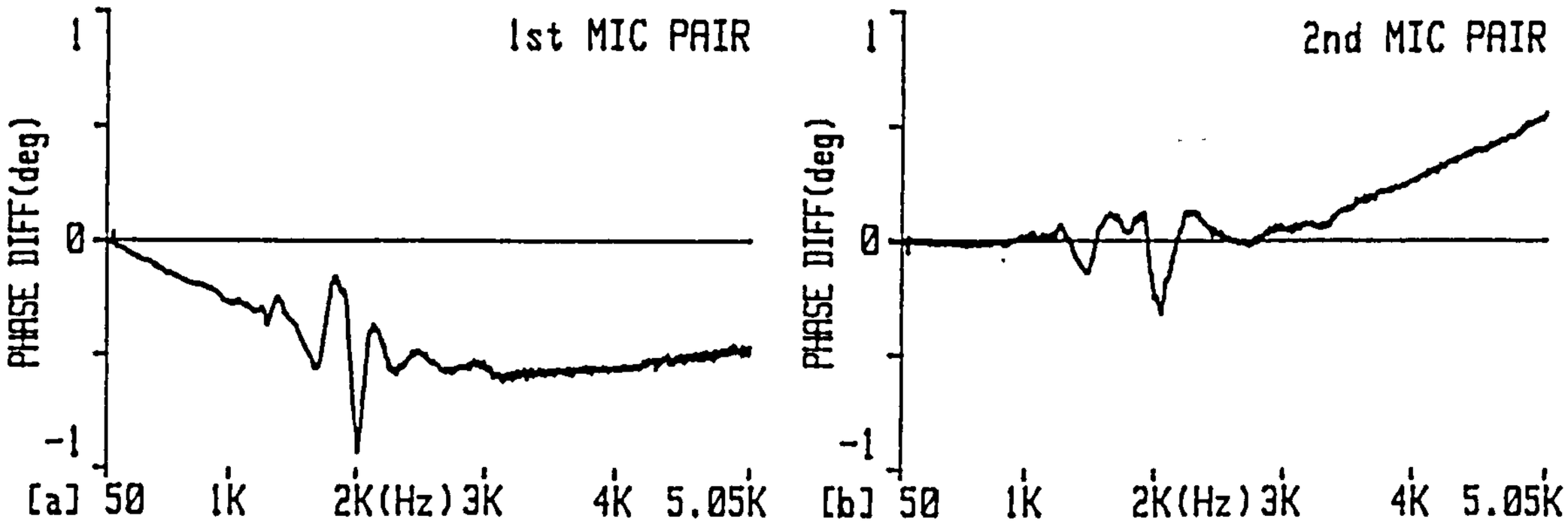

Fig.3.5 Measured phase difference for a) microphone pair 1 b) microphone pair 2

intensity will always be measured. The residual index can be used to predict the measurement error in sound power using eqn. (A.12) in conjunction with the measured average difference between sound pressure and intensity as outlined in appendix A.

The difficulty arises in subjecting each microphone to identical pressure. A special cavity, B & K type 3541, was randomly excited to accomplish this. The similarity in pressure for both microphones was monitored. Two 1/2" microphone pairs, type 4181, were used during this investigation. For microphone pair 1 used in the original factory testing programme reported in section 4.1 the residual pressure intensity index is as plotted in Figs.3.4a and 3.4b for narrowband and synthesised 1/3 octaves. The residual index increased linearly from 17 dB at 200 Hz to 21 dB at 5 kHz. Microphone pair 2 was used for site testing and the second program of factory testing reported in sections 4.2, 4.3 and 4.4. It's performance is better than pair 1 as illustrated in Figs.3.4c and 3.4d. From 150 Hz to 1.8 kHz, the range in which the phase error is most problematic, the value was in general appreciably above 24 dB.

The performance can be directly related to the microphone phase characteristic measured using the transfer function technique outlined by Frederiksen[55]. For microphone pair 1 the phase, given in Fig.3.5a, increases linearly up to 2 kHz, yielding a flat index. After a glitch at 2 kHz the phase was constant and the index increases linearly. The low frequency region of microphone pair 2 has a phase of within ±0.03° up to 1 kHz as given in Fig.3.5b. For a narrow frequency band at 1.8 kHz the phase increases to 0.2° relating to a residual index of 18 dB, but above this

frequency the phase increases linearly to 0.6° at 5 kHz relating to residual index of 21 dB.

3.3.4.3 Analyser performance

For an F.F.T. based intensity system it is important to assess it's performance as this may limit the system capability. The two analogue signals should be sampled synchronously. The effects of sampling phase distortion, electrical noise and arithmetic implementation of the F.F.T. and their increase with the dynamic range can be assessed by injecting common pink electrical noise signals to both inputs. The dB difference between the indicated sound pressure level spectrum and the indicated sound intensity level indicates the residual index of the analyser.

For pink noise with a sound pressure level equivalent to 44 dB in each line (an overall level of 73 dB), the indicated residual pressure intensity index is commonly above 30 dB below 500 Hz and greater than 35 dB above 500 Hz. For pink noise with a sound pressure level equivalent to 84 dB in each line the indicated residual pressure intensity index is commonly above 35 dB below 500 Hz and above 40 dB above 500 Hz. For these levels of input noise which are typical of those encountered, with high levels in low frequency band and lower levels in the high frequency band, the F.F.T. does not limit the overall residual pressure intensity index given in Fig.3.4c. The analyser dynamic range of 80 dB is necessary to analyse broadband sources with spectral levels that varied over the frequency range. The unweighted maximum level of 100 dB S.P.L. at 50 Hz or 100 Hz set the low range of the instrument at 20 dB, which allowed a signal to noise ratio of 25-30 dB for the typical narrowband S.P.L.'s encountered. To fully utilise this auto ranging was up and down. The internal noise

floor, when not determined by the 80 dB dynamic range was 270 nV per line generally, with a maximum of 8μV at supply frequency harmonics. This corresponds to 2.6 dB and 32 dB sound pressure for the 1/2" microphones therefore being insignificant.

3.3.4.4 **Synopsis**

The measurement system performance has been evaluated for both microphone pairs and found to be within manufacturer's specification. Microphone pair 1 performance could be better and may result in problems in the extreme conditions of background noise found within the factory. Microphone pair 2, used for the site and later factory testing, has a very high residual index. This high quality instrumentation is fundamental to obtaining accurate results in hostile conditions.

3.4 SOUND POWER DETERMINATION

3.4.1 Principle of source sound power determination

The sound intensity technique can be employed for sound power determination in the presence of strong extraneous noise. The method uses two means to suppress background noise commonly referred to as local and global suppression. For local suppression extraneous noise is reflected back from the source surface through the measurement surface it entered causing cancellation. Global suppression employs Gauss's Integral Theorem, by which the volume integral of the divergence of any field vector may be expressed in terms of the integral over the enclosing surface of the component normal to the surface :

$$\int_{vol} \nabla \mathbf{I}\, dV = \int_{s} \mathbf{I}.\mathbf{n} ds = \int_{s} I_n .\, ds = \sum_{i=1}^{N} I_{ni} A_i = W_s \qquad 3.8$$

where W_s is the net mean sound power generated by the source mechanism within the enveloping surface and N is the number of segment areas into which the enclosing surface is divided. Normal components of sound intensity generated by steady source mechanisms operating external to S do not contribute to the surface integral and hence not to W_s provided the source contains no absorption.

3.4.2 Measurement procedure

To obtain an acceptable level of measurement accuracy the measurement procedure has to be optimised. For the specific measurement problems encountered the following parameters required assessment.

i) Form and size of the segments into which the measurement surface is subdivided.

ii) The geometric configuration of the scan path.

iii) The maximum permissible scan speed.

iv) The indicators of quality of sound power determination.

v) Confidence limits of sound power determination accuracy.

In regions of high background noise the measurement surface should conform to the machine surface. The sub-divided sections should facilitate a continuous, well controlled probe traverse. Each area should be less than $1m^2$. The sub-division should ideally separate regions of high intensity as insufficient averaging over a "hotspot" may yield poorer results. These should be identified ideally using a portable real time analyser or alternatively by a sound level meter or the ear.

Small regions of high intensity are more accurately measured by discrete points. The measurement distance used was commonly 10cm except in regions of too high air velocities near couplings for example. This increased the signal to noise ratio (the source to background noise ratio) and utilised local suppression most fully. Nearfield measurements can cause problems due to reactive fields, but at 10cm from reasonably thick plate (10mm to 27mm) this should not be prohibitive[30].

The measurement scan pattern was dependant upon the sub-section geometries. For a $1m^2$ region, the most commonly encountered, the scan consisted of parallel lines joined at the ends by semi-circles. Orthogonal overlay does not appear to improve accuracy. The compromise adopted between scan speed and line density for a fixed averaging time was a line separation of 12cm and a scanning speed of $0.25ms^{-1}$. This is within the recommended speed of $0.3ms^{-1}$ and general practice of the Nordic group[41]. 200 averages were commonly adopted for each scan, which for a 6.25 Hz line bandwidth, resulted in a scanning duration of 32s. The topic of measurement accuracy assessment is discussed in the following section.

3.4.3 Correlation of measured sound power to sound pressure

It is very important for noise control purposes to understand the composition of sound pressure level. Obviously applying acoustic treatment to an item of equipment, which contributes only weakly to the sound pressure field will have little benefit. Unfortunately sound pressure, the source of the environmental problem, is seldom simply related to the source sound power. Simple relationships only exist in the far field of any source situated in a free field or a fully diffuse reverberant field. The

measured sound power for each component can still approximately be related to the free field sound pressure level using the wave divergence formula[57] :

$$L_{p\theta} = L_w + DI_\theta - 10 \log (A) \qquad 3.10$$

where $L_{p\theta}$ is the sound pressure level in dB in the angular direction θ, L_w is the sound power level in dB, DI_θ is the directivity index of the source in the angular direction θ and A is the area noise is emitting into at a defined distance.

The predicted sound pressure will be an underestimation of the actual sound pressure level at 1m due to a number of factors namely reverberation, geometric error, absorption of low levels of energy and the direct and reverberant background noise.

i) **Reverberation** For a similar power station Reiniche[12] estimated that the increase in sound pressure level due to reverberation was 4.5 dB. For the investigated power station, with only two turbine generator units on the top level, the main reverberation results from reflections from the solid floor doubling the sound pressure i.e. increasing the S.P.L. by 3 dB. The level will be further raised by reflections from the station walls. This increase can be estimated using a Sabinian model from the reverberation time, hall volume and total sound power for 2 generator units.

ii) **Geometric error** The sound pressure at 1m from a distributed source such as a generator surface is contributed to by not only the normal adjacent intensity component, but also by the interference pattern of the complete source. In other words the scalar sound pressure is the summation of the intensity components from all the different angles of incidence. Probst[56] claims that the difference between sound pressure and intensity measurements on large machines is between 1 and 3 dB.

iii) **Absorption** The measured generator unit components can be liable to an underestimation due to small levels of power absorption from the diffuse field. The power absorption P_α, of any structure in a diffuse field is given by[49,57]

$$P_\alpha = S\ \alpha_s\ \frac{p^2}{4\rho c} \qquad 3.11$$

where S is the area of the measurement object, α_s it's Sabine absorption coefficient, p is sound pressure and ρc is the acoustic impedance of air. Hübner suggests that the factor of 1/4 in eqn. (3.11) is only applicable for reverberant rooms and presents experimental results indicating that the multiplication factor should be between 0.4 and 0.8 for reverberant fields and 0.8 and 1.6 for direct extraneous noise in practice.

iv) **Background noise** The sound pressure beside the generator unit will also be increased by direct and reverberant noise from other plant. This will be assessed in other sections.

3.5 SOUND INTENSITY VECTOR MEASUREMENTS

The rate and direction of flow of sound energy is a more revealing and discriminating measure of the distribution and strengths of sound sources. Plotting of vector intensity distributions in a sound field can pinpoint major noise sources, especially when the source has small dimensions. Intensity measurements conducted over a reference grid can characterise acoustic emission effectively even in the presence of background noise in some simple instances[58]. The probe however can only measure the net intensity at a point and not discriminate between the contribution of one machine, the source, and that from other machines. In complex multi-source environments intensity vector characterisation has it's limitations. The magnitude of sound intensity from background sources can be investigated to assess it's influence on S.P.L.

3.6 SOUND PRESSURE SURFACE VIBRATION COHERENCE

In general the relationship between sound power radiation and surface vibration is complex. It is dependant not only upon the vibration velocity distribution on the surface, but also on the radiation efficiency of the structure, which is determined by the interference pattern created by an infinite number of mass injection elements in the radiating surface. For diesel engines the sound power has been calculated successfully from measured vibration data by assuming a radiation efficiency of 1, although for a structure with the size and complexity of vibration behaviour as a generator this is not feasible.

Coherence techniques have proved successful for noise source identification in power plant applications[46]. The coherence function is a measure of statistical similarity

between two signals. These signals may be related by cause and effect, or they may only be similar due to the fact that they arise from a common phenomenon. For a linear system with statistically independent multiple inputs, the coherence function between each signal and the output of the system gives an unambiguous indication of the causal relation between them. The value of coherence varies between 0 and 1 if the system has extraneous noise input, is non linear or has other additional inputs.

For noise source identification the input signals can be near field sound pressures or vibration accelerations measured on individual portions of a machine with the output being the sound pressure at a location of interest, usually at 1m from the machine surface. In cases where the sources are incoherent, the best case being many independent machines, and where representative inputs can be designated, which are free from contamination from other inputs, the technique can prove a very effective tool aiding noise source identification. Yet for more complex systems where inputs are not strictly incoherent such as in a line of co-functioning equipment like a generator unit caution must be exercised in the use of this method.

The coherence function was computed using a dual channel spectrum analyser, the HP3562A. Input signals were piezo-electric accelerometers supported on a magnetic bases and nearfield sound pressures. The output was sound pressure at different locations 1m from the generator unit. The vibration velocity squared spectral composition was also compared to the sound pressure spectra for a variety of distances from 5cm to 1m to investigate source generation mechanisms.

3.7 SOUND PRESSURE PARTICLE VELOCITY COHERENCE

The coherence between sound pressure and particle velocity indicates whether the sound field is produced by one or more sound sources. The coherence between the sound pressure, p, and the particle velocity, u, in the measurement direction is by definition

$$\gamma^2_{pu}(\omega) = (|S_{pu}(\omega)|^2)/(S_{pp}(\omega)S_{uu}(\omega)) \qquad 3.12$$

where $S_{pu}(\omega)$ is the cross-power spectrum of sound pressure and particle velocity and $S_{pp}(\omega)$ and $S_{uu}(\omega)$ are the power spectra of sound pressure and particle velocity respectively.

Another useful, closely related quantity is the frequency band coherence defined in eqn. (3.13). In cases where the intensity spectrum changes in sign within the frequency band the frequency band coherence can be small even where the coherence tends to unity. The influence of bandwidth on the frequency band coherence can yield further information about the nature of the sound field.

$$\gamma^2_{pu}(\omega_o, \Delta\omega) = \left| \int_{\omega_a}^{\omega_b} S_{pu}(\omega).d\omega \right|^2 / \left[\int_{\omega_a}^{\omega_b} S_{pp}(\omega).d\omega \int_{\omega_a}^{\omega_b} S_{uu}(\omega).d\omega \right] \qquad 3.13$$

The sound pressure particle velocity coherence can be derived from the signals of two closely spaced pressure microphones in conjunction with intensity measurements using the following expressions[59] :

$$S_{pp}(\omega) = (S_{11}(\omega) + S_{22}(\omega) + 2C_{12}(\omega))/4 \qquad 3.14$$

$$S_{uu}(\omega) = (S_{11}(\omega) + S_{22}(\omega) - 2C_{12}(\omega))/(\omega\rho\Delta r)^2 \qquad 3.15$$

$$S_{pu}(\omega) = (-2Q_{12}(\omega) + j\,(S_{22}(\omega) - S_{11}(\omega)))/(2\omega\rho\Delta r) \qquad 3.16$$

where S_{11} and S_{22} are the power spectra of each pressure signal, C_{12} is the real part and Q_{12} is the imaginary part of the cross spectrum of the two pressure signals, and

Δr is the microphone separation distance. The coherence function can be calculated by substituting eqns. (3.14) - (3.16) into eqn. (3.12).

The potential value of the coherence indicator can be demonstrated as follows. L_p, sound pressure level, could be significantly greater than L_I, sound intensity level, due to a diffuse field generated by the source, or a diffuse field from extraneous sources, or due to near field effects. If L_p exceeds L_I because of near field effects, the coherence is high irrespective of spectral resolution, provided measurements are not made too close to a thin plate. Tichy[30] illustrated that for a 10mm thick undamped steel plate the percentage of negative intensity in each third octave varied from 25% at 200Hz to 5% at 1kHz for a measurement distance of 100mm. In a diffuse field generated by one source the coherence is high only for very narrow measurement bandwidth.[59] This is due to the bias error introduced by inadequately fine frequency resolution. In a reverberant field containing a single, coherent source the coherence between pressure and particle velocity should tend to unity. However the bias error introduced by reflections delayed longer than the individual record lengths can be significant in reducing the measured coherence. For multiple uncorrelated sources coherence will always be low.

4. EXPERIMENTAL RESULTS

4.1 FACTORY TESTS INVESTIGATION

It is often a contractual requirement to test the generator and it's excitation system on a factory test berth prior to despatch to customer. There is no drive capability to run generators at full load in the factory. Tests are therefore designed, including measurements on open circuit, short circuit and unexcited running, to prove contractual compliance to the various full load electrical and mechanical specifications. One notable exception to the performance verification is the noise specification, normally quoted as the sound pressure level at 1m. Initially it may be expected that the factory environment, in the absence of the turbines, control valves and boiler feed pumps, is the best to accredit noise from the generator alone. In practice noise levels beside the generator are actually 10 dB less on site than in the factory. This is due to four principal reasons.

Associated with the temporary test arrangements are equipment such as the drive motor (open vented), gearbox, associated couplings and temporary brushgear used to supply field current, when the generator is tested uncoupled to the exciter. There are a number of assembly differences which effect it's noise emission. For the generator these include the rear end coupling being uncovered and the front end coupling running uncovered as opposed to being encased in the thicker L.P. turbine pedestal. Temporary baffles and enclosure seals are often fitted to the exciter. Reverberation characteristics are different to those on site. Finally all operating conditions cannot be achieved in the factory.

Under these conditions standard sound pressure measurements will have limited value in characterising the true noise emission of the generator unit. Sound intensity

techniques afford many advantages, but the severe extraneous noise conditions impose very stringent requirements on the measurement practice and instrumentation. The sound intensity surveys discussed in the following sections for a variety of machine power ratings and constructions examine the measurement techniques to their limitations. As well as providing a valuable insight into the measurement techniques some level of noise quantification and identification of the source mechanisms was obtained.

4.1.1 Generator investigation

4.1.1.1 Sound power determination

The noise emission from two hydrogen cooled generators was measured during factory testing. Both units, 350MW and 985MW, were basically similar in design and construction with the larger power output obtained by increasing physical dimensions. The typical test arrangement is illustrated in Fig. 4.1. Within the test line out there are a number of compact background noise sources with large acoustic outputs. The influence of these is discussed in more detail in section 4.1.1.2.

For both units, as the generator was symmetrical and due to access difficulties, the sound power emission was determined by measuring one eighth of the generator from shaft centre line upwards and appropriate scaling of the area ratios to obtain a total figure. The approximate area measured is illustrated in Fig. 4.2 within the dashed lines. For the 350MW unit the machine side was divided into 32 areas, the F.E. 5 areas and the R.E. 3 areas. The 985MW unit side was divided into 38 areas and the F.E. and R.E. were each divided into 3 areas. The results obtained for both units were similar despite lower background noise for the 985MW unit and will be discussed together to allow comparison. Measurements were conducted on normal rated voltage with the terminals

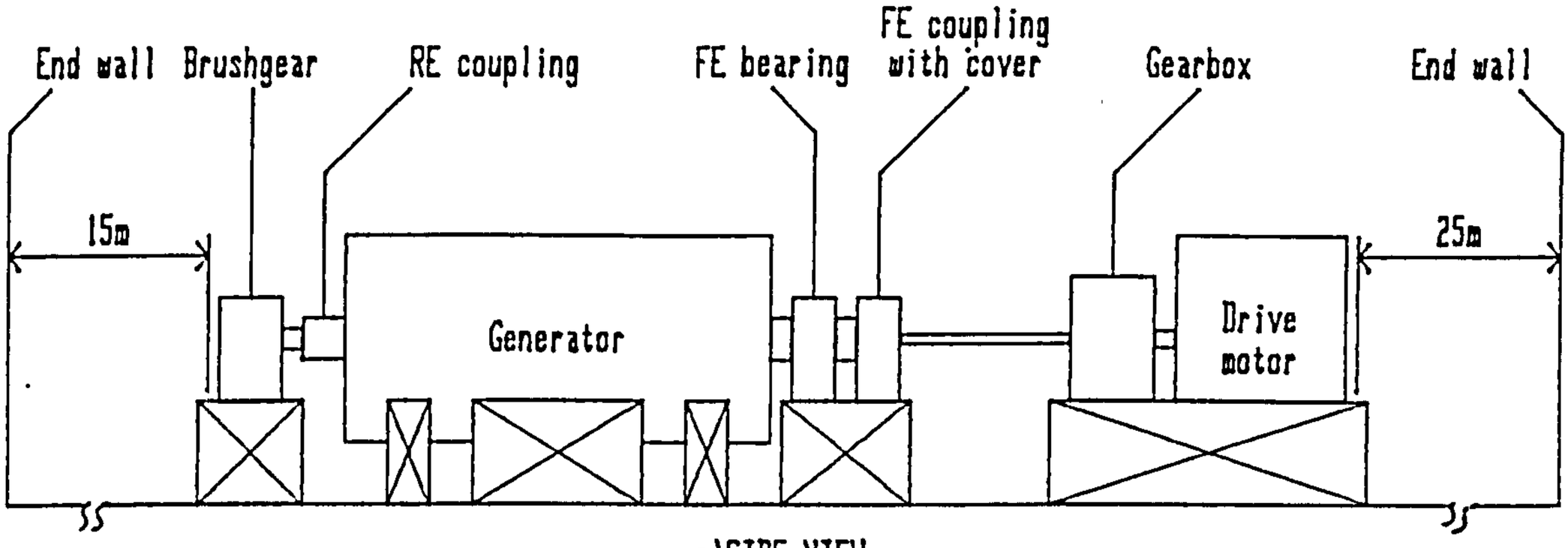

a)SIDE VIEW

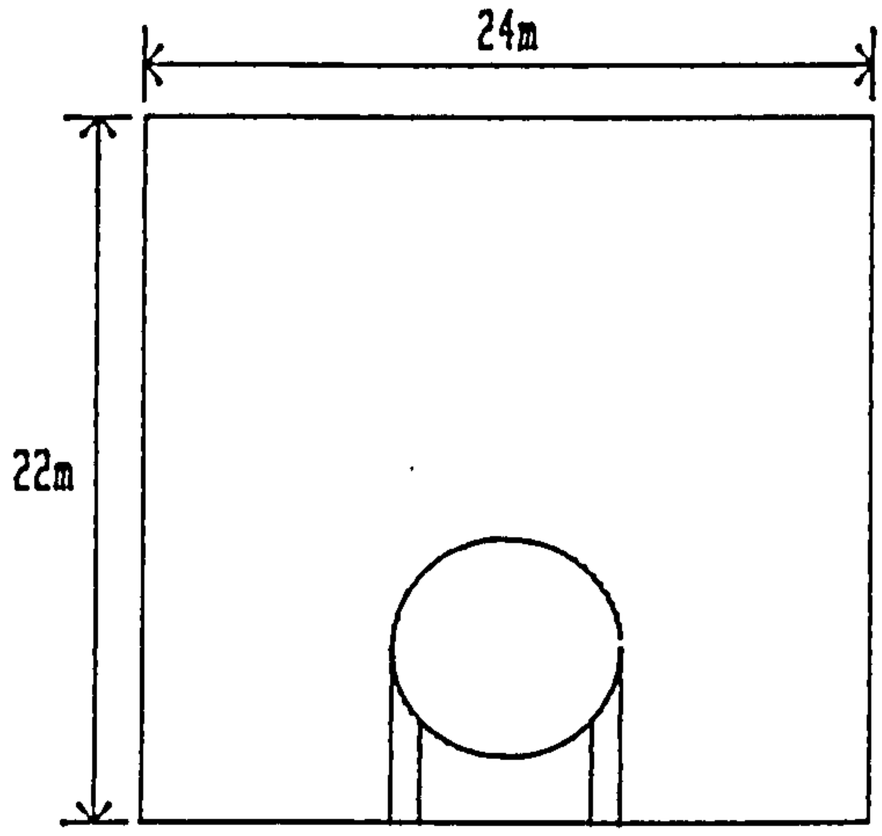

b)END VIEW

Fig.4.1 Generator factory test layout

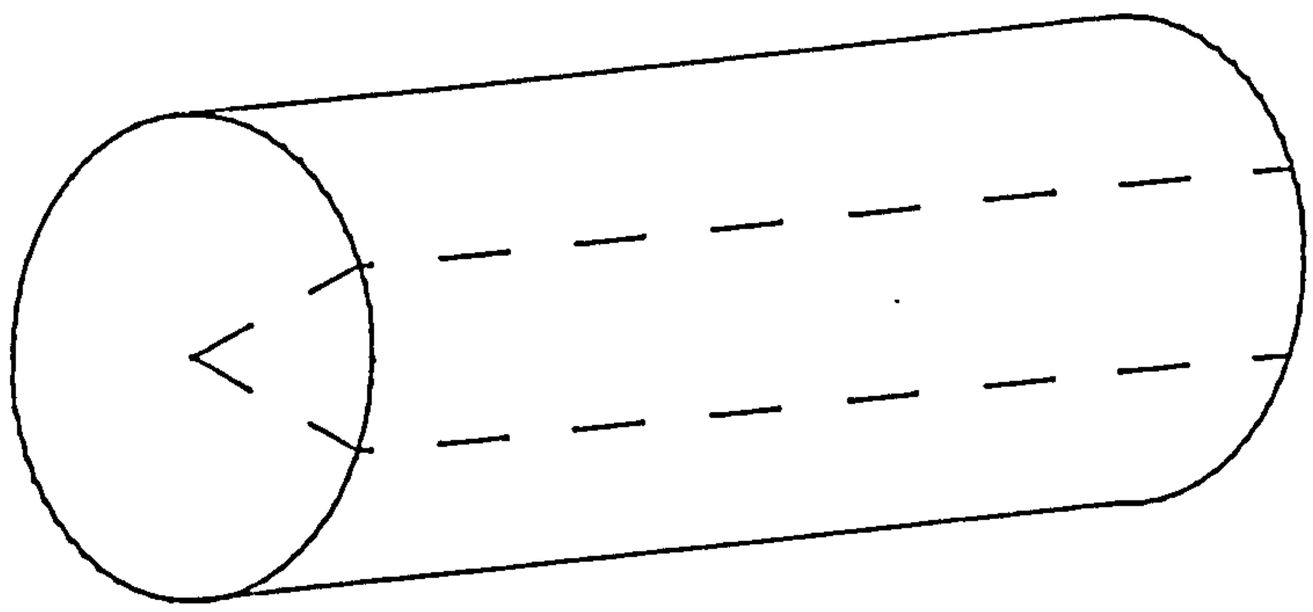

Fig.4.2 Generator measurement area (1/8 of total)

open circuited. The twice supply frequency magnetically induced vibration is a maximum under these conditions[18]. The noise output should therefore be representative of that under load conditions.

The measurement results for the 350MW and 985MW units are summarised in table A and B respectively. The determination of sound power was not straight forward, so to facilitate measurement accreditation the data is presented as three groupings of measurements, the complete 1/8 of the generator, including the end brackets, the side only and the side minus areas close to (within 0.5m) the generator edge. The measured sound power level is given in row 1. The error in sound power level due to phase mismatch calculated using eqn. (A.7) is given in row 2 and the corrected sound power level obtained by subtracting this from the measured levels is given in row 3. This was computed using the calibration data for microphone pair 1 in section 3.3.4.2. The average sound pressure levels and the sound power absorbed using a diffuse field model given in eqn. (3.11) with these S.P.L.'s and an estimated absorption coefficient of 0.03 were also presented. Where feasible the free field sound pressure level was estimated using the source divergence formula eqn. (3.10).

	Measurement area groupings		
	Side-ends	Side	Side + end brackets
Measured sound power level (dB(A))	-83.7	95.9	-105.5
Phase mismatch sound power level (dB(A))	-93.8	-95.8	-100.6
Corrected sound power level (dB(A))	93.3	98.9	-103.8
Average sound pressure level (dB(A))	101.2	102.1	105.7
Sound power absorbed (dB(A))	90.2	92.1	96.8
Estimated free field sound pressure level from corrected power (dB(A)) at 1m	81.6	86.4	-

Table A: Summary of 350MW generator unit sound power measurements and phase mismatch corrections for 1/8 of total generator area

	Measurement area groupings		
	Side-ends	Side	Side + end brackets
Measured sound power level (dB(A))	-85.7	-81.3	- 96.4
Phase mismatch sound power level (dB(A))	-96.5	-97.3	- 99.6
Corrected sound power level (dB(A))	96.1	97.1	96.7
Average sound pressure level (dB(A))	97.6	98.0	99.7
Sound power absorbed (dB(A))	88.9	89.9	92.2
Estimated free field sound pressure level from corrected power (dB(A)) at 1m	81.8	82.2	-

Table B: Summary of 985MW generator unit sound power measurements and phase mismatch corrections for 1/8 of total generator area

The measured sound power for 1/8 of the complete surface including the end brackets for both units was negative for the overall level and for the majority of the sound power spectra as illustrated in Figs. 4.3a and 4.3b. This is due to excessive levels of incident background noise on the F.E. and R.E. brackets. For the 350MW unit the average S.P.L. in these regions was 110 dB(A) and for the 985MW unit the average S.P.L. was 105 dB(A). Theoretically the application of Gauss's Integral Theorem should compensate for this, but in extreme cases of background noise the effectiveness of this has a practical limit. A similar effect was noted for site measurements illustrated in section 4.2.2.1.

To further investigate generator noise output the measurements on the generator side are considered as a separate entity. For the 350MW generator the measurement represented a net output of 95.9 dB(A) with a complex spectrum given in Fig. 4.3c representing net output up to 4 kHz. The 985MW unit measurement represented an input of 81.3 dB(A) with bidirectional flow up to 3 kHz and negative power above this, Fig. 4.3d. The discrepancy arose because of more acoustic energy fringing around the edges of the 350MW generator from the background sources.

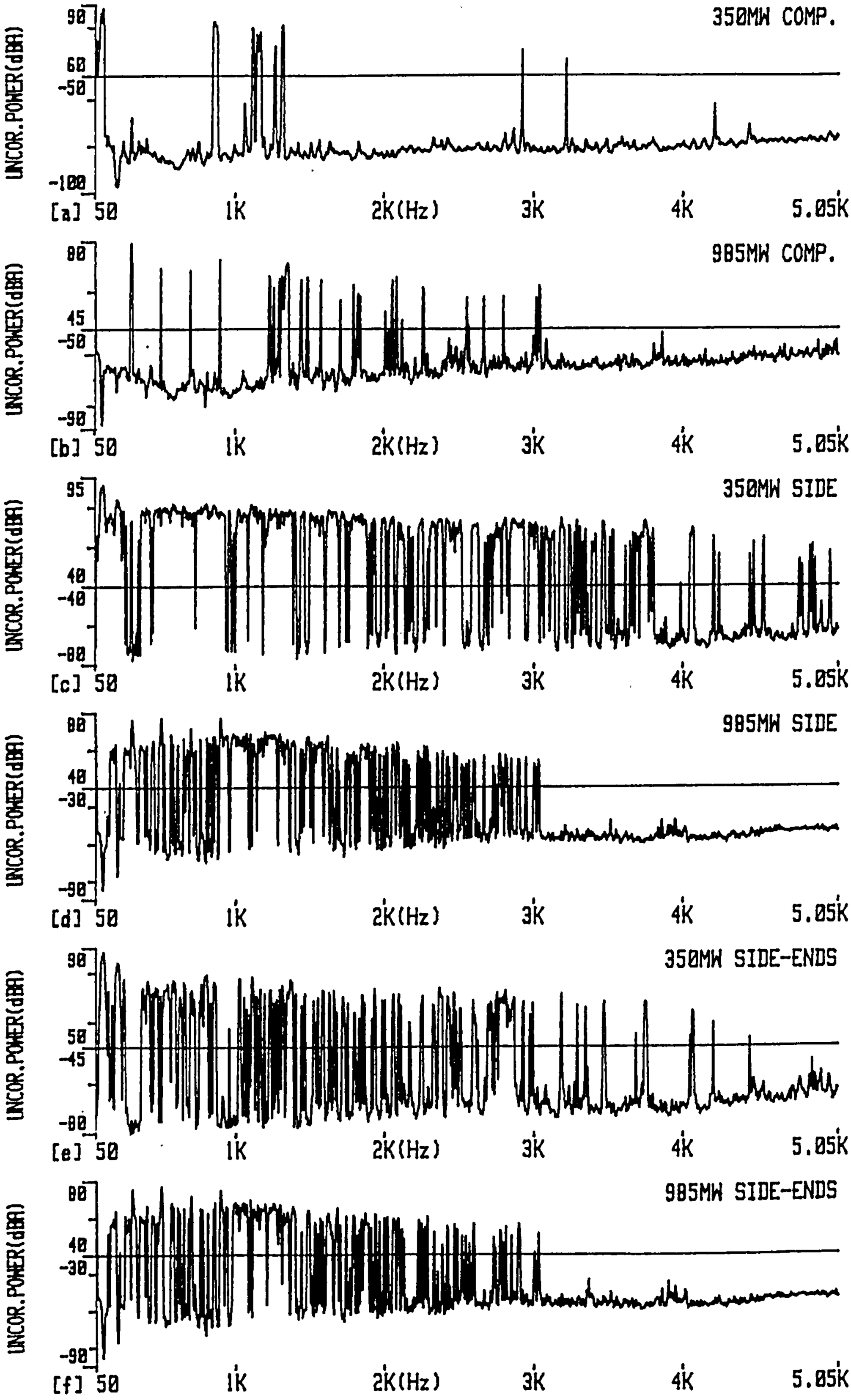

Fig.4.3 Narrowband sound power levels for 350MW and 985MW generators

This can be proven by considering measurements on the generator side excluding those close to the edge. Both generators exhibit net low levels of sound power input corresponding to complex spectra with bidirectional or purely input frequency ranges, Fig. 4.3e and 4.3f. Complex bidirectional flow due to circulating energy in the nearfield of thin vibrating steel plates[30] or near a plate with strong normally incident background noise ideally should be cancelled by application of the surface integral. Failure to achieve this implies the problem posed from background noise is severe.

The F_3 indicator can be used to assess phase mismatch errors and more generally accredit the sound power determination. F_3 for the 350MW and 985MW generator sides is given in Figs. 4.4a and 4.4b respectively. The value commonly exceeds the residual pressure intensity index as illustrated in Figs. 4.4c and 4.4d implying that the quoted levels are invalid. This correlates with other work. The average S.P.L. of 102.1 dB(A) and 98.0 dB(A) for the 350MW and 985MW units respectively exceed typical site levels of 92 dB by an appreciable amount. Even assuming that generator alone sets the site S.P.L., for which there is considerable evidence to the contrary (section 4.2.2), there will be a large difference between the output sound intensity and the S.P.L. measured during factory testing. The measurement error cannot be calculated using eqn. (A.12) in such cases, but it is apparent it will be large. Similarly the spatial sampling random error cannot be calculated when F_3 exceeds the residual pressure intensity index.

It is interesting, under such extreme background noise conditions, to investigate application of Jacobsen's[33,34] phase mismatch correction. Fahy[2] claims that a biased intensity measurement cannot be corrected, when the residual pressure intensity index is exceeded by F_3. Jacobsen disputes this and provides a supporting formulation. For

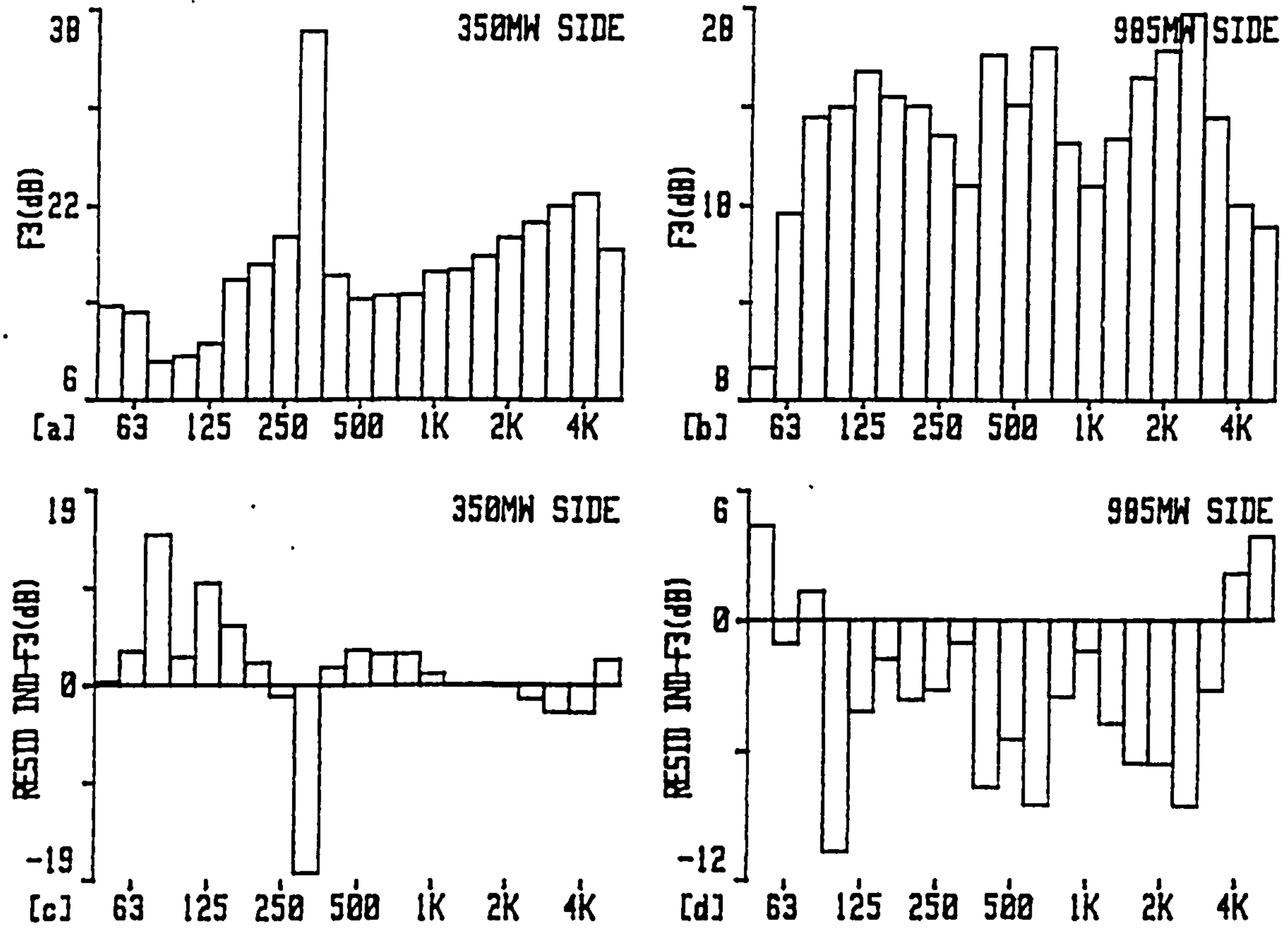

Fig.4.4 Generator side measurements uncorrected for phase mismatch a), b) F_3 & c), d) Residual index - F_3

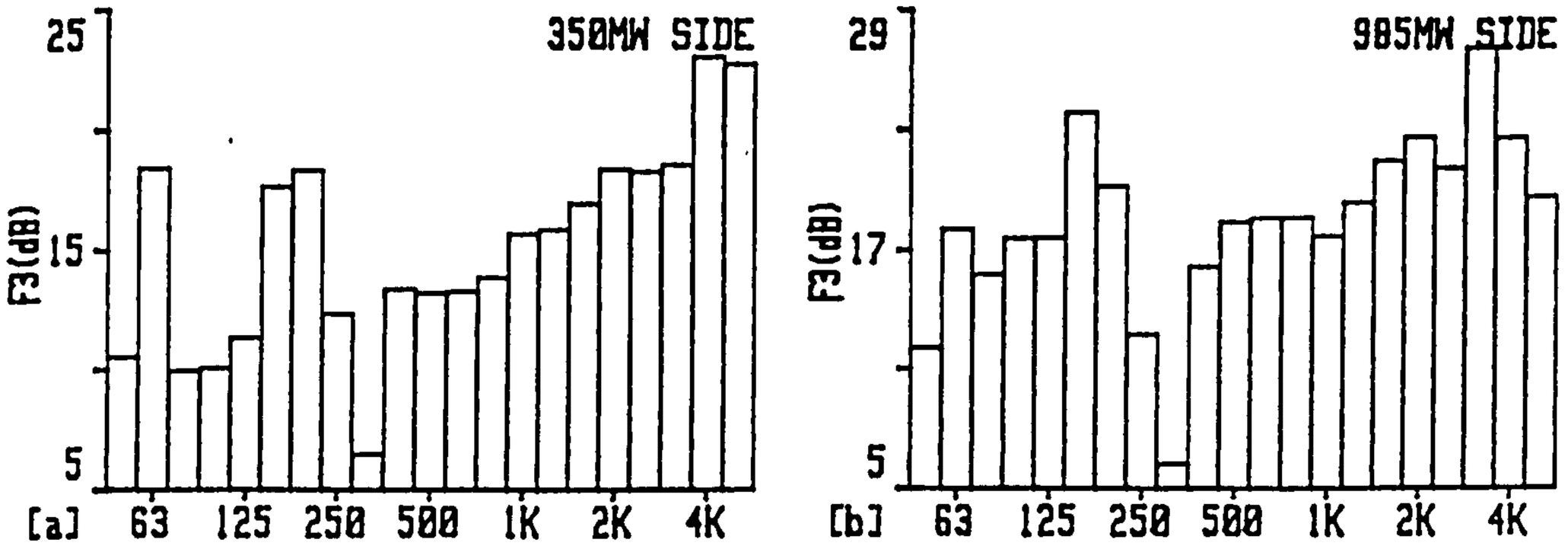

Fig.4.6 Generator side measurements corrected for phase mismatch a), b) F_3 and c), d) Residual index - F_3

the microphone pair used during this work the residual pressure intensity index is within specification ranging between 18 and 21 dB, Fig. 3.4b, but is markedly less good than that realised by the microphone pair 2, Fig. 3.4d. Application of eqn. (A.7) increases the sound power measurement as the sign of phase error has tended to cause an underestimation in sound power level. This is reflected by comparing the corrected and uncorrected sound powers in rows 3 and 1 for both machines in tables A and B. The influence of phase mismatch correction is readily apparent by comparing Figs. 4.5a-f with the uncorrected spectra in Figs. 4.3a-f.

The generator side spectra illustrate a marked change. The 985MW generator side sound power spectrum in Fig. 4.3d is bidirectional up to 3 kHz and negative above these frequencies. The adjusted spectrum, Fig. 4.5d, is clearly positive up to 3 kHz, but still negative from 4 kHz. The spectrum is intrinsically broadband with a prominent 100 Hz tone. A similar problem was observed for the 350MW unit. For measurements on the generator side excluding the end regions to minimise the influence of energy fringing around the ends of the generator the influence of phase correction is equally pronounced for both units. The exception to the spectra sign alteration is the sound power determination for the complete unit, which remains intrinsically negative due to the excessive power input in the end bracket regions. This implies that the measurement inaccuracy caused by this is more fundamental than a phase mismatch error and cannot be corrected simply. It appears that in such extreme cases of background noise the sound power determination of low outputs is impossible.

Even for the phase corrected sound power spectra Figs. 4.5a-f above 4 kHz the power is negative for all cases. This is believed to represent an underestimation in output

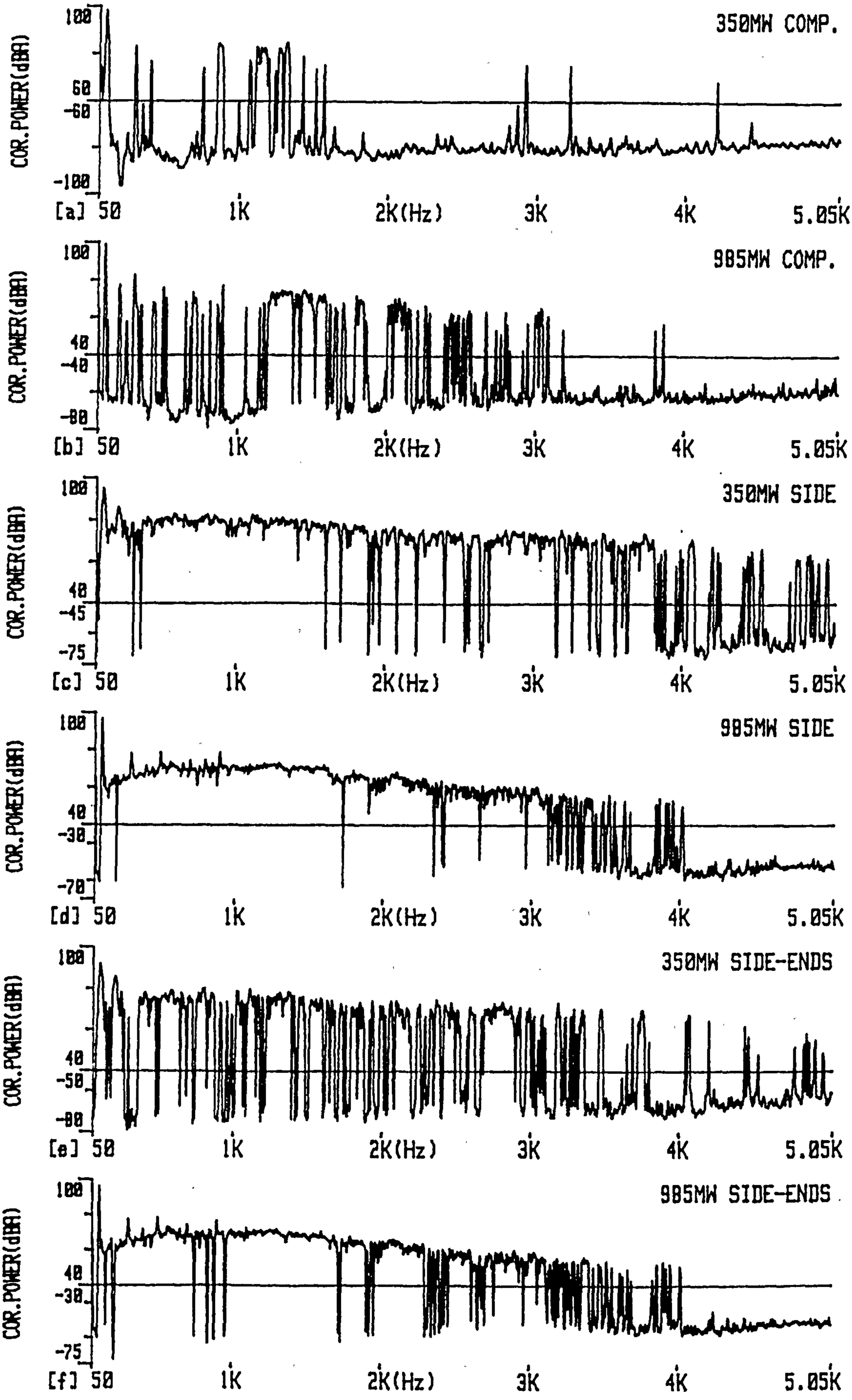

Fig.4.5 Narrowband sound power levels corrected for phase mismatch for 350MW and 985MW generators

sound power due to low levels of power absorption, which is not inconsequential when the true output power is low. For the 350MW generator the phase corrected sound power level of 93.3 dB(A) for side-ends will be liable to a significant underestimation of 1.7 dB for the predicted absorbed power of 90.2 dB(A). For the 985MW generator the mean S.P.L. is 4 dB less, resulting in lower level of absorption of 88.9 dB(A). This would result in the measured sound power level of 96.1 dB(A) being an underestimation of 0.8 dB. The reason for this surprising physical phenomenon is explained in more detail in section 5.2 on generator source mechanisms due to the high transmission loss limiting high frequency intensity output.

If the corrected sound power for the 350MW and 985MW generator side-ends is assumed valid and absorption not considered the levels of 93.3 dB(A) and 96.1 dB(A) scale up to total generator sound powers of 102.3 dB(A) and 105.1 dB(A). These relate to free field sound pressure levels of 81.6 dB(A) and 81.8 dB(A) at 1m respectively assuming uniform radiation.

Even for the corrected data, despite net power emission for most frequency bands, the F_3 indicator remains relatively large. For both units the value of F_3 tends to 19 dB for many bands, Figs. 4.6a and 4.6b, causing the residual pressure intensity index to be exceeded, Figs. 4.6c and 4.6d. The phase error limits predicted from eqn. (A.12) are either large or not quantifiable and subsequently so are the spatial sampling random errors.

For eqn. (3.9) to be applicable the measurement distribution or probability density should be Gaussian. The relative occurrence chart[60] is also a useful indicator of potential measurement problems. The relative occurrence chart is in general non

Gaussian for all the uncorrected data as illustrated in Figs. 4.7a and 4.7b, for the frequency range 50-5050 Hz and 250-2000 Hz respectively for measurements conducted on the 985MW generator side. The phase mismatch corrected data is more Gaussian. The degree of this is dependant upon the frequency range. For some frequency bands, for example 50-5050 Hz given in Fig. 4.7c, the relative occurrence chart only approximates to Gaussian. For 250-2000 Hz, given in Fig. 4.7d, the Gaussian nature is more pronounced. Similar results were found for the 350MW unit.

4.1.1.2 Influence of background noise

The sound power levels from the main background noise sources are given in table C and the spectra are given in Figs. 4.8a-d.

Component	Sound power level (dB(A))
350MW F.E. coupling cover	122.6
985MW F.E. coupling cover	115.8
985MW R.E. coupling	112.4
985MW temporary test brushgear	113.2

TABLE C: Net sound power levels for background noise sources during generator factory testing

These sound power levels are high and larger than that from the generator contributing significantly to the direct and reverberant sound pressure levels. This is illustrated by the sound pressure spectra 1m from the 985MW generator F.E. and R.E. in Figs. 4.9a and 4.9b respectively. The spectra exhibit a large degree of similarity due to the significant reverberation influence and resemble the background noise components plotted in Figs. 4.8b-4.8d. The F.E. spectrum, Fig. 4.9a, bears a closer resemblance to the F.E. coupling power spectrum, Fig. 4.8b, due to the greater influence of direct noise transmission and the R.E. spectrum, Fig. 4.9b, has more prominent R.E. coupling and

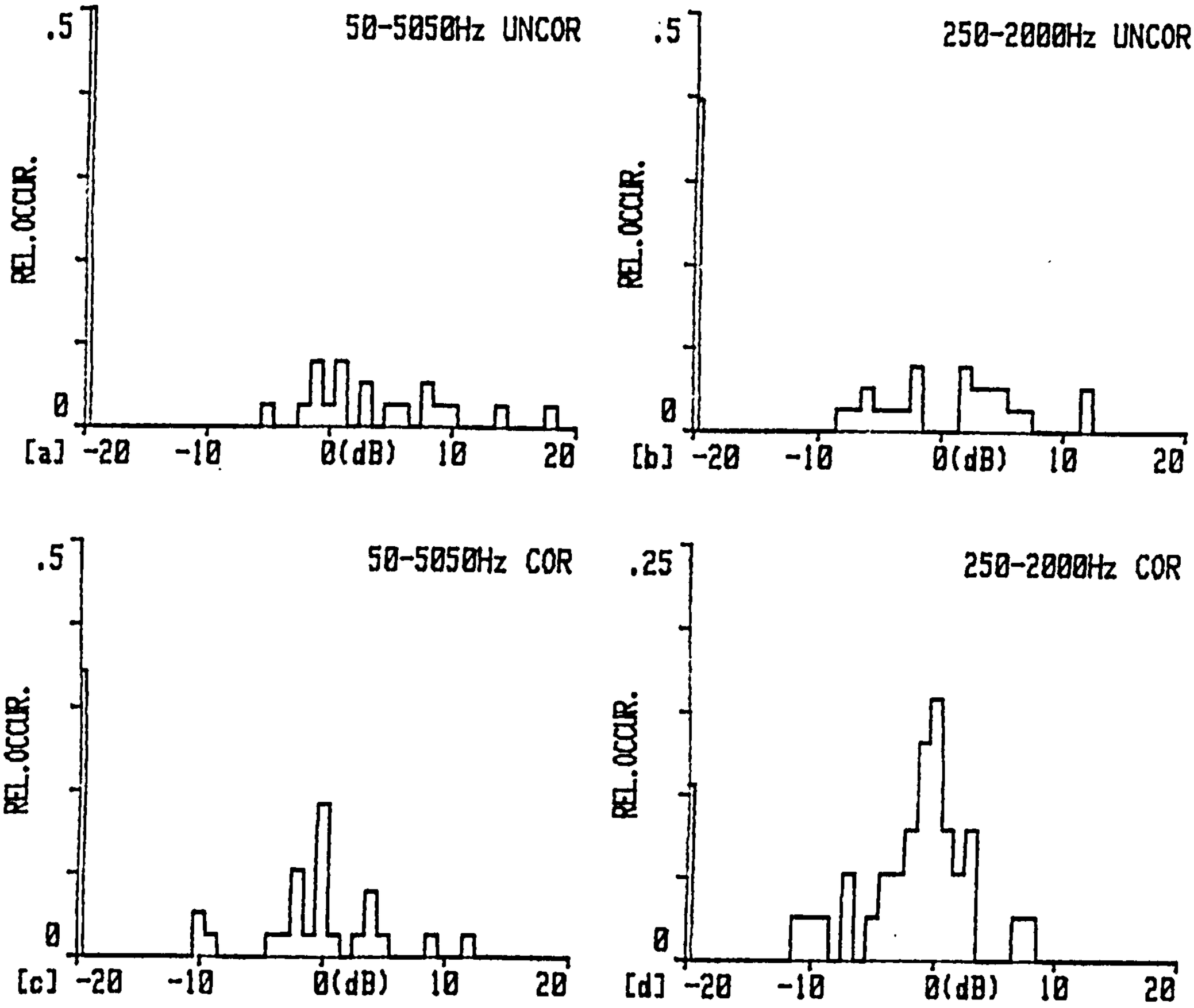

Fig.4.7 Probability density for 985MW side measurement a), b) without phase mismatch correction and c), d) with phase mismatch correction

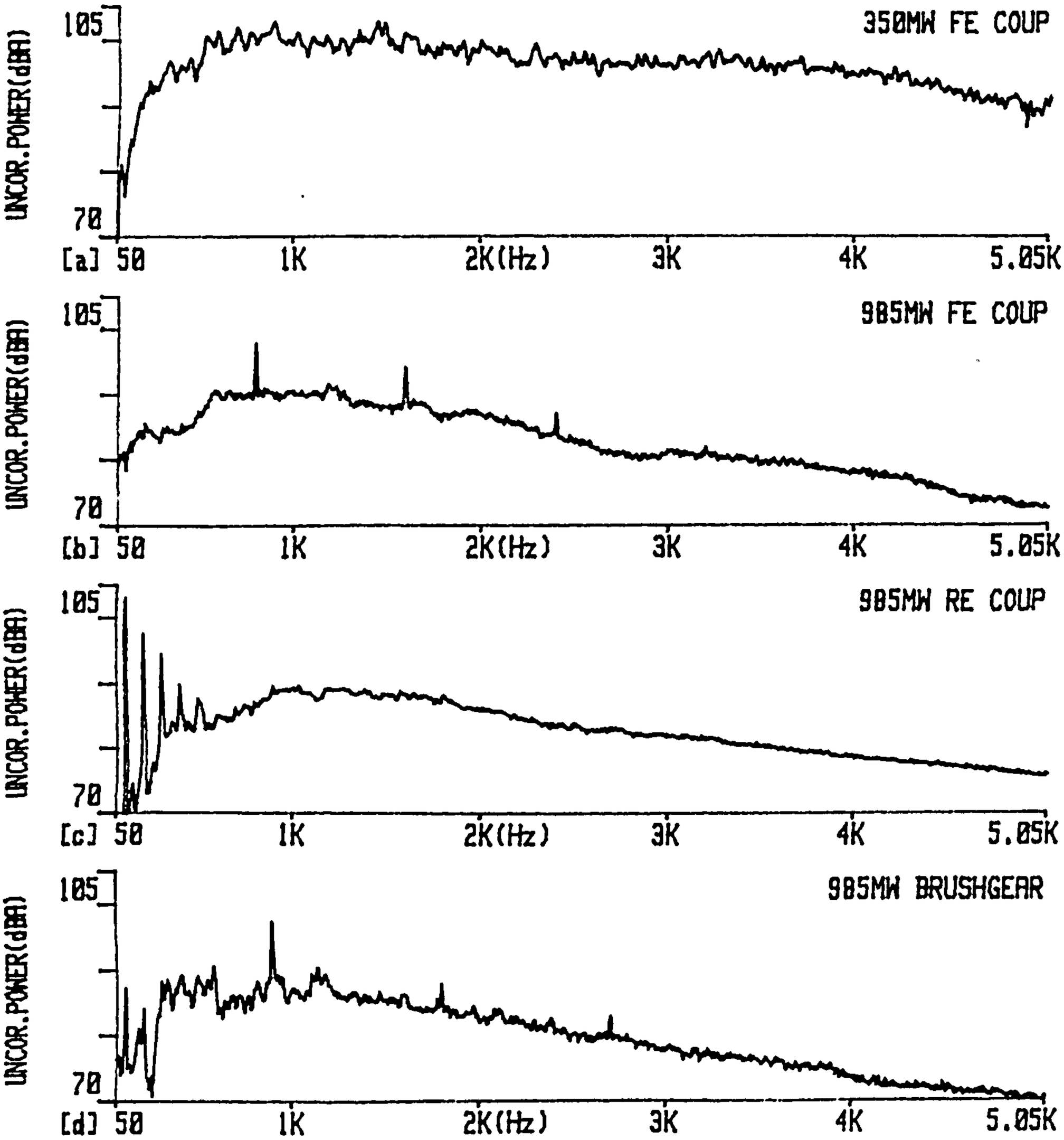

Fig.4.8 Narrowband sound power levels for principal generator test background sources

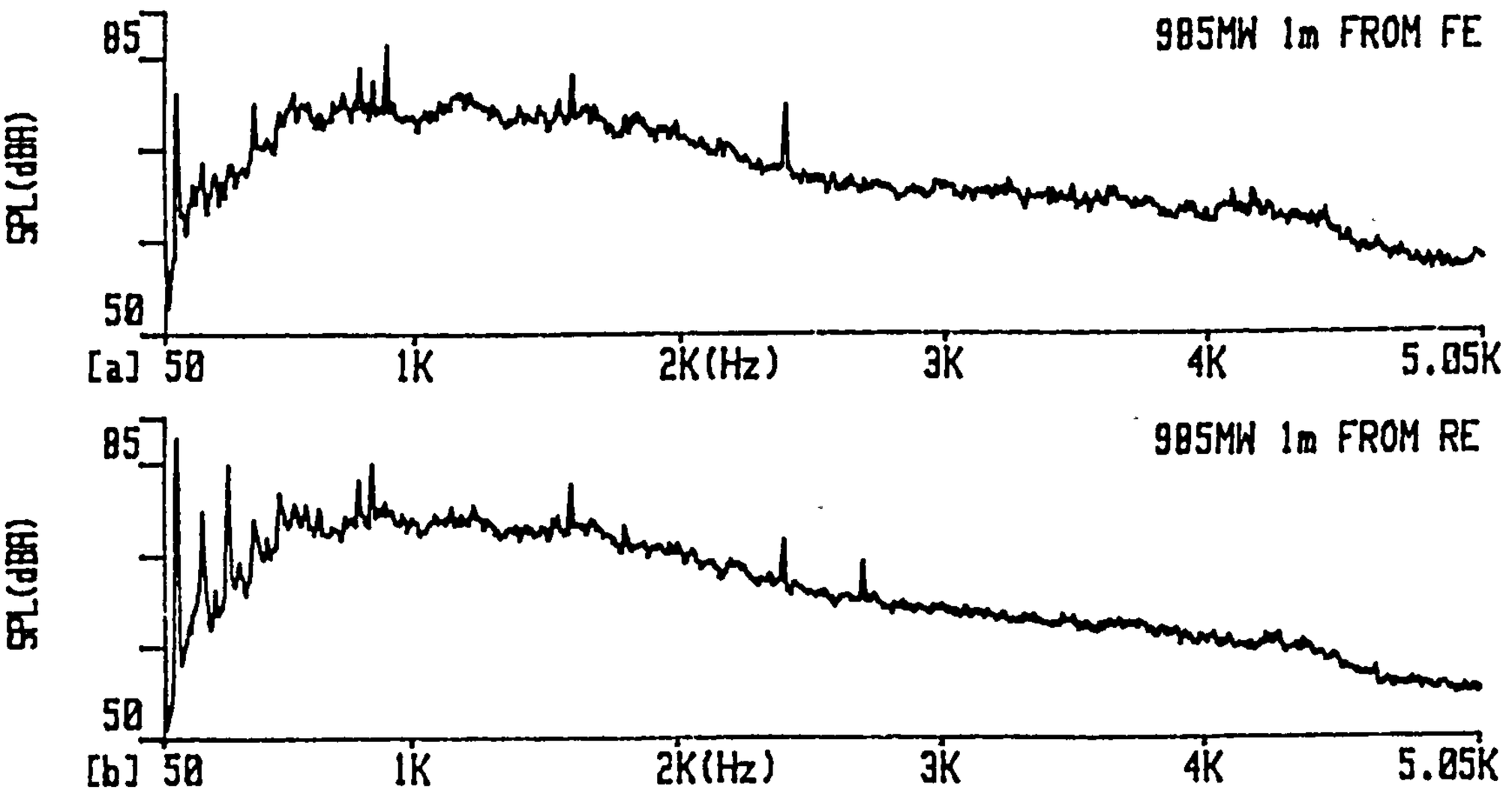

Fig.4.9 Narrowband sound pressure level for 985MW generator

brushgear tones, Figs. 4.8c and 4.8d, for the same reason.

4.1.1.3 Summary of generator factory testing findings

It is evident that the generator emitted low levels of noise relative to the background noise sources. Measured sound power levels are commonly negative and the F_3 indicator exceeds the residual pressure intensity index. Application of phase mismatch correction increases the sound power levels to positive values, but the residual pressure intensity index is still exceeded for many 1/3 octaves. Due to this, measurement accuracy is questionable and it appears that under such circumstances the validity of the correction is uncertain. Application of the correction will itself introduce a bias if the true output intensity is a lot smaller than the corrected intensity component set by the sound pressure and the instrumentation. The influence of low levels of power absorption is not insignificant when the background sound pressure levels are high and the source emission is low, therefore reducing the effective residual index.

It is probable that even the phase mismatch corrected sound power levels are liable to large unquantifiable inaccuracies. It is therefore necessary to either increase the residual pressure intensity index improving measurement capability or reduce the background noise or preferably both. Despite the measurement problems a number of important factors about generator noise emission can be gleaned. The generator emission is relatively low. The emission has a significant component at twice supply frequency due to magnetically induced vibration. The remaining emission is broadband with the most significant emission below 3 kHz. The R.E. and F.E. couplings are significant noise sources, however on site the F.E. coupling is not prevalent as it is enclosed in the very solid low pressure turbine pedestal.

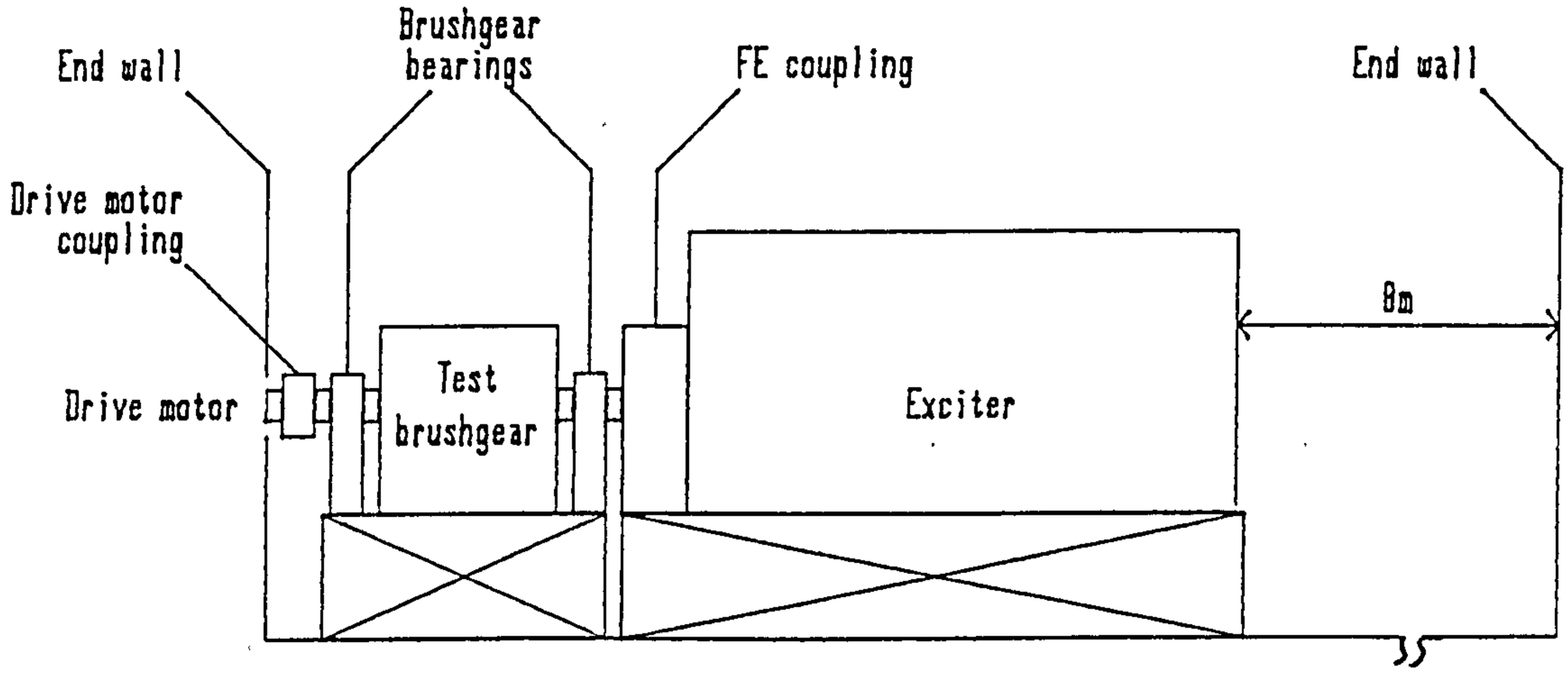

Fig.4.10 Exciter factory test layout

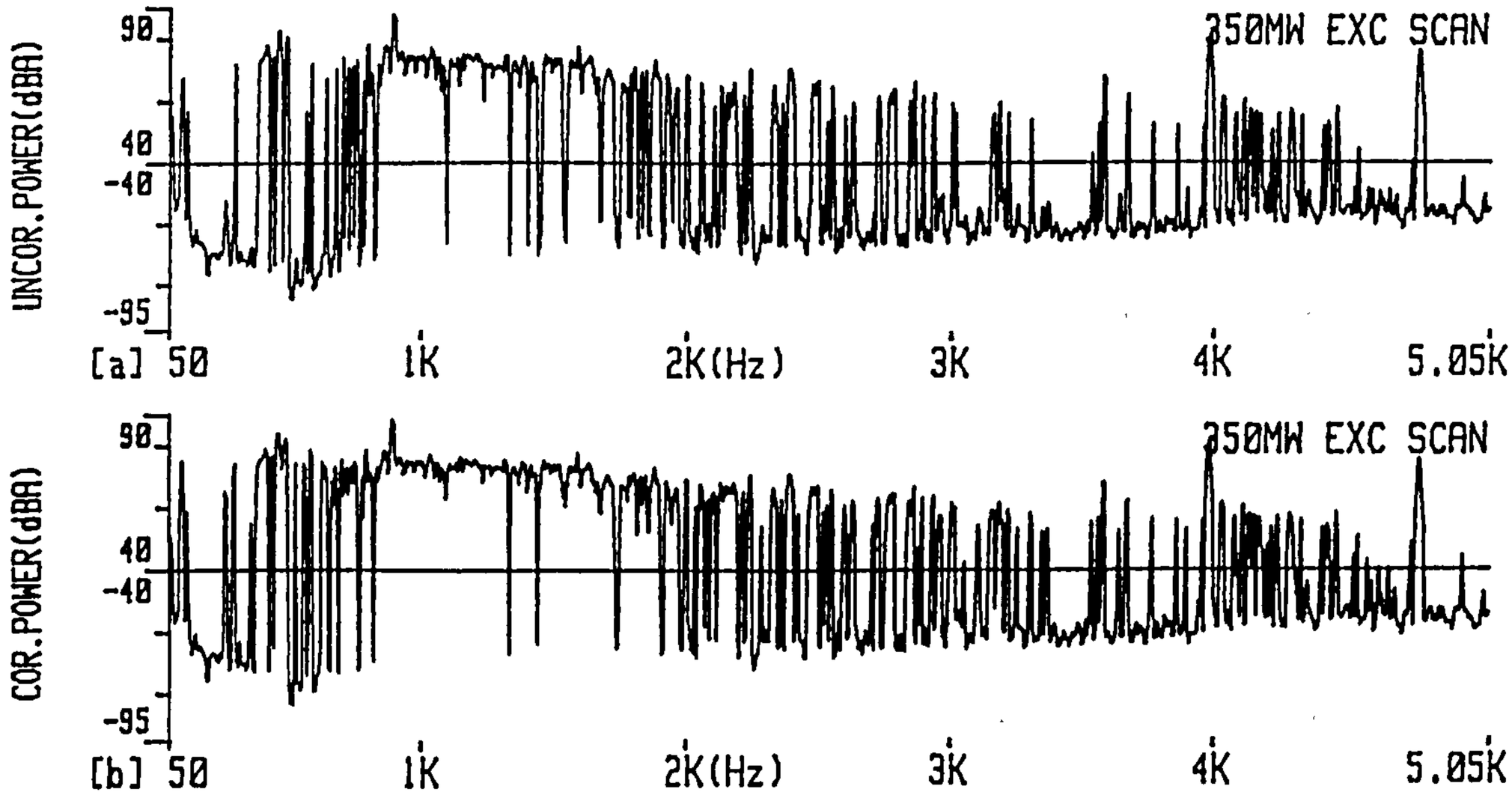

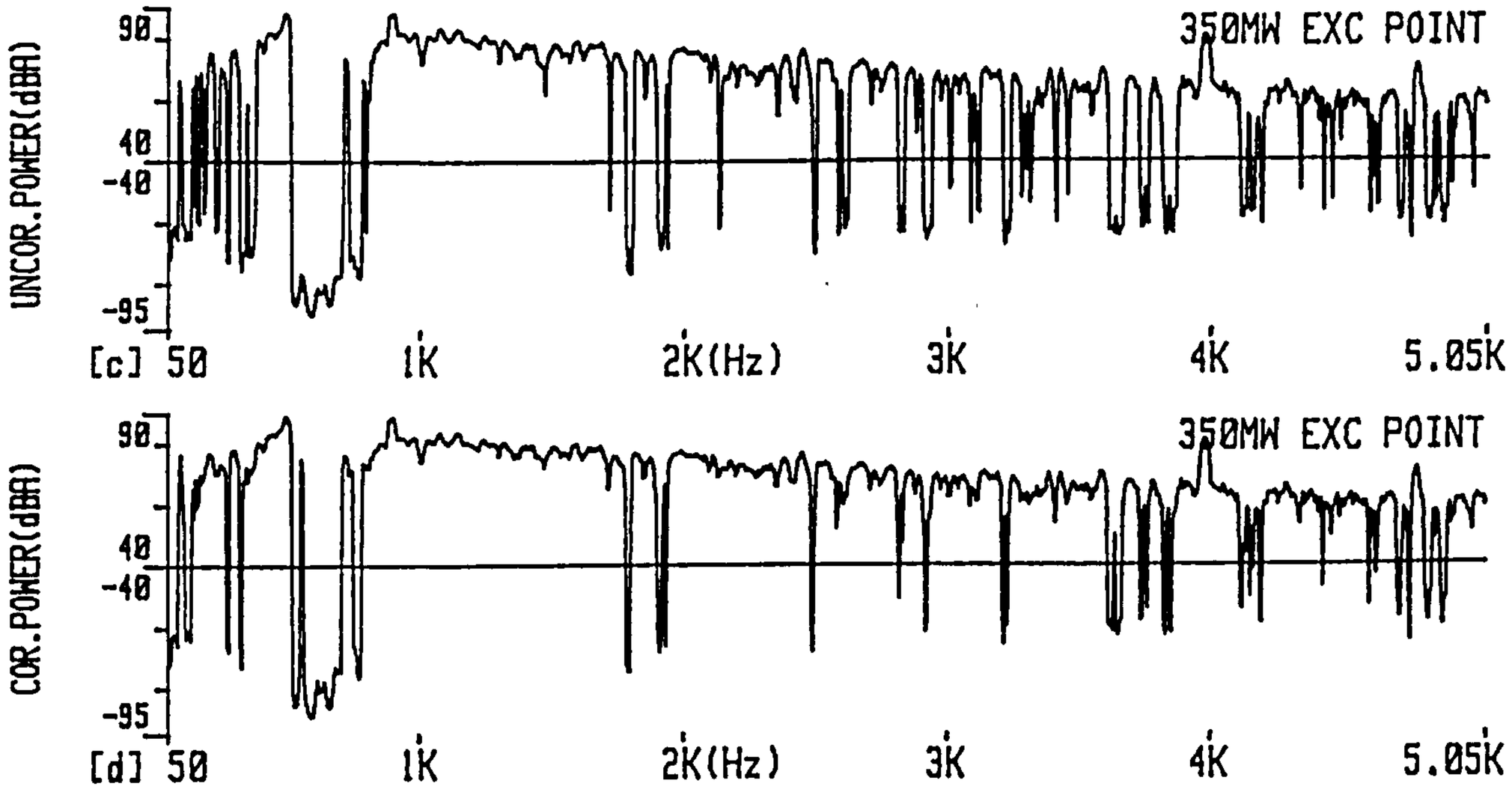

Fig.4.11 Narrowband sound power levels of complete 350MW exciter from a), b) scan measurements and c), d) point measurements

4.1.2 Exciter investigation

4.1.2.1 Sound power determination

The noise emission from one brushless exciter used to provide the field current for a 350MW generator was measured during factory testing. The test arrangement is illustrated in Fig. 4.10. Within the test lineout there are a number of sources of background noise including the brushgear, various couplings and the drive motor, although the latter's influence is minimised by being situated behind a partition wall. The exciter enclosure contains the main exciter, rotating rectifier and pilot exciter. The F.E. exciter coupling is acoustically enclosed, although the actual site sealing baffle was replaced by a wooden one for test purposes.

As the exciter is symmetrical the noise emission was determined from one side and half the F.E. and R.E. faces, which represents approximately 1/3 of the total area. The side was measured with 12 area scans and 3 scans were conducted on the F.E. and R.E. To further investigate noise emission these levels were compared with 18 point measurements on the side and 5 on each face. The sound power was also measured from the F.E. coupling cover and temporary test brushgear. Measurements were conducted with the exciter operating on full load condition.

The strong direct background noise from the temporary test brushgear complicated exciter sound power determination. To assist with measurement interpretation constituent regions as well as the total will be considered. These results are summarised in table D. The influence of phase mismatch bias on measurements is assessed by applying Jacobsen's correction in eqn. (A.7). The phase compensated sound power levels are quoted in brackets.

Region	Net sound power level in dB(A) with phase mismatch corrected levels given in brackets	
	Scan measurements	Point measurements
total exciter measurements	91.1 (95.3)	94.7 (97.3)
side face	99.3 (99.8)	98.5 (99.2)
1/2 front end face	-99.2 (-98.7)	-96.8 (-95.9)
1/2 rear end face	90.7 (91.4)	88.5 (89.3)
side - F.E. side measurements	95.6 (96.3)	95.2 (96.1)
1/2 F.E. exciter coupling	-95.2 (-93.2)	-98.5 (-97.7)
1/2 temporary test brushgear	105.5 (105.7)	-

Table D **Summary of exciter unit sound power measurements for 1/3 of the total exciter area with phase mismatch corrected levels given in brackets**

From the scan measurements the overall exciter sound power level was 91.1 dB(A). The sound power spectrum, Fig. 4.11a, is complex with net output power only between 800 Hz and 1600 Hz and at tones of 4 kHz and 4.8 kHz. The remainder of the spectrum is negative or bidirectional. Application of phase mismatch correction increases the level to 95.3 dB(A), but the spectrum is only a little less negative, Fig. 4.11b.

The sound power level of 94.7 dB(A) determined from point measurements was higher and the spectrum was noticeably more positive, Fig. 4.11c. The negative power measurement occurs only between 525 Hz and 700 Hz due to insufficient suppression of the brushgear noise and some negative components above 2 kHz. The phase mismatch correction raises the power level to 97.3 dB(A). The number of negative peaks above 2 kHz is reduced by half, but in general the spectrum Fig. 4.11d is unaltered. The main measurement difficulty is posed by the strong directional

power output from the test brushgear at the F.E. of the exciter. This is illustrated by relatively large inputs of 99.2 dB(A) from scan measurements and 96.8 dB(A) from point measurements for the F.E. face which virtually negate the side outputs of 99.3 dB(A) and 98.5 dB(A) from both techniques. From the average S.P.L. of 101.7 dB(A) the estimated power absorbed from eqn. (3.11) for an absorption coefficient of 0.03 is 90.4 dB(A) implying the point power level of 94.7 dB(A) is an underestimation of 1.4 dB(A).

The potential measurement difficulties are suggested by the indicators F_3 and F_3-F_2 plotted in Figs. 4.12a and 4.12b respectively for the scan measurements on the exciter. F_3 has a value of 20 dB for many 1/3 octave bands with some bands greater than 20 dB such as the 500 Hz and 625 Hz 1/3 octaves, which is related to the prominent brushgear power, Fig. 4.18. The F_3 indicator exceeds the residual pressure intensity index in 7 bands implying invalid measurements and the phase mismatch error in other bands was commonly ±3 dB, Fig.4.12c. In bands, where the residual index is exceeded by F_3, the random error prediction is invalid, but the value calculated from eqn. (3.9) shows a large basic trend of 5 dB, Fig. 4.12d. The error is larger in those bands, where F_3 is large. For the phase corrected scan data, despite the increase in magnitude of 4.2 dB the power level, the value of F_3 is basically unaltered for the scan data and subsequently likewise for the phase error. The random error is slightly reduced to 4 dB, but the basic trend is high.

For the point measurements conducted on the exciter enclosure the value of F_3 is significantly reduced with all 1/3 octave above 625 Hz less than 10 dB, Fig. 4.13a. The F_3-F_2 indicator, Fig. 4.13b, is subsequently reduced to less than 3 dB above 625

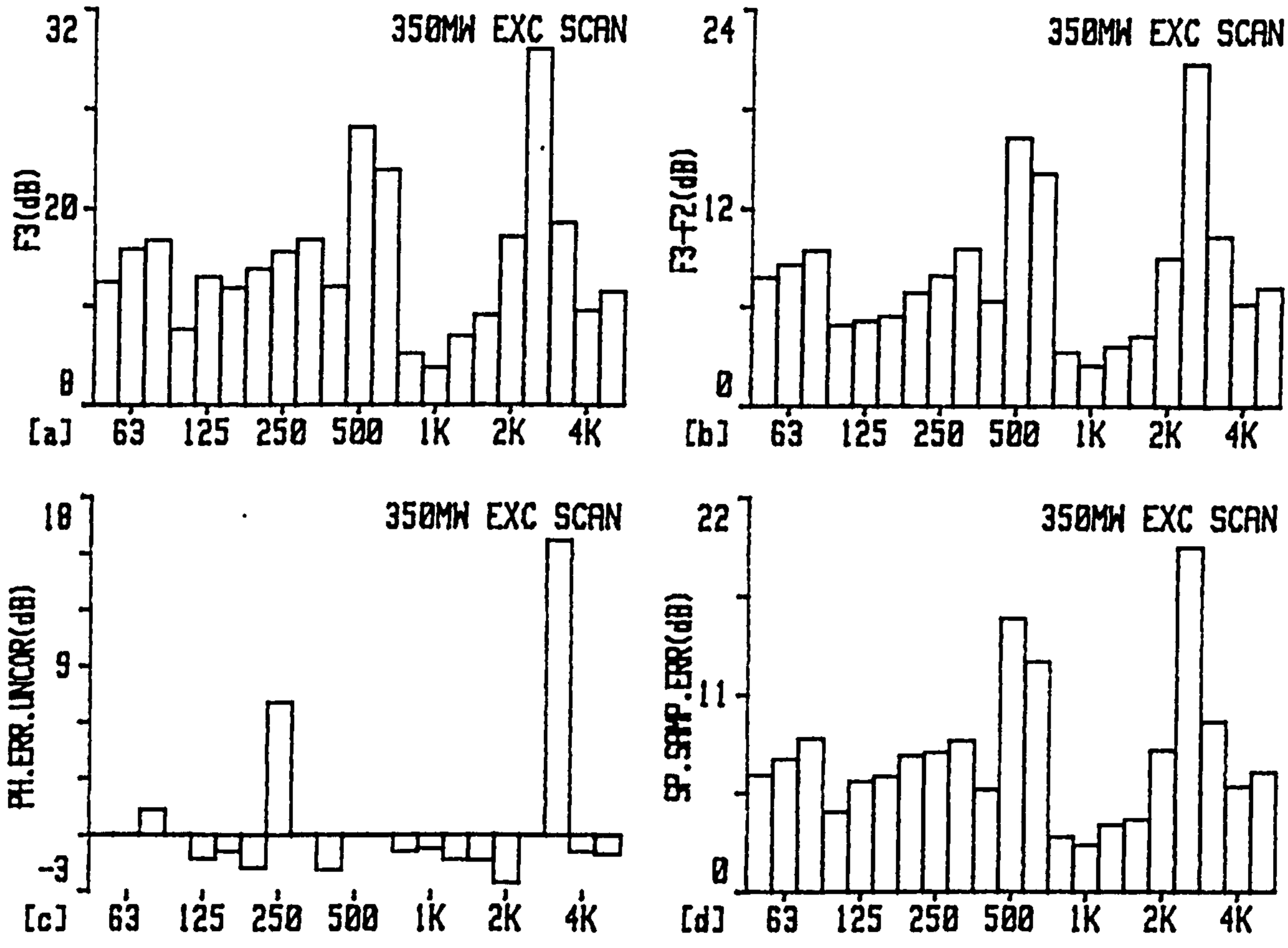

Fig.4.12 Exciter scan measurements a) F_3 b) F_3-F_2 c) Phase mismatch error d) Spatial sampling error

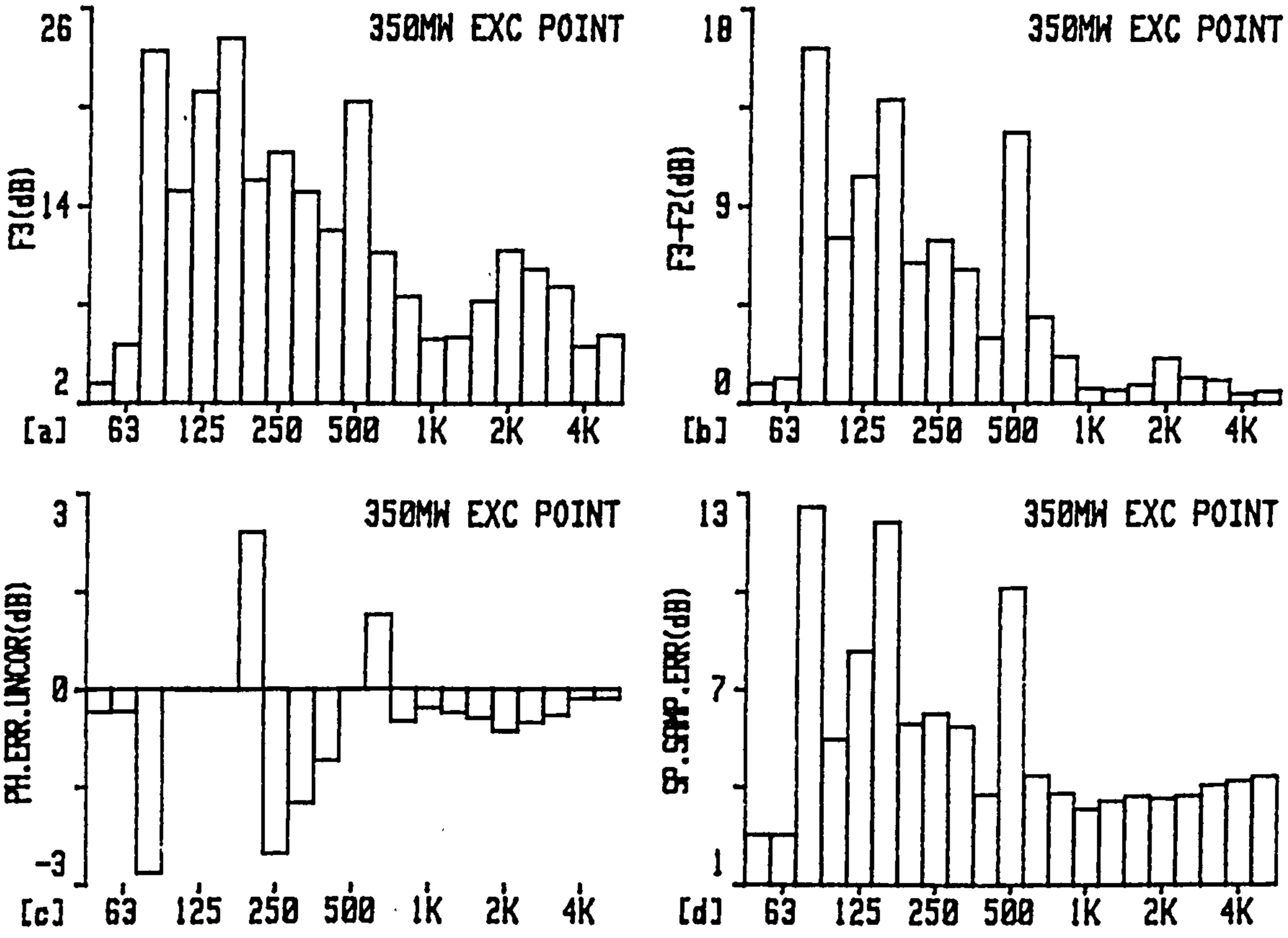

Fig.4.13 Exciter point measurements a) F_3 b) F_3-F_2 c) Phase mismatch error d) Spatial sampling error

Hz, which is within the acceptance criteria given in ISO 9614. F_3 exceeds the residual pressure intensity index in 4 low frequency bands, but the phase mismatch error is commonly less than 1 dB (Fig. 4.13c). The random error calculated from eqn. (3.9) is valid for point measurements. The value is 3.5 dB for bands above 500 Hz, Fig. 4.13d, which as expected suggests more measurements are necessary.

The sound power was measured as a net input for the F.E. exciter coupling of 95.2 dB(A) and 98.5 dB(A) for the scanning and discrete point techniques respectively. Ideally using eqn. (3.8), the application of Gauss's Integral Theorem, should cancel the background noise from the brushgear. However due to the temporary wooden baffle on the F.E. the measurement on this region represented not only a negative power due to fringing, which should be cancelled by measurement on the side, but also absorbed power. The point measurement sound power spectrum, Fig. 4.14, is dominated by the power absorbed by the cover in the range 500-700 Hz from the brushgear. Under these circumstances irrespective of the measurement practice the true output power cannot be obtained unless it is substantially greater than the background noise source. The measurement difficulty is not clearly indicated by F_3, Fig. 4.15, as the majority of measurements are negative.

In summary it is readily apparent that the background noise caused severe problems to exciter sound power emission. The overall exciter sound power level from the scanning technique of 91.1 dB(A) is liable to a significant underestimation. The potential errors are reflected by indicators F_3 and F_3-F_2 and whereas these errors cannot be quantified it is apparent they will be large. The point measurement value of 94.7 dB(A) is a more accurate figure with more favourable indicator values.

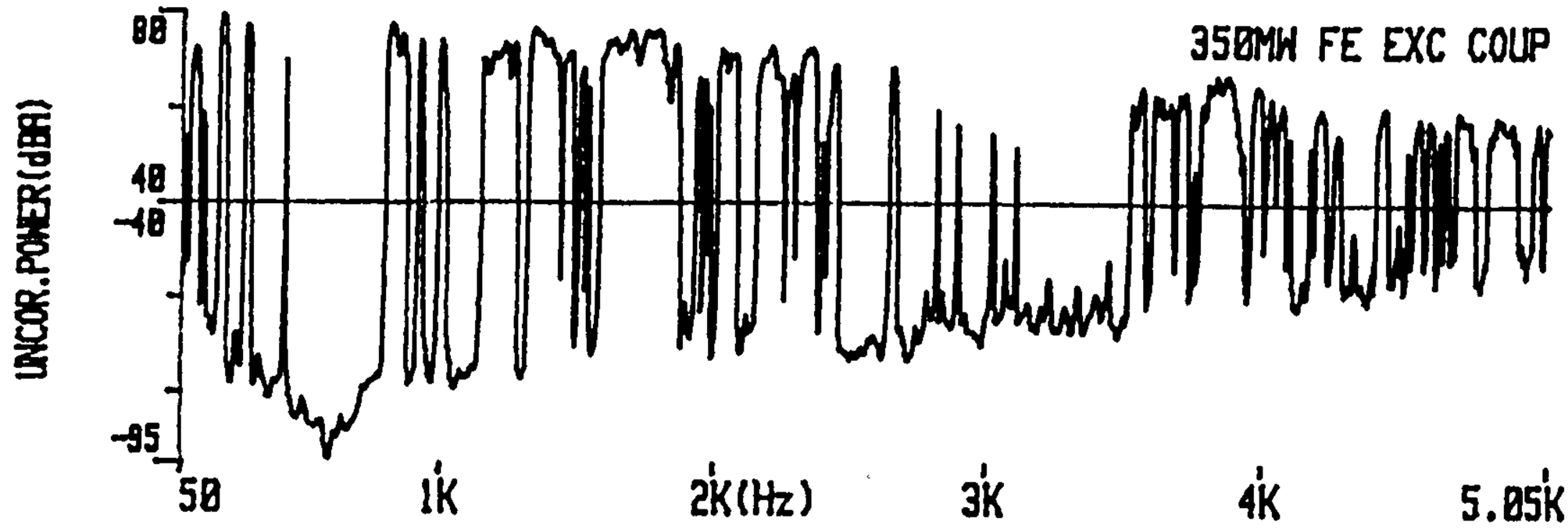

Fig.4.14 Narrowband sound power level for the F.E. exciter coupling cover

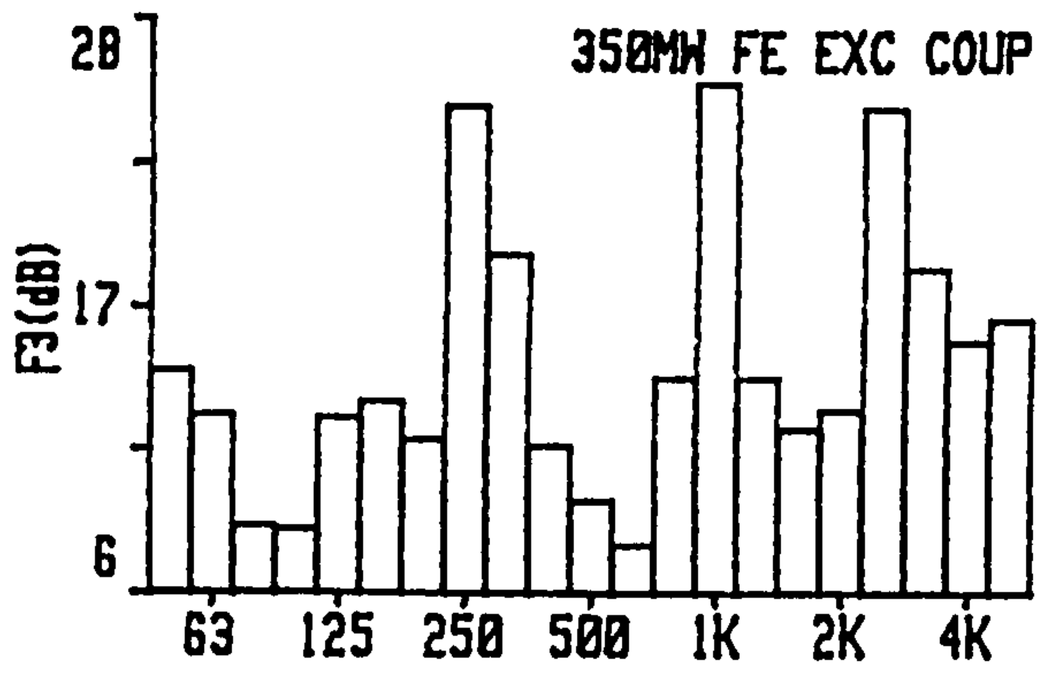

Fig.4.15 F.E. exciter coupling point measurements F_3 indicator

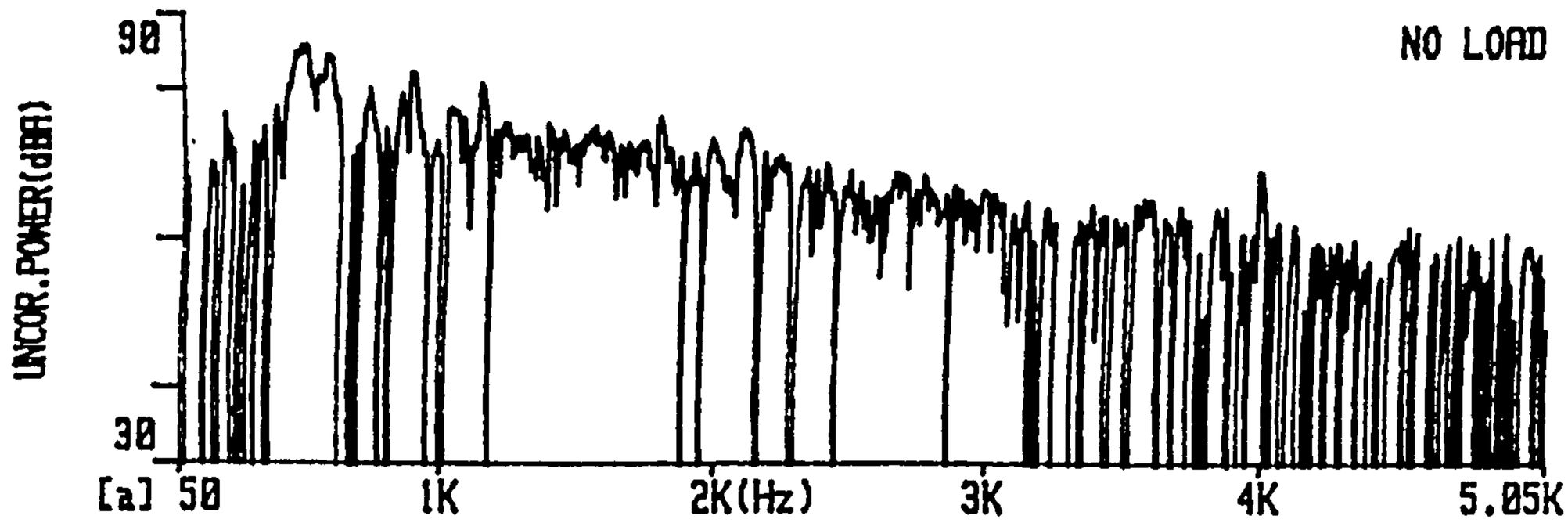

Fig.4.16 Narrowband sound power level for half the exciter side on a) no load b) full load

The phase error is relatively low, ±1 dB, but the spatial sampling error is 3.5 dB implying that for a source of this size more points are necessary under these conditions. It is believed that the point measurements give better results as for the F.E. face measurement they provided better local suppression of the normally incident background noise, as well as incorporating less of the fringing noise. The overall level of 94.7 dB(A) would relate to a total exciter value of 99.5 dB(A) after scaling for the area ratios. This relates to free field pressure at 1m of 80.2 dB(A). This level is liable to an underestimate of approximately 1.4 dB due to power absorption.

4.1.2.2 **Point sound intensity vector measurements**

A comparison of full load and no load sound pressure levels at 1m from the exciter indicates no significant differences, in part due to the dominance of background noise. The partial sound power was measured using 8 equi-spaced point measurements on the exciter enclosure on no load and full load. The no load sound power from 1/2 the exciter enclosure side was 95.1 dB(A) with a spectrum as plotted in Fig. 4.16a. The full load power level is slightly higher being 95.9 dB(A), although the spectrum is basically similar, Fig. 4.16b. The only difference is that the 900 Hz tone is 86.2 dB(A) on full load, which is 4.1 dB greater than the no load case, and the 3600 Hz tone is 68.2 dB(A), which is 3 dB greater than the no load condition. These differences have only a minor influence on overall levels implying electrical loading is not very significant for this type of exciter.

Due to the strong background noise it is difficult to identify the major source components inside the enclosure from the intensity measurements. A measurement

5cm from the air make-up filter does however provide some more insight into source mechanisms. As there was very limited airflow through the vent the major portion of the noise measured was not created by this airflow. Instead the acoustic intensity was due to noise being generated inside the enclosure and is therefore a clearer indication of the main noise generation mechanisms than measurements at other points beside the exciter. The spectrum, Fig. 4.17, has pronounced peaks at 800 Hz, 1.6 kHz, 4 kHz and 4.8 kHz, but the overall level of 104.6 dB(A) is principally due to broadband noise in the range 400 Hz to 1.8 kHz. The source mechanisms will be discussed in more detail in section 5.2, but are mainly aerodynamic in origin.

4.1.2.3 **Influence of background noise**

The influence of the main background noise source, the temporary test brushgear, has been illustrated in detail in the preceding sections. It made accurate sound power determination from the exciter difficult due to large negative measurements on the F.E. face imposing stringent demands upon global and local suppression. The brushgear, half of which emitted 105.5 dB(A), had a characteristic spectrum illustrated in Fig. 4.18. The spectrum had a large band of power from 500 Hz to 700 Hz and a fan blade passing frequency tone of 900 Hz. As is evident from table D the brushgear contributes more substantially to the S.P.L. beside the exciter than the exciter itself. The sound pressure spectrum 1m from the exciter centre, Fig. 4.19a, has a strong spectral similarity to the test brushgear sound power spectrum, Fig. 4.18. The spectral similarity is also evident in the radial and axial intensity components at this position, Figs. 4.19b and 4.19c. The overall S.P.L. of 99.0 dB(A) has a large direct contribution from the axial sound intensity of 96.3 dB(A) and the radial intensity of 92.7 dB(A) emanating from the brushgear region.

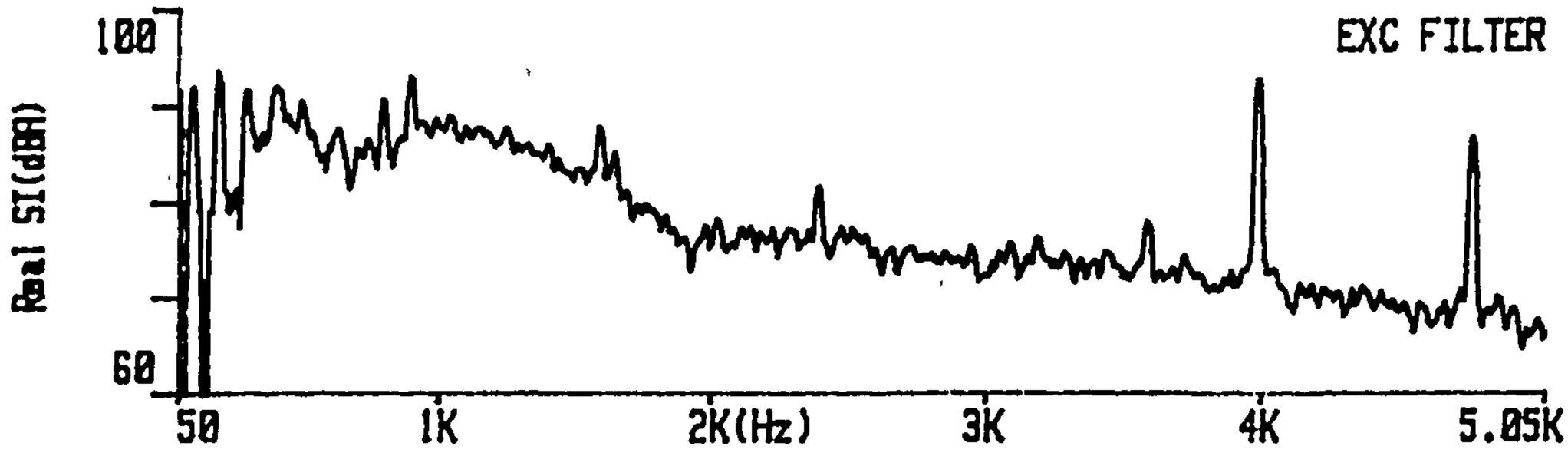

Fig.4.17 Narrowband sound intensity 5cm from 350MW exciter air make-up filter

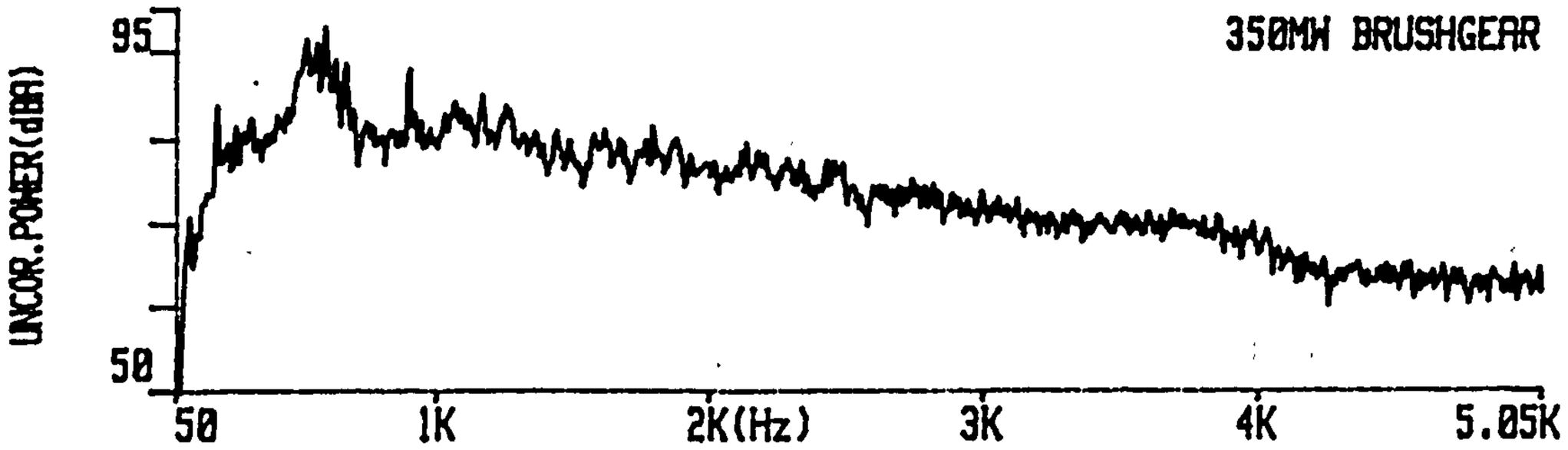

Fig.4.18 Narrowband sound power levels for half temporary test brushgear

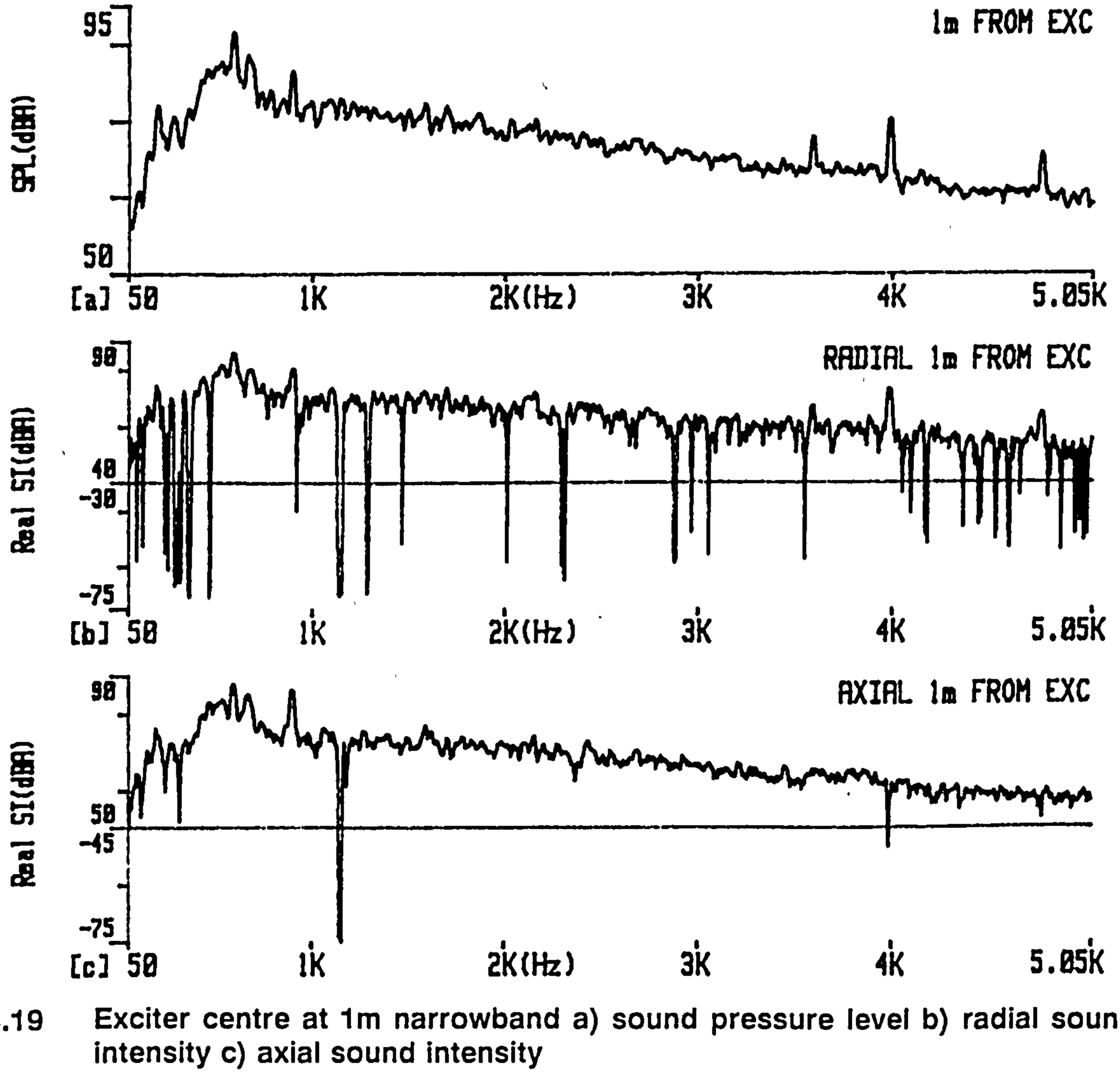

Fig.4.19 Exciter centre at 1m narrowband a) sound pressure level b) radial sound intensity c) axial sound intensity

4.2 SITE INVESTIGATION

The site measurement survey was conducted in a power station containing two 660MW steam turbine generator units. The detailed study concentrated upon the hydrogen cooled generator unit and it's excitation system consisting of the main exciter, the rotating rectifier, the pilot exciter and associated couplings with a layout as given in Fig. 4.20. The station contains a multitude of co-functioning equipment, illustrated in Fig. 4.21, with 4 turbines driving each generator and many auxiliary pumps, valves, steam lines and condensers. The turbine hall has dimensions 58m x 144m x 31m and the turbine generator units were the only plant on the top level of 3 floors. The turbine hall reverberation time was approximately 3s from 125 Hz to 4 kHz. This was measured prior to the commissioning of the station with the majority of the plant installed. Both units had a stable loading condition of 660MW.

The full variety of different measurement techniques outlined in chapter 3 were utilised to investigate the difficult reverberant, multi source acoustical environment found in power stations. The aim of this analysis is to provide a unified explanation of the noise problem by fulfilling the following objectives :

1. To quantity site sound pressure levels.
2. To determine the sound power from the constituent items comprising the generator unit enabling ranking of noise sources.
3. To predict the S.P.L. due to the generator unit components alone.
4. To fully explain the S.P.L. beside the generator unit.
5. To investigate the nature of the sound fields.

A full commentary on a variety of sound field indicators, observations on the

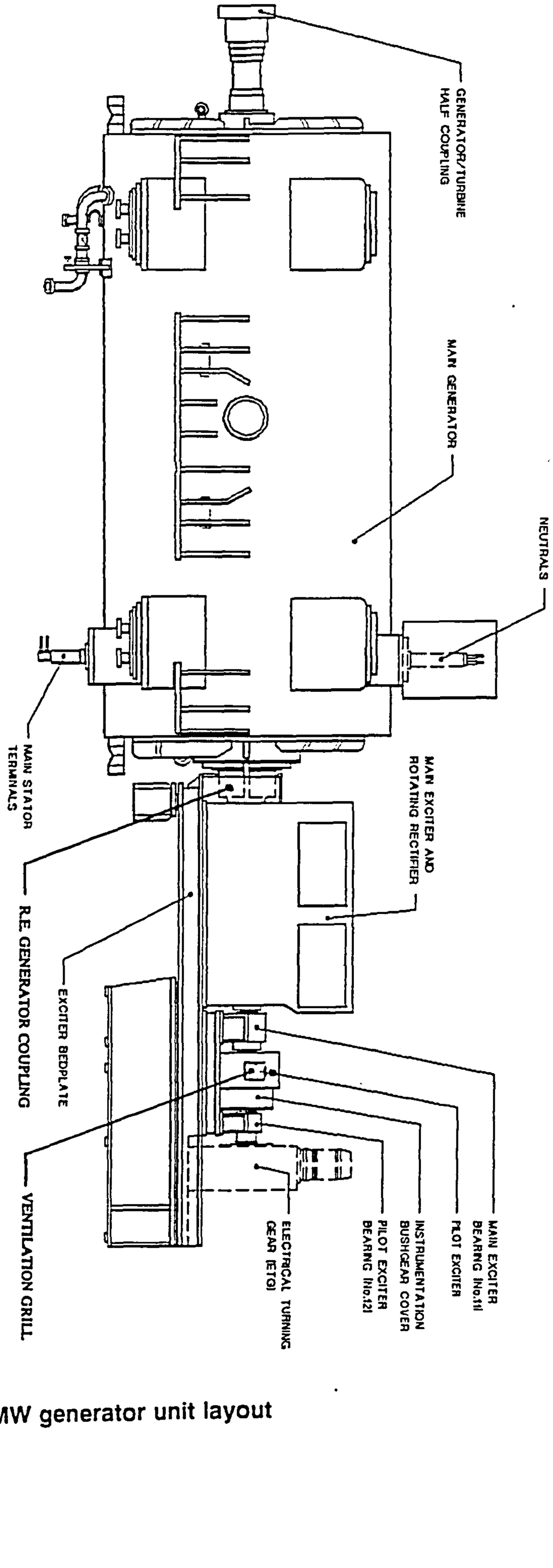

Fig.4.20 660MW generator unit layout

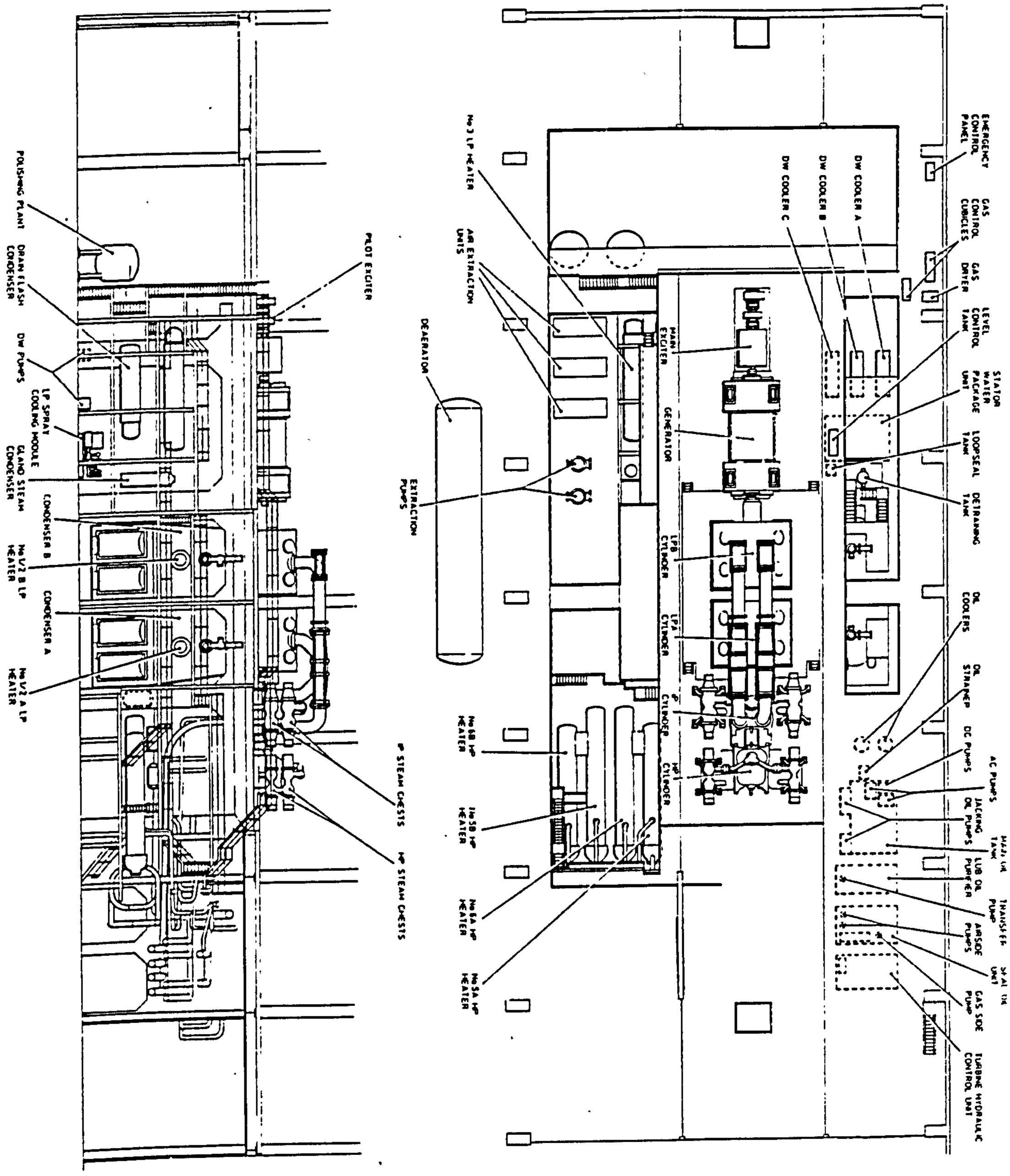

Fig.4.21 Typical power plant in turbine hall

measurement techniques and deductions about the main noise generation mechanisms of each component are presented in the following chapter.

4.2.1 Sound pressure level

The overall A-weighted sound pressure levels and their measurement locations 1m from the generator unit are illustrated in Fig. 4.22. For comparison purposes to assess the influence of background reverberant noise the S.P.L. measured on unit 1 without unit 2 in operation is quoted in brackets. Both units are identical on parallel axes 80m apart.

The sound pressure level was on average 92.5 dB(A) beside the generator except towards the rear end, where the level increased to 96.5 dB(A). 1m from the exciter, levels approached 97 dB(A) at the front end, decreased to 94.9 dB(A) in the centre and increased to 97.4 dB(A) at the rear end. 1m from the pilot exciter S.P.L. was 102 dB(A).

Typical sound pressure levels 1m from other plant items include 93-96 dB(A) beside the low pressure turbines, 92-93 dB(A) beside the high and intermediate pressure turbines and localised levels of 100 dB(A) beside connecting pedestals. General basement auxiliary plant levels were 91 dB(A) with exceptions including 98-101 dB(A) beside the main boiler feed pump turbine and 102 dB(A) beside a lubricating oil pump.

The general reverberant level was assessed by measuring the S.P.L. beside unit 2 generator with only unit 1 in operation. As the generator shielded this point from

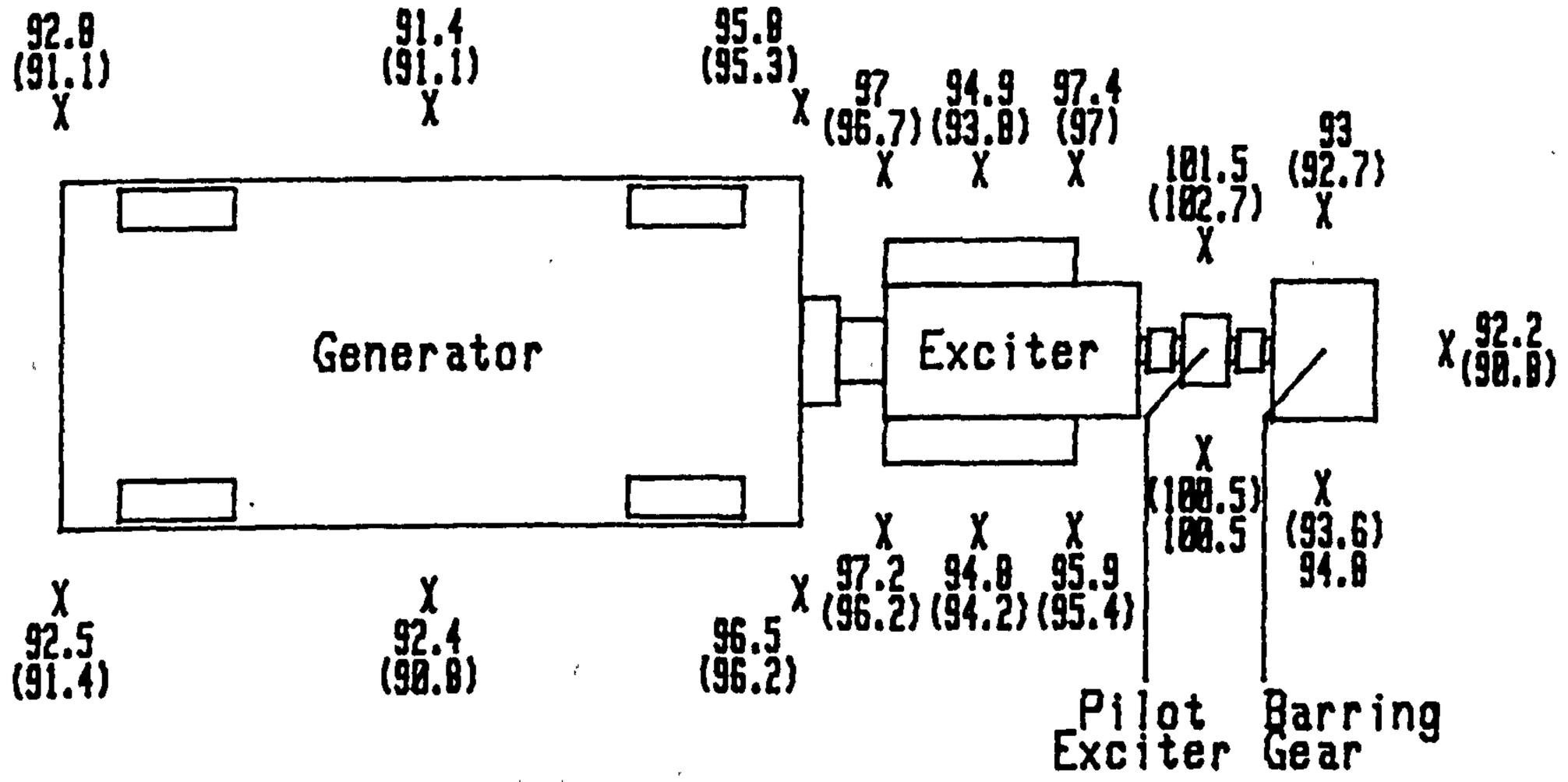

Fig.4.22 660MW sound pressure level at 1m from the generator unit (dBA)

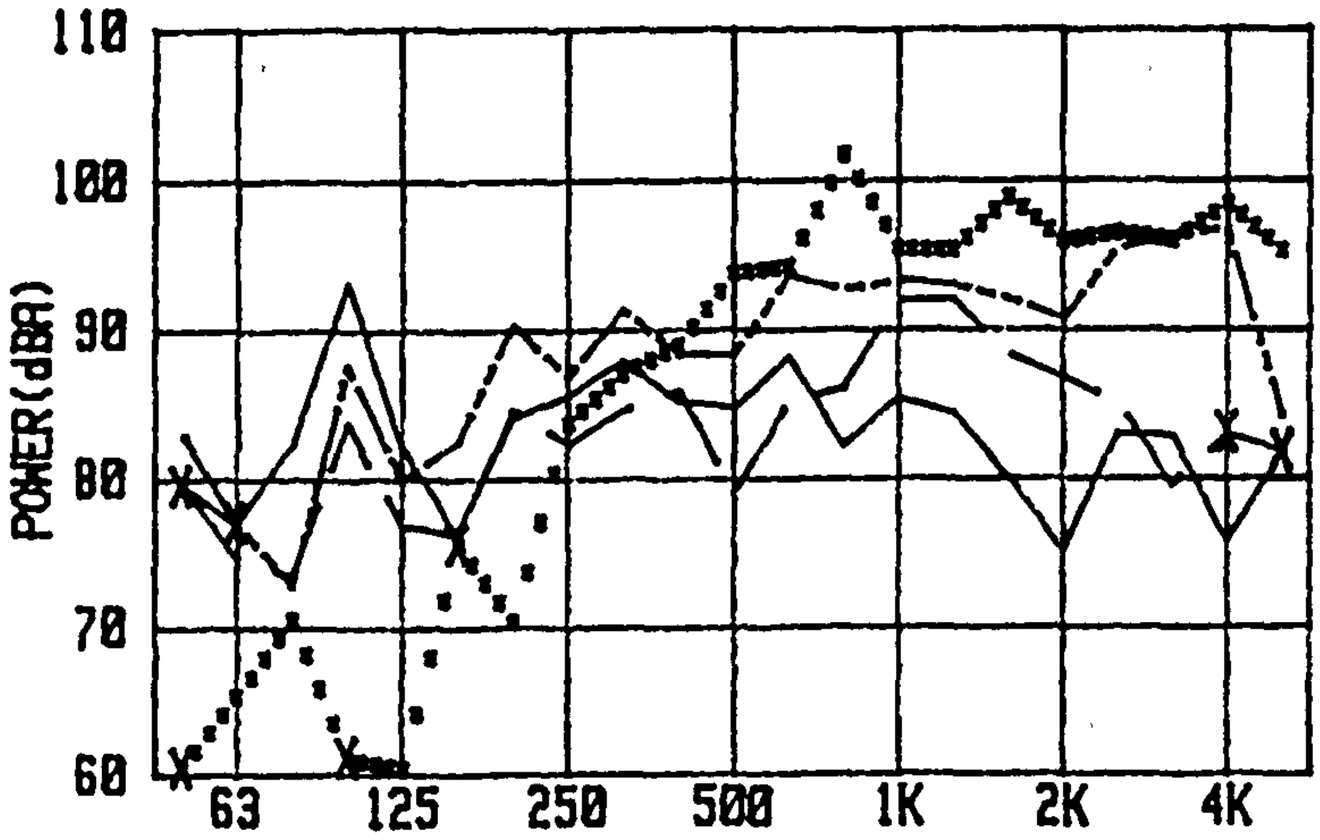

Fig.4.24 A-weighted 1/3 octave sound power for generator unit components

– – – – R.E. Coupling Cover

——— Generator

· · · · · · · Pilot Exciter

– – – Exciter

× Negative Sound Power Level

direct noise flow the measured level of 87.5 dB(A) represents the general reverberant level of one unit. The general reverberant level for the station due to two units is hence doubled to 90.5 dB(A). This reverberant level contribution is reflected in the difference between S.P.L. measured beside unit 1 with and without unit 2 in operation. For example at the generator F.E. the S.P.L. was increased 1.7 dB(A) by 87.9 dB(A) to 92.8 dB(A). The S.P.L. increase from 93.8 dB(A) to 94.9 dB(A) at the exciter centre relates to an extra 88.4 dB(A). Both these increases due to unit 2 approximise to the 87.5 dB(A) reverberant S.P.L. due to one unit.

4.2.2 Sound power determination

4.2.2.1 Sound power from each constituent component

As the generator is symmetrical it's sound power emission was determined by scanning one third of the generator from floor level to top dead centre and appropriate scaling of area ratios to obtain a total figure. The exciter, R.E. generator coupling and pilot exciter were each completely scanned, when measuring their sound power. Measurement repeatability was investigated.

The sound power emission for the generator unit constituent components are given in table E. The quoted error limits are based upon instrument errors and statistical considerations as discussed in the following section. The A-weighted narrowband sound power levels are plotted in Figs. 4.23a-d and the A-weighted 1/3 octave sound power level are given in Fig. 4.24.

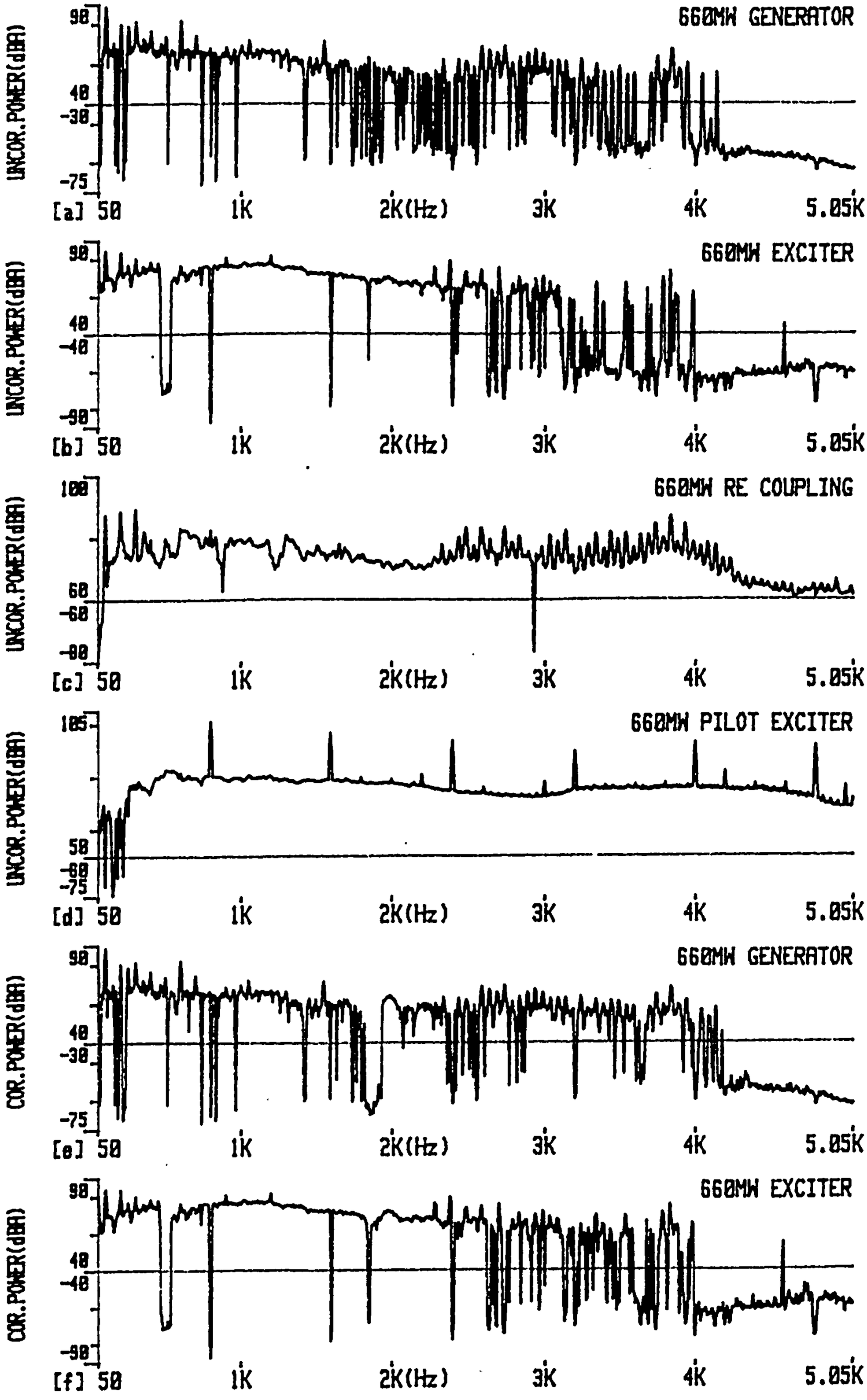

Fig.4.23 Narrowband sound power levels for 660MW unit a) generator b) exciter c) R.E. generator coupling d) pilot exciter uncorrected for phase mismatch & e) generator f) exciter corrected for phase mismatch

Component	Net Sound Power Level in dBA
Generator	97.3 ± 2
R.E. generator coupling	103.5 ± 1.25
Exciter	96.8 ± 3
Pilot Exciter	106.7 ± 1.5

TABLE E : Net sound power levels for generator unit constituent components

The sound power of one third of the generator wrapper from floor level to top dead centre was 92.5 dB(A), which scales up to 97.3 dB(A) for the total wrapper. The sound power is mainly related to low radial intensities of typically 75-76 dB(A), which are reasonably uniformly distributed over the side of the machine.

The determination of sound power emission from the R.E. generator face was complicated by the high sound pressure levels of 104 dB(A) generated by the R.E. coupling. A negative sound power of 94.2 dB(A) was measured. As the sound pressure was 28 dB greater than the average generator wrapper sound intensity, contravening the residual index, it is probable that the sound power determination on the bracket will be invalid due to the instrument capability being exceeded irrespective of the measurement grid definition.

The F.E. generator face had an overall sound power output of 80.8 dB(A), which was mainly due to 84.6 dB(A) at 100 Hz. If that tone is excluded the net input sound power is 82.2 dB(A). The sound pressure in this region was typically 95 dB(A) and the average intensity was 76 dB(A). The sound power is negative for most

frequencies. As the residual intensity varies in sign for different frequencies it is unlikely that the phase mismatch causes the measured input of power. The generator surface will absorb and scatter small amounts of energy as outlined in section 3.4.4. From eqn. (3.11) with a sound pressure of 95 dB(A) and an absorption coefficient of 0.03 the absorbed power is 80 dB(A) from the diffuse field. The direct intensity component of 83 dB(A) from the turbines would result in an absorption of 74.2 dB(A) yielding a total sound power absorption of 81.2 dB(A). It is therefore feasible that this energy is being absorbed. This correlates with Bühlmann's[61] claim that for direct flow the practical limit on reactivity is closer to 15 dB than the residual index of 22 dB due to this absorption effect.

Due to the large absorption of energy at the R.E. generator face the generator wrapper sound power was chosen to be representative of the generator and the appropriate figure to relate to free field generator sound pressure. Care was taken to minimise the overestimation effect by measuring close to the side of the generator to shield the R.E. coupling energy.

The generator wrapper side narrowband sound power, as illustrated in Fig. 4.23a is mainly broadband noise output with predominant peaks at 100 Hz and harmonics thereof. Above 4 kHz the spectrum denotes low levels of power absorption. The range between 2 kHz and 4 kHz contains some negative power tones. To investigate this phenomenon the sound power was adjusted using Jacobsen[33] phase mismatch correction as outlined in Appendix A. The overall sound power level differed by less than 0.1 dB. However, the narrowband adjusted spectrum in Fig. 4.23e differed from the unadjusted power in Fig. 4.23a within the 2 kHz to 4 kHz region, due to the number of the

negative tones being reduced by a factor of 4. The majority of the spectrum at other frequencies was unaltered. This implies that many of the negative power tones were due to the phase mismatch error being significant, because of the low intensity emission. Above 4 kHz the sound power was largely unaltered implying the presence of low levels of power absorption as suggested by Reiniche.[12] By contrast the sound power measured from the rear and front end brackets was unaltered by the phase error compensation for both level and spectral composition.

The measured exciter sound power of 96.8 dB(A) was complicated by stronger directional noise from the pilot exciter and the rear end generator coupling. The accuracy of this sound power determination is dependant upon the effectiveness of the global suppression, based upon Gauss's Integral Theorem, of the strong background noise effects. The value of cancelling energy fringing can be illustrated by considering the rear end measurements. The rear end face of the exciter was measured as an input of 93.3 dB(A) due to energy from the pilot exciter. However, when measurement areas on the side and roof adjacent to the rear end face are included, the net sound power became an output of 93.2 dB(A). The sound power from the exciter sides was 94.1 dB(A) and 94.6 dB(A). These levels should not be considered in isolation because of fringing effects, but the spectra are not dominated by the pilot exciter tones at 800 Hz and harmonics thereof, Fig. 4.23d, nor the rear end coupling cover tones in the 2.5 kHz to 4 kHz range, Fig. 4.23c. This implies that even without the benefit of complete measurement enclosure background noise is still suppressed to a reasonable extent. A similar situation exists for the roof.

The sound power spectrum as illustrated in Fig. 4.23b contains negative power above

3 kHz due to low level absorption and insufficient suppression of background noise. The phase mismatch error is less significant for the exciter than the generator. This is reflected in the smaller difference between the sound power spectrum compensated for phase mismatch, in Fig. 4.23f, and the uncompensated sound power spectrum in Fig. 4.23b. Apart from more positive sound power tones in the range 3.5 kHz to 4 kHz the spectrum is unaltered.

The R.E. coupling sound power was determined using the scanning and discrete point sound intensity measurement techniques for comparison purposes. The cover was 86cm in diameter and 62cm long. One end is flush with the generator bearing bracket and the other end has a 2.5cm clearance to the exciter cover. The slit emits sound intensity an order of magnitude greater than that from the cover. A small area of high intensity can pose measurement problems. For accurate sound power determination using the scanning technique it is important that the probe spends a proportion of averaging time on the "hot spot", which is directly proportional to the area fraction of the high region to the total area. The total sound power was determined using 4 scans on the cover. For comparison the coupling power was also measured by determining the cover power emission by 8 point measurements at 45° increments on the cover centre and the gap power by 4 point measurements at 90° increments. The total power was the sum of both these powers.

The average sound intensity from the point measurements was 101 dB(A) on the cover and 109.5 dB(A) on the slit. This relates to sound powers of 102 dB(A) from the cover and 98.2 dB(A) from the slit yielding a total power of 103.5 dB(A). The average scan sound intensity of 103.5 dB(A) relates to a sound power of 105.8 dB(A).

It is believed that the semi circles joining the line scans spent too great a proportion of scanning time over the slit causing an overestimate in average intensity. The 103.5 dB(A) sound power is therefore the more correct level.

The sound power emission was determined for the pilot exciter and other equipment outboard of the main exciter rear end using scanning and discrete point sound intensity measurements. Point measurements were used for small areas of potentially high emission such as the grill on the instrument slipring cover and also for comparison purposes on the most important regions of acoustic output, the pilot exciter ventilation grills.

The total pilot exciter sound power including the F.E. grill sound power was measured as 106.7 dB(A). The ventilation grills on both sides, Fig.4.20, and the F.E. contribute 105.6 dB(A) sound power to this total figure. The sound power from the enclosure itself was 100.5 dB(A), but this level is increased by fringing of sound from the grills. The measurements on the grills compared to a series of discrete point sound intensity measurements to within 0.5 dB. The narrowband sound power spectrum is given in Fig. 4.23d.

The barring gear was disengaged and hence should be silent. The measured input of 88.6 dB(A) sound power represents an average residual error intensity of 80 dB(A) in regions of 95 dB(A) S.P.L. This represents reasonably good global suppression of background noise considering that the barring gear is subjected to strong direct intensity as well as a strong diffuse field. This level of suppression is similar to that suggested for the generator F.E. bracket.

4.2.2.2 **Measurement error assessment**

Error assessment associated with sound power determination using sound intensity measurement can be complex, which is the drawback to counterbalance the substantial benefits afforded by the technique over traditional sound pressure techniques.

i) **Generator error assessment**

For the generator sound power determination the finite difference error is not significant. The majority of acoustic emission, Fig. 4.23a, is below 1 kHz implying small errors of less than 0.03 dB.

The main measurement problems for the low levels of generator sound power determination was due to a diffuse sound field created mainly by other sources. Under these circumstances the largest measurement error is due to microphone phase mismatch.

For measurements on the generator wrapper, the indicator F_3 commonly has a value of 18 dB, with some higher bands (Fig. 4.25a). The logarithmic difference between F_3 and the residual pressure intensity index, $\delta_{|poIo|}$, is plotted in Fig. 4.25b. For the 4 kHz 1/3 octave band the value of F_3 exceeds $\delta_{|poIo|}$ implying an unclassified error. The phase error was calculated using $\bar{3}$ formulations to investigate if the F_3 indicator is more appropriate for quantifying phase errors than F_2, which is contrary to ISO 9614, but more theoretically correct as explained in chapter 2.

	Indicator	**Error formulation**	**Figure**
a)	F_3, biased by phase error	biased error eqn. A.12	4.25c
b)	F_3, corrected for phase error	unbiased error eqn. A.11	4.25d
c)	F_2, biased by phase error	biased error eqn. A.12	4.25e

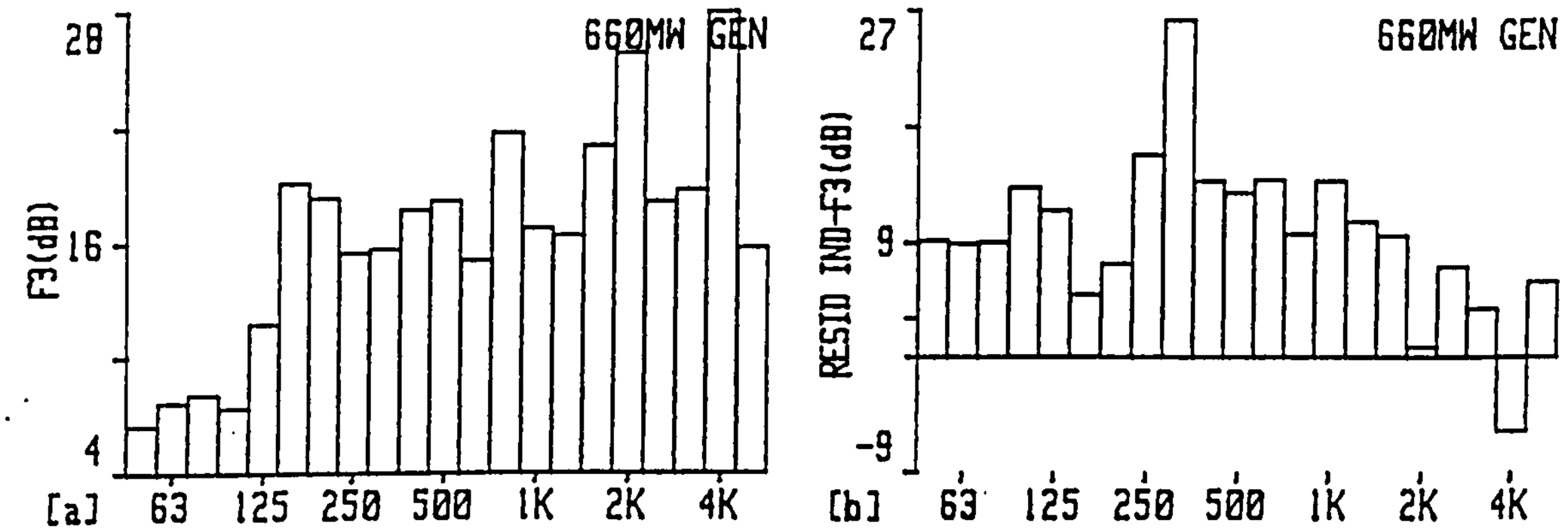

Fig.4.25 Generator measurements a) F_3 b) Residual index - F_3 & phase mismatch error, c) uncorrected for phase mismatch d) corrected for phase mismatch e) uncorrected for phase mismatch and calculated using F_2

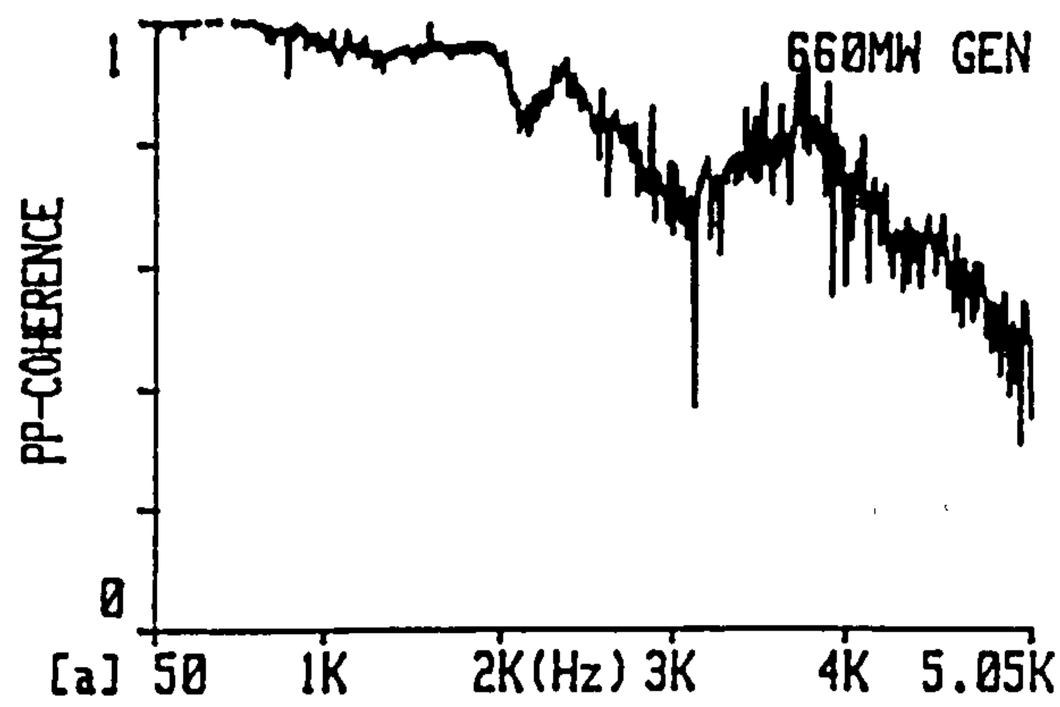

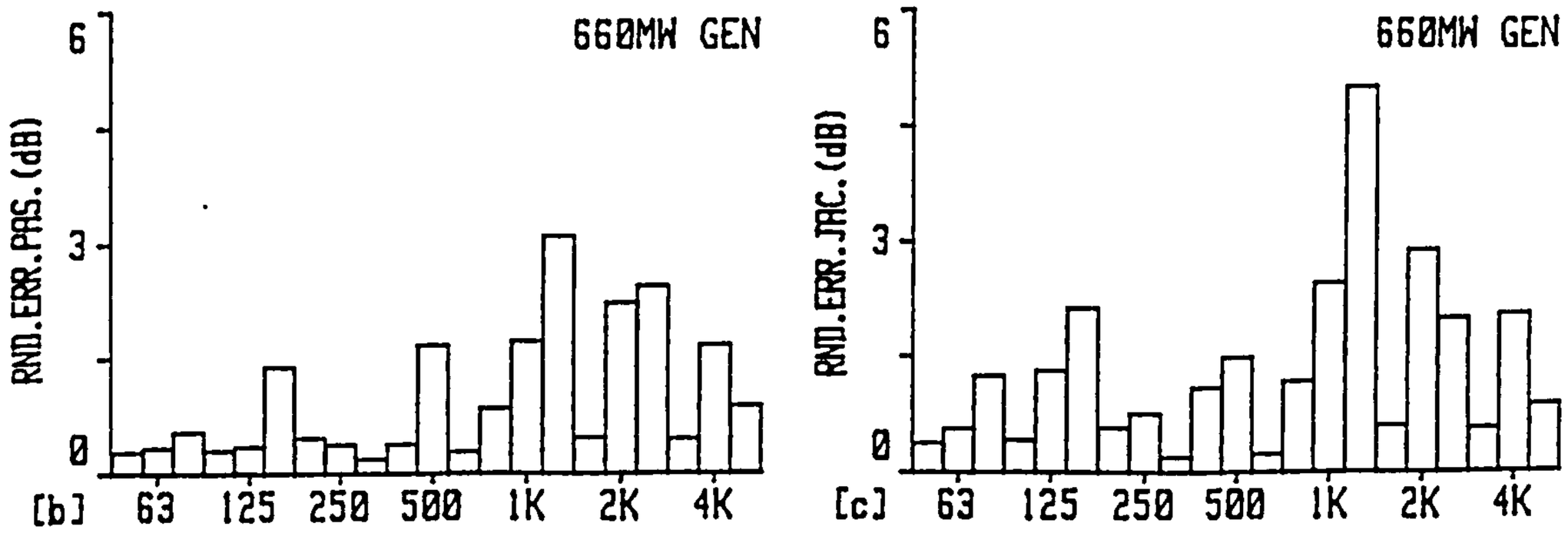

Fig.4.26 0.1m from generator centre a) sound pressure coherence & random error using b) Pascal's c) Jacobsen's formulation

By comparing Figs. 4.25c and 4.25d it is apparent that the error predicted from the biased and corrected F_3 indicator is the same provided the appropriate error formulation (Appendix A) is applied. With the exception of the 4 kHz band, for which the error was unclassified for the biased case, the error differs by less than 0.1 dB. The phase error is typically ±0.5 dB up to 1.6 kHz, above which the increased generator measurement error is reflected by the increased negative sound power measured (Fig.4.23a). The phase error predicted using F_2 (Fig.4.25e) is less than ±1 dB for all bands and is commonly less than ±0.25 dB, which appears to be an underestimation for such a complex noise field especially in the range 2 kHz - 4 kHz.

The random error due to finite sampling tones was assessed from point measurements at 10cm from the generator, the measurement distance for the sound intensity scans. The random error computed from Pascal's[35] eqn. (3.6) is illustrated in Fig.4.26b. Despite the low intensity emission from the generator and correspondingly low phase difference the interchannel coherence tending to 1 up to 1.5 kHz (Fig. 4.26a) limits the error. The error was further assessed from Jacobsen's[36] eqn. (3.7) and plotted in Fig. 4.26c. The coherence between sound pressure and particle velocity is small (Fig. 4.46a) due to the diffuse field creating many positive and negative frequency components in a band, which suggests a reasonably large random error. The two predictions for random error, Figs. 4.26b and 4.26c, are similar implying that despite the complexity of the bidirectional intensity at a point the bandwidth must be narrow enough for both integrals in eqn. (3.7) to be assumed independent of frequency. The overall error is ±0.5 dB up to 1 kHz, ±3 dB from 1.25 kHz to 4 kHz and ± 1 dB at 5 kHz.

The spatial sampling error cannot be predicted accurately[51] for the scanning technique. The error was assessed using the indicator F_4 and eqn. (3.9) despite the potential overestimation due to the scanning technique more closely representing the surface integral. The random error is plotted in Fig. 4.27a for the 66 measurement locations for the 95% confidence limits and $t_s = 1.67$. For most bands up to 1 kHz the error is between 1 dB and 1.5 dB, however above 1 kHz the error is substantially larger. Interestingly there is a correlation between the F_3 indicator (Fig. 4.25a) and the spatial sampling error (Fig. 4.27a).

An alternative means for error evaluation was to repeat every 4th measurement 4 times and calculate the error using eqn. (3.9). The random error is plotted in Fig. 4.27b for $t_s = 2.35$ and confidence limits of 95%. The error has a similar spectral composition to the complete sample population in Fig. 4.27a with smaller magnitudes. Up to 1.25 kHz the error is less than 1 dB for all but one 1/3 octave band at 800 Hz. This coincides with the general observation that 80% of the measurements were repeatable to within 1 dB for 2 scans.

This analysis and prediction of random errors is valid only if the measurements have a normal distribution and the probability density is Gaussian. Figs. (4.28a) to (4.28c) illustrate the relative occurrence chart for the frequency range 50 Hz - 1.25 kHz, 1.6 kHz - 4 kHz and 4 kHz - 5 kHz. For the frequency range 50 Hz - 1.25 kHz (Fig. 4.28a), where most of the generator sound power is contributed and the 5 kHz band (Fig. 4.28c), where the majority of measurements are negative the distribution is approximately Gaussian. The offset regions are due to some measurements having a sign opposite to the mean. For the frequency range 1.6 kHz to 4 kHz there was much

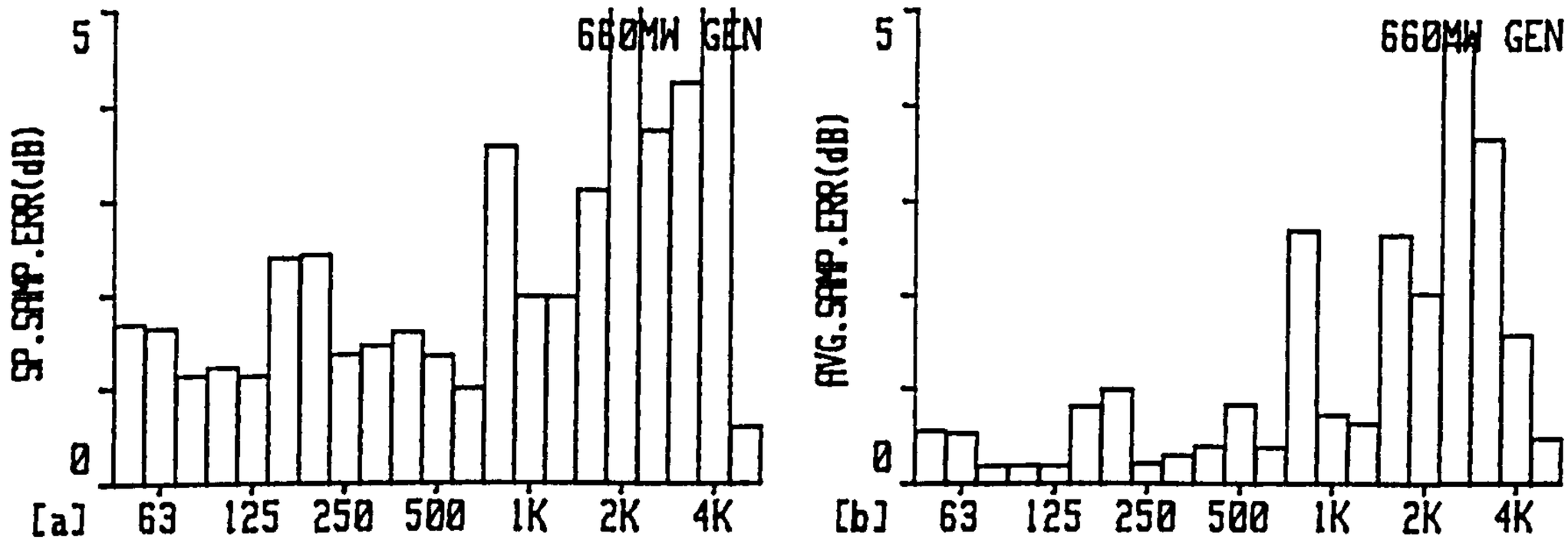

Fig.4.27 Generator spatial sampling error a) all 66 areas b) 4 repeated averages of 17 areas

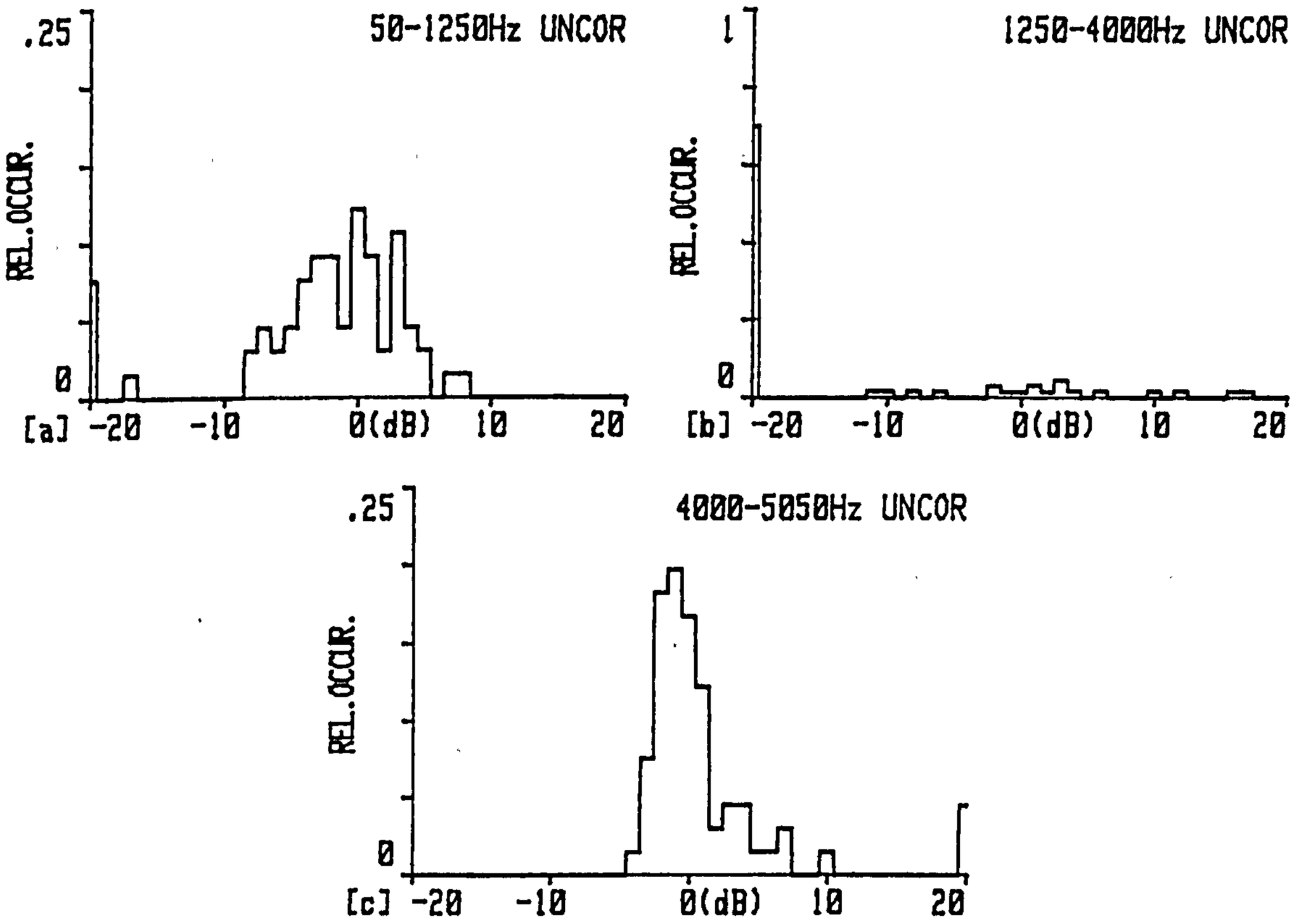

Fig.4.28 Probability density of generator sound intensity measurements

Fig.4.29 Total error for generator sound power

positive and negative power flow resulting in a low positive average, Fig.4.23a. The intensity for each measurement location differed largely from the mean resulting in a distribution, which was not Gaussian at all, Fig. 4.28b. This implies that the error calculation in this band may be invalid or larger, but for other frequencies it can be estimated.

Summary of generator errors

The total error was estimated by summating the phase mismatch error (Fig.4.25c), the random time sampling error at a "typical" point at the generator centre (Fig. 4.26b) and the random sampling error from the 4 repeated average sound intensities (Fig. 4.27b). The result is plotted in Fig. 4.29. In general up to 1.25 kHz the total error is ±2 dB. From 1.6 kHz to 3.2 kHz the error is between 4 and 8 dB with that at 4 kHz being unclassified. The 5 kHz error is 3 dB for the measured input, but is meaningless for the true output power. The relative errors correlates with the sound power spectrum (Fig. 4.23a) for which the majority of energy output was below 1.5 kHz. From 1.5 kHz to 4 kHz the net effect was emission, but at some frequencies negative sound power was measured. Above 4 kHz all measured power was negative.

The most applicable error limits for the overall sound power level determination are those for the bands, which contribute the majority to the overall level. The appropriate levels are therefore those up to 1.5 kHz being ± 2 dB.

ii) **Exciter error measurement**

Similar to the generator sound power determination the finite difference error is not significant. The majority of acoustic emission, Fig. 4.23b, is below 2 kHz implying

small errors of less than 0.15 dB.

Exciter sound power determination was complicated by the stronger directional noise from the pilot exciter and R.E. generator coupling. The value of F_3 was lower than that for the generator typically being less than 13 dB (Fig. 4.30a). From the difference between the residual pressure intensity index and F_3 (Fig. 4.30b) it is apparent the phase error will be small except below 160 Hz and above 4 kHz. The phase error (Fig. 4.30c) is less than ±0.25 dB within these limits calculated using both the biased measured intensity and phase mismatch corrected formulations given in eqns. (A.12) and (A.11) respectively.

The random error due to finite sampling error was assessed from a typical point measurement 10cm from the centre of the exciter. The error calculated from Pascal's eqn. (3.6) (Fig. 4.31a) and Jacobsen eqn. (3.7) (Fig. 4.31b) are similar to those for the generator as expected for similar low values of sound pressure particle velocity coherence (Fig. 4.46d). The difference in exciter random error using Pascal's and Jacobsen's eqns. is due to extensive nature of the bidirectional flow at a point implying that integrals in eqn. 3.7 are no longer frequency independent.

The spatial sampling random error was initially assessed using eqn. (3.9). The error plotted in Fig. 4.32a is liable to overestimation due to the scanning sampling representing the true surface integral better than suggested by the point sampling formulation. Also the number of negative power areas, 17, due to strong directional extraneous noise increases the estimated sampling error. These factors influence the error value of ±4 dB. Hübner[48,49] suggested that the random error may be more

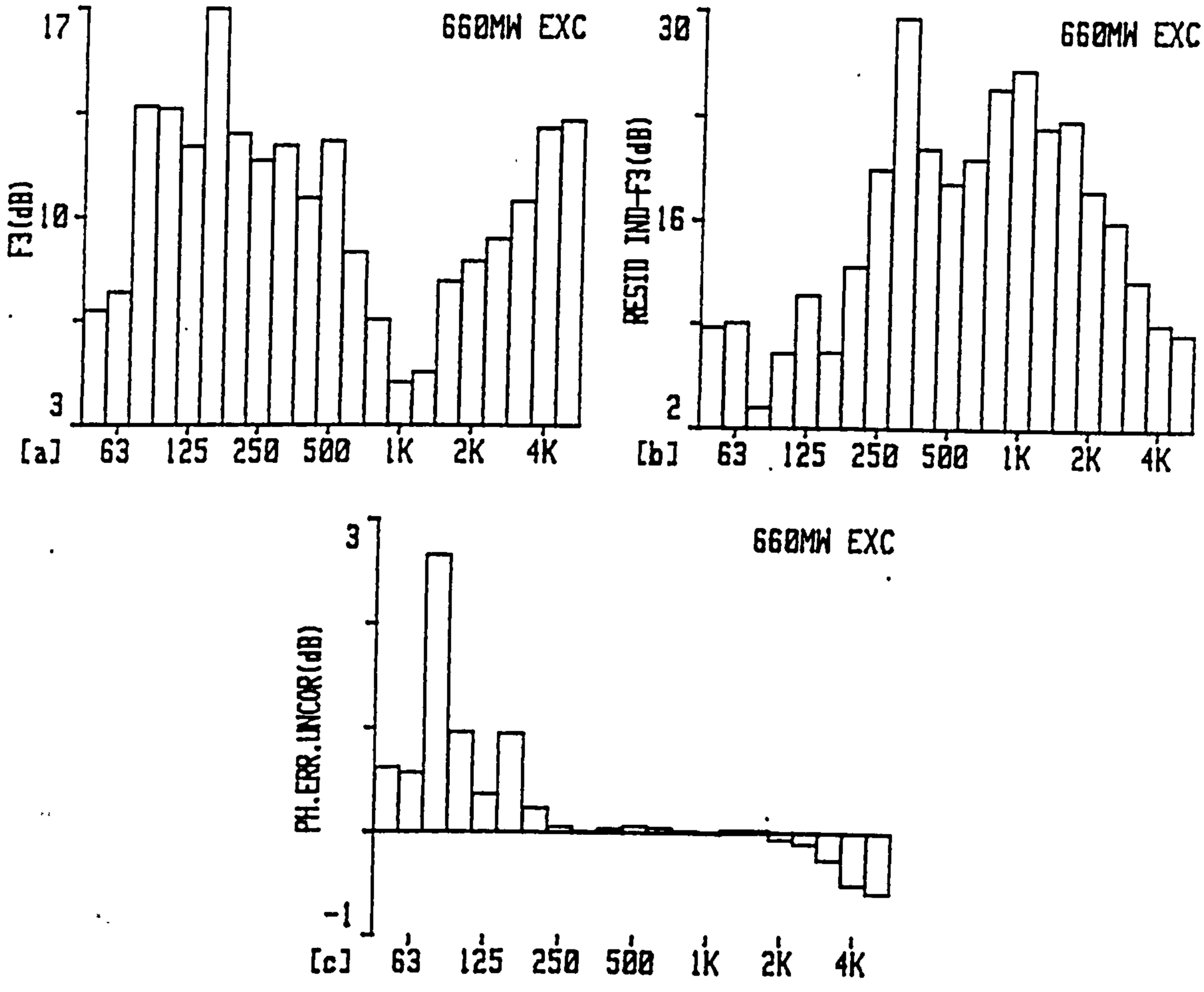

Fig.4.30 Exciter measurements a) F_3 b) Residual index - F_3 c) Phase mismatch error

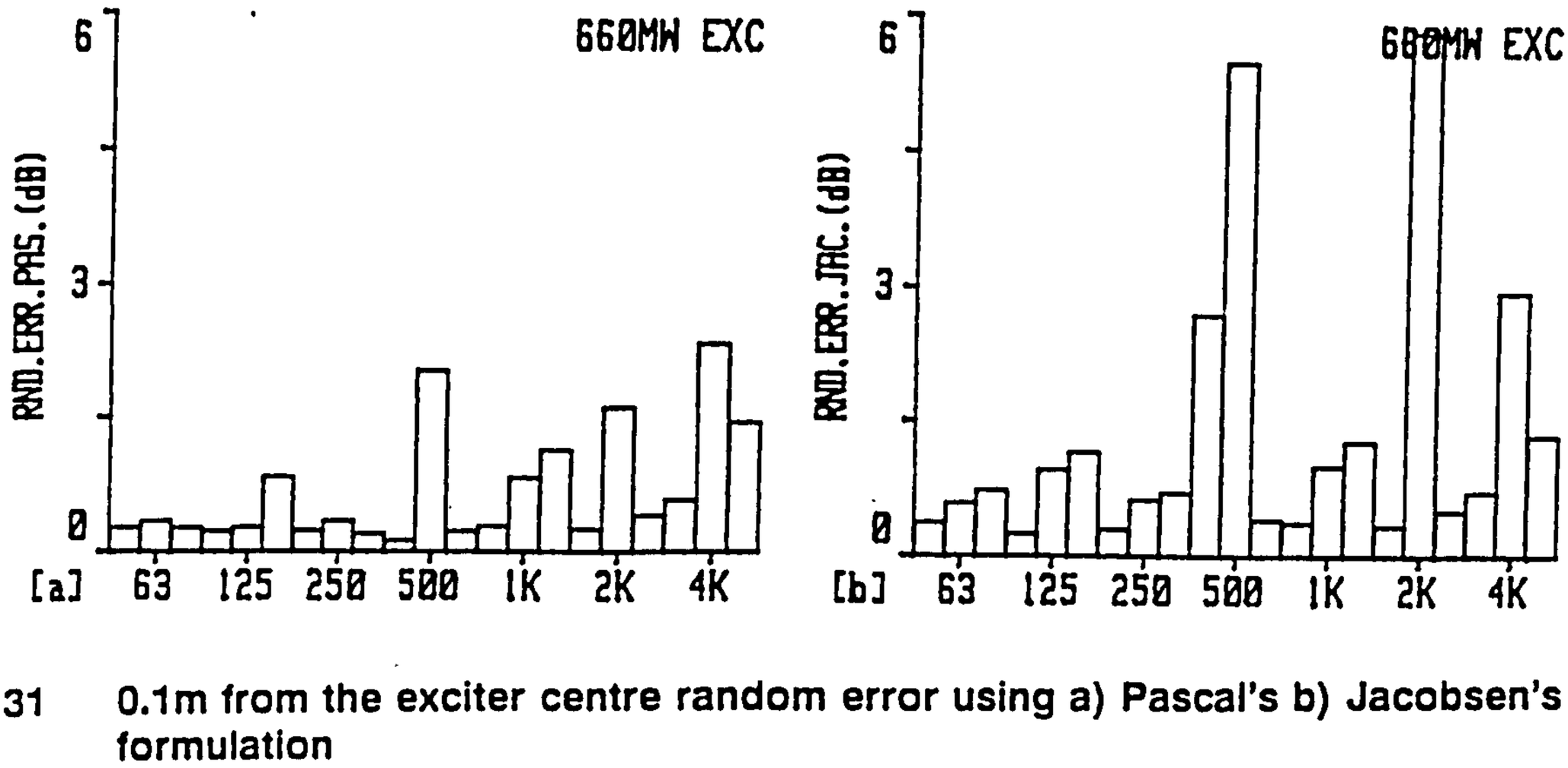

Fig.4.31 0.1m from the exciter centre random error using a) Pascal's b) Jacobsen's formulation

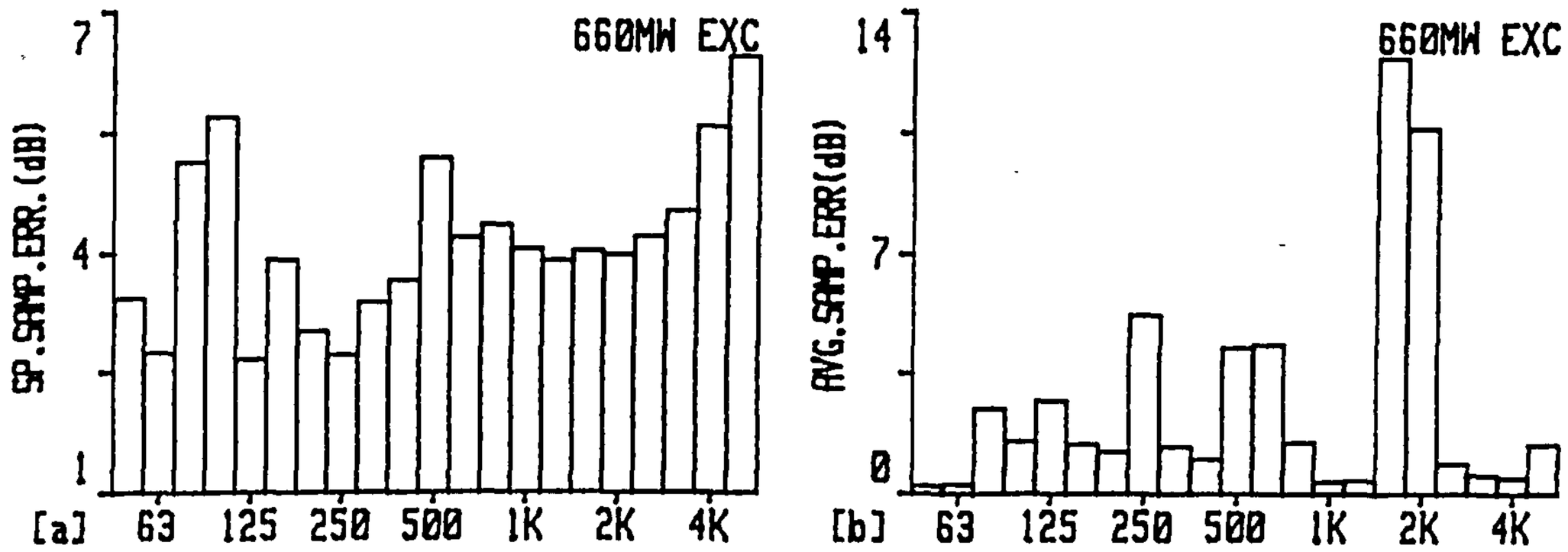

Fig.4.32 Exciter spatial sampling error for a) all 64 areas & 4 repeat averages of b) all c) positive only d) negative only measurements

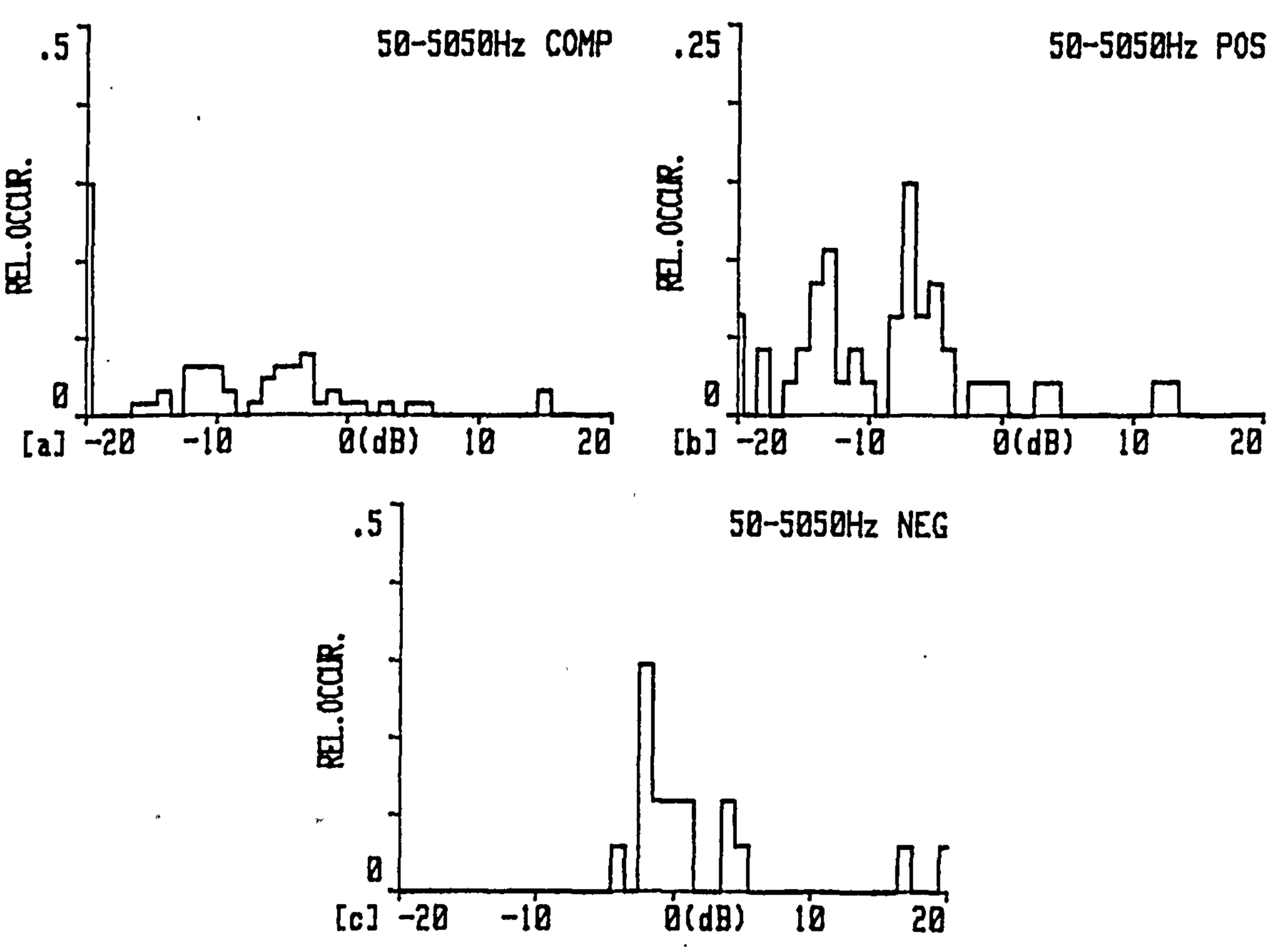

Fig.4.33 Probability density of exciter sound intensity for a) all b) positive only c) negative only measurements

appropriately evaluated for negative areas separately in these cases. For the positive areas the error was 3 dB and for the negative areas above 400 Hz it was 2 dB, which is less than the error predicted from the total sample population despite fewer measurements.

The random error was also investigated by repeating every 4th measurement 4 times and calculating the error using eqn. (3.9). The random error is illustrated in Fig. 4.32b for t_s = 2.35 and confidence limits of 95%. Unlike the generator case the spectral composition differs from that for the complete measurement survey, Fig. 4.32a. The reason for this was the extra variance created by the negative power areas. In general the measurement error was ±2 dB except for bands at 400 Hz, 500 Hz, 1.6 kHz and 2 kHz. If the error is calculated for the positive areas alone the error is less than 2 dB for all but 1 frequency band as indicated in Fig. 4.32c and similarly for the error evaluated only from the negative areas, Fig. 4.32d. It is therefore apparent that the negative intensities significantly increase the spatial sampling error.

The relative occurrence chart for the 64 exciter intensity measurements is illustrated in Fig. 4.33a. The distribution is only very approximately Gaussian with a large negative offset due to the number of negative intensities. By contrast the probability density for the positive and negative measurements alone, in Figs. 4.33b and 4.33c respectively, more closely resemble the Gaussian distribution.

Summary of exciter errors

The total error was estimated by summating the phase mismatch error (Fig. 4.30c),

the random time sampling error at a "typical" point at the exciter centre (Fig.4.31b) and the random sampling error from the 4 repeated average sound intensities (Fig. 4.32b). The result is plotted in Fig. 4.34a. Most values are less than 3.25 dB except bands at 500 Hz, 1.6 kHz and 2 kHz. As the 1.6 kHz and 2 kHz represent reasonably strong noise emission from the exciter, Fig. 4.24, it is believed that the error is overestimated due to the many negative intensities caused by strong extraneous noise. If the spatial sampling error calculated from 11 positive areas repeated 4 times, Fig. 4.32c, is used as the appropriate sampling error the total error, as plotted in Fig. 4.34b, is less than 3 dB for the majority of bands. This approach of considering sampling errors prevalent to a set of positive and a set of negative intensities was suggested by Hübner[48,49] and seems apt. Despite the average intensity emission from the centre being of the order of 4-5 dB greater than that from the generator, the sound power determination was subject to greater error limits of 3 dB due to the strong directional extraneous noise incurring greater spatial sampling errors.

iii) **R.E. generator coupling error measurement**

For the strong component source the R.E. generator coupling represents, the main measurement problem is due to correct sampling of the high intensity region, the clearance slit. The F_3 indicator for the 12 point measurements on the coupling cover and gap, as illustrated in Fig. 4.35, is less then 5 dB above 160 Hz. This implies low phase mismatch errors of less than 0.2 dB, which is relatively negligible.

The influence of the time sampling random error can be accurately assessed for the point measurements by considering a typical point 0.1m from the R.E. generator coupling. The interchannel coherence is high tending to 1 across the complete

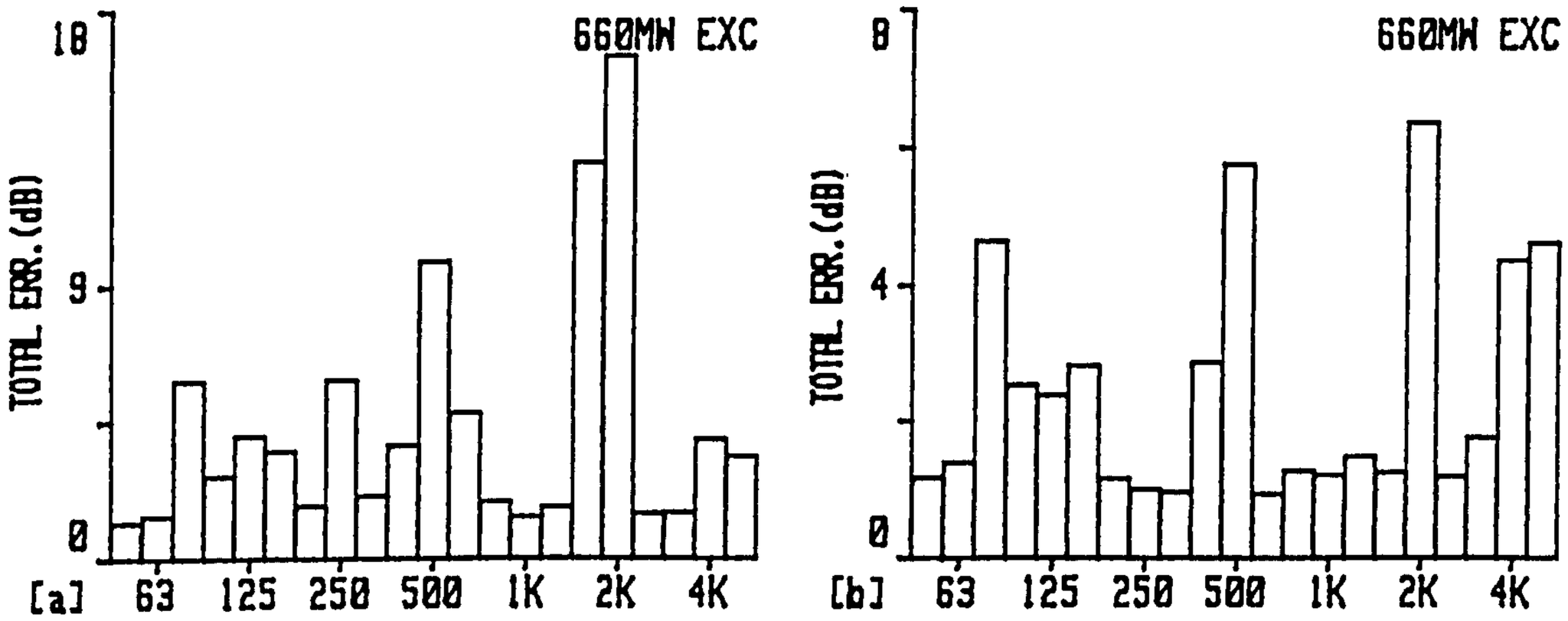

Fig.4.34 Total error for exciter sound power using spatial sampling error for a) all b) positive only measurements

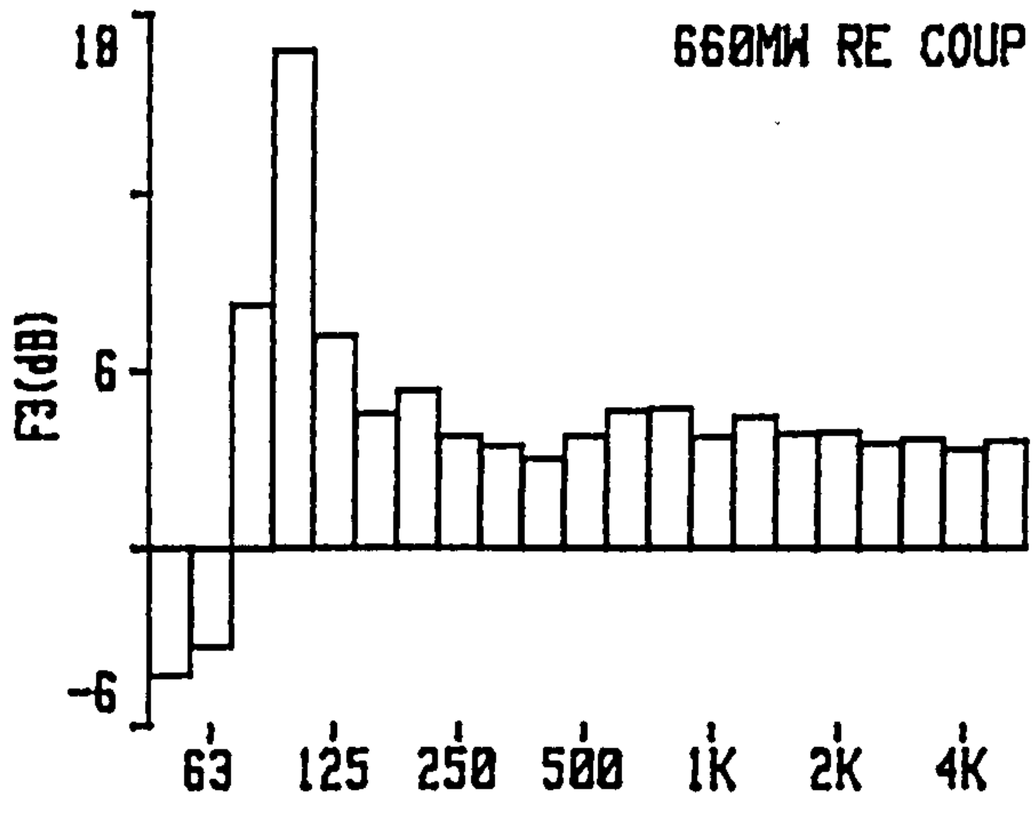

Fig.4.35 R.E. generator coupling measurements F_3 indicator

frequency band, 50 Hz to 5.05 kHz, (Fig. 4.36a). The sound pressure particle velocity coherence is higher than other examples tending to 0.5 dB, Fig. 4.46f. Under these circumstances the random error is similar using Pascal's and Jacobsen's formulation, as given in Figs. 4.36b and 4.36c respectively. The value of low frequency error is increased by the low phase difference and bidirectional flow below 150 Hz, but this is not significant. Above 250 Hz the error tends to ±0.5 dB. For the constant average reactivity illustrated in Fig. 4.35 the error decreases with increasing frequency for each 1/3 octave band as the bandwidth increases. For the 2 kHz to 4 kHz 1/3 octaves, which contribute the majority of the overall level, the error is less than 0.25 dB and is relatively minor.

For the 12 point measurements the random spatial sampling error can be calculated using eqn. (3.9) in accordance with ISO 9614. The typical error was 2 dB for all 1/3 octaves above 160 Hz as illustrated in Fig. 4.37a. By contrast, despite fewer measurements, the error for the 8 measurements on the cover and the 4 measurements on the gap was less than 2 dB and 1 dB respectively as indicated in Figs. 4.37b and 4.37c. This implies that the complete estimate is an overestimate and limits of ±1 dB are more apt. Interestingly the error implied by the 4 scan measurement was less than 1 dB for the main frequency bands, as illustrated in Fig. 4.37d. In this case it is believed that the "hot spot" of the coupling cover clearance gap was less well sampled by the scanning. Despite this and the fewer measurement locations the sampling error from scanned measurements will tend to be less than that from point measurements.

The overall error limits will be principally comprised of the time sampling random

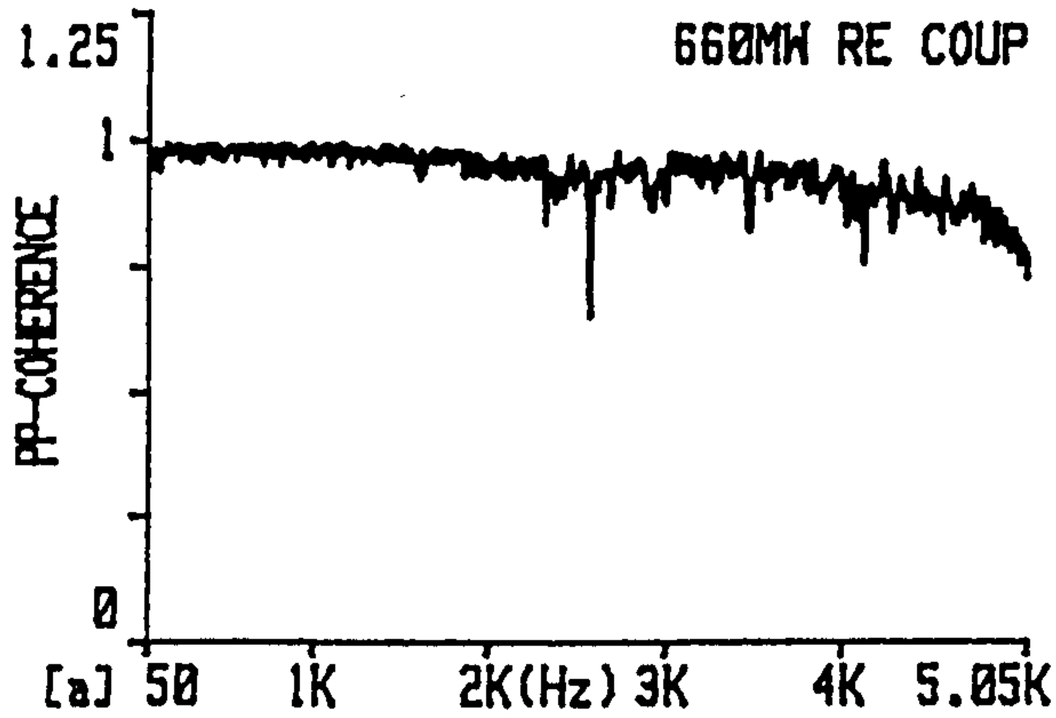

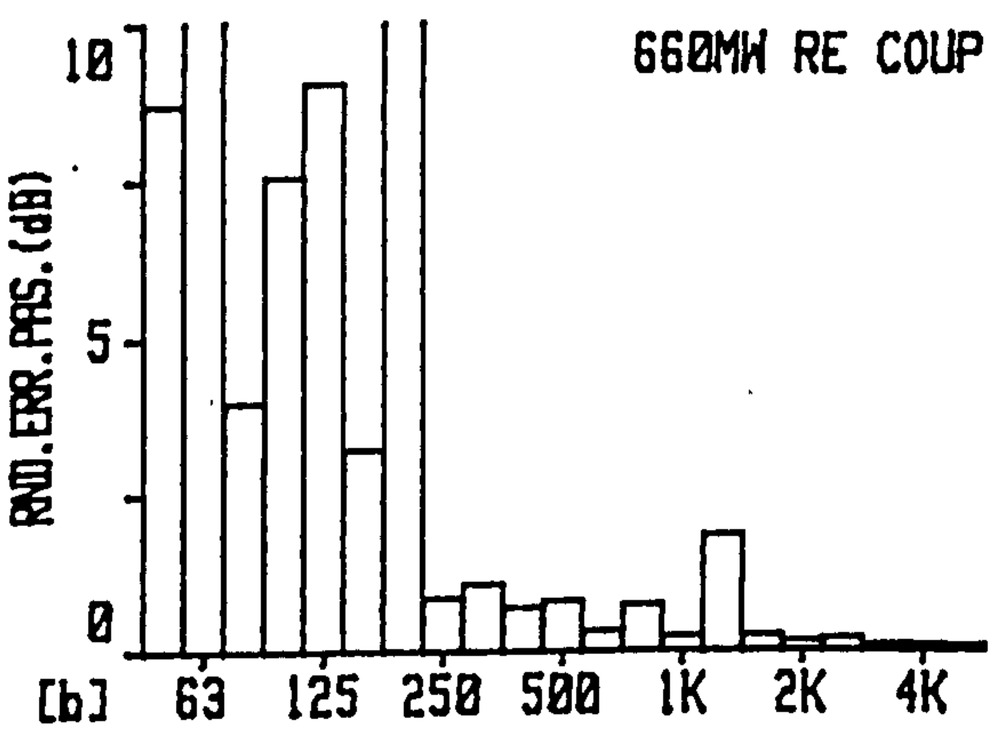

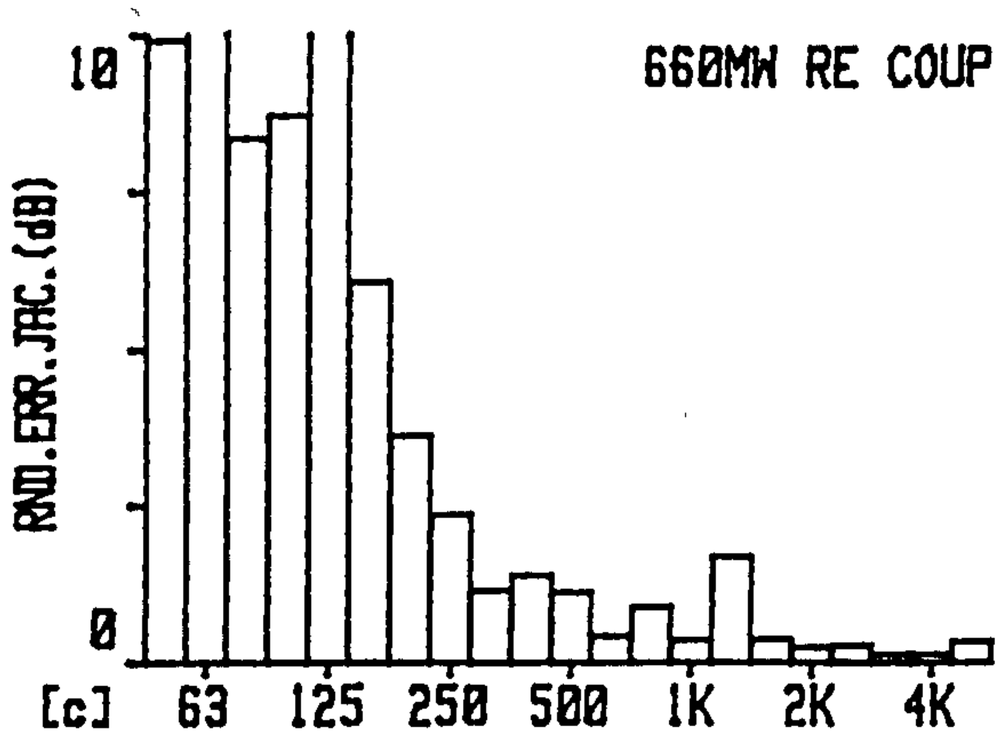

Fig.4.36 0.1m from R.E. generator coupling a) sound pressure coherence & random error using b) Pascal's c) Jacobsen's formulation

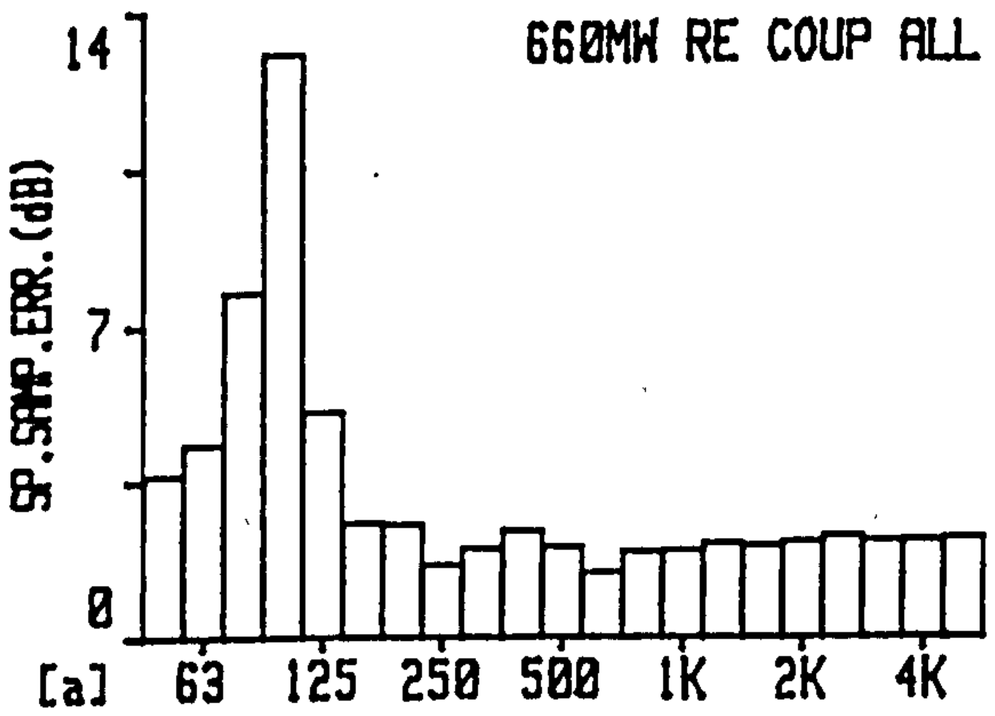

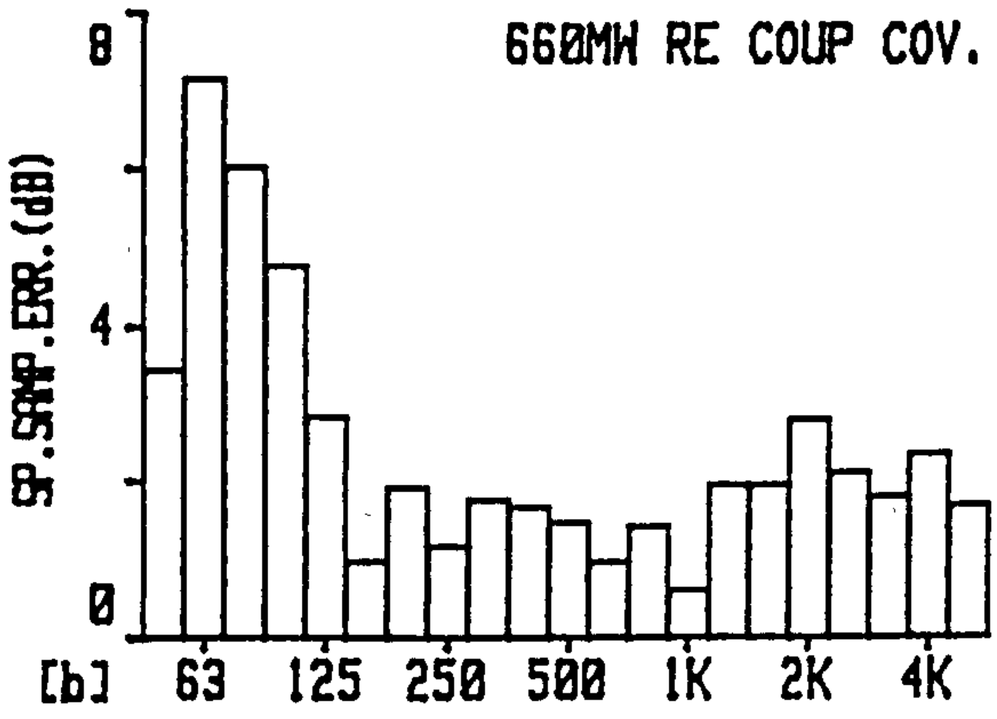

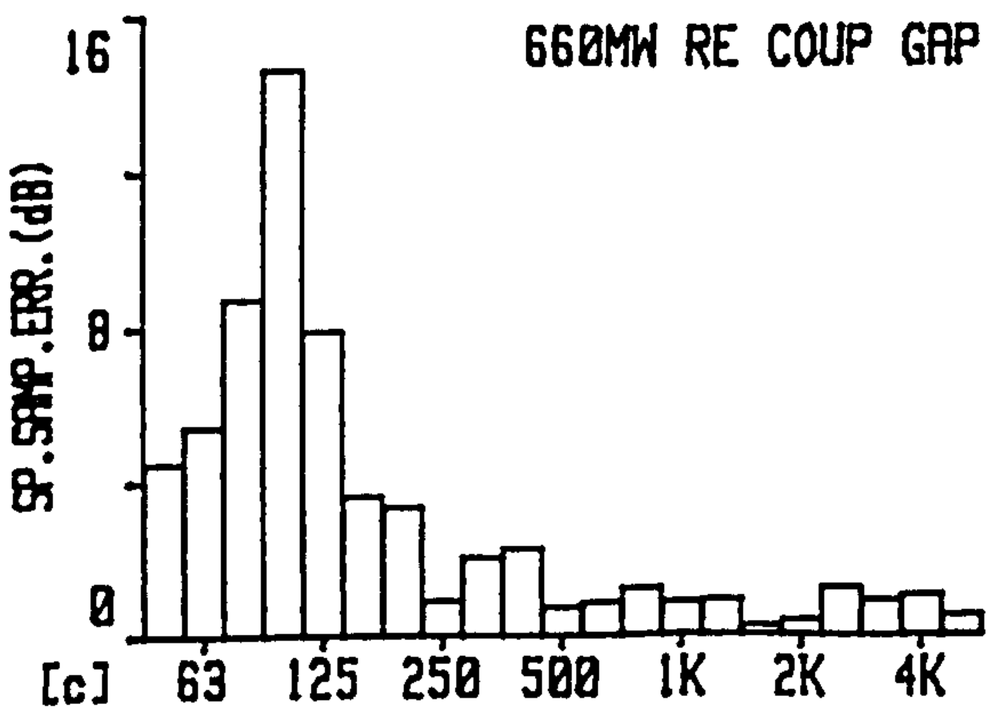

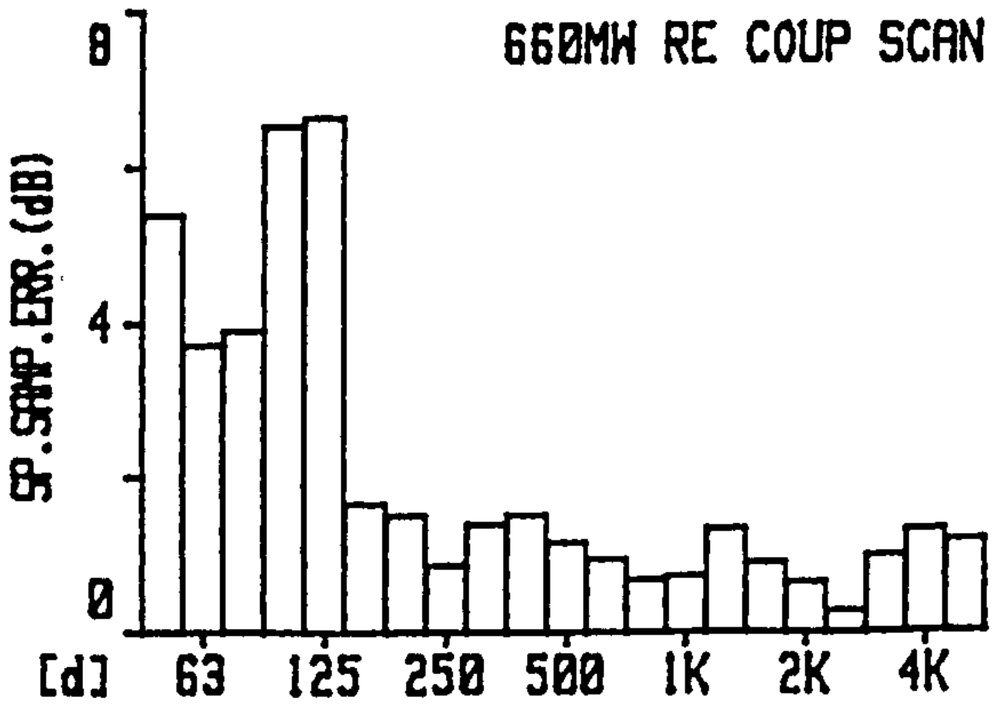

Fig.4.37 R.E. generator coupling spatial sampling error for a) cover + gap points b) cover only points c) gap only points d) cover + gap areas.

error of 0.25 dB and the spatial sampling error of 1 dB with negligible phase errors yielding a total of ±1.25 dB.

iv) **Pilot exciter error measurement**

Similar to the R.E. generator coupling the main measurement problem is associated with correct sampling of the high intensity regions. To some extent this is already minimised by defining the measurement grid to consider the high intensities regions, the grills, as separate areas. The F_3 indicator for the 20 area scans on the pilot exciter enclosure was illustrated in Fig. 4.38, was less than 5 dB above 400 Hz implying phase mismatch errors of the order of ±0.1 dB.

The influence of the time sampling random error was assessed by a point measurement 1m from the pilot exciter enclosure level with one of the side ventilation grills. The interchannel coherence is high tending to 1 across the complete frequency band, 50 Hz to 5.05 kHz, as illustrated in Fig. 4.39a. The sound pressure particle velocity coherence is the highest of all 4 components tending to 0.8, as illustrated in Fig. 4.46i, implying similar random time sampling errors from Pascal's and Jacobsen's formulations, plotted in Figs. 4.39b and 4.39c. The error was very low being less than ±0.2 dB above 250 Hz.

The predicted random spatial sampling error predicted for the 20 scan measurements was ±2 dB for frequencies above 250 Hz is given in Fig. 4.40a. This error is overestimated as the grid definition should correctly measure the high power regions. The error for the measurements on the grills was ±1.5 dB as indicated in Fig. 4.40b, which should more correctly represent the total error as phase mismatch and time

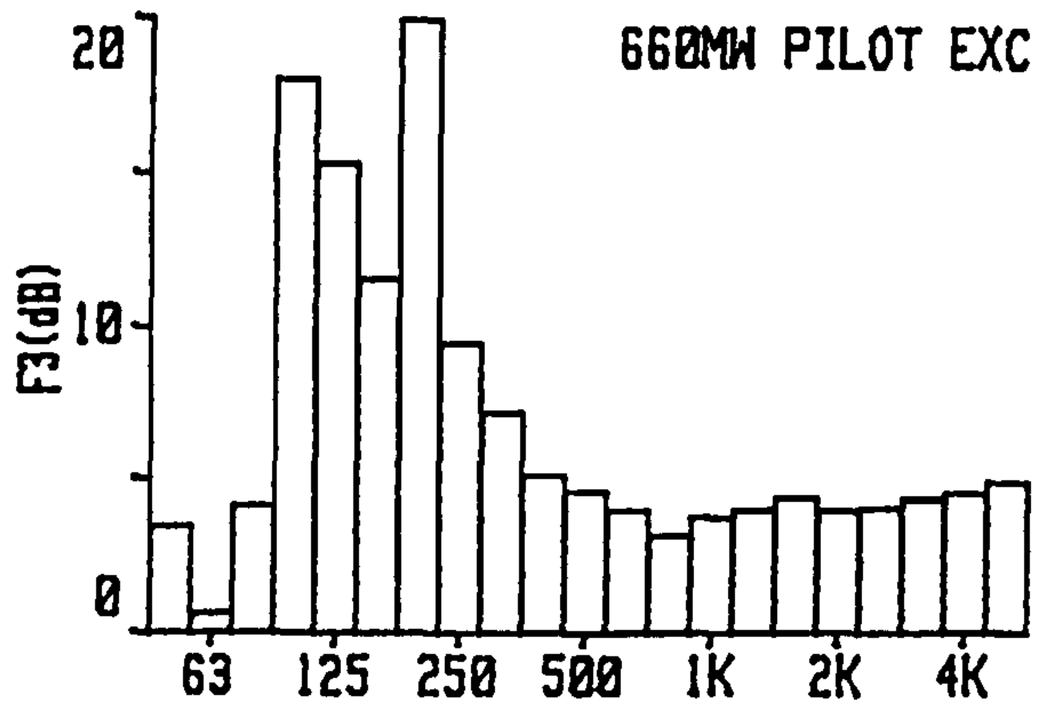

Fig.4.38 Pilot exciter measurements F_3 indicator.

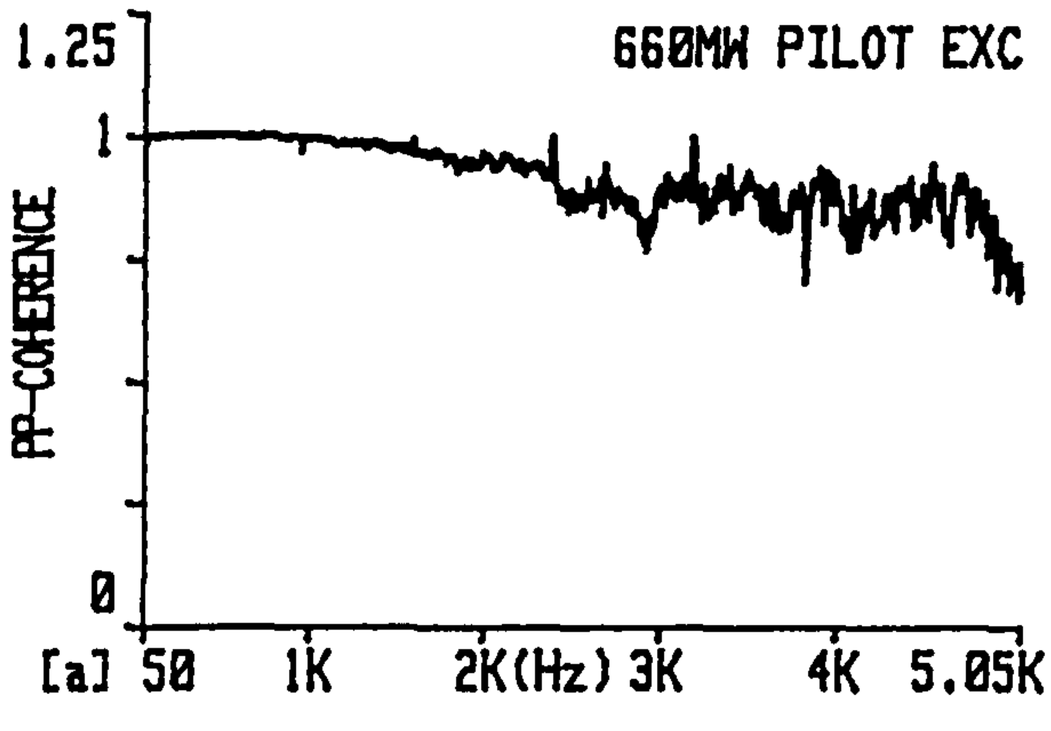

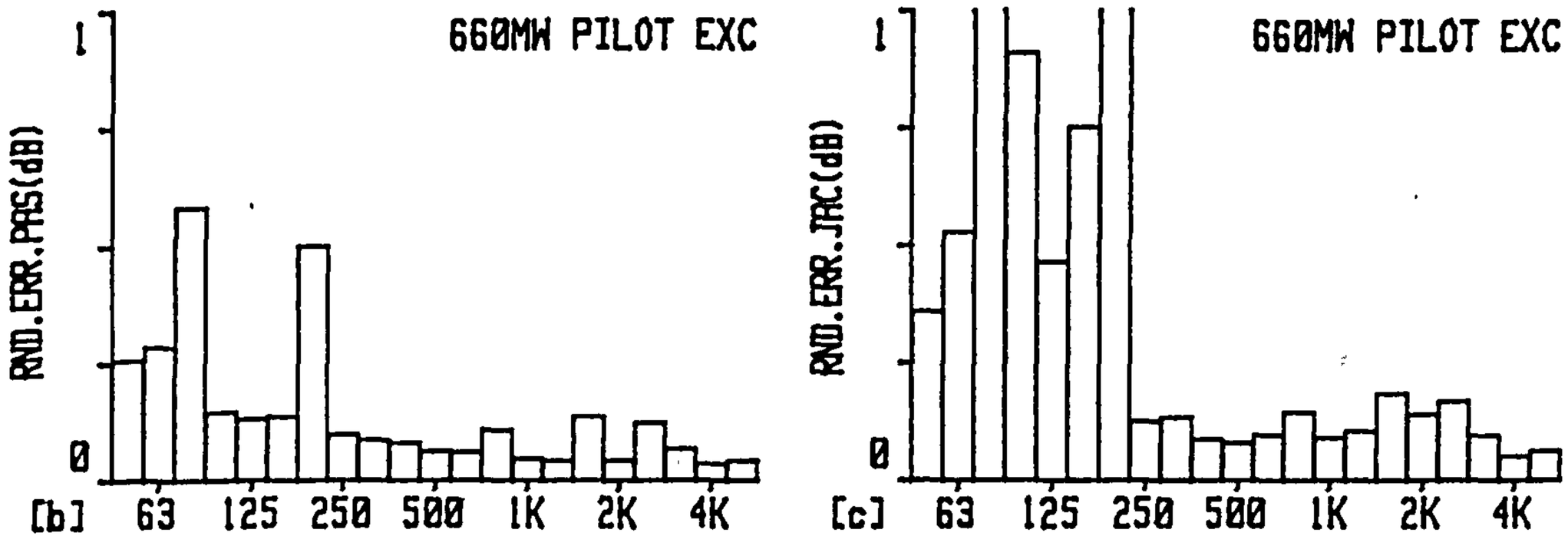

Fig.4.39 0.1m from pilot exciter a) sound pressure coherence & random error using b) Pascal's c) Jacobsen's formulation

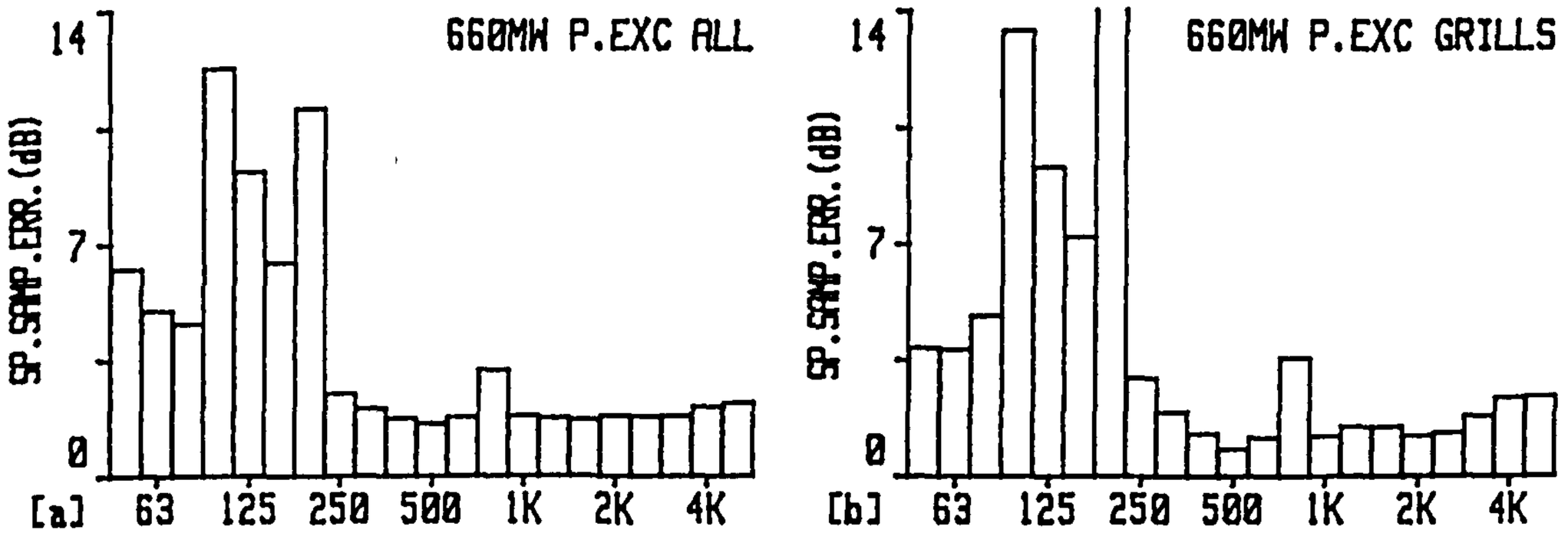

Fig.4.40 Pilot exciter spatial sampling error for a) all areas b) grill areas only.

sampling random errors were reasonably inconsequential.

4.2.2.3 **Correlation of measured sound power to sound pressure**

The practical value and approach for correlating measured sound power to site sound pressure from each component has been outlined in section 3.4.4. The sound power levels in table E can be related approximately to free field sound pressure level using the wave divergence formula, eqn. (3.10). The results for each component are presented in row 1 of table F.

Component	Generator	R.E. Coupling Cover	Exciter	Pilot Exciter
Predicted free field sound pressure level at 1m from measured sound power level	74.2	94.3	78.5	95.2
Increase due to reverberation	4.5	1.5	4.5	4.5
Increase due to geometric interference	2.5	-	1.5	-
Increase due to power absorption	1.2	-	1.5	-
Predicted site sound pressure level	82.4	95.8	86.0	99.7

Table F: Predicted sound pressure levels due to each of the generator unit components (all levels are in dB(A))

The estimated increase in noise levels due to reverberation is 4.5 dB for all components except the R.E. generator coupling cover. It is principally above a floor opening between the exciter and the generator reducing the reverberation influence to approximately 1.5 dB.

Reiniche[12] evaluates that for a structure with the length of the generator the underestimation of sound pressure from the intensity due to geometric interference

effects was 2.5 dB, as explained in 3.4.4. For the shorter exciter the underestimation is approximately 1.5 dB. The more compact pilot exciter and R.E. generator coupling sources are not influenced by this superposition effect.

The measured generator sound power of 92.5 dB(A) for one third of the total area and subsequently the total level of 97.3 dB(A) are liable to an underestimation due to small levels of power absorption from the diffuse and direct fields. This is manifested by the negative generator sound power spectrum in the range 4 kHz - 5 kHz, Fig. 4.23a. The sound power for the generator side was mainly from the diffuse field due to shielding of the direct noise by the F.E. and R.E. brackets. For an absorption coefficient of 0.03 and the average sound pressure of 92 dB(A) approximately 87.5 dB(A) sound power would be absorbed meaning the measured sound power was an underestimate of the total figure by 1.2 dB. Similarly the exciter would absorb low sound power levels causing an underestimate in the total figure of 1.5 dB, if the absorption coefficient was 0.03. For the pilot exciter and rear end generator coupling cover the absorption relative to emission is insignificant.

The predicted sound pressure levels and the influence of these extra factors are given in table F. The approximate pilot exciter and R.E. generator coupling sound pressure levels are 99.7 dB(A) and 95.8 dB(A). The generator and exciter levels of 82.4 dB(A) and 86 dB(A) are significantly less.

4.2.3 Point sound intensity vector measurements

The point intensity vector measurements clearly showed that the predominant flow was not from the generator and exciter but from the neighbouring equipment such

as the turbines, R.E. generator coupling and pilot exciter. This is illustrated in Fig. 4.41. This correlates with the predicted low levels of generator and exciter sound power.

The A-weighted sound pressure spectrum, given in Fig. 4.42a, at the generator front (turbine) end was raised by the direct flow of 86.5 dB(A) due to sound intensity from the turbines. Towards the rear end the sound pressure at 1m has increased due to a number of tonal components in the range 2.5 kHz to 4 kHz, as illustrated in Fig. 4.42b. The resultant sound intensity is 92.7 dB(A) from the R.E. generator coupling. This value and the spectral similarity between R.E. coupling sound power, Fig. 4.23c and sound pressure, Fig. 4.42b, indicate a significant influence of the coupling on S.P.L. beside the generator. At the generator centre the overall intensity is from the turbine in the range 4 kHz - 5 kHz, from the rear end coupling in the range 2.5 kHz - 4 kHz and bidirectional at lower frequencies as indicated in Fig. 4.42c. The resultant sound intensity levels of 86.5 dB(A) and 92.7 dB(A) at the front and rear ends are an order of magnitude greater than the typical generator near field output intensities of 75-76 dB(A) therefore clearly illustrating the influence of background noise on the sound pressure level beside the generator. This also explains the measurement difficult associated with generator sound power determination.

Beside the exciter F.E. the sound pressure spectrum and level are similar to those at the generator R.E. with 94.2 dB(A) direct intensity flow from the coupling at 1m. 1m from the exciter rear end the S.P.L. of 97.4 dB(A) is significantly contributed to by the 95.4 dB(A) sound intensity from the pilot exciter. The sound pressure spectrum, shown in Fig. 4.43a, differs markedly to that at the F.E. with tones at 800 Hz and

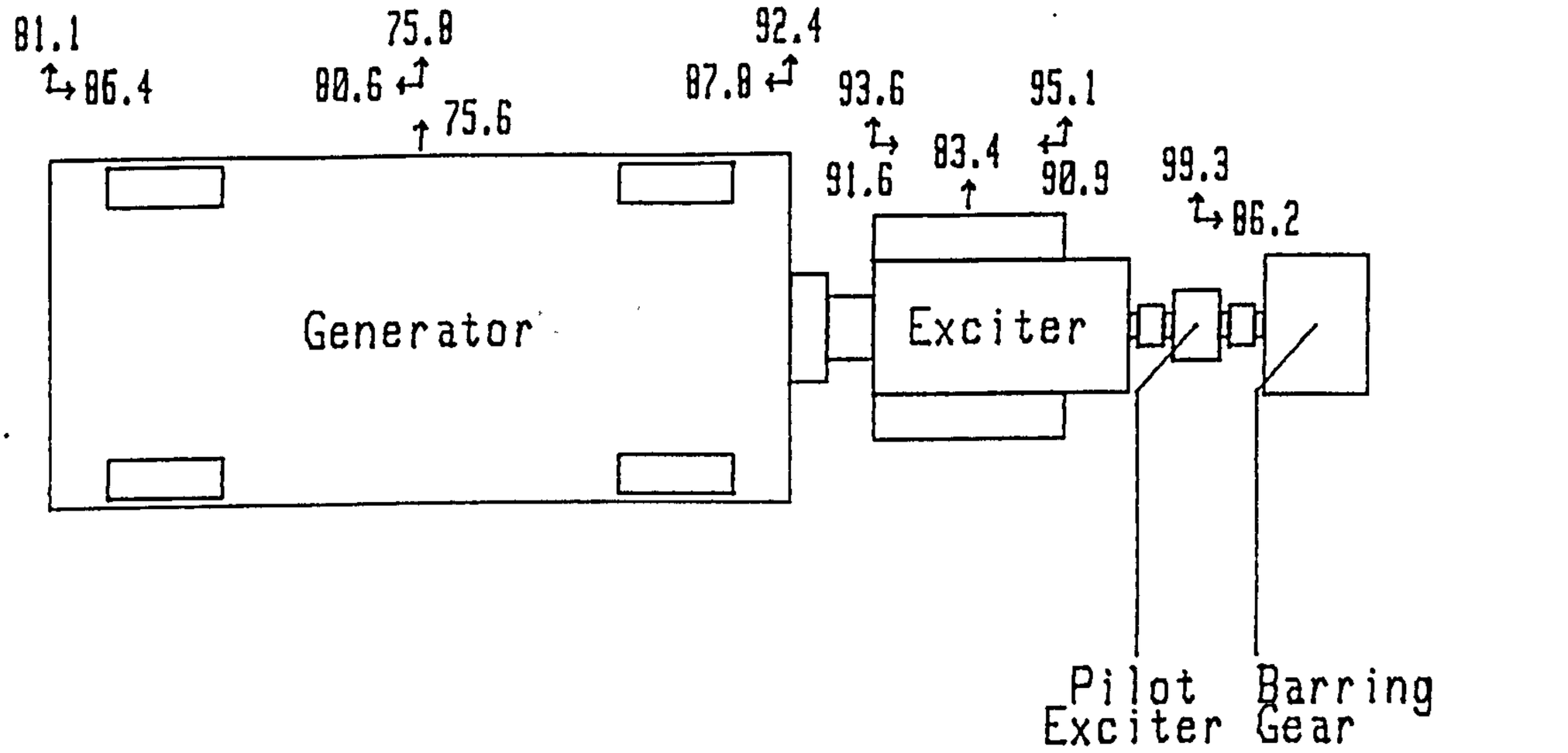

Fig.4.41 Sound intensity distribution around the generator unit (dB(A)).

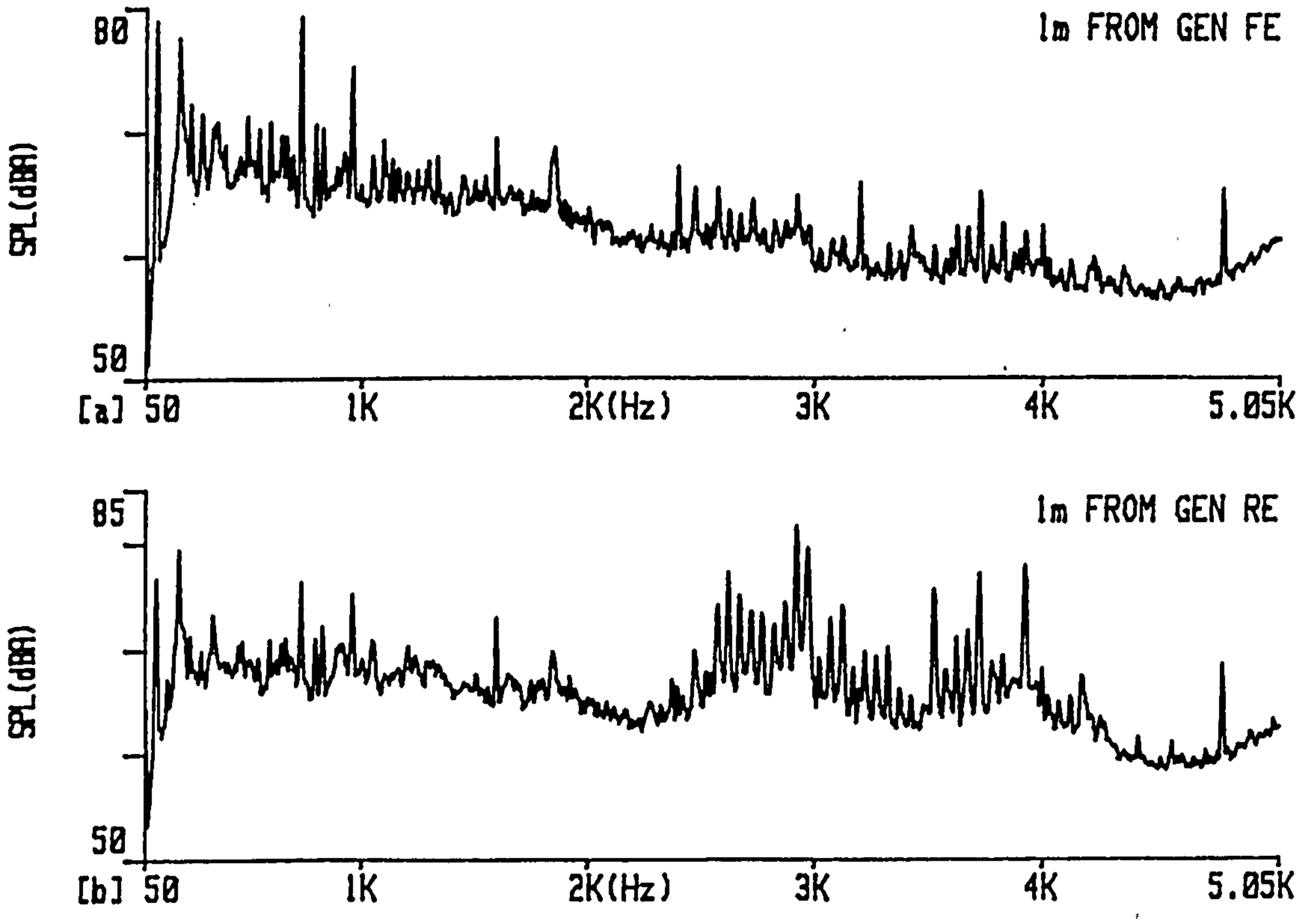

Fig.4.42 Narrowband sound pressure level 1m from generator a) F.E. & b) R.E. c) Narrowband axial sound intensity 1m from the generator centre (+ve from F.E.).

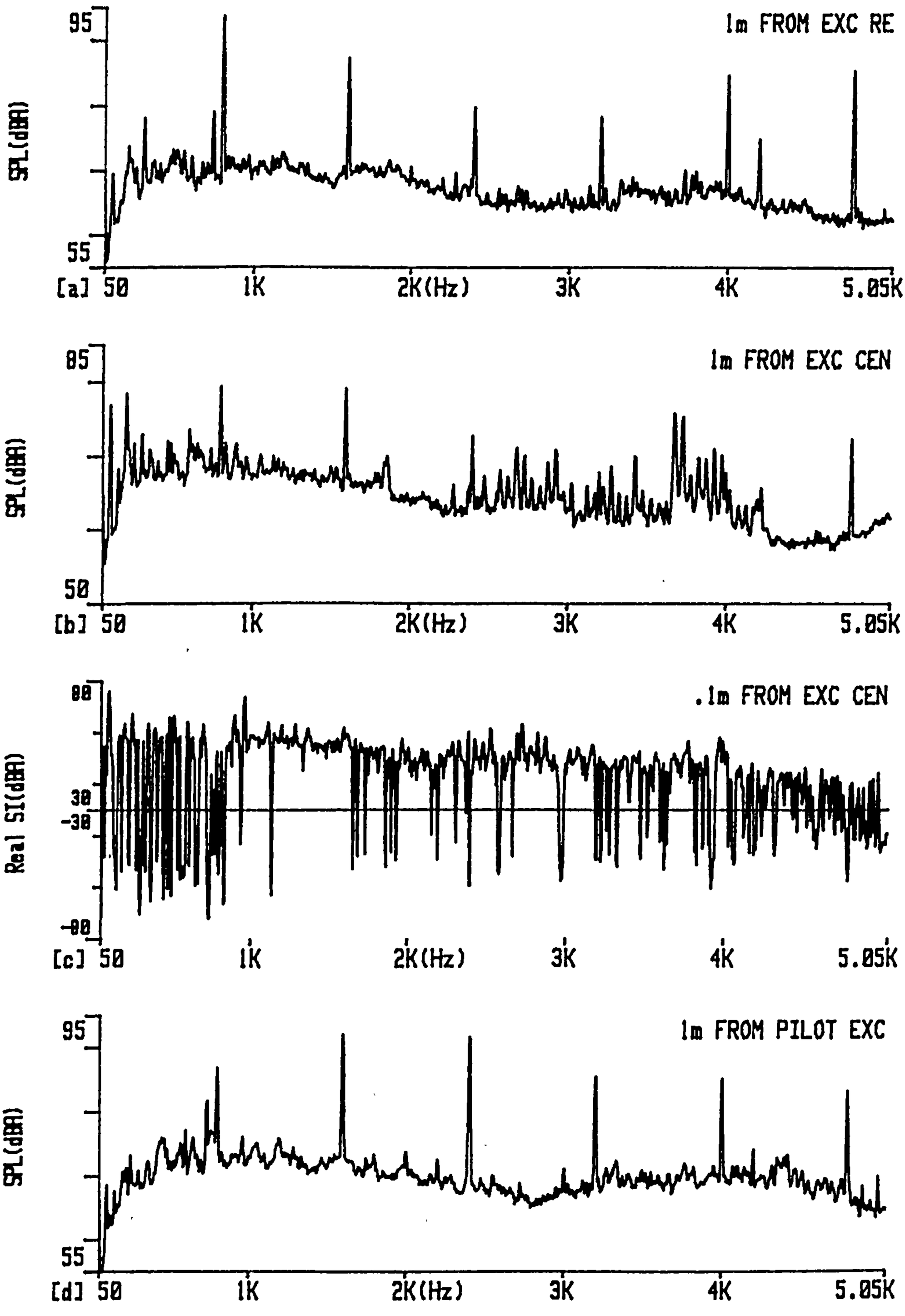

Fig.4.43 Narrowband sound pressure level 1m from the exciter a) R.E. b) centre c) Narrowband radial sound intensity 0.1m from the exciter centre d) Narrowband sound pressure level 1m from the pilot exciter.

harmonics thereof emanating from the pilot exciter, Fig. 4.23d. At 1m from the exciter centre sound pressure spectrum shows the contribution from both the R.E. coupling and the pilot exciter, as illustrated in Fig. 4.43b. The radial sound intensity 10cm from the exciter at its centre was 83.4 dB(A) with a complex spectrum, Fig. 4.43c, due to circulating energy near steel plates[30] and background noise effects. The intensity is still clearly a net output of low levels of exciter emission relative to the pilot exciter and R.E. coupling and it's difference to the measured sound pressure spectra illustrate that the S.P.L. is largely set by other sources. The pilot exciter sound pressure level of 102 dB(A) at 1m had the characteristic spectrum given in Fig. 4.43d.

4.2.3.1 Composition of sound pressure level at 1m

It is important when assessing sound pressure level to decompose the level into its contributing influences rather than assume it is due to equipment directly adjacent. The preceding analysis has decomposed the level into 3 influences, namely, the general reverberant sound field, direct sound intensity from other background noise sources and the predicted sound pressure due to equipment directly. This analysis can be compared to the measured levels by summating the 3 factors. The results are summarised in table G. These explain the site S.P.L. to within 1 dB at all locations and more commonly to within 0.5 dBA. This clearly illustrates the influence of general reverberation and direct background noise on S.P.L. beside the exciter and the generator. It is apparent that the exciter and generator do not set the S.P.L. beside them.

Equipment	Generator			Exciter			Pilot Exciter
Location	F.E.	Centre	R.E.	F.E.	Centre	R.E.	
Reverberant S.P.L.	90.5	90.5	90.5	90.5	90.5	90.5	90.5
Predicted S.P.L. due to equipment	82.4	82.4	82.4	86.0	86.0	86.0	99.7
Direct background intensity component	86.5	80.6	92.7	94.2	89.1	95.4	-
Total predicted S.P.L. at 1m	92.4	91.5	95.0	96.2	93.7	97.0	100.2
Measured S.P.L. at 1m	92.8	91.4	95.8	97.0	94.9	97.4	101.5

Table G: Comparison of predicted S.P.L. due to reverberation, direct background noise and predicted plant level with measured levels (all levels are in dB(A))

4.2.4 Sound pressure surface vibration coherence

The coherence between sound pressure at 10cm and surface vibration at the generator centre is low commonly tending to 0 except for a few tones in range 50 Hz to 1 kHz as shown by Fig. 4.44a. The vibration velocity squared spectrum (Fig. 4.44b) and the unweighted sound pressure spectrum (Fig. 4.44c) are not comparable except for a limited number of tones at 100 Hz and harmonics thereof.

The sound pressure vibration coherence is similarly low beside the exciter, as shown by Fig. 4.44d except for tones at 2281 Hz, 2400 Hz and 2700 Hz. By contrast the coherence between sound pressure at 1m from the exciter front end and coupling cover vibration is clear for the coupling cover tones at 100 Hz and harmonics thereof and in the range 2.5 kHz to 4 kHz. This is illustrated by Fig. 4.44e. The spectral similarity between cover vibration velocity squared and unweighted sound pressure 1m from the exciter front end can be seen by comparing Fig. 4.44f and 4.44g. Similarly between pilot exciter cover vibration and the sound pressure at 1m from the exciter rear end there is strong coherence between tones at 800 Hz and harmonics thereof as can be seen from Fig. 4.44h. The coherence measurements therefore correlate with the sound

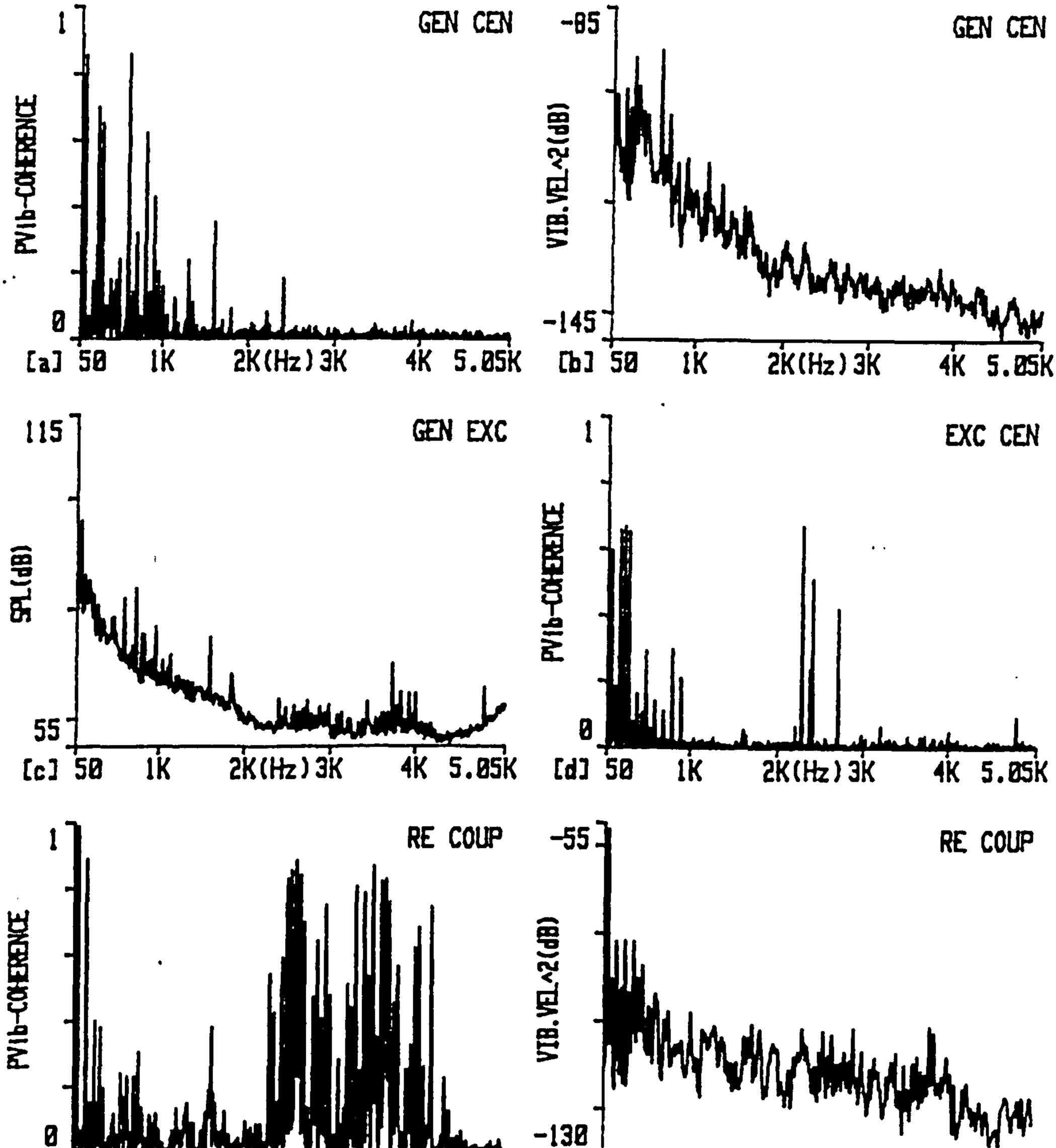

Fig.4.44 Relationship between vibration on and sound pressure close to a)-c) generator centre, d) exciter, e)-g) R.E. generator coupling and h) pilot exciter.

intensity point measurements indicating the value of this alternative technique for source location.

The coherence technique was also investigated using pressure microphone signals as inputs. The influence of noise emission from the side ventilation grill of the pilot exciter was investigated by measuring the coherence between sound pressure at 10cm and 1m from the grill. The coherence Fig. 4.45a tends to 1 at 800 Hz and harmonics thereof and has some bands between 0.2 and 0.5. The coherence is higher than that for the cover vibration showing that it contributes to the sound pressure more significantly, but still lower than may be expected for such a clear relationship between cause and effect. This effect was noticed in [62] for a radial fan where only the discrete tones produced high coherence and the broadband noise coherence was commonly less than 0.1. This is due to the random nature of the broadband noise, although it may be more complex depending upon the variety of source mechanism causing this aerodynamic noise.

For the air makeup filter in the exciter enclosure there was a strong localised intensity of 105.8 dB(A). This was predominantly of broadband aerodynamic origin. The coherence between sound pressure measured at 10cm from the filter and the sound pressure at 40cm and also 1m from the filter is as plotted in Figs. 4.45b and 4.45c. The coherence for the 30cm microphone separation, Fig. 4.45b, has a large band of high coherence (>0.8) from 600 Hz to 1400 Hz as well as tones at 2281 Hz, 2406 Hz and 2706 Hz. The coherence has been reduced to less than 0.3 for the 90cm separation (Fig. 4.45c) due to incoherent sound from other sources. The high intensity low power, 88.7 dB(A), make-up filter contributes an estimated 85.8 dB(A) to the 91.6 dB(A) radial intensity at 1m, which correlates with the diminished coherence.

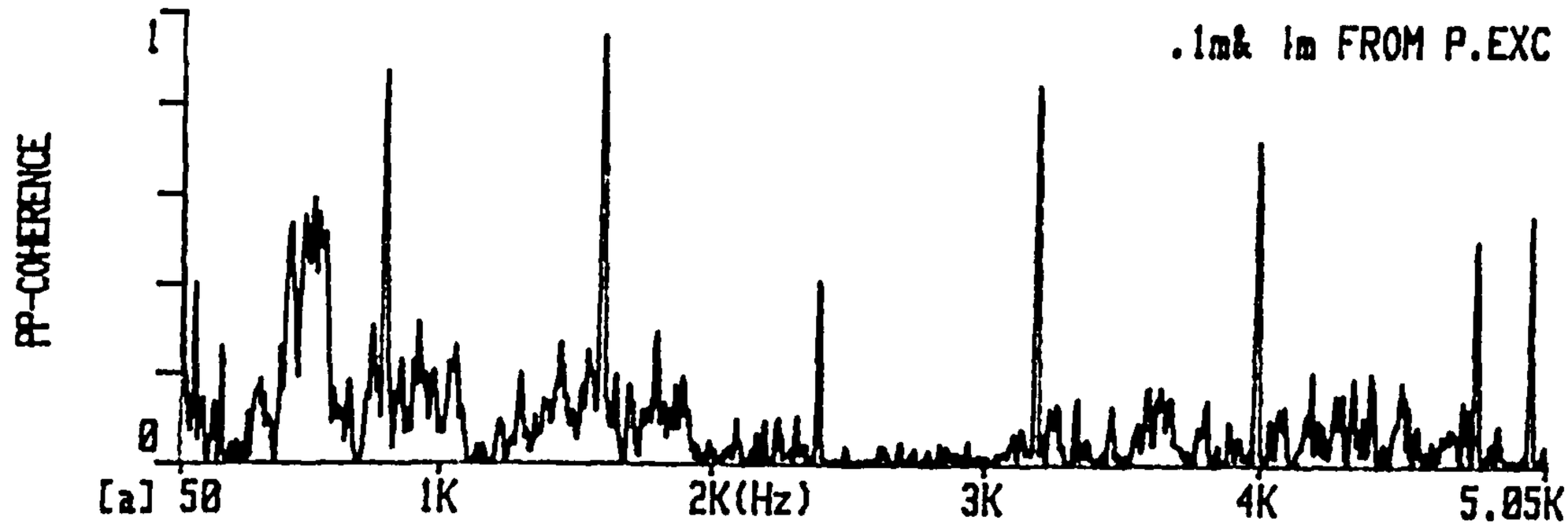

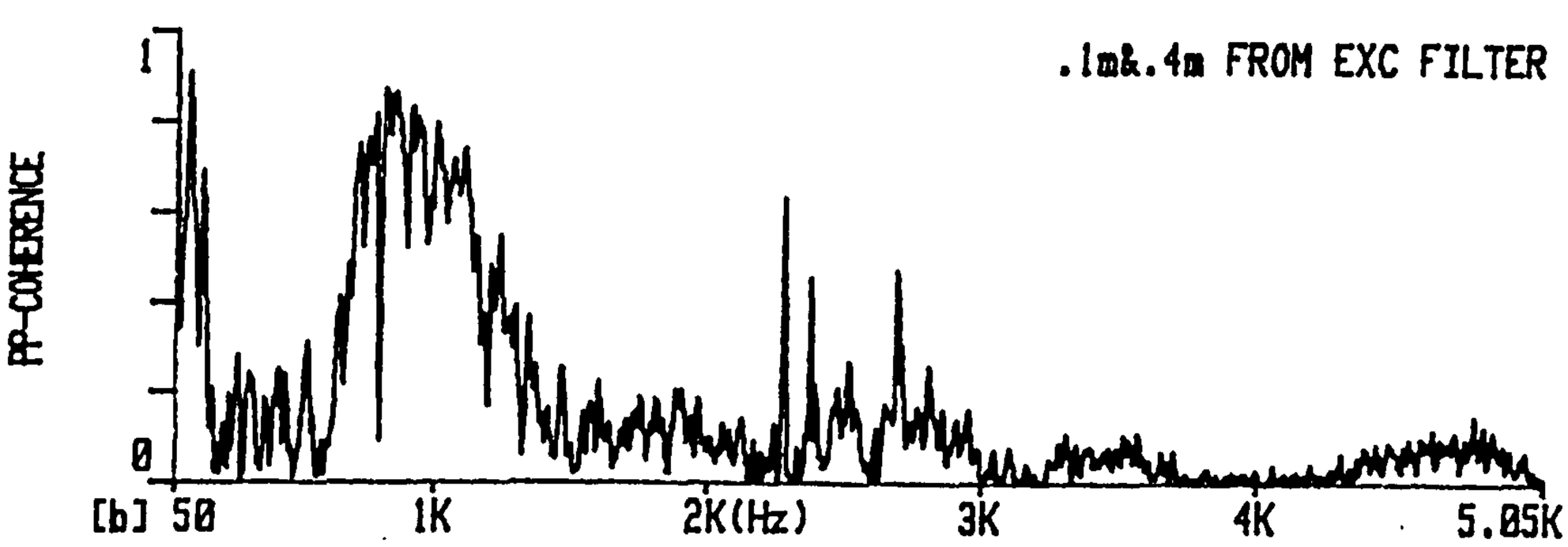

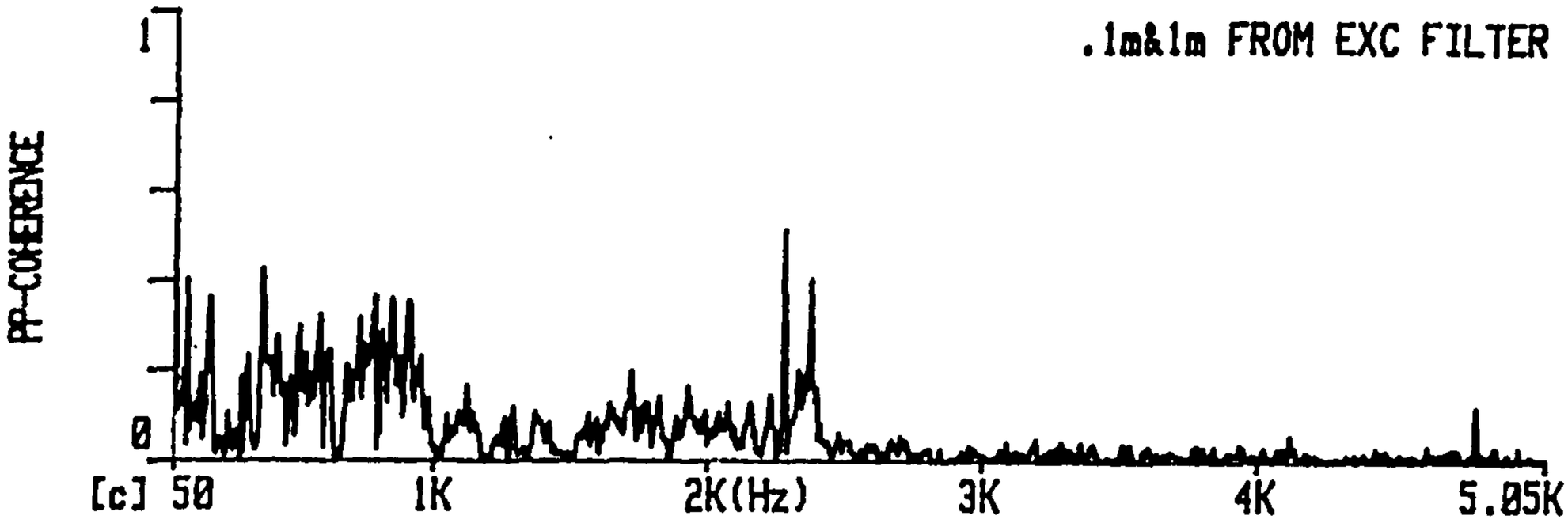

Fig.4.45 Narrowband coherence between sound pressure signals.

These results illustrate that sound pressure signals can act as valuable inputs identifying contributions to the farfield pressure. It should be pointed out that sound pressure signals can often be contaminated by noise components from many different items of equipment leading to inappropriate deductions about cause and effect being made. For aerodynamic noise coherence between nearfield and farfield pressures is also not necessarily high even when there is an obvious relationship in spectral similarity.

4.2.5 Sound pressure particle velocity coherence

The sound pressure particle velocity coherence measured at fixed points 0.1m from the generator centre is plotted for the frequency ranges 50-5050 Hz and 50-1050 Hz in Figs. 4.46a and 4.46b for a line bandwidth of 6.25 Hz. For comparison purposes the measurement was repeated with the finer spectral resolution of 1.25 Hz as illustrated in 4.46c. For all frequencies above 1 kHz the coherence is very low (<0.1) and only at a few discrete frequencies lower than 1 kHz does the coherence approach unity. As the coherence is low in general, especially above 1 kHz, and independent of spectral resolution, evident from comparing 4.46b and 4.46c, the field beside the generator is due to multi-source diffuse fields, with the generator making a relatively weak contribution. This is consistent with the low sound power and radial intensity measurements.

The coherence measured at 0.1m from the exciter centre was higher than that for the generator, but still generally low. The value is commonly between 0.15 and 0.5 for a number of tones throughout the frequency range 50-5050 Hz as illustrated in Fig.

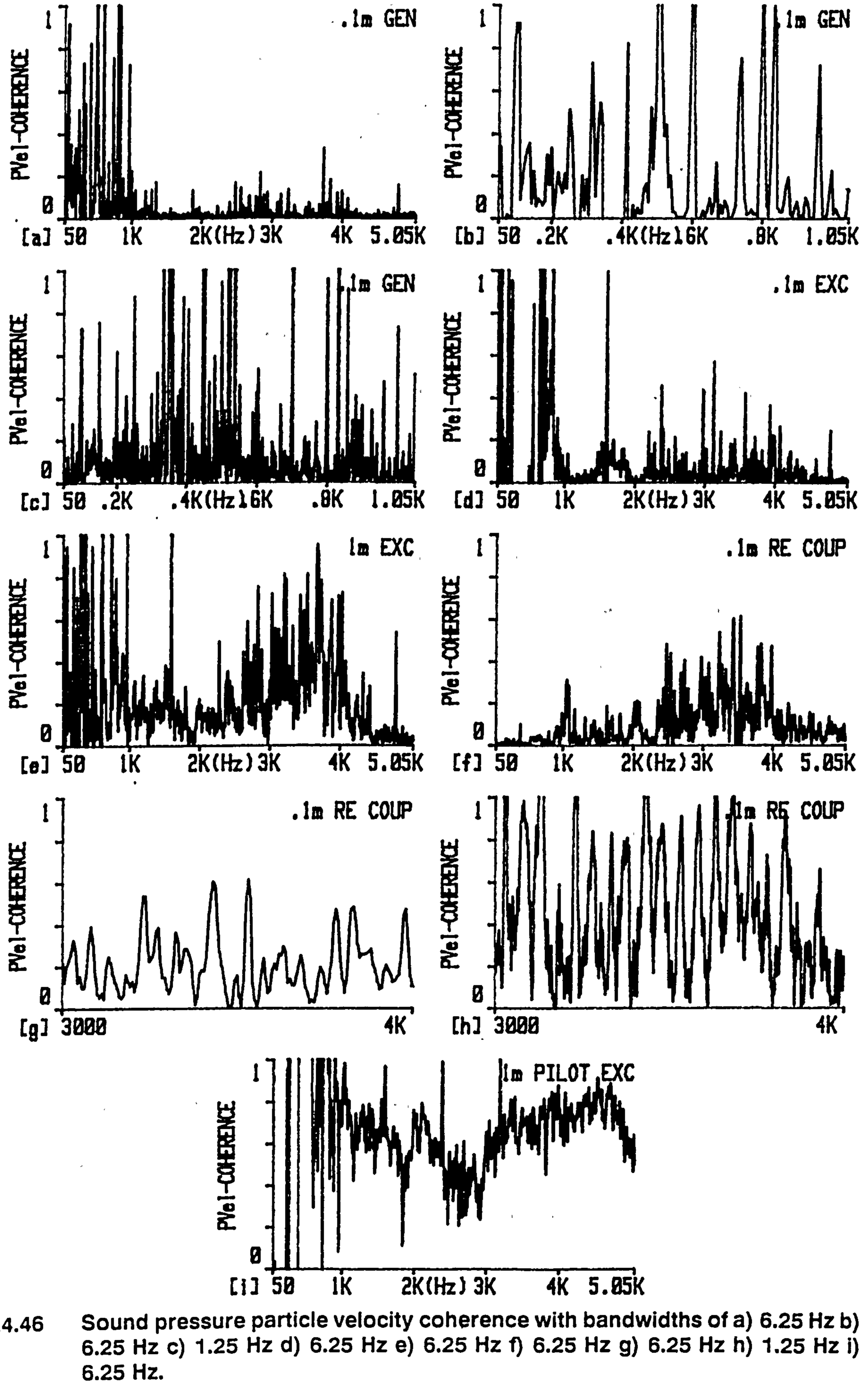

Fig.4.46 Sound pressure particle velocity coherence with bandwidths of a) 6.25 Hz b) 6.25 Hz c) 1.25 Hz d) 6.25 Hz e) 6.25 Hz f) 6.25 Hz g) 6.25 Hz h) 1.25 Hz i) 6.25 Hz.

4.46d. The coherence is invariant with spectral resolution. At 1m from the exciter the stronger direct background noise is not shielded by the exciter to the same extent. The coherence, which is greater than 0.8 for the coupling cover and pilot exciter tones, as illustrated in Fig. 4.46e, indicates that at 1m from the exciter there is a strong direct field, which will significantly raise the sound pressure level.

At a distance of 0.1m from the rear end generator coupling, the coherence has a value of 0.5 at frequencies coinciding with the sound power tones (Fig. 4.23c) for the 6.25 Hz measurement line bandwidth as seen in Figs. 4.46f and 4.46g. For the finer spectral resolution of 1.25 Hz the coherence has increased to 1 for the tones in the range 3 kHz to 4 kHz (Fig. 4.46h). The increase in coherence with decrease in spectral resolution is due to a bias error. This indicates that the coupling region between the generator and exciter bodies contains a reverberant field generated by one main source.

The coherence 1m from the pilot exciter side for this range 50-5050 Hz with a 6.25 Hz bandwidth is high, commonly greater than 0.7. This is illustrated in Fig. 4.46i. The coherence is invariant of spectral resolution indicating the field beside the pilot exciter is the strong direct field from one source. This is consistent with the high sound power and radial intensity measurements.

4.3 INVESTIGATION OF AIR COOLED GENERATORS

4.3.1 Generator investigation

The design and construction of large air-cooled generators differs from that of the hydrogen cooled generators discussed in sections 4.1 and 4.2 in a number of significant ways. From the acoustic viewpoint the most significant is the outer casing, as the

internal rotor and stator construction have similar profiles and dimensions. The hydrogen-cooled generator casing is in effect a thick (20-25mm) pressure vessel capable of not only retaining hydrogen at 4-5 bar pressure, but also in the unlikely event of an explosion. Instead the air cooled generators have a stand alone acoustic enclosure 10mm thick, mounted on the bedplate, which forms part of the ventilation circuit. The air-cooled generator layout is given in Fig. 4.47.

The noise emission of a 110MW generator was investigated. The internal pressure measurements conducted at full load yield not only an appreciation of typical internal levels, but also from the spectral content, speed dependence and variation with load insight into generator source mechanisms. External sound intensity measurements were not conducted due to the limitations imposed by the background noise similar to the hydrogen cooled units presented in 4.1.

4.3.1.1 Internal sound pressure measurements

The internal generator acoustic enclosure sound pressure was measured at one location 1.5m above shaft centre line in the rear end rotor inlet duct as indicated in Fig. 4.47. The microphone employed was of the ½" pre-polarized B & K type 4155 with a foam windshield, which was suitable for the air temperature and velocity. The location was chosen to give a representative level for the cover as a whole. The microphone was reasonably close to the major aerodynamic sources the axial fan and rotor endwinding region.

The sound pressure level measured for full open circuit voltage was 112.8 dB(A) and 122.3 dB(lin) with octave levels tabulated as follows.

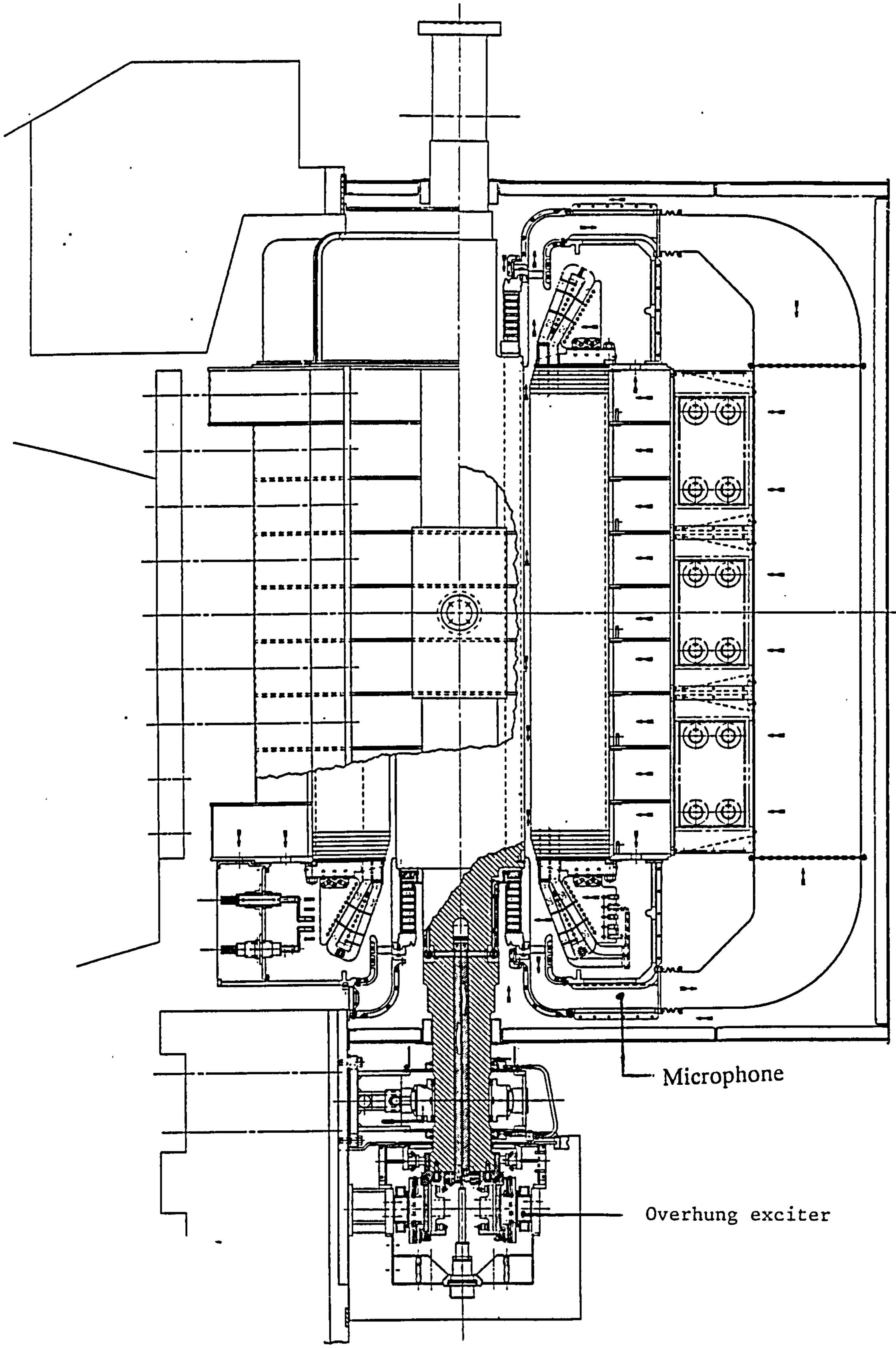

Fig.4.47 Large air cooled generator and overhung exciter layout.

	Octave band centre frequency (Hz)										
	31.5	63	125	250	500	1K	2K	4K	8K	16K	Overall
Sound pressure level dB(lin)	112.9	116.8	118.6	112.3	107.9	107.6	104.5	102.6	94.0	84.8	122.3
Sound pressure level dB(A)	73.9	90.8	102.6	103.3	104.9	107.6	105.5	103.6	93	77.8	112.8

Table H : Measured internal octave sound pressure levels in 110MW air-cooled generator

The narrowband A weighted sound pressure spectra in the frequency ranges 50-5050 Hz, 20 Hz - 20 kHz and 20-1020 Hz measured on full open circuit voltage is illustrated in Figs. 4.48a to 4.48c respectively. The source mechanisms will be discussed in more detail in section 5.2, but it is readily apparent due to the predominantly broadband nature of the spectra, that the main noise generation is related to aerodynamic effects especially vortex shielding and unsteady flow effects. A number of tones commonly 3 dB greater are superimposed on the broadband noise. The 100 Hz tone level of 100 dB(A) is increased by 4 dB by electrical loading, however by comparing the load and no load spectra in Figs. 4.48a and 4.48d respectively, the remainder of the spectrum and the overall dB(A) S.P.L. are unaltered. Tones exist at blade passing frequencies of 1150 Hz and harmonics thereof but are of relatively low magnitude.

At other frequencies corresponding to half wavelengths of the duct dimensions acoustic resonances are evident e.g. 660 Hz, 855 Hz and 1068 Hz. The existence of these frequency components is independent of the rotational speed, as is evident from Figs. 4.48d to 4.48f, but the actual magnitude is dependent on the acoustic "excitation"

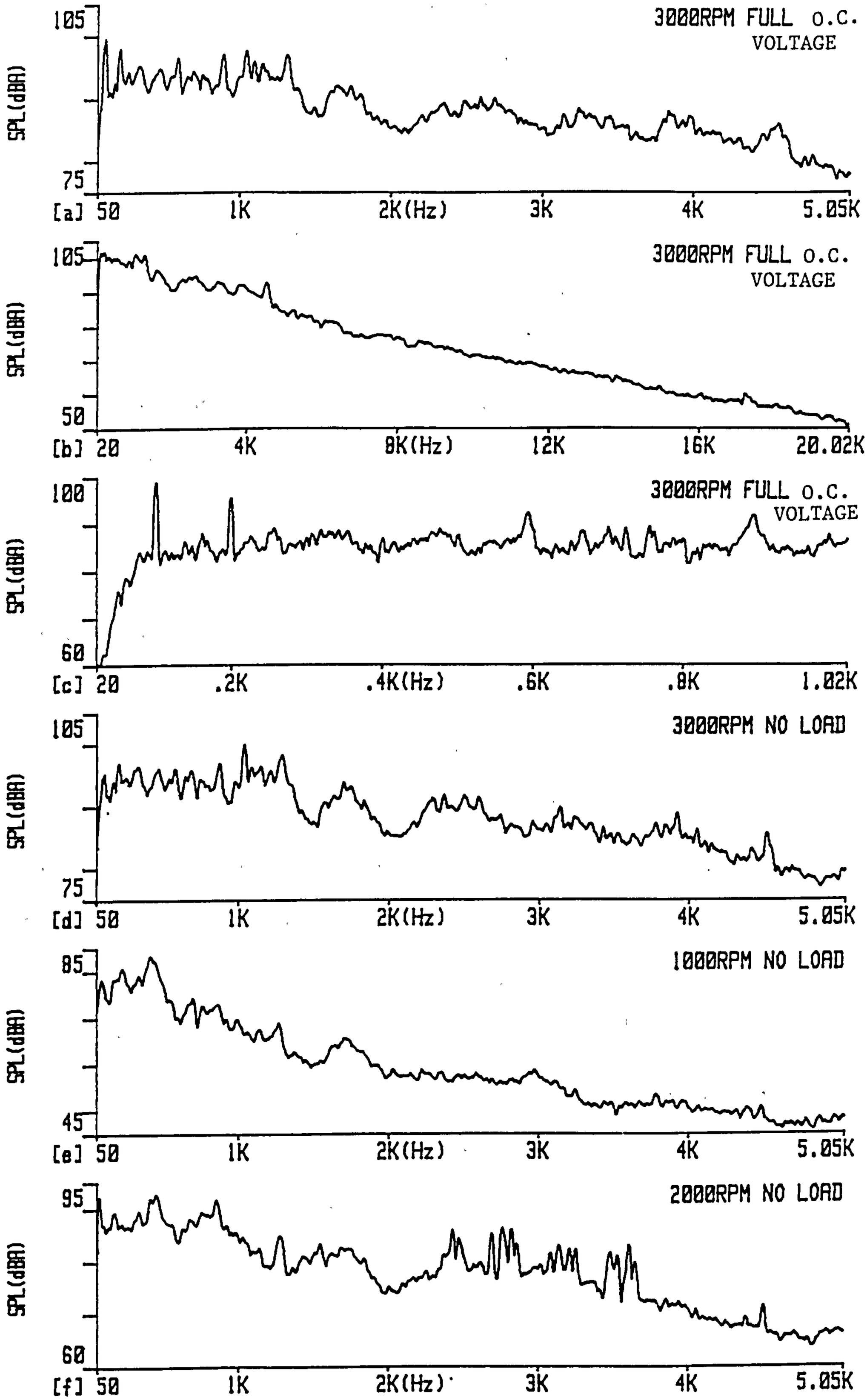

Fig.4.48 Large air cooled generator internal sound pressure levels.

spectra, which is speed dependent. The fibre glass ducting and the acoustic treatment lining the enclosure damp these resonances down so that they do not have a major influence on the overall noise level.

The variation in sound pressure level with rotational speed is given in Fig. 4.49. The A-weighted level varies as a 4.8th power of velocity and the unweighted level varies as a 3rd power of velocity. The difference is due to the shift of low frequency noise to the audible range as the velocity increases. The power of velocity is similar to the 5th power measured by Hübner[20] for induction motor rotors. From these graphs it is possible to scale the measured levels for larger diameter rotors and 60 Hz generators.

4.3.2 Exciter investigation

An alternative excitation system construction to that considered in sections 4.1 and 4.2 is the overhung brushless exciter as illustrated in Fig. 4.47. The arrangement is appreciably more compact with the rotating rectifier on a hub inside the exciter rotor. The noise emission was investigated without the unit's separate acoustic enclosure fitted. This enables source strength to be quantified and from the measurement spectra on full load and no load conditions much can be evaluated about the source mechanisms. Source identification was supplemented with sound intensity measurement without the exciter cooler attached. This facilitated direct field measurements to be made on the exciter. Measurements on the exciter/generator coupled running enabled accreditation of the contract F.E. exciter enclosure sealing baffle.

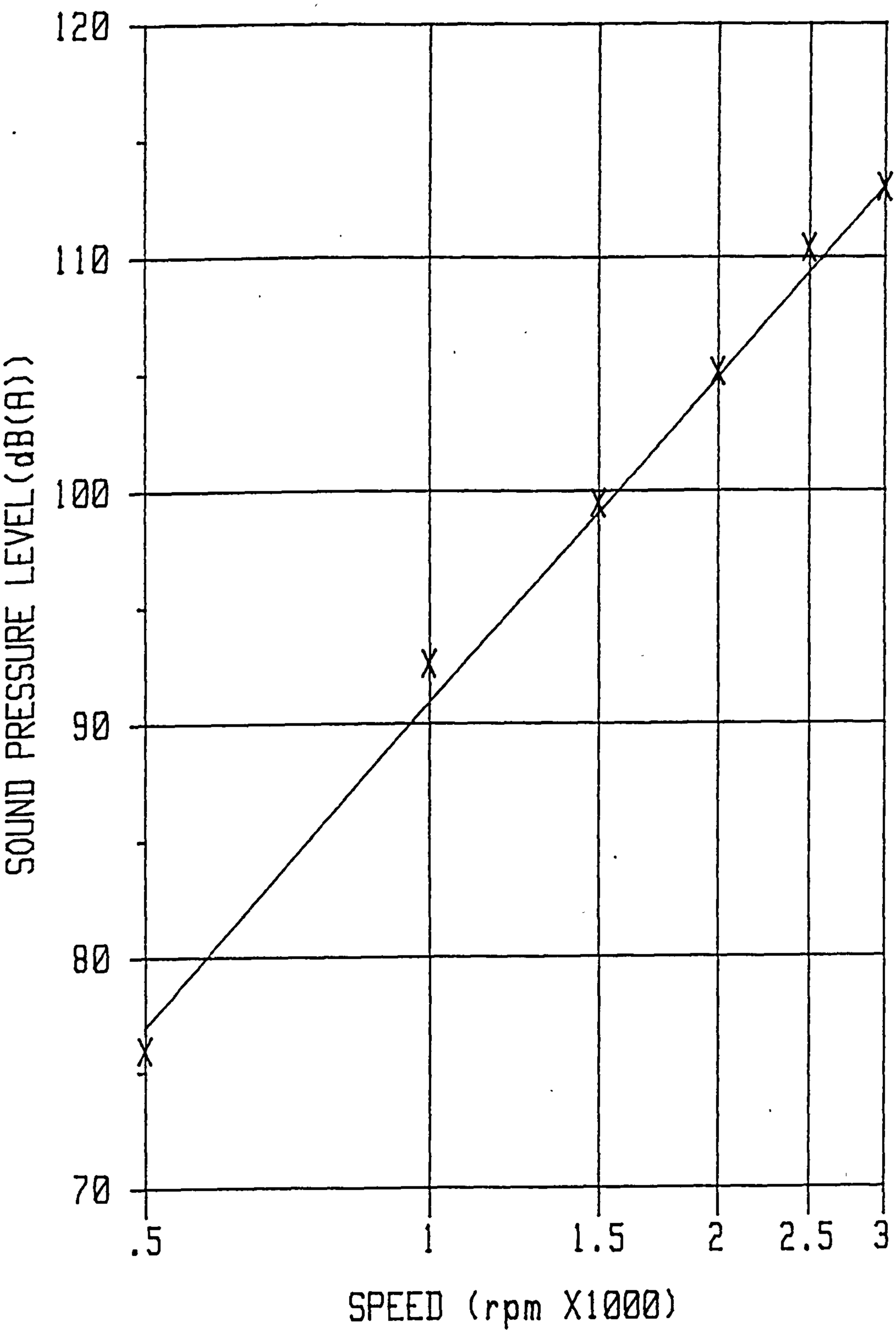

Fig.4.49 Variation of internal sound pressure level with rotational speed.

4.3.2.1 **Sound power determination without acoustic cover fitted**

The noise emission from one overhung brushless exciter, used to provide the field current to a 110MW air cooled generator, was measured during factory testing. Large ratings up to those necessary for 1300MW generators can be achieved from similar compact exciters by using hydrogen as the cooling medium. The test arrangement is similar to that for other exciters tested in the factory reported in section 4.1 (Fig.4.10). The temporary test brushgear is a less predominate background noise source as the lower power rating output from the exciter does not require forced cooling from a fan. The R.E. brushgear coupling, however, contains large boltheads, which represent a more significant noise source. The contract F.E.exciter sealing baffle was replaced by a wooden one for test purposes altering it's noise emission characteristics.

The exciter sound power level was determined by enclosing the unit with 30 scan measurements during full load operation. Background influences including the F.E. exciter temporary wooden baffle, the test brushgear and the R.E. test brushgear coupling were also quantified as outlined in the following section. In general sound power determination was less difficult than on the previous factory exciter case study, in section 4.1.2. The direct flow of sound from the main background noise source, the R.E. brushgear coupling was shielded from the exciter by the brushgear housing itself. Experimental practice aimed to maximise this and also shield acoustic flow from the F.E. sealing baffle from other measurements. The measurement situation was further improved by the exciter output being greater improving the signal (source strength) to noise ratio and also by the microphone pair used having substantially better phase mismatch characteristics (see section 3.3.4.2).

The sound power levels for the exciter and it's constituent regions, as well as the principal background noise sources, are summarised in table I for full load operating conditions. The overall sound power level for the exciter unit excluding measurements on the temporary F.E. baffle was 104.0 dB(A). The measured sound power spectrum, Fig. 4.50a, is mainly positive with a limited number of negative tones. The overall level is significantly contributed to by a 3.5 kHz tone with a magnitude of 99.3 dB(A). The spectrum also contains tones at 800 Hz with harmonics thereof and 1175 Hz with tones at 800 Hz multiples of this. Phase correction has a limited influence on the spectral composition, Fig. 4.50b, and the overall level, which is only raised by 0.2 dB on application of eqn. (A.7). The detailed discussion of source mechanisms will be presented in section 5.2.

Region	Net sound power level in dB(A)
complete exciter excluding temporary F.E. baffle	104.0
pilot exciter	98.6
main exciter	87.2
endcover	99.4
cooler	99.5
temporary F.E. baffle	104.8
temporary test brushgear	103.6
R.E. brushgear coupling	111.7
jury shaft coupling	100.3
contract F.E. baffle	99.3

Table I : Summary of full load overhung exciter sound power measurements

The sound power spectra of the exciter constitute regions are given in Figs. 4.50c-f. In general the sound power spectra for the pilot exciter, endcover and cooler and the overall levels 98.6 dB(A), 99.4 dB(A) and 99.5 dB(A) respectively are similar, which

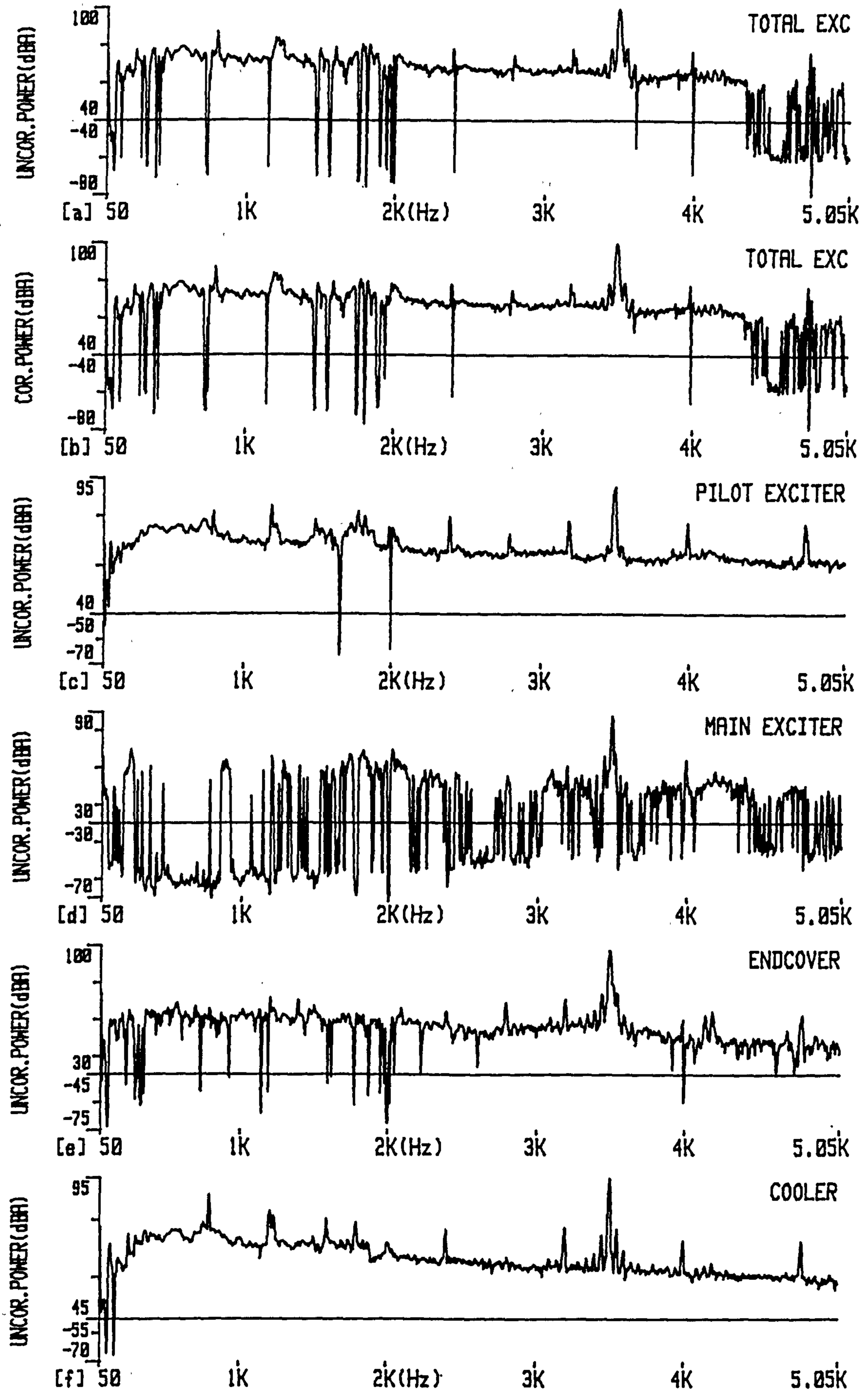

Fig.4.50 Narrowband sound power level for overhung exciter and constitute items.

is to be expected as the plant items are closely situated and there is little internal partitioning. The 3.5 kHz tone is prominent for all components. The tonal components are less prominent in the endcover spectrum as it is slightly further from the pilot exciter frame. The main exciter level is noticeably lower being 87.2 dB(A) with a spectrum denoting low levels of bidirectional flow except at 3.5 kHz, which determines the overall level, Fig. 4.50d.

For the reasons outlined earlier in this section the potential problems due to extensive background noise are not as severe as encountered on previous factory tests. This is reflected by the measurement indicators and subsequent error limits. F_3 is less than 18 dB for the majority of the frequency bands, Fig. 4.51a. F_3 exceeds the residual pressure intensity index in only one 1/3 octave and the difference is commonly 15 dB (Fig. 4.51b) implying low phase mismatch errors. This results in error limits, above 200 Hz, of ±0.4 dB (Fig. 4.51c). The relatively low phase mismatch error is consistent with the small effect of applying the phase mismatch correction. The spatial sampling error, as calculated approximately from eqn. (3.9), is plotted in Fig. 4.51d. This is not strictly correct for the scanning technique, but still serves as a reasonable indication of this error, which is less than 1.25 dB for most bands.

The sound power was not determined for the complete exciter on no load, but the influence of electrical forcing is still clear from partial sound power measurements conducted in some areas. Comparison of the no load (Fig. 4.52a) and full load (Fig. 4.52b) sound power spectra on the R.E. of the endcover illustrate the majority of the spectral composition is identical with the notable exception being the 3.5 kHz tone. The difference in power levels of 86.6 dB(A) on no load and 97.1 dB(A) on full load

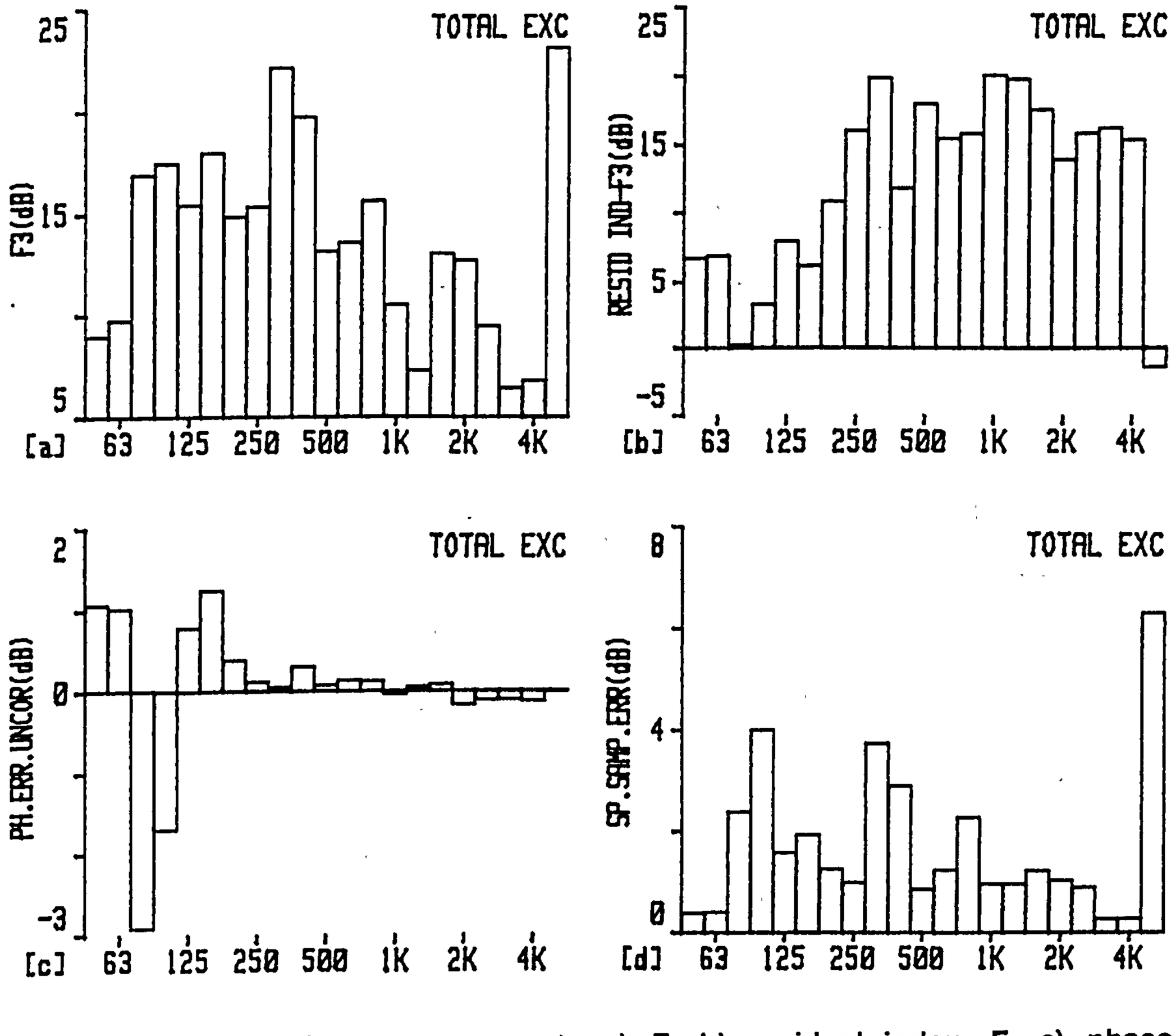

Fig.4.51 Overhung exciter measurements a) F_3 b) residual index $-F_3$ c) phase mismatch error d) spatial sampling error.

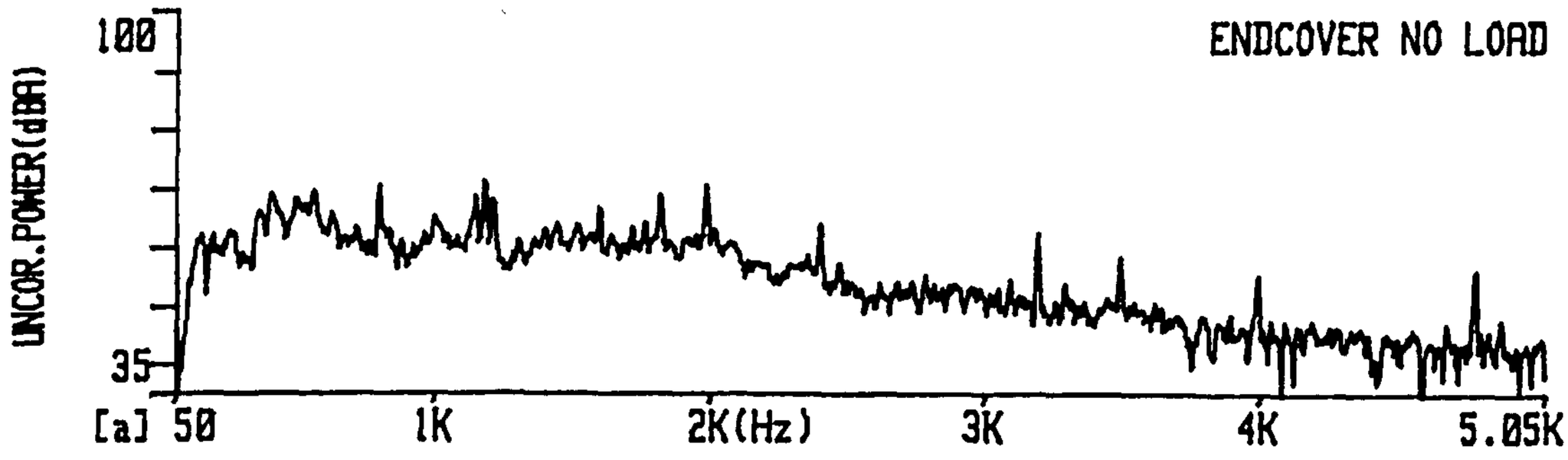

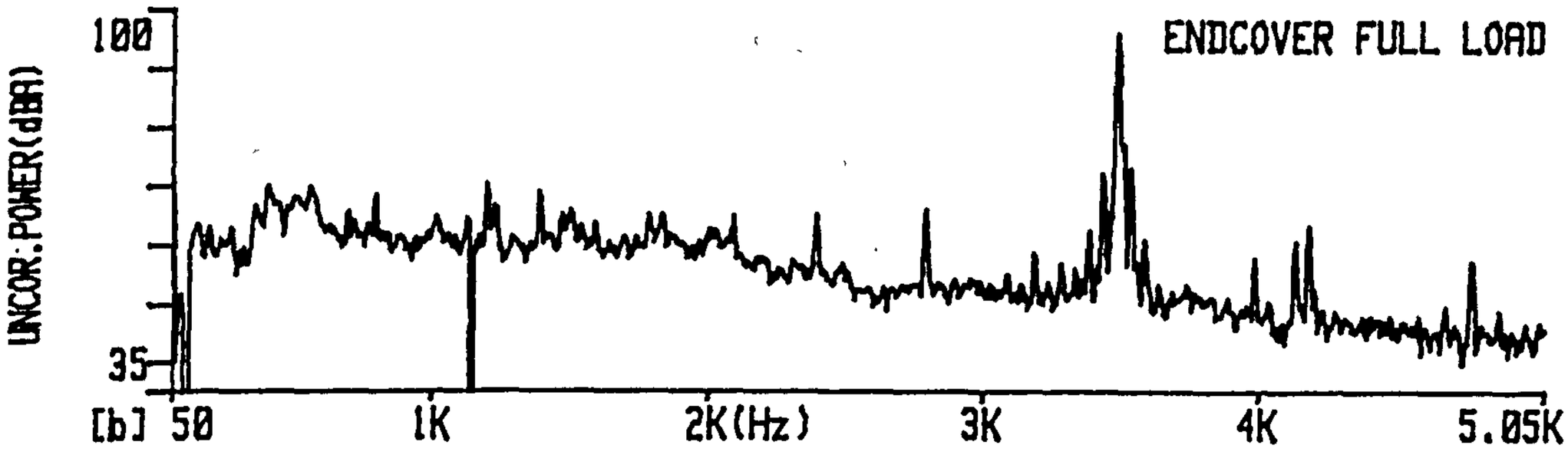

Fig.4.52 Narrowband sound power level for R.E. cover a) no load b) full load.

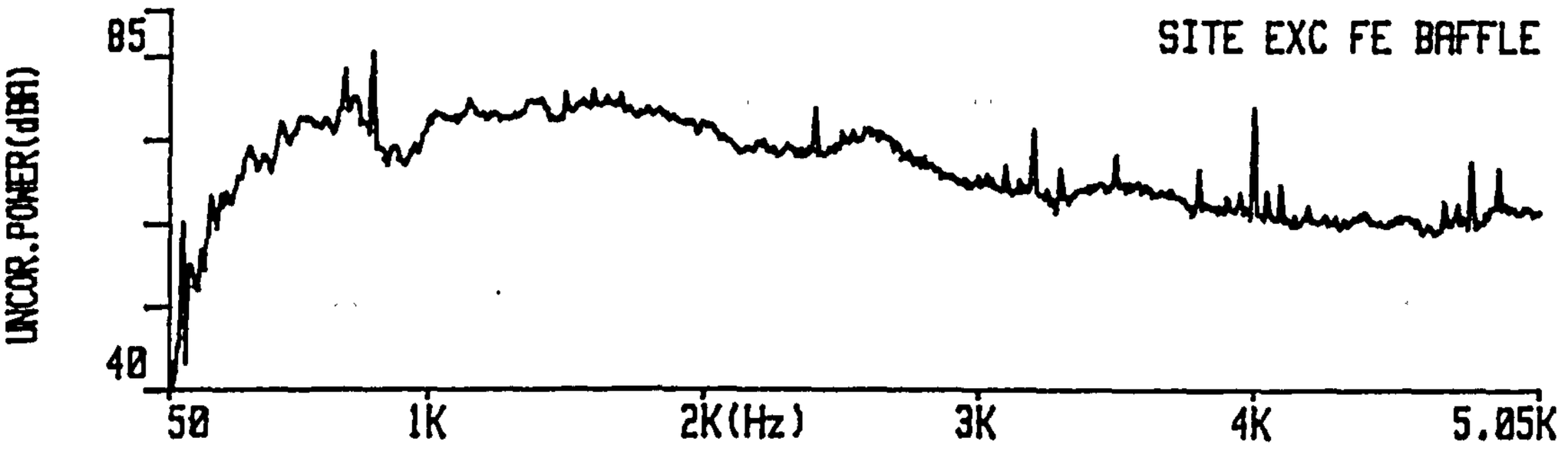

Fig.4.53 Narrowband sound power level for contract F.E. exciter baffle plate.

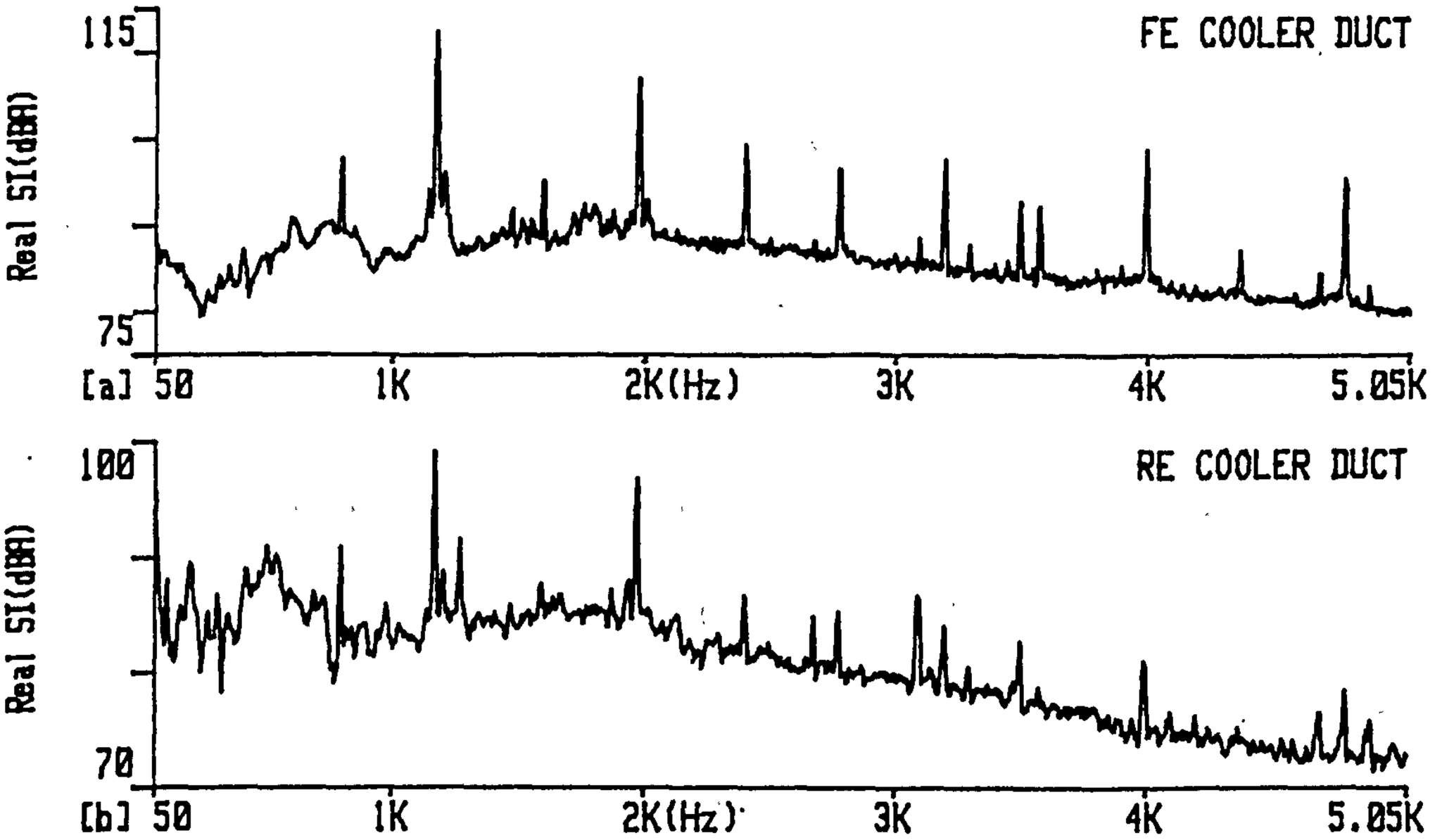

Fig.4.54 Narrowband radial sound intensity from cooler ducts a) F.E. b) R.E.

is almost solely due to the 3.5 kHz tone. The influence of the 3.5 kHz tone is apparent in all the narrowband spectra, Figs. 4.50a-f, and it contributes approximately 40% of the total sound power level for the exciter unit of 104.0 dB(A).

There was a large noise emission from the temporary F.E. baffle of the exciter enclosure of 104.8 dB(A), so this level was considered as a separate entity. On a later test the sound power was measured from the actual site contractual baffle during running with the exciter/generator coupled. The overall sound power level was 99.3 dB(A) with a spectrum (Fig. 4.53), which is basically broadband with superimposed tones at 800 Hz and harmonics thereof.

4.3.2.2 Sound intensity measurements without the coolers attached

Limited intensity measurements were conducted with the exciter coolers disconnected to assist with noise source identification on no load operation. 30cm from the R.E. duct opening the sound pressure was 113 dB(A) and the radial intensity was 110.6 dB(A), which is a power output of 105 dB(A). 30cm from the F.E. duct opening the sound pressure was 118.8 dB(A) and the radial intensity was 117.3 dB(A), which is a power output of 111.7 dB(A). At 1m from the F.E. duct the sound pressure was 115.3 dB(A) and the radial intensity was 114.2 dB(A). The sound intensity spectra for the front and rear end ducts are illustrated in Figs. 4.54a and 4.54b.

4.4 FACTORY TESTS INVESTIGATION INTO DESIGN CHANGES TO PILOT EXCITER AND R.E. GENERATOR COUPLING

It has been illustrated, in section 4.2 for a 660MW generator unit, with a layout given in Fig. 4.20, that the pilot exciter and R.E. generator coupling had significant noise output. New covers have been designed for these components as illustrated in Figs.

4.55 and 4.56.

The performance of these new designs was investigated by quantifying sound power emission and relating this emission to S.P.L. at 1m. To make this work compatible with earlier analysis at site the F.E. exciter coupling will be referred to as the R.E. generator coupling.

The test arrangement is identical to that used for the 350MW exciter illustrated in Fig. 4.10. The F.E. generator coupling site sealing baffle was replaced by a wooden one for test purposes so it's performance should be carefully monitored. Tests were conducted with the pilot exciter on open circuit as the primary source mechanisms were aerodynamic and the permanent magnets will still induce stator vibration. The F.E. exciter coupling will generate similar noise levels to the site R.E. generator coupling arrangements.

4.4.1 Sound power determination

The sound power level was determined for the pilot exciter and R.E. generator coupling by completely enclosing both components with 28 and 6 sound intensity scan measurements respectively.

The overall sound power levels and those for different constitute areas of each component are summarised in table J. The total pilot exciter sound power level was measured as 95.3 dB(A). The narrowband sound power spectrum illustrated in Fig. 4.57a has the characteristic tonal components of 800 Hz and harmonics thereof evident for the original cover (Fig. 4.23d), but these are substantially reduced in magnitude. The opening at the pilot exciter F.E. to facilitate cooling air to enter the

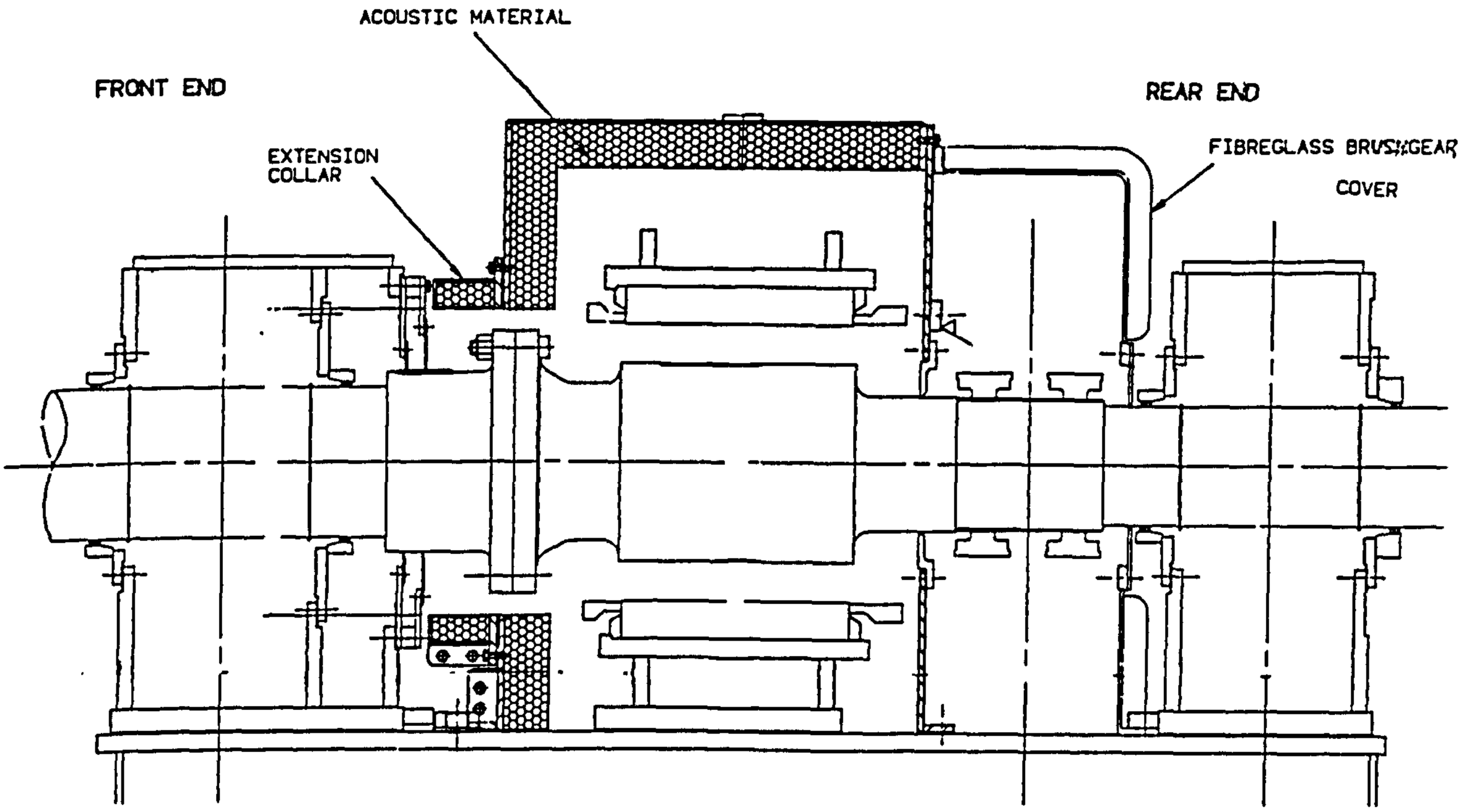

a) side view

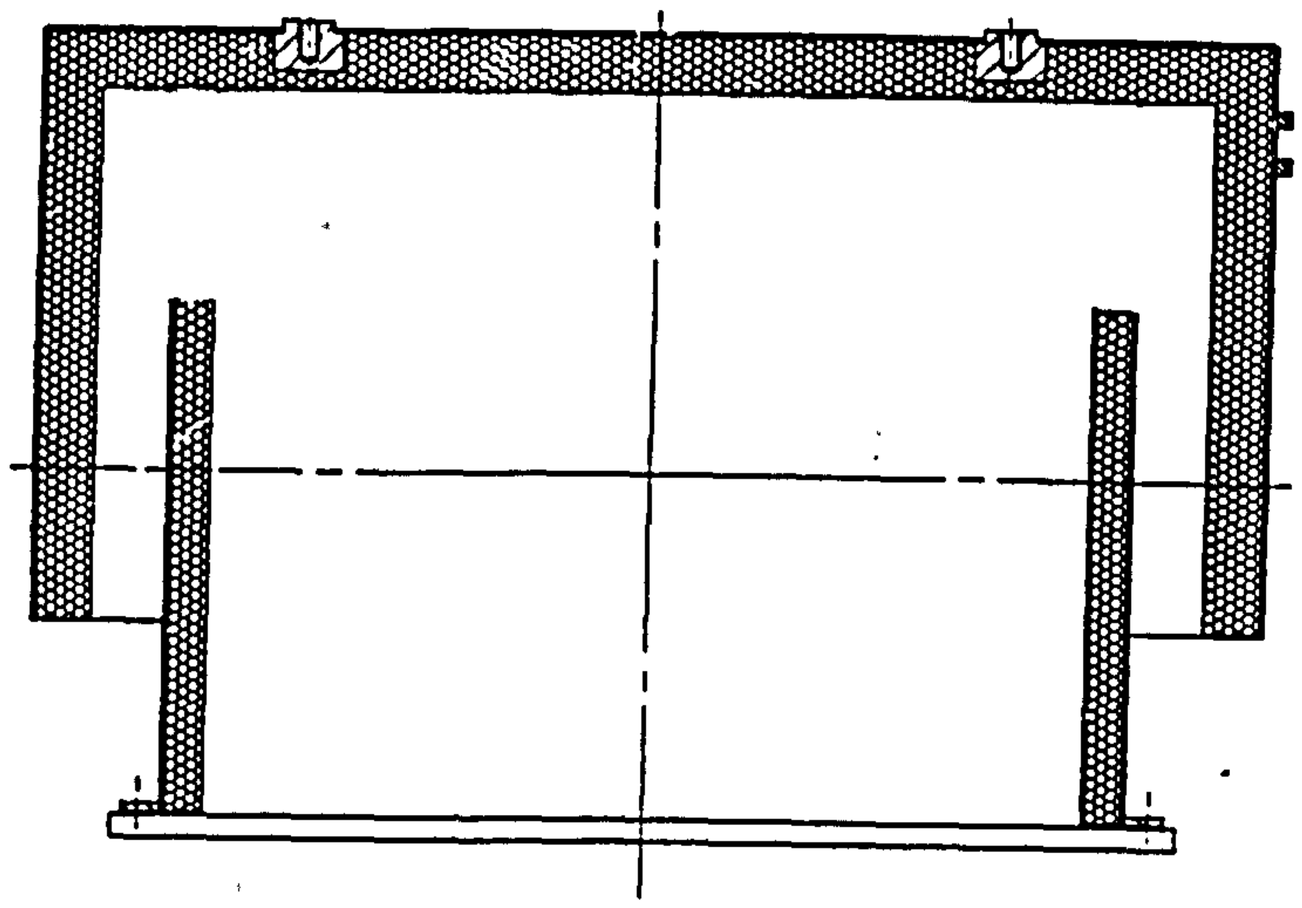

b) front view.

Fig.4.55 Pilot exciter acoustic cover

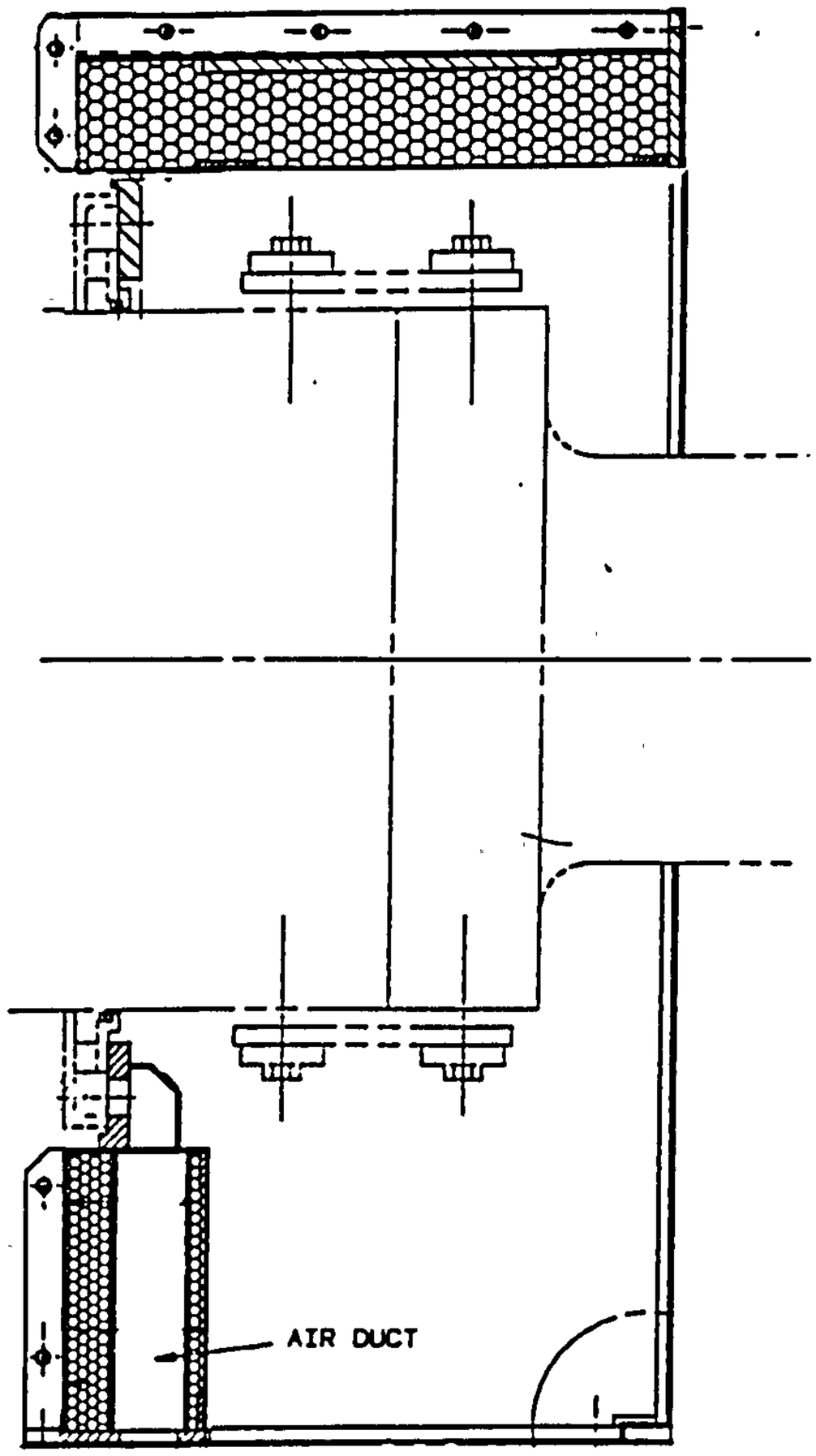

Fig.4.56 R.E. generator coupling acoustic cover.

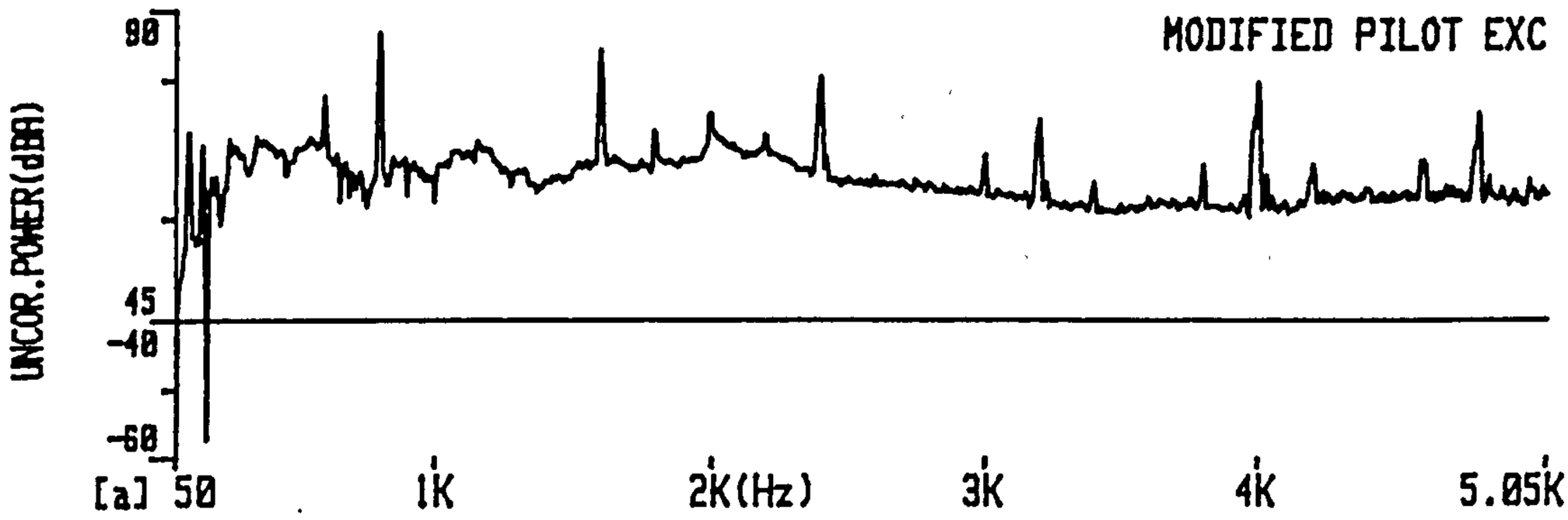

Fig.4.57 Narrowband sound power level for a) pilot exciter b) R.E. generator coupling.

enclosure contributes 94.2 dB(A) sound power output to the total figure. Relatively little noise is emitted from the enclosure's outlet ventilation ducts, 83.3 dB(A), indicating that the baffling arrangement has been successful. From the remainder of the pilot exciter enclosure the emission is 88.1 dB(A). 98.6 dB(A) sound power was emitted from the R.E. generator coupling of which 96.3 dB(A) emanated from the front face comprised of a temporary wooden baffle. The narrowband sound power spectrum plotted in Fig. 4.57b is predominantly broadband with tonal components at 100 Hz and harmonics thereof and a tonal component at 800 Hz of 92.7 dB(A).

Region	Net sound power level in dB(A)
Complete pilot exciter	95.3
Pilot exciter F.E. shaft	94.2
Pilot exciter side ducts	83.3
Pilot exciter enclosure excluding openings	88.1
Instrument slipring cover	81.8
R.E. generator coupling cover	98.6

Table J : Net sound power levels for modified 660MW pilot exciter and R.E. generator coupling covers

Measurement accuracy can be assessed from the field indicator F_3. F_3 for the pilot exciter, Fig. 4.58a, is less than 7.5 dB for all 1/3 octaves above 200 Hz implying low phase mismatch errors of ±0.2 dB, Fig. 4.58b. The predicted random spatial sampling error for the 28 area measurements was ±2.5 dB for most 1/3 octaves, Fig. 4.58c. This error is overestimated as it is raised by measurements on the F.E. grill, which should be correctly measured because of the grid definition. The error for the

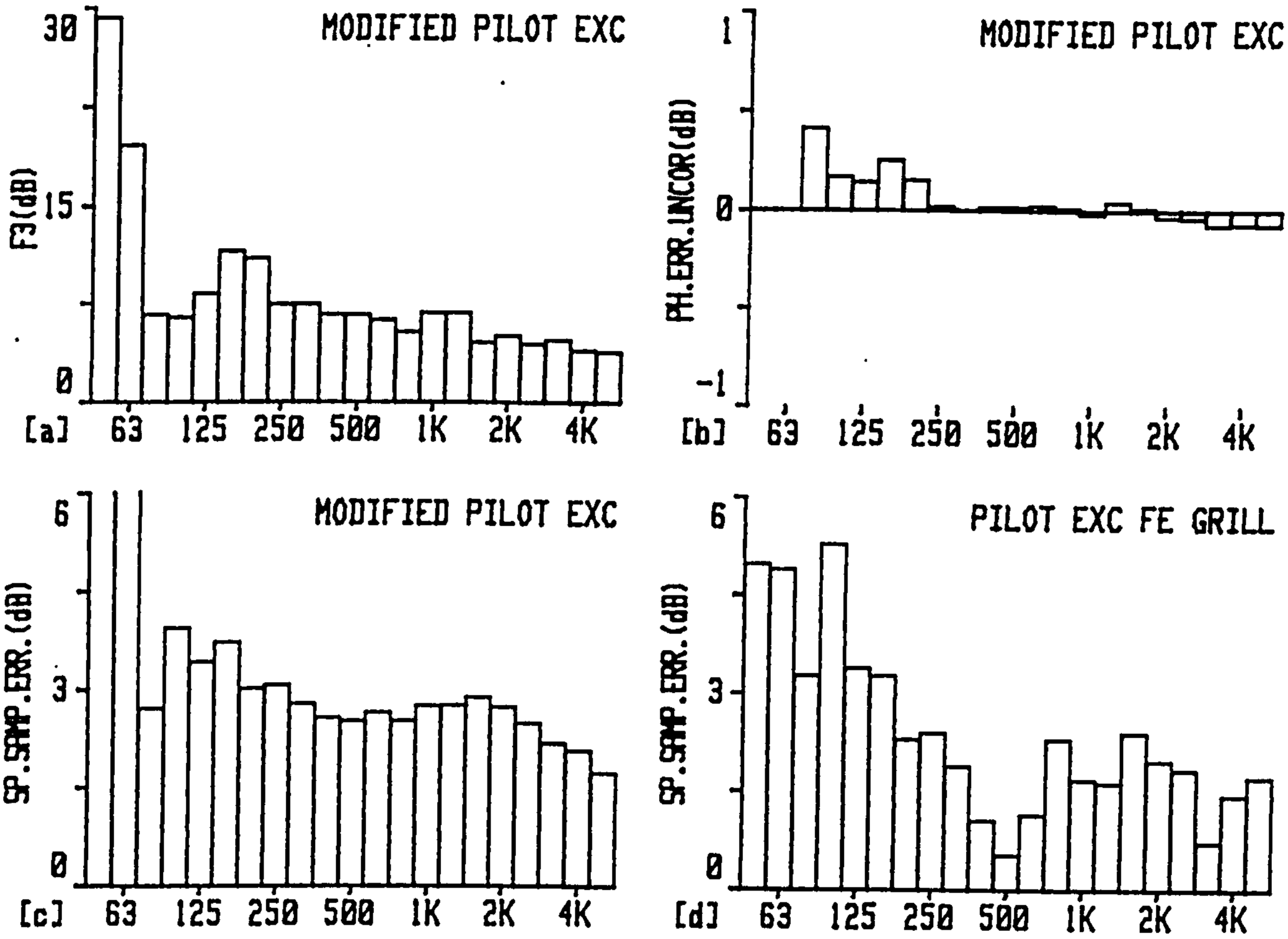

Fig.4.58 Pilot exciter measurements a) F_3 b) Phase mismatch error & spatial sampling error for c) all measurements d) F.E. grill measurements only.

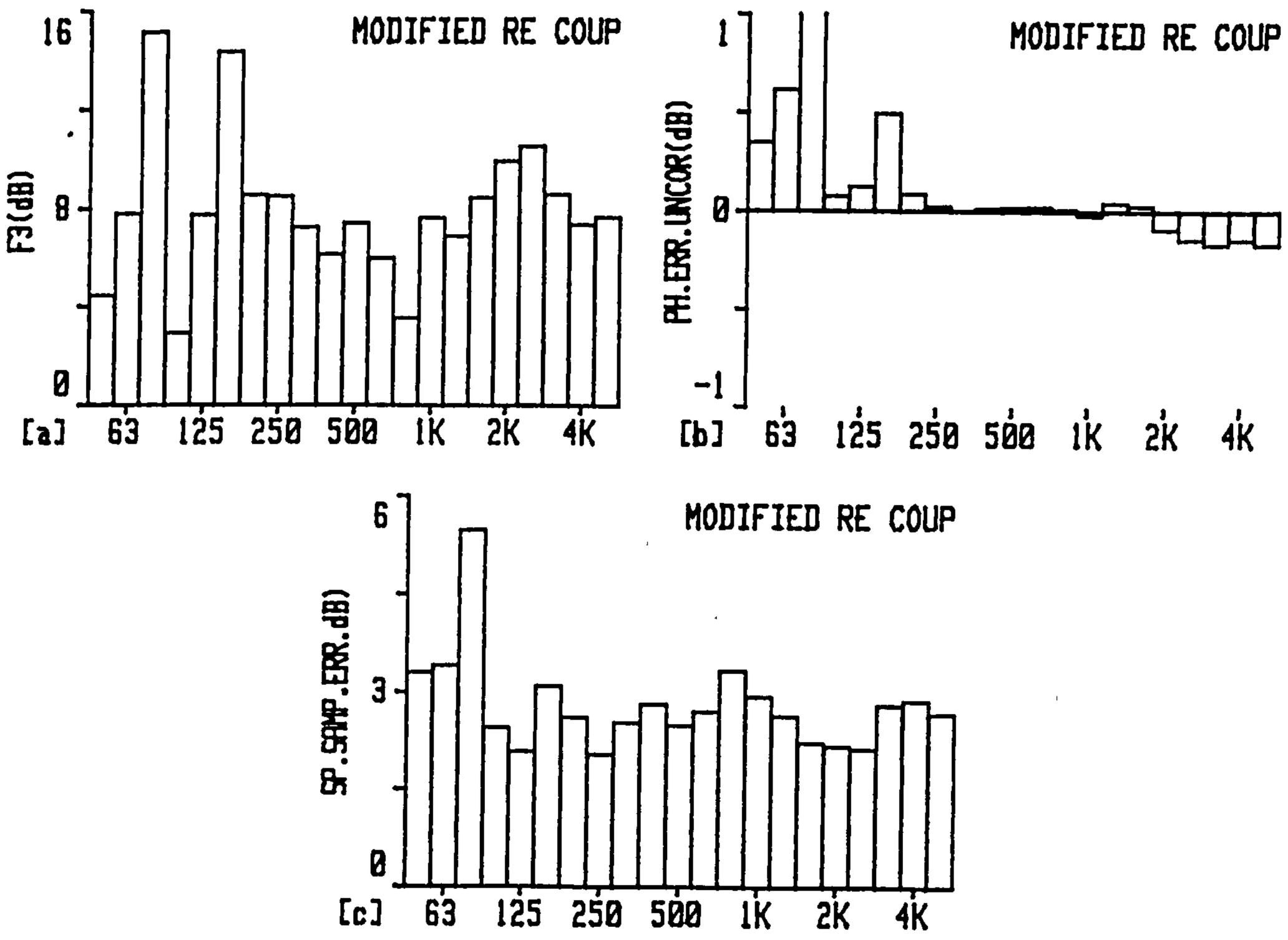

Fig.4.59 R.E. generator coupling cover a) F_3 b) phase mismatch error c) spatial sampling error.

F.E. grill is ±1.5 dB as indicated by Fig. 4.58d, which should represent the total error for the pilot exciter as phase mismatch is relatively inconsequential.

For the R.E. generator coupling cover $F_3 < 10$ dB for all 1/3 octaves above 200 Hz, Fig. 4.59a, implying a phase mismatch error of ±0.2 dB, Fig. 4.59b. The spatial sampling error indicated in Fig. 4.59c will tend to ±2.5 dB, which is liable to an overestimation. All measurements were repeatable to within 1 dB and both the pilot exciter and R.E. generator coupling sound powers were reproduced to within 0.4 dB on repetition a second time suggesting an overestimation in sampling error for scanned measurements from the spatial variance used in eqn. (3.9).

The sound power levels can be approximately related to free field sound pressure using the wave divergence formula, eqn. (3.10). 1m from the pilot exciter the 95.3 dB(A) sound power relates to a free field sound pressure of 82.2 dB(A). The R.E. generator coupling sound power of 98.6 dB(A) relates to a free field sound pressure of 88.2 dB(A) 1m from the exciter F.E. The actual sound pressure can be increased by a number of factors. For small strong sources, relative to the exciter and generator dimensions, the geometric error and power absorption are insignificant. Only the estimated reverberation of 4.5 dB for the pilot exciter and 1.5 dB for the R.E. generator coupling, estimated in section 4.2.2.3, are important. The uniform acoustic emission assumption made in using (eqn. 3.10) is not correct for the pilot exciter, because of the high levels of emission from the compact F.E. shaft opening. This is discussed in the following section.

4.4.2 **Point sound intensity vector measurements**

The S.P.L. 1m from the pilot exciter was 94.3 dB(A) with a narrowband spectrum as

illustrated in Fig. 4.60a. The direct sound intensity radial and axial components are 86.6 dB(A) and 88.0 dB(A) respectively, representing a total contribution to the S.P.L. of 88.9 dB(A). As expected due to the reduced pilot exciter sound power emission the sound pressure spectrum (Fig. 4.60a) is noticeably different to that at site, Fig. 4.43d. This in part is due to the effectiveness of the re-designed cover and also the contribution of background noise from the temporary test brushgear, half of which outputs 105.5 dB(A) sound power, discussed in section 4.1.2.3. The influence of background noise on S.P.L. is reflected by some differences in spectral composition between sound pressure (Fig. 4.60a) and radial sound intensity (Fig. 4.60b).

The intensity of the F.E. pilot exciter gap between the collar and bearing was high, but because of the small area the sound power is reasonably small minimising it's ability to emanate to the far field. The magnitude of radial sound intensity decreased markedly with distance from the gap with a value of 100.5 dB(A) at 5cm, 94.3 dB(A) at 50cm, 89.8 dB(A) at 1m and 88.0 dB(A) level with the gap 1m from the pilot exciter cover.

The S.P.L. of 102 dB(A) 1m from the R.E. generator coupling is contributed to by the temporary brushgear. The strong flow from both sources is indicated by the axial intensity beside the R.E. brushgear pedestal, which contains many bi-directional components, Fig. 4.60c.

4.4.3 Composition of sound pressure level at 1m

The pilot exciter free field S.P.L. at 1m was predicted from the measured sound power as 82.2 dB(A), which would be raised by reverberation effects by approximately 4.5 dB to 86.7 dB(A). The measured sound intensity 1m from the pilot exciter had a vector

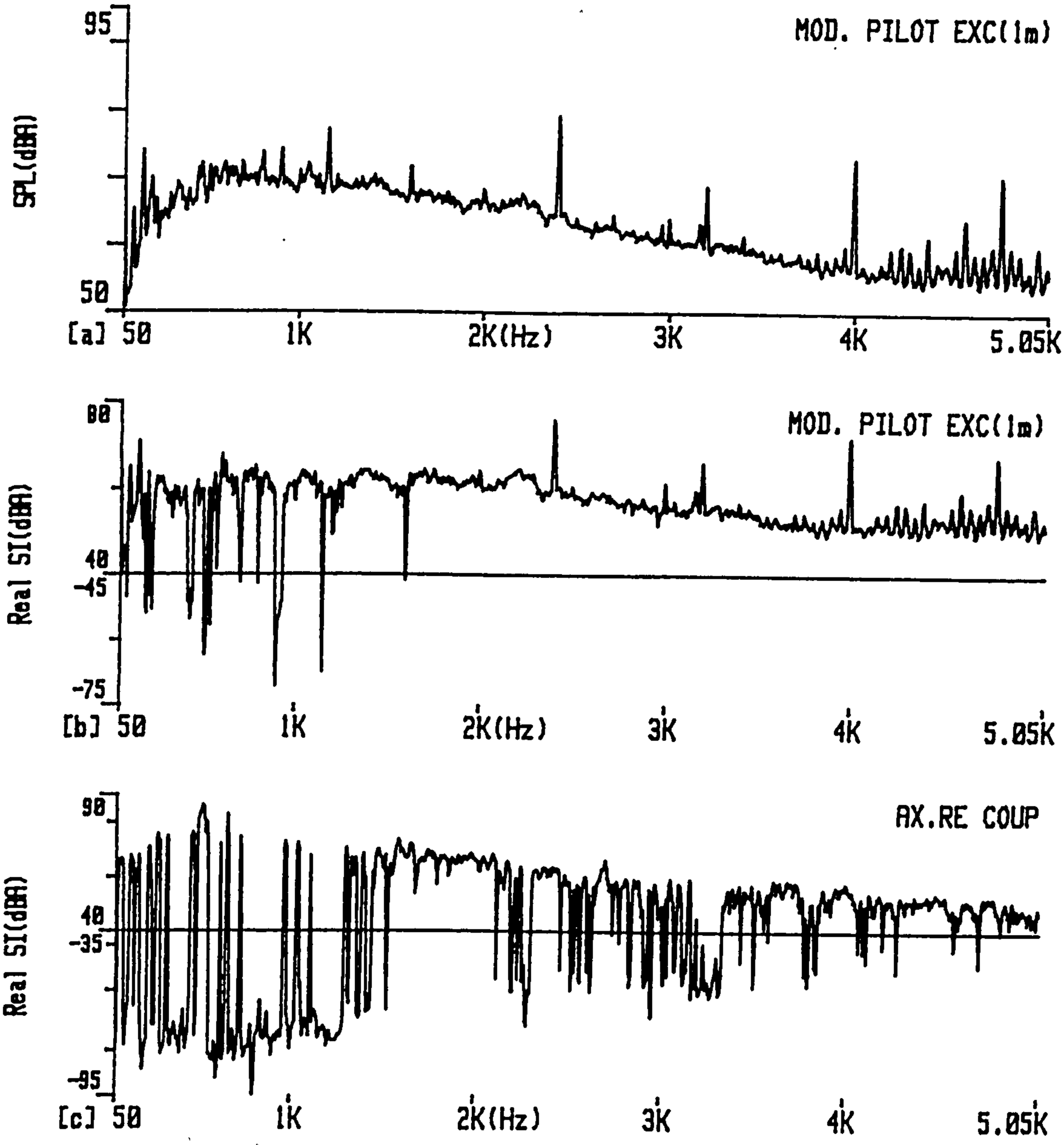

Fig.4.60 1m from the pilot exciter narrowband a) sound pressure level & b) radial sound intensity, c) axial sound intensity between R.E. generator coupling and brushgear.

magnitude of 88.9 dB(A) from the F.E. pilot exciter gap. This intensity level includes some component of reflection from the floor, the major reverberation contribution. Site measurements have shown that this effect raises the actual sound pressure level by 2 dB above the radial intensity level. The maximum S.P.L. due to the pilot exciter will therefore be 88.9 + 2 = 90.9 dB(A). At site this will be raised by 90.5 dB(A) general background noise reverberation yielding an S.P.L. of 93.7 dB(A).

The R.E. generator coupling sound power measured as 98.6 dB(A) relates to a free field sound pressure of 88.2 dB(A) at 1m from the exciter F.E. which is raised by approximately 1.5 dB reverberation resulting in an actual level of 89.7 dB(A). This level will be raised by 90.5 dB(A) general background reverberation and 86.0 dB(A) from the exciter yielding a total level of 93.9 dB(A). It is expected that the R.E. generator coupling noise emission measured will be greater than that on site because the transmission loss, T.L., of the temporary wooden baffle used for test purposes will be less than the contract baffle. Using Beranek's[13] approximate expression, eqn.(4.1) for the transmission loss of composite structures the T.L. of the test arrangement was calculated as 20.6 dB as opposed to 26.2 dB for the contract baffle. The difference was due to lower transmission loss of plywood than polyester glass mat and the larger shaft clearance for the test arrangement.

$$T.L. = -10 \lg \left[\left(\sum_{i=1}^{N} S_i \tau_i \right) / S_T \right] \qquad 4.1$$

where T.L. is the transmission loss in dB of composite structure comprising of N different materials with a total area S_T, S_i is the area of the ith element and $\tau_i = 1/\text{antilog}_{10} (TL_i/10)$.

It is expected that the 96.3 dB(A) sound power emanating through the wooden baffle

on test will be reduced by 5.6 dB to 90.7 dB(A). This emission plus the 94.7 dB(A) from the side regions yield 96.2 dB(A) implying site sound power emission will be 2.4 dB(A) less. The actual site sound pressure level due to the R.E. coupling alone would be 87.3 dB(A), which would be raised by exciter and reverberant background noise to 93.1 dB(A).

In summary effective muffling of air inlets and outlets reduced the pilot exciter sound power by 11.4 dB to 95.3 dB(A). The removal of R.E. generator coupling standing waves by absorbent material and more effective sealing has reduced noise emission by 7.3 dB to 96.2 dB(A).

5. ACCREDITION OF MEASUREMENT TECHNIQUES AND SOURCE MECHANISMS

5.1 MEASUREMENT TECHNIQUE INDICATORS

"Field indicators" are useful tools, which can be calculated from measurements using the intensity technique that either describe the measurement accuracy or show some characteristics of the sound field. Sound power determination within acceptable, quantifiable levels of accuracy is achieved as an iterative process of measurement, calculation of measurement indicators and measurement refinement. Despite standardisation of sound power determination using point sound measurement[5] there is discrepancy in the literature about the correctness of the point standard indicators and their applicability to scan measurements. In particular there is disagreement whether F_2 or F_3 more accurately quantifies phase error and also if F_4 overestimates the number of measurement points required. In this chapter the measurement data obtained from a variety of different acoustic environments will be used to accredit the standard indicators, their applicability to the scan technique and ability to classify sound fields.

Unfortunately the field indicators are inextricably related to the measurement error they are being used to quantify. Ideally the "true" sound power emitted by one of the components being investigated, such as the 660MW generator, should be used as a datum level. This, however, for the previously discussed reasons is not possible as the sound intensity in situ represents the best alternative to find the "true" sound power. The alternative approach of incorporating a reference source into the study may have yielded some useful comparative results. However the primary objective was to quantify generator unit emission and identify the main source mechanisms and as the secondary objective was to assimilate the application of the sound intensity technique to real sources in real environments the use of a reference source would be of lesser

value. There is still a solid basis for accrediting the value of the indicators to quantify errors. The data presented was from a series of measurements conducted on a diversified range of sources in differing conditions. Also the supplementary measurement of S.P.L., vector sound intensity, coherence, vibration and the relative magnitude of sound power all combined to produce a clear picture of the source relative to its surroundings.

Furthermore the value of reactive intensity, sound pressure particle velocity coherence and the probability density to supplement the standard indicators is illustrated. This approach has been discussed only briefly in the literature for laboratory measurements, but seldom in real industrial conditions. The F_6 indicator recently suggested by Hübner[49,64] for strong direct extraneous noise is also discussed.

5.1.1 Standard sound field indicators

Since phase mismatch is the principal factor that influences measurement accuracy indicators related to it are more important than the others. There is discrepancy in the literature if the indicator should be based on the absolute value of intensity (the unsigned intensity), F_2, or the integrated signed intensity, F_3. These indicators for a number of measurement surveys considered in chapter 4 are summarised in table K and their applicability is discussed as follows. The pilot exciter test rig results are given for comparison purposes. The sound power level is calculated from S.P.L., Lw(P), signed sound intensity Lw(I) and absolute sound intensity Lw(|I|).

Component	Lw(P) dB(A)	Lw(I) dB(A)	Lw(|I|) dB(A)	F3 dB	F2 dB	F3-F2 dB	Measurement classification
660MW pilot exciter test rig (factory)	112.4	110.3	110.3	2.1	2.1	0.0	Strong source direct field
660MW pilot exciter (site)	111.5	106.7	107.0	4.8	4.5	0.3	Strong source direct field
660MW R.E. generator coupling (site)	110.7	103.5	104.7	7.2	6.0	1.2	Strong source reverberant field
660MW generator (site)	113.5	97.3	99.6	16.2	13.9	2.3	Weak source diffuse background field
350MW generator (factory)	113.4(1/8) =122.4(1/1)	95.9(1/8) =104.9(1/1)	102.6(1/8) =111.6(1/1)	17.5	10.8	6.7	Weak source strong direct background field
660MW exciter (site)	106.3	96.8	99.4	9.5	6.9	2.6	Weak source diffuse and direct background fields
350MW exciter (factory) point measurements	112.8(1/3) 117.6(1/1)	94.7(1/3) 99.5(1/1)	104.1(1/3) 108.9(1/1)	18.1	8.7	9.4	Weak source strong direct background field
350MW exciter (factory) scan measurements	111.1(1/3) 115.9(1/1)	91.1(1/3) 95.9(1/1)	99.1(1/3) 103.9(1/1)	20.0	8.0	12.0	Weak source strong direct background field

Table K **F_2, F_3 and F_3-F_2 sound field indicators for sound power measurement surveys**

The pilot exciter test rig was a strong, uniform source operating in the absence of any significant background noise with low reverberation. F_3 and F_2 were the same with a low value of 2.1 dB. This is due mainly to nearfield measurement effects and limited floor reflections. Phase mismatch is negligible for this case.

On site the 660MW pilot exciter had it's enclosure attached. The value of overall power emission Lw(I) was reduced by 3.6 dB and the indicators were slightly higher with F_3 = 4.8 dB. The F_3-F_2 indicator was still low equalling 0.3 dB. The increase was due to the majority of the sound power emanating from limited measurement areas, i.e. the ventilation grills, which contribute to the pressure fields at all positions, but only weakly to the intensity in shielded areas. The R.E. generator coupling is also a strong source operating in the absence of other predominant sources indicated by F_3-F_2 = 1.2

dB, which is still relatively small. The value of F_3 has increased to 7.2 dB due to the greater reverberation influence due to the bodies of the adjacent exciter and generator. The value will still yield low phase mismatch errors.

The site 660MW generator intensities measurements had a large value of $F_3 = 16.2$ dB, with F_3-$F_2 = 2.3$ dB. The low power level, the large value of F_3 and F_3-$F_2 < 3$ dB implied that the generator was a weak source operating in a stronger diffuse background field. This implies that if the residual pressure intensity index of the measurement probe is high i.e. $\geq$ 21 dB and that source absorption is reasonably low, sound power determination is feasible albeit with reasonably large error limits. This was in fact the case.

The factory measurements on a 350MW generator had a slight increase in F_3 to 17.5 dB with a large value of F_3-$F_2 = 6.7$ dB. This illustrated that not only has the level of background noise increased, it is appreciably more directional in nature, in this case emanating from the couplings at each end of the generator and the test brushgear. Under these circumstances suppression of the background noise by Gauss's Integral Theorem, eqn. (3.8) has stringent demands placed upon it, as well as on the instrumentation, and for such extreme background the sound power determination is probably invalidated.

The 660MW exciter at site emitted stronger sound intensity than the generator indicated by the lower value of $F_3 = 9.5$ dB. The influence of directional background noise is more noticeable with F_3-$F_2 = 2.6$ dB, which is expected for many positive and negative intensity measurement areas. The value of F_3-$F_2 < 3$ dB is still acceptable inferring reasonable sound power determination in difficult conditions.

For the 350MW exciter operating on factory testing the background noise from the test brushgear is much greater than that of the exciter. This is indicated by the high value of F_3 = 18.1 dB and 20.0 dB for the point and scan surveys respectively. The values of F_3-F_2 = 9.4 dB and 12.0 dB for the point and scan surveys respectively are very high clearly identifying the presence of the strong directional background noise. These indicator values determined from the overall levels may be misleading. The sound power determination from the scan measurements was complex with net output power only between 800 Hz and 1600 Hz (Fig.4.11a), which is reflected by F_3 tending to 20 dB for all but the frequency range 800-1600 Hz (Fig.4.12a). The overall sound power level determination has large probably unacceptable inaccuracy. For the point measurements the sound power spectrum (Fig.4.11c) was positive except between 525 Hz and 700 Hz due to insufficient suppression of the main brushgear noise frequency band. This is reflected by $F_3 < 11$ dB (Fig.4.13a) and F_3-$F_2 < 2$ dB (Fig.4.13b) above 800 Hz implying correct measurement in these regions. The overall indicator values overestimated the errors in the point, but not the scan, measurement surveys and it is therefore necessary to relate errors to 1/3 octave indicator values. The point measurements produced a better sound power estimate as the F.E. face measurement provided better local suppression of the normally incident background noise, as well as incorporating less of the fringing noise.

The indicator F_4, the variance coefficient V_n, can be used to predict the spatial sampling random error using eqn. (3.9). It is necessary to assess if F_4 overestimates the error and also if it is applicable for scanned sampling. The value for F_4 is summarised in table L for a variety of measurement surveys.

For the 660MW R.E. generator coupling the emission from the gap between the exciter

enclosure and coupling cover was 10 dB greater than the remainder of the cover. For the 12 point measurements F_4 = 1.13 and the sampling error was 2.1 dB. The error predicted for measurement groupings on the gap and cover was less being 0.8 and 1.1 dB. Under these circumstances where the intensity hotspot has been identified and measured separately, Hübner's[48,49] estimated error obtained by using F_4 and the ratio of sound power for the sub-regions to the total obtains a more representative error of 1 dB. The 4 scans on the cover despite an even distribution with a low sampling error of 0.9 dB is believed to overestimate the power due to spending too great a proportion of the measurement time over the "hotspot".

Component	Measurement grouping	No. of measurements N	F4	Student's T ts 95% confi-dence limits	error (dB)
660MW R.E. Generator coupling (site)	coupling cover only point	8	0.40	1.90	1.1
	gap only point	4	0.15	2.35	0.8
	cover + gap point	12	1.13	1.80	2.1
	cover + gap scan	4	0.16	2.35	0.9
660MW pilot exciter test rig (factory)	scan	19	0.56	1.73	0.9
350MW exciter (factory)	scan	18	8.3	1.74	6.5
	point	28	5.6	1.7	4.5
350MW generator (factory)	side-ends scan	24	18.3	1.71	8.8
	side scan	32	3.0	1.7	2.9
	total scan	40	3.6	1.68	2.9
660MW generator (site)	side scan	66	2.06	1.67	1.5
660MW exciter (site)	total scan	64	5.27	1.67	3.2

Table L : F_4 sound field indicator and spatial sampling error for sound power measurement surveys

For the scanned measurements on the 660MW pilot exciter test rig the value of F_4 = 0.56 implies an error of 0.9 dB. The complete measurement survey was repeated 4 times with different scan patterns to within 0.1 dB. The implication that the error is

overestimated is consistent with the belief that the scan measurement more closely represents the continuous surface integral.

For the 350MW exciter tested in the factory F_4 was high for both the scan and point measurements. Due to the aforementioned reasons the scan techniques will tend to overestimate the error. The point error of 4.5 dB may be representative. Under these circumstances the direct incident intensity should be reduced by shielding and also the number of measurement should be increased by a factor of 2-3.

The factory sound power determination of a 350MW generator was largely invalid because even after phase mismatch correction the residual pressure intensity index was exceeded by F_3. Under these circumstances the F_4 indicator will be high and of limited quantitative value. The value of F_4 for the side-ends region excluding direct background noise was 18.3 implying an error of 8.8 dB. Including the direct measurements reduced the error to 2.9 dB, but as this includes many negative measurements this is misleading.

The value of $F_4 = 2.06$ and the subsequent error of 1.5 dB for the 660MW generator at site was appreciably lower, which was expected for the more favourable measurement conditions. For the 660MW exciter due to the number of negative intensities created by the strong directional background noise the average is low, which results in the large value of $F_4 = 5.27$. The error is subsequently large equalling 3.2 dB. The sampling error for the positive and negative areas separately is 2 dB, which infers that the 3.2 dB may be an overestimate.

To further assess the spatial sampling error every 4th measurement on the 660MW generator and exciter was repeated 4 times. The estimated errors for these surveys and

that for the pilot exciter test rig, which also had every measurement repeated 4 times is given in table M.

Component	No. of repeated averages	F4	Student's T ts 95% confidence limits	error (dB)
660MW pilot exciter test rig (factory)	4	0.014	2.35	0.08
660MW generator (site)	4	0.033	2.35	0.18
660MW exciter (site)	4	0.31	2.35	1.53

Table M **F_4 sound field indicator and spatial sampling error for 4 repeated sound power measurement survey averages**

It is apparent by comparing tables L and M that the variance coefficient F_4 and the error are substantially smaller for the repeated averages. One consequence of this is that the measurement error converges in accordance with the central limit theorem implying that the distribution is Gaussian and the error formulation given in eqn.(3.9) is valid. It was also observed that for the pilot exciter test rig the sound power was repeated 4 times to within 0.1 dB. This is consistent with the error predicted from the repeated averages of 0.08 dB, but not with that predicted from the complete sample population of 0.9 dB. The overall 660MW generator error from the repeated averages was 0.18 dB, which is due to the important contribution of the 100 Hz tone to the total sound power level (Fig.4.24), whereas that calculated for the complete survey was 1.5 dB. The complete generator sound power was repeated twice to within 0.3 dB. The error calculated from the repeated averages for the 660MW exciter was 1.5 dB as opposed to the 3.2 dB predicted from the complete survey. The overall exciter sound power was repeated to within 0.2 dB. These results imply that the overall spatial sampling error from scanned measurement will be an overestimation using eqn.(3.9).

For comparison purposes the spatial sampling error associated with sound pressure measurement is tabulated below for some cases.

Component	Measurement grouping	No. of measurements N	F4	Student's T ts 95% confi-dence limits	error (dB)
660MW R.E. generator coupling (site)	coupling cover only point	8	0.18	1.90	0.52
	gap only point	4	0.1	2.35	0.55
	cover + gap point	12	0.55	1.80	1.13
	cover + gap scan	4	0.11	2.35	0.63
660MW pilot exciter test rig (factory)	scan	19	0.43	1.73	0.7
350MW exciter (factory)	scan	18	0.77	1.74	1.23
	point	28	0.96	1.70	1.19
350MW generator (factory)	side-ends	24	0.19	1.71	0.29
	side	32	0.50	1.70	0.62
	total	40	1.31	1.64	1.31
660MW generator (site)	side	66	0.158	1.67	0.14
660MW exciter (site)	total	64	1.08	1.67	0.89

Table N : Spatial sampling error for sound pressure measurements

The error associated with sound pressure is commonly half that of sound intensity sampling as is evident from comparing tables L and N. Similar to the 660MW R.E. coupling the complete error is overestimated unless Hübner's[48,49] partial variance approach is adopted yielding an error of 0.54 dB. For near field sampling the pilot exciter test rig error was 0.7 dB, which may also be an overestimation. For the 350MW exciter there was a large reduction in error. This was due to the pressure variation being uniform and independent of the sampling technique, whereas the sound intensity distribution was very dependant upon the ability to suppress background noise. The relationship between pressure and intensity distributions is not necessarily

straightforward as illustrated for the 350MW generator side-ends measurement. The error is only 0.29 dB for the pressure distribution, but 8.8 dB for an invalid intensity distribution. The variation for the total survey is greater due to the strong background noise at the ends causing a greater variation. The 660MW generator at site was in an even diffuse field yielding a low error of 0.14 dB whereas the exciter error of 0.89 dB was raised by the strong direct background noise.

5.1.2 Reactive intensity

As reactive intensity is high in the near field of an idealised point source the quantity may be used to indicate a "source". Fahy[2] points out that as strong reactivity is present near very inefficient radiators and also in reverberant enclosures the convergence of reactive vectors does not necessarily indicate active sources. The value of reactivity as a sound field indicator has been discussed by Jacobsen[59,65] and is predicted theoretically by others for idealised situations. Jacobsen[59] presents laboratory results, but despite the interest in the quantity little experimental data obtained in industrial environments is available.

For a variety of measurement situations the reactive and active intensity can be investigated to see if they can classify the nature of the sound field. 10cm from the ventilation grill on the side of the 660MW pilot exciter at site the radial sound intensity was high being 108 dB(A), Fig.5.1a. The reactive intensity is also strong with positive values except for 3 of the siren tones at 1.6 kHz, 2.4 kHz and 4 kHz, Fig.5.1b. Below 300 Hz the reactive intensity is greater, but above this frequency the real intensity is commonly 10 dB greater than the reactive component. This is illustrated more clearly by the logarithmic difference between pressure and real intensity, Fig.5.1c, and that of the pressure and reactive intensity, Fig.5.1d. This is to be expected for near field

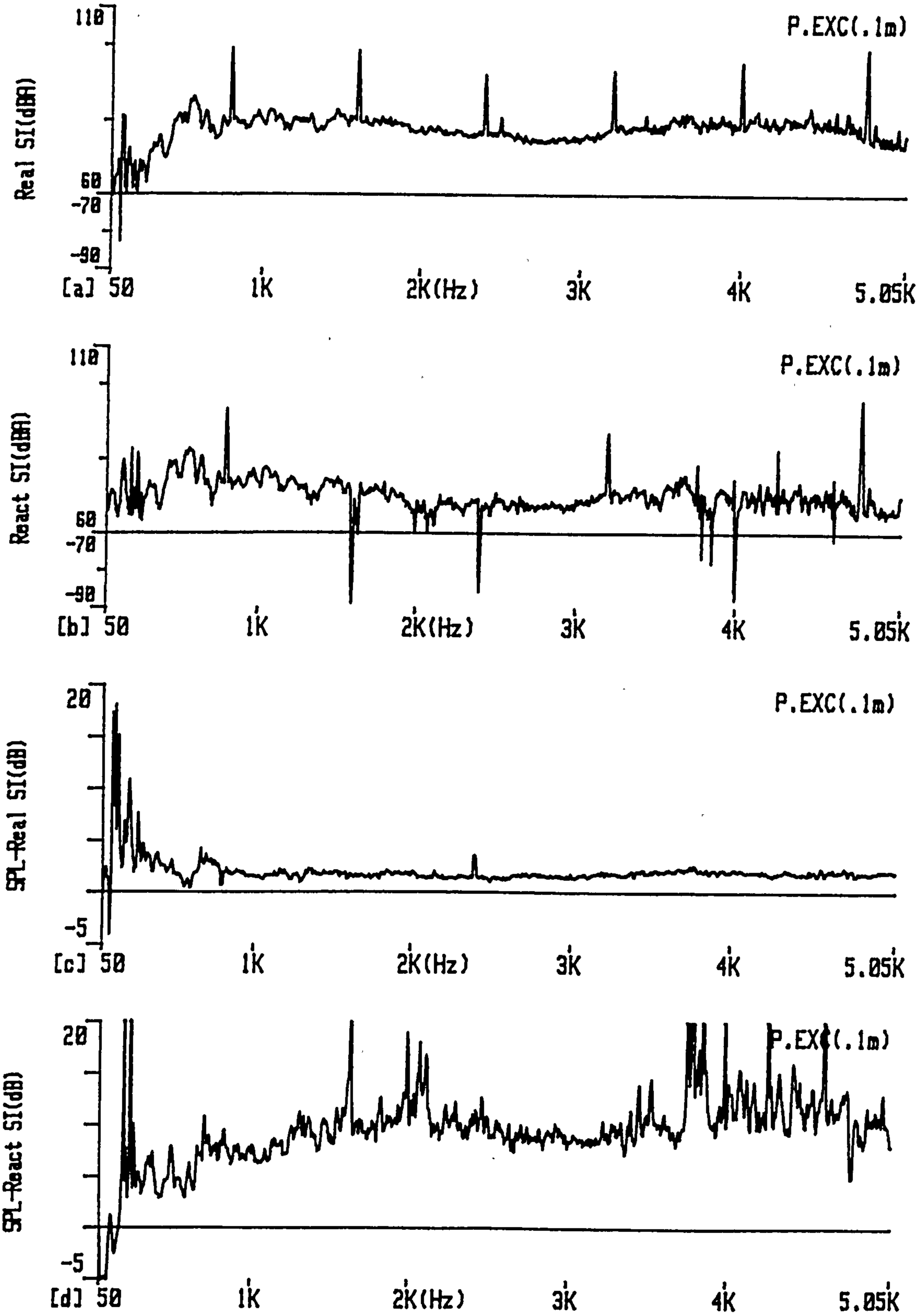

Fig.5.1 0.1m from the 660MW pilot exciter a) real intensity b) reactive intensity & logarithmic difference between sound pressure and c) real intensity d) reactive intensity.

measurements on a monopole or dipole source in the absence of reflections or significant background noise.

In the nearfield of the R.E. generator coupling the maximum emission was in the frequency range 3 kHz- 4 kHz containing many pure tones, Fig.5.2a. By contrast the reactive sound intensity contains many negative and positive peaks, 5-10 dB less than the real intensity, Fig.5.2b. This is due to the reverberant field created by the generator and exciter bodies on either side of the strong source the R.E. coupling represents. The sharp variation in pressure amplitude gradient for the different frequency components creates the negative reactive components.

10cm from the 660MW generator casing at site the net intensity output was typically 75 dB(A) created by a bidirectional frequency composition. The reactive intensity, Fig.5.3a had a definite pattern of large frequency bands of positive and negative flow. This pattern was also evident near to the centre of the 660MW exciter. As illustrated by the indicators in the preceding section the generator is a weak source situated in a strong diffuse field. It is believed that the phenomenon evident in the reactive intensity is due to the interference pattern created by a diffuse field incident upon a rigid surface. The interference pattern for the pressure field, p, is given by

$$p = A \cos kx = A \cos \{(2\Pi f/c)\ x\} \qquad 5.1$$

where A is a constant, k is the acoustic wave number, x is the distance from the rigid surface, f is frequency and c is the acoustic velocity. The two pressure, p_1 and p_2, from a sound intensity probe with microphone spacing Δr and distance, d, from the centre of the probe to the rigid body is

$$p_1 = A \cos \{(2\Pi f/c)\ (d - \Delta r/2)\} \qquad 5.2a$$

$$p_2 = A \cos \{(2\Pi f/c)\ (d + \Delta r/2)\} \qquad 5.2b$$

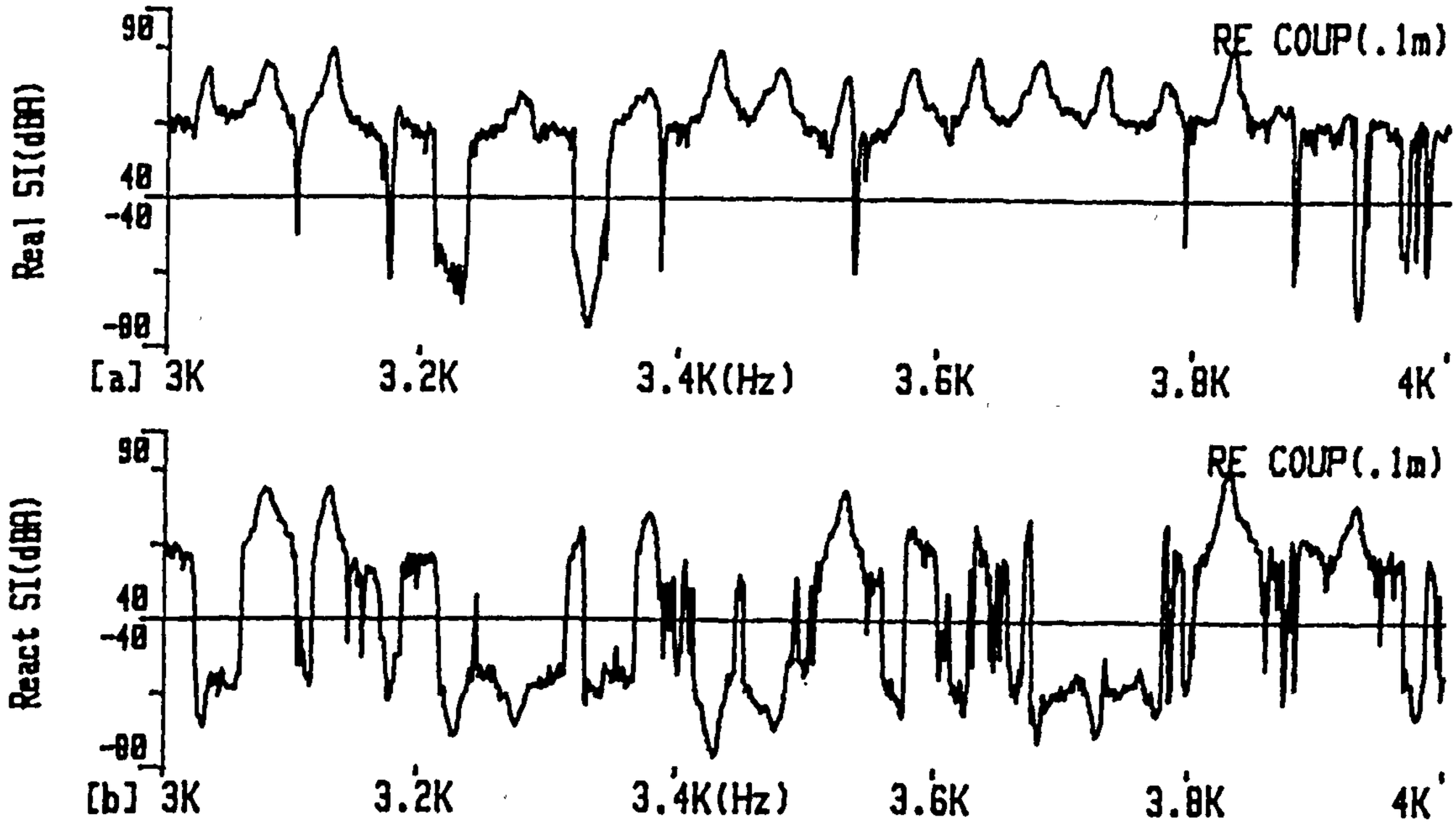

Fig.5.2 0.1m from 660MW R.E. generator coupling a) real intensity b) reactive intensity.

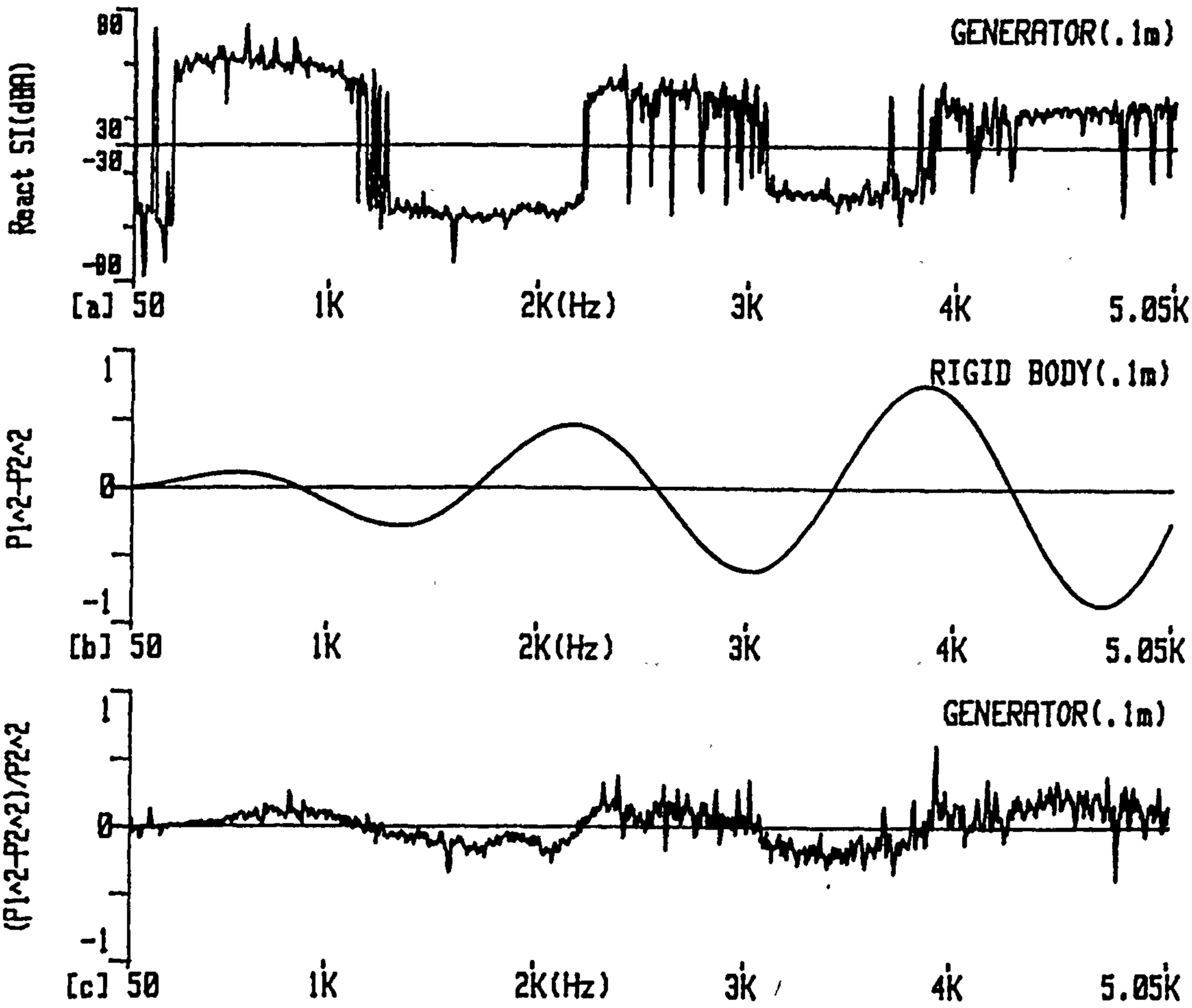

Fig.5.3 a) Measured reactive intensity 0.1m from 660MW generator Difference in pressure squared for microphone pair
b) predicted 0.1m from rigid surface and c) measured 0.1m from 660MW generator

The reactive intensity is proportional to the difference of the pressure squared for each microphone, eqn. 3.4. The variation in this quantity with frequency with $\Delta r = 12mm$ and $d = 10cm$ is given in Fig.5.3b. It is apparent that the sign of the predicted pressure amplitude gradient, Fig.5.3b, is the same as the measured reactive intensity, Fig.5.3a. The correlation is further illustrated by plotting the ratio of measured difference between pressure squared for the two microphones to pressure squared for the 2nd microphone, Fig.5.3c.

To summarise the reactive intensity when considered in conjunction with real intensity can prove a useful indication of the sound field nature. When both real and reactive intensity are high and of the same sign the field is that of a strong source nearfield. High real intensity in conjunction with high bidirectional reactive intensity is indicative of a reverberant region dominated by 1 source. Low levels of bidirectional real intensity in conjunction with a reactive intensity distribution similar to that predicted from eqns.5.2a and 5.2b is characteristic of a weak source in a strong diffuse field.

5.1.3 Sound pressure particle velocity coherence

The theory and experimental results for a 660MW generator unit at site for sound pressure particle velocity coherence have been presented in sections 3.7 and 4.2.5 respectively. The quantity proved very successful in field classification. The coherence was high beside the pilot exciter and invariant of spectral resolution indicating a strong direct source. Beside the R.E. generator coupling the indicator was high only for very narrow resolution indicating a strong source in a reverberant region. The coherence was low close to the generator and exciter irrespective of spectral resolution identifying that these regions are low power output in stronger multi-source background fields. The coherence increased with distance from the exciter as the shielding of direct noise from

adjacent plant was reduced indicating direct and not diffuse background.

5.1.4 Relative occurrence of sound intensity distribution

Quantitive determination of spatial sampling errors is dependant upon the measurement distribution having a normal (Gaussian) distribution. From the relative occurrence distribution, summarised in table O for a variety of conditions, with frequency bands, it is also possible to identify the measurement environment.

For the 660MW generator the distribution was Gaussian for the frequency range 50-1250 Hz. The distinctly non Gaussian appearance of the 1600-4000 Hz region coincides with low net output in this frequency range. Despite the measurement of negative power in the 5 kHz 1/3 octave the distribution is clearly Gaussian. This adds further credence to a correct measurement of the physical phenomenon of power absorption.

The 660MW exciter measurement had a non Gaussian distribution with a large negative offset due to the number of negative measurements on the ends of the exciter caused by strong background from the adjacent plant. The positive and negative measurements themselves were distributed in a Gaussian manner.

The measurements on the 985MW generator in the factory are non Gaussian for all data not corrected for phase mismatch irrespective of the frequency resolution. The phase mismatch corrected data is more Gaussian, but this is only prominent for the 250-2000 Hz range. This may however be misleading as the validity of the phase correction is questionable.

Component	Measurement description (phase correction if applied, frequency band)	Relative occurrence distribution	Fig.No.	Sound power spectral composition
660MW generator (site)	Uncorrected 50-1250 Hz	Gaussian with limited offset	4.28a	Net low levels of emission
	Uncorrected 1600-4000 Hz	Clearly not Gaussian with large neg. offset	4.28b	Bidirectional power flow
	Uncorrected 5000 Hz	Gaussian	4.28c	Low levels of power absorption
660MW exciter (site)	Uncorrected 50-5050 Hz	Only very slightly Gaussian with large neg. offset	4.33a	Net power emission up to 3 kHz, bidirectional 3k to 4k, negative above 4 kHz
	Uncorrected 50-5050 Hz - Pos measurements only	Approximately Gaussian with neg. offset	4.33b	-
	Uncorrected 50-5050 Hz - Neg measurements only	Gaussian	4.33c	-
985MW generator side (factory)	Uncorrected 50-5050 Hz	Not Gaussian	4.7a	Bidirectional to 3 kHz, neg. >3 kHz
	Uncorrected 250-2000 Hz	Not Gaussian	4.7b	Bidirectional with small net output
	Corrected 50-5050 Hz	Slightly Gaussian with large neg. offset	4.7c	Net low levels of emission <3 kHz Net absorption > 3 kHz
	Corrected 250-2000 Hz	Gaussian	4.7d	Net low levels of emission
660MW pilot exciter test rig (factory)	Uncorrected 50-5050 Hz	Generally Gaussian with peak on either side of mean	5.4a	Strong broadband plus tonal components
	Uncorrected 800 Hz	Basically Gaussian with peak on either side of mean	5.4b	Strong tonal component

Table O : Summary of relative occurrence distribution for a variety of different source regions

For the 660MW pilot exciter test rig the relative occurrence distribution was generally Gaussian with a peak on either side of the mean value. This was the case for both the complete frequency band from 50-5050 Hz, which contained approximately equal tonal and broadband noise, and the 800 Hz 1/3 octave, which is dominated by a pure tone. The Gaussian influence is more prominent for the former case. This coincides with the standardised probably density function of a sine wave in Gaussian noise given by Bendat[60]. The more significant the sinusoidal wave the less pronounced is the mean

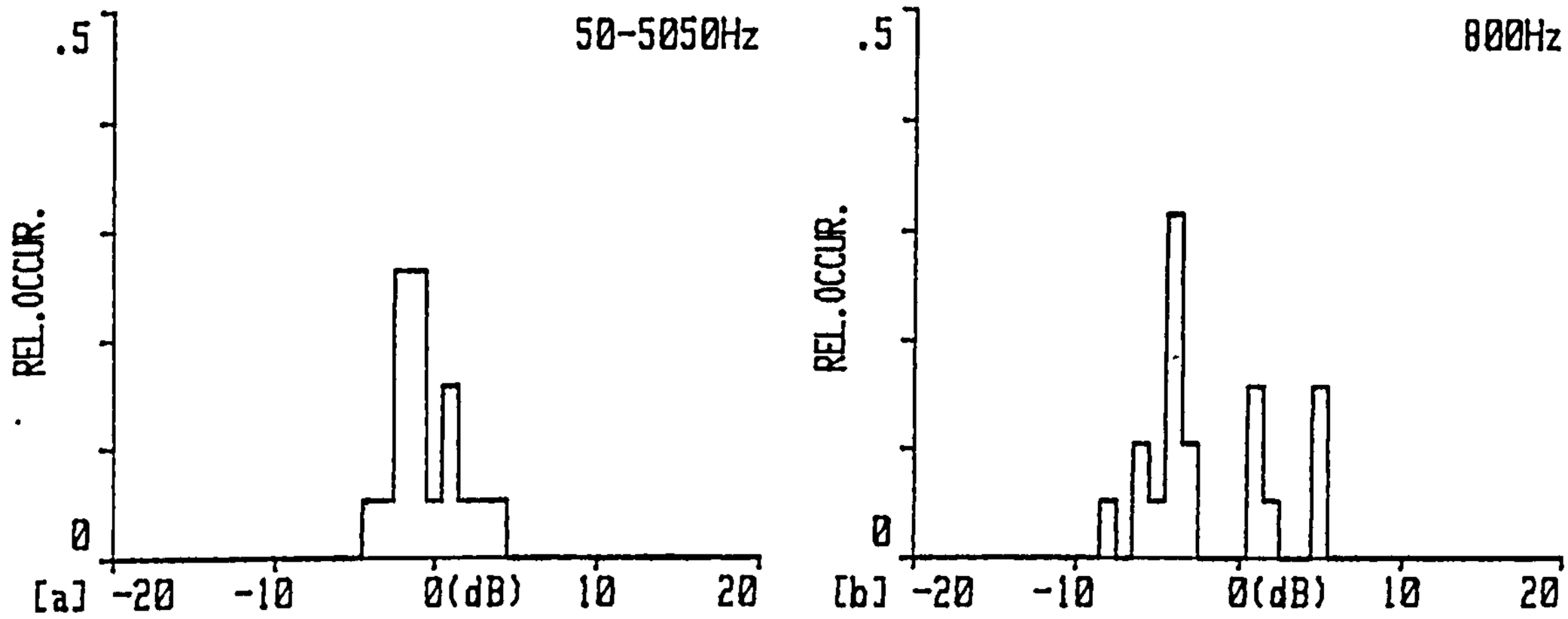

Fig.5.4 Probability density for 660MW pilot exciter test rig sound intensity measurements.

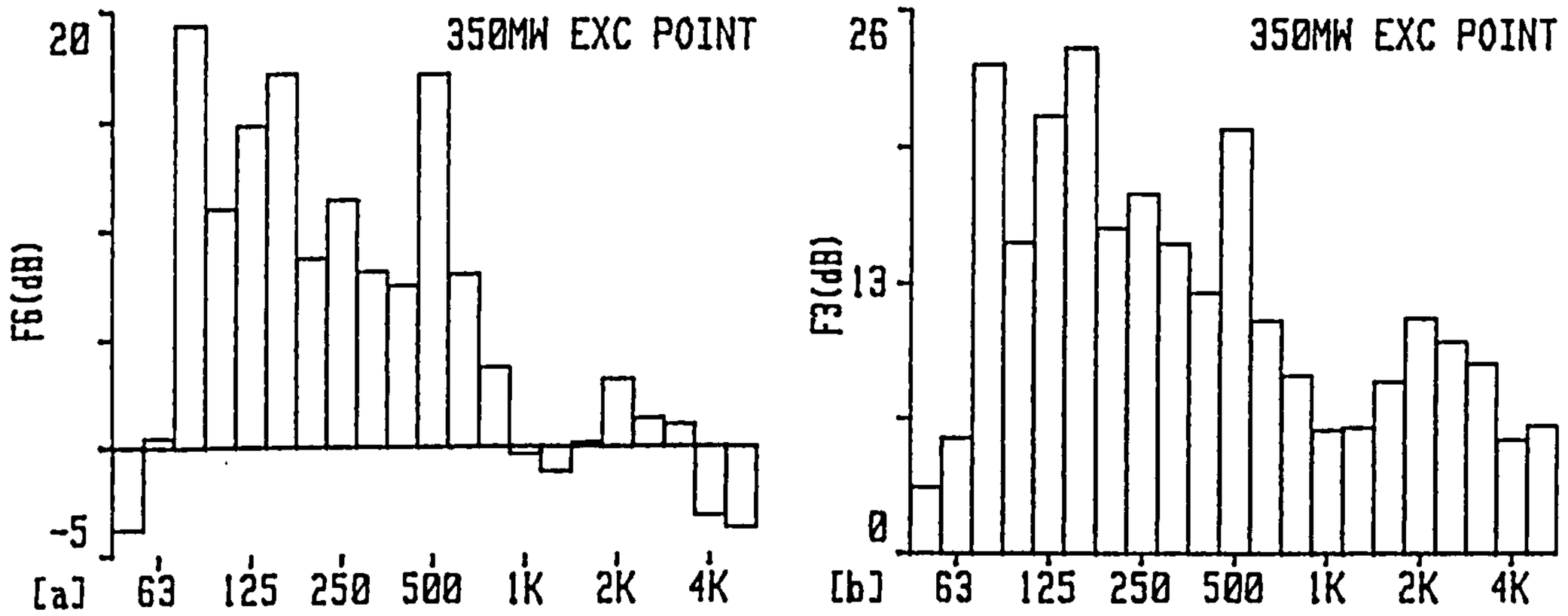

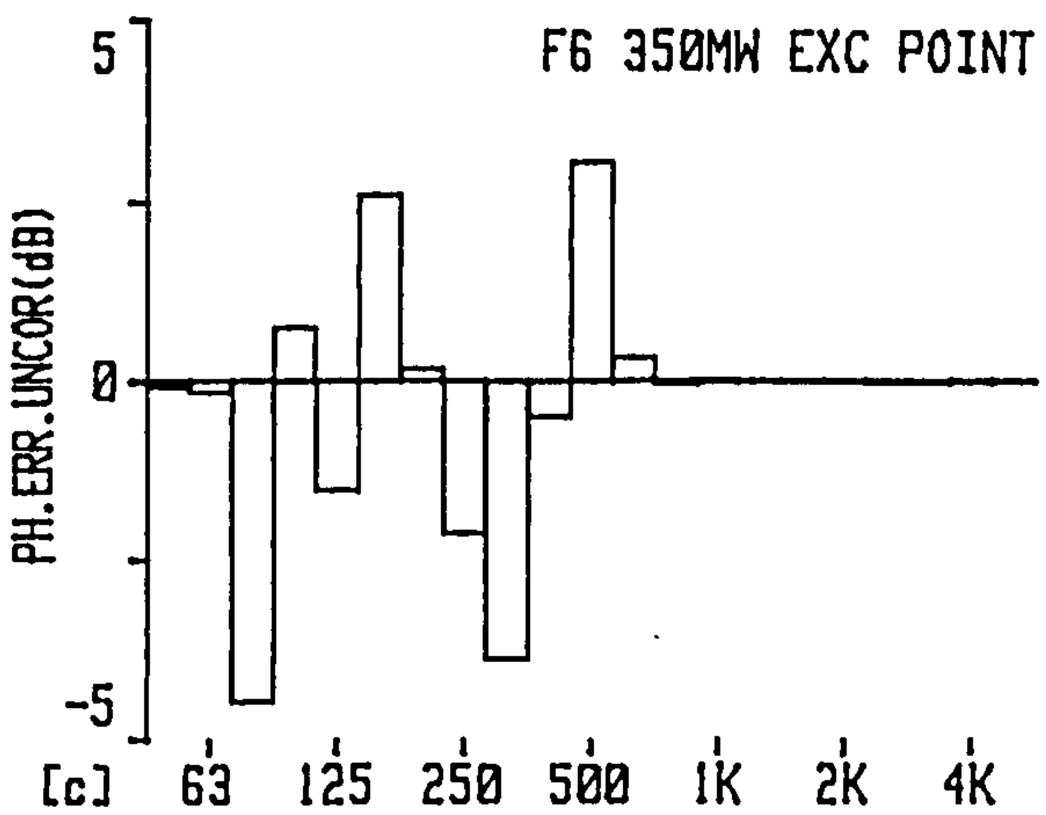

Fig.5.5 350MW exciter point measurement a) F_6 b) F_3 c) Phase mismatch error predicted from F_6.

value, which is the case for these examples.

The relative occurrence distribution is therefore not only useful in assessing measurement error, but also in accrediting the sound intensity measurement population. A Gaussian distribution is indicative of a good measurement survey even if the net sound power emission is low. If the distribution is non Gaussian the overall sound determination has the potential for inaccuracy unless the global suppression of background noise is good.

5.1.5 F_6 indicator

It is claimed by Hübner[49,64] that F_2 and F_3 overestimate the bias error for point measurements conducted in the presence of direct extraneous noise. He suggests that under these circumstances a new indicator F_6, calculated from the mean tangential intensity, $\bar{I}_t$, and the mean normal sound intensity component, $\bar{I}_n$ is used to calculate the bias error, E_r

$$F_6 = 10 \log (\bar{I}_t) - 10 \log (\bar{I}_n) \quad dB \qquad 5.3$$

$$E_r = -10 \log (1 - 10^{0.1(F6-\delta po|Io|)}) \quad dB \qquad 5.4$$

where $\delta_{po|Io|}$ is the residual pressure intensity index.

The indicator was calculated from the point sound intensity data for the 350MW exciter reported in section 4.1.2. The F_6 indicator is plotted in Fig.5.5a and the F_3 indicator is also plotted in Fig.5.5b for comparison purposes. Up to 800 Hz F_6 has a similar spectral content to F_3 with levels approximately 6 dB less. The main background noise is below 800 Hz, which is evident from the 350MW exciter point sound power spectrum, Fig. 4.11c. Above 800 Hz the F_6 indicator is negative indicating the normal intensity component is greater than the tangential. F_3 <10 dB above 800 Hz indicates less

measurement difficulties for the frequency bands above 800 Hz. The phase error is similar when predicted from F_6 (Fig.5.5c) and F_3 (Fig.4.13c) except above 800 Hz when that from predicted F_6 tends to 0 dB and that from F_3 tends to 0.5 dB.

It has been illustrated that F_3 predicts the measurement error reasonably well for a number of different circumstances in accordance with Jacobsen's theoretical prediction[34]. For the 350MW exciter, in the presence of one source of background, F_6 and F_3 imply similar errors although F_6 underestimates the error when the normal component is greater than the tangential component as sound pressure may still be high due to nearfield or reverberant effects. For the case when the background is directly incident upon one face of a machine the background is not tangential and the potential problem will not be indicated by F_6. Also in the case of two strong sources at either end of a machine, which is a situation commonly encountered for distributed lineouts of rotating plant, the tangential intensity will tend to average to an unrepresentatively low value underestimating the error.

5.1.6 Summary

The standard sound field indicators F_2, F_3 and F_3-F_2 have proven reliable for describing the measurement environment and indicating refinement of measurement procedure for both scanning and point techniques. It has been illustrated that F_3 not F_2 determines the bias error introduced by phase mismatch and should be adopted for the point standard as well. F_6 under certain circumstances, namely strong direct background noise from one source, is similar to F_3, but in general underestimates the measurement error. The F_4 indicator clearly overestimates the spatial sampling error for scanned measurements and also for point measurements when certain regions contribute strongly to the total level. For scanned measurements spatial sampling errors may be better assessed using

repeated measurements with different patterns. To some extent if the measurement procedures outlined in section 3.4.2 are adhered to, including slow scanning rates, and "hot spots" are identified and measured separately the spatial sampling errors may be reasonably small and certainly less than the bias errors. The overestimation in sampling error for point measurements can be reduced by employing Hübner's[49] error formulation based on partial variance as this approach weights the error according to the importance of the various regions to the overall sound power level.

The sound pressure particle velocity coherence and relationship between real and reactive sound intensity have been shown to reflect the nature of the sound field. Measurements conducted in an industrial environment have identified a weak source in a multi-source diffuse field, a strong direct source and a strong source in a reverberant region. This information clearly correlates with relative sound power levels, point vector sound intensity and sound pressure levels of the plant items. The field classification is similar to that inferred from F_2 and F_3. It is suggested that limited measurement of coherence or reactive intensity could be conducted at the start of a sound power survey to assist with sound field classification and allow optional measurement procedures to be adopted. This could optimise measurement time as measurement, calculation of indicators and refinement can prove a time consuming process. Alternatively these measurements can be conducted after a sound power survey to add further credence to sound power levels, when a component is deemed to contribute weakly to the surrounding noise fields.

The relative occurrence distribution can also indicate potential measurement difficulties and situations where good global suppression of background noise is essential. The indicators F_2 and F_3 already indicate this clearly, but the probability density distribution still requires assessment before the spatial sampling error can be quantified with confidence.

5.2 NOISE GENERATION MECHANISMS

Understanding the fundamental cause of noise generation and the subsequent transmission through and radiation from, enclosing structures is essential for effective noise control. This is a prerequisite of long term design modifications to reduce noise emission at source and of substantial benefit in implementing optimal short term acoustic treatments.

Little comprehensive information of this nature exists for the generator unit constitute components especially in comparison to the extensive treatises on electric motor noise. This is largely due to the extra aforementioned practical difficulties associated with source identification or even quantification for a generator unit.

Much new experimental data for a wide range of generator plant, from a variety of sophisticated measurement techniques, has been presented. This has enabled quantification of noise levels in rank order and improved understanding of many source mechanisms. For electric machinery the source mechanisms can be broadly categorised as being due to magnetically induced vibration, mechanically induced vibration and aerodynamic origin with many further sub-divisions. Analysis is further complicated by transmission and radiation of this noise. Therefore each mechanism for each component cannot be fully quantified, not only due to time restrictions, but

also technical feasibility. Interpretation of the experimental data is broadly discussed with the relative importance of each mechanism for each component given. The worst noise source, the pilot exciter, is the subject of indepth analysis so it is only briefly introduced in this section.

5.2.1 Generator noise

The majority of the measurement data and subsequent theoretical studies have concentrated on the large hydrogen cooled generators, although much of this information is also applicable to air cooled generators. Magnetic forcing and it's dependence on load conditions is analysed. Aerodynamic noise generation is also discussed in detail with the transmission loss through the generator casing calculated.

5.2.1.1 Magnetically induced vibration

For small motors magnetic noise is of primary importance and for large induction motors, whereas aerodynamic noise is generally more important, magnetic noise is seldom negligible. A generator has a number of significant differences, which tend to reduce the magnetic noise generation. Firstly the generator air gap is appreciably greater than that of an induction motor being typically 10cm as opposed to 1-2mm. This reduces the flux ripple caused by variation in rotor and stator slot permeance and air gap eccentricity subsequently reducing fluctuating magnetic forces. Saturation non-linearities are prevalent for both machines. The second major factor is the smaller stator voltage and current harmonic content for a generator. These are important extra noise sources for motors especially those with inverter drives.

From the site measurement data it is evident that the generator emits low levels of noise and does not determine the sound pressure level beside it. Magnetic noise creates

discrete tones and the presence of these can be identified from the narrowband measurement spectra. The sound power (Fig.4.23a) and vibration (Fig. 4.44b) spectra indicate a prominent 100 Hz component due to magnetically induced vibration transmitted directly to the casing. The tone and it's harmonics were added and constituted half of the overall power level of 97.3 dB(A). The sound pressure surface vibration and sound pressure particle velocity coherences are both low apart from for these tones coinciding with the earlier observations on low emission. This illustrates the significance of these magnetic tones. The sound pressure spectrum at 1m especially towards the generator R.E. (Fig.4.42b) is also raised by the 100 Hz and higher harmonics emitted from the R.E. generator coupling with the sound power spectrum given in Fig.4.23c.

The link between the 100 Hz tone and magnetic forcing was partly illustrated by the increased internal S.P.L. with electrical loading for the air-cooled generator (section 4.3.1.1). The magnetic core vibration is more important for hydrogen than air cooled generators as it is transmitted more directly to the radiating outer casing as for air cooled machines the outer cover is free standing. Vibration isolation between the core and the outer casing reduces the transmitted vibration by at least a factor of 2. Typical contractual vibration limits for a 985MW generator were 50 and 25μm peak to peak displacement on the core and outer casing respectively.

For small (fractional horsepower) motors magnetic noise can be predicted. The magnetic forcing is calculated from the flux density fluctuation and related to a vibration distribution via a measured or predicted structural mechanical response. This can then be related to sound power output for the predominate modes of vibration. However whereas the generator core vibration level and distribution can be calculated the

complexity of the transmission of this to the outer casing is such that the sound power cannot be accurately predicted.

The relative influence of magnetic forcing can still be analysed. Tampion et al[18] used Maxwell's stress equations to determine the distribution of electromagnetic forces on the stator bore to investigate the variation of double frequency stator core vibration with load and power factor. Structural finite element analysis was then used to relate these forces to relative vibration levels. An alternative approach was adopted here to calculate the force variation. The average radial and circumferential flux density acting on a stator tooth were calculated for 1 complete cycle from the 2D finite element flux distribution. The radial and circumferential stress can then be calculated from the flux distribution using Maxwell's eqns.

radial stress	$\sigma_r = (B_r^2 - B_\theta^2)/2\mu_0$	5.5
circumferential stress	$\sigma_\theta = B_r B_\theta/\mu_0$	5.6

Where B_r = radial flux density and B_θ = circumferential flux density

The variation in force waveforms for two operating conditions, full open circuit stator voltage and full load with 0.8 lagging power factor, are presented in Figs.5.6a and 5.6b respectively. These waveforms are very similar to those presented by Tampion[18]. The force harmonics are expressed in table P. For comparison purposes the average open circuit vibration velocity harmonics are also tabulated for 156 measurements equispaced along 50% of the length and 90% of the circumference of a 500MW generator casing.

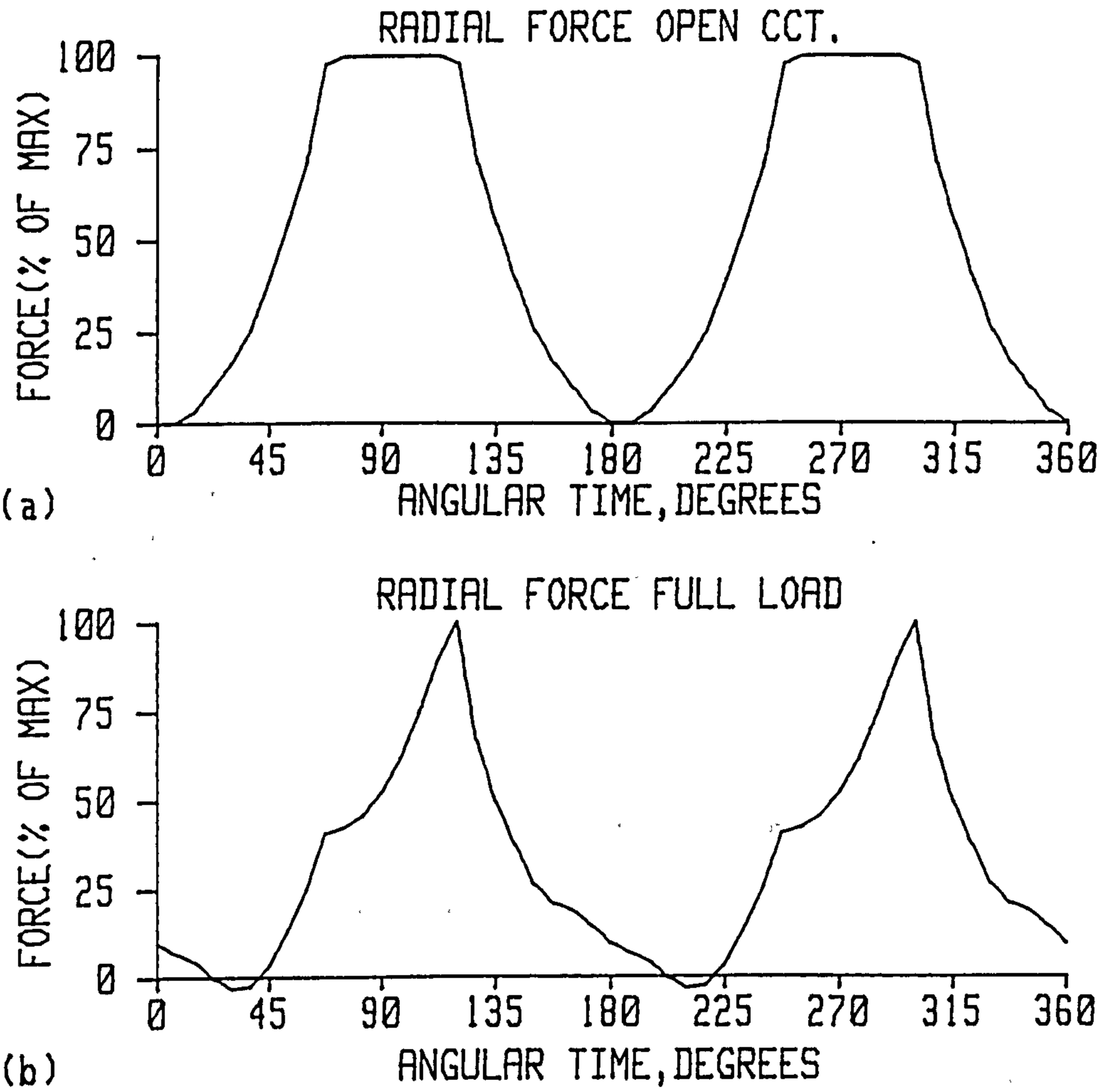

Fig.5.6 Force on one tooth as a function of time expressed relative to maximum force for a) open circuit b) full rated load with 0.8 power factor lag.

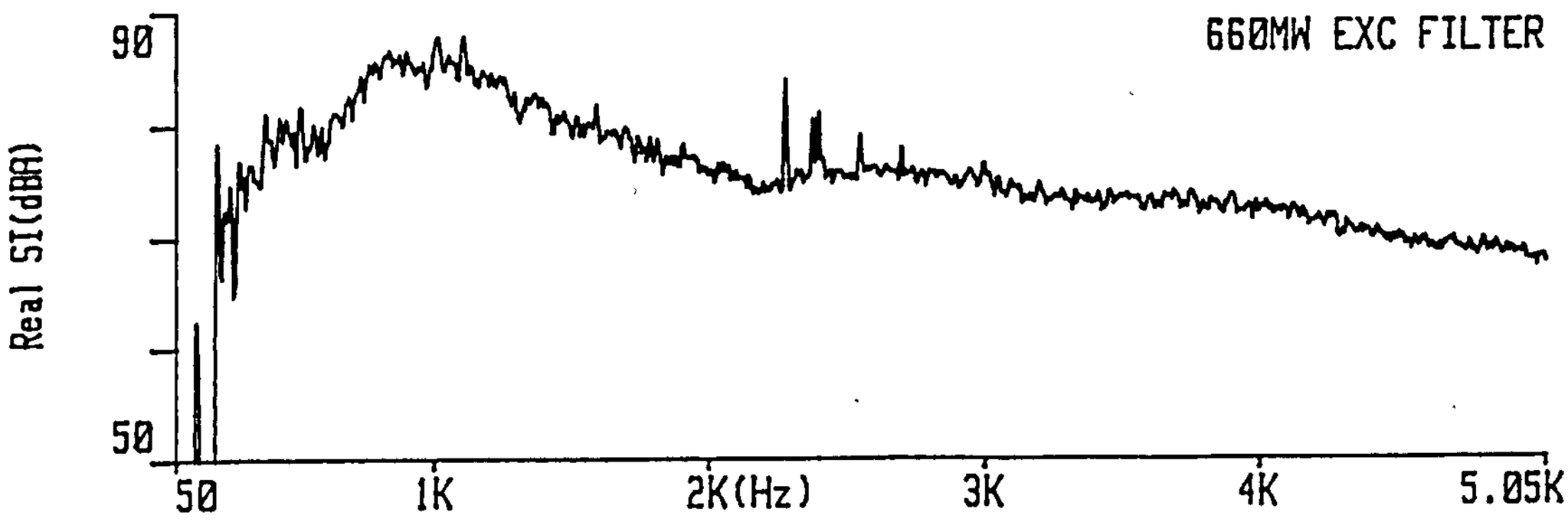

Fig.5.7 Narrowband sound intensity 5cm from 660MW exciter air make-up filter.

Frequency (Hz)	Shaft order (Harmonic)	Open Circuit Predicted % of Force harmonics	Full load Predicted % of Force harmonics	Open circuit Measured % of vibration velocity harmonics
100	2	100	100	100
200	4	3.2	20.4	3.4
300	6	8.6	23.4	4.7
400	8	8.0	14.1	2.8
500	10	1.9	5.1	1.8
600	12	0.9	3.8	1.4
700	14	3.2	6.6	1.3
800	16	2.7	4.2	0.7
900	18	0.7	2.4	0.6

Table P: Comparison of harmonic content for predicted radial forces on open circuit and full load and measured open circuit vibration expressed relative to the twice supply component

On open circuit the twice supply frequency force component dominates the overall level with the next component, the 6th harmonic, being only 8.6%. For full load conditions with 0.8 lagging power factor the 4th and 6th harmonics increase to over 20%, which is to be expected from the more distorted flux and force waveforms. The twice supply frequency force component was increased by 14% from open circuit to full load 0.8 lagging power factor. The actual vibration velocity level can only be approximately compared to the force spectrum because of the obvious influence of the structural response. To some extent for such a large vibration survey this will be averaged out and there is a definite correlation with the predicted forces. Unfortunately test data was not available for validation of full load results.

Tampion's[18] results were not completely consistent. Whereas the twice supply component decreased markedly from leading to lagging power factor, the variation with increase in MW was a decrease for one machine and an increase for another. The discrepancy was due to approximising the rotor M.M.F. as a sine wave omitting the 3rd and 5th harmonics, which when included resulted in a slight increase in vibration with increased MW. The finite element approach more correctly models the rotor M.M.F. and probably also saturation.

The acoustic emission is proportional to the mean velocity squared, but also the radiation behaviour of the generator casing. The later relationship is complex. The force harmonic squared is therefore approximately related to velocity squared and sound power. The 4th and 6th force harmonics squared are between 12 and 14 dB less than the fundamental. The A weighting alters these components, but the relative harmonic magnitudes is reflected in the measured sound power spectrum for the 660MW generator, Fig.4.23a.

5.2.1.2 **Aerodynamic noise**

In general for large induction motors the major noise source is aerodynamic generating of the order of 75% of the total level. The solid generator rotor can have larger dimensions implying a similar trend. The 660MW generator considered at site had a rotor diameter of 1.14m and fan OD of 1.28m corresponding to peripheral velocities of $179ms^{-1}$ and $201ms^{-1}$ respectively. The total generator hydrogen flow is large being 10.2 m^3s^{-1}.

For the air cooled generator the measured internal S.P.L. was 112.8 dB(A). The spectrum (Figs. 4.48a to 4.48c) was mainly broadband implying that the major source mechanisms are vortex shedding and unsteady flow effects. Siren mechanisms at the rotor slot passing frequency are not prominent for large air gap machines. For many electrical machines the fan is the dominant noise source, but for the generator the large rotor length relative to that of the fan and the small ratio of the outer diameters of the components suggests that rotor noise is more important. This is reflected by the presence, but not dominance of the fan blade passing frequency, for the air cooled generator. Similarly for the 660MW hydrogen cooled generator the fundamental blade

passing frequency of 1550 Hz was present in the sound power spectrum (Fig.4.23a), but the value of 71 dB(A) was low.

The variation of A weighted level had a 4.8th power relationship with speed, Fig. 4.49, which was similar to the 5th power measured by Hübner[20] for induction motor rotors.

From the speed relationship it is estimated that the 660MW generator levels will be 3 dB greater than the air cooled generator because of a greater rotor diameter. The acoustic cover manufacturer estimated the reverberant build up for the air cooled generator will be reduced by 3 dB from that of a unlined steel cover implying an internal S.P.L. for the 660MW generator of approximately 120 dB(A).

For the high internal levels outer generator casing transmission loss is expected to be high to explain the measured low output levels. The generator transmission loss was calculated using the statistical energy analysis outlined in [22] by considering the response of the generator cylinder to broadband diffuse noise and the consequent acoustic re-radiation. Transmission due to resonant and non-resonant vibration is determined. For this analysis the resonant transmission is determined in terms of modal density and radiation efficiency of the structure. Standard flat plate theory is used to calculate non-resonant transmission with adaptation to the particular vibrational behaviour of cylinders by a statistical method. The transmission loss for each 1/3 octave from 31.5 Hz to 10 kHz is given in table Q.

1/3 Octave Centre frequency (Hz)	Non-resonant TL (dB)	Resonant TL (dB)	Total TL(dB)	Measured Internal S.I. (dB(A))	Predicted External S.I. (dB(A))	Measured External S.I. (dB(A))
31.5	17.6	55.5	17.6	69.0	51.4	-
40	20.4	56.0	20.4	77.9	57.5	-
50	23.0	56.5	23.0	85.0	62.0	61.8
63	25.6	57.0	25.6	85.8	60.2	56.0
80	28.4	57.5	28.4	93.1	64.7	61.0
100	31.0	58.0	31.0	101.7	70.7	71.7
125	33.6	58.5	33.6	95.1	61.5	60.8
160	36.6	59.1	36.5	98.1	61.6	56.6
200	39.3	59.1	39.2	101.3	62.1	63.0
250	42.1	59.1	42.0	101.3	59.3	64.2
315	45.3	55.4	44.9	102.1	57.2	66.4
400	42.4	73.7	42.4	102.4	60.0	63.8
500	44.0	76.5	44.0	106.1	62.1	63.3
625	45.6	79.9	45.6	107.1	61.5	66.7
800	47.4	83.3	47.4	107	59.6	61.3
1000	48.9	86.3	48.9	109.1	60.2	63.5
1250	50.5	89.3	50.5	109.6	59.1	63.1
1600	52.1	92.5	52.1	107.1	55.0	59.4
2000	53.6	95.4	53.6	104.3	50.7	52.4
2500	54.9	97.3	54.9	107.4	52.5	60.0
3150	56.1	100.3	56.1	106	49.9	58.6
4000	56.9	98.4	56.9	102.6	45.7	-55.7
5000	57.0	92.6	57.0	99.6	42.6	-61.4
6250	55.1	91.5	55.1	91.4	36.3	-
8000	-	66.7	66.7	90.1	23.4	-
10000	-	69.5	69.5	87.9	18.4	-

Table Q: Predicted transmission loss (TL) for generator casing (dB) and comparison of predicted and measured external sound intensity.

The sound pressure levels inside the air cooled generator enclosure, with appropriate scaling for extra reverberation and larger rotor dimensions, were related to the transmission loss to predict approximate external sound intensity levels. These levels were compared to the average measured sound intensity on the generator wrapper.

The theoretical model and the comparison with actual levels is approximate due to a number of necessary assumptions regarding internal sound pressure levels, structural damping and behaviour of the endbrackets etc. It does illustrate a number of important points.

i. The structural transmission loss of the wrapper is large increasing from 31 dB at 100 Hz to 57 dB at 4 kHz.

ii. For frequencies less than 7.5 kHz the acoustic attenuation is mass controlled and above 7.5 kHz damping controlled.

iii. Low level power absorption was observed in the 4 kHz and 5 kHz octaves, but no others. As the transmission loss increases with frequency it appears that a value is reached at 4 kHz, where the reduced output is exceeded by low levels of input.

iv. The predicted low levels of surface sound intensity of 74.9 dB(A) coincides closely with the average measured intensity of 75.6 dB(A), which will be raised by 3 dB by magnetic noise transmitted directly from the core to the other casing. This analysis therefore explains that despite large levels of aerodynamic noise generated by the fans and rotor the transmission loss of the wrapper is so large as to attenuate levels of radial sound intensity to the order of 75 dB(A).

5.2.1.3 **Mechanical noise**

All plant considered in the preceding chapter operates on sleeve bearings, which are not normally an important noise source for electrical machines[11]. The main vibration component is at running speed, but these levels are already subject to stringent specification, typically 25μm p-p absolute pedestal vibration. At site the 660MW F.E. generator pedestal emitted 65 dB(A) at the running speed of 50 Hz, which is relatively insignificant.

For a generator rotor unbalance will create relatively little extra direct airborne noise and due to the large airgap the unbalanced magnetic pull due to dynamic eccentricity

is also insignificant.

Most modern generator units have brushless excitation systems obviating the need for brushgear. Brush noise is in general less significant for the smooth sliprings occasionally employed than for the sliding contact of current brushes against commutator segments used in d.c. machines.

5.2.1.4 Summary

In general magnetic and aerodynamic noise generated similar noise levels for a hydrogen cooled generator. The large transmission loss of the thick generator outer casing is important in minimising the latter. Mechanical noise is relatively unimportant. For air cooled generators the ratio of aerodynamic to magnetic noise is increased as the magnetic noise is more greatly attenuated by a free standing cover. The average free field intensity is approximately 3 dB greater for the air cooled unit due to lower transmission especially below 1 kHz.

5.2.2 Exciter noise

5.2.2.1 Traditional excitation systems

The traditional brushless excitation systems discussed in sections 4.1 and 4.2 have the main exciter, pilot exciter and rotating rectifier as separate components on the same shaft. For the 350MW arrangement considered in the factory all these components were in an enclosure and for the 660MW exciter arrangement considered at site the main exciter and rotating rectifier were in the same enclosure. Under these circumstances source identification opportunities are limited. The sound intensity sound power technique can only be utilised to compare sound power from components, which can be measured separately and not to distinguish between components inside one cover. The

use of vector measurements for source location is also restricted in the presence of stronger flow from nearby noise sources, which alters the net direction. The cover generates a reverberant internal field, which leads to further loss of directional information.

In general the exciter noise emission was relatively low, but greater than that for the generator. The 660MW exciter emitted 96.8 dB(A) sound power which relates to a free field sound pressure level at 1m of 78.5 dB(A) and a site S.P.L. of 86.0 dB(A). For the 350MW exciter the total sound power level of 99.5 dB(A) relates to a free field level of 80.2 dB(A) and a site S.P.L. of 87.6 dB(A).

Despite the aforementioned difficulties some information about exciter noise generation is evident. The sound power spectrum for the 350MW and 660MW exciter enclosures illustrated in Figs.4.11c and 4.23b respectively are predominantly broadband. Measurements close to the air make-up filters provide further insight into the source mechanisms as the transmission loss is low and the airflow is very limited implying the majority of the noise measured was not created by flow through the vent. These spectra in Figs.4.17 and 5.7 for the 350MW and 660MW exciters are predominantly broadband and it is this broadband noise, which determines the overall noise level from the exciter. The source of noise is aerodynamic with vortex shedding from the exciter rotor periphery, the fans and the rotating rectifier with diodes, fuses, attaching bolts and electrical connections.

A number of tones of lesser importance exist and can be related to their probable sources. For the 350MW exciter unit the sound power (Fig.4.11c) and air make-up filter intensity (Fig.4.17) spectra show tones at 800 Hz and harmonics thereof, especially at

4 kHz and 4.8 kHz. These tones are created by the pilot exciter siren action and will be discussed further in section 5.2.4. Other tones exist at 900 Hz and 3.6 kHz, which were increased from no load to full load conditions, as is evident from Figs.4.16a and 4.16b. The 3.6 kHz tone is due to flux ripple imposed at the rotor slot passing frequency. The 900 Hz is also due to magnetic forcing and may be a function of the rectifier action. This tone is evident also on no load due to the diode module passing frequency of the rotating rectifier. Tones at 100 Hz and harmonics thereof are due to the rotating rectifier field connections.

The sound power spectrum (Fig.4.23b) and the air make-up filter intensity spectrum (Fig.5.7) for the 660MW exciter exhibit many similar tones. The tones at 100 Hz and harmonics are present due to field connections. The flux ripple created at exciter armature slot passing frequency of 2700 Hz is also evident. Tones at 1200 Hz and 2400 Hz are related to the number of fan blades and also the number of diode modules (24). The 100 Hz and harmonics thereof, 2400 Hz and 2700 Hz tones are also evident in the sound pressure surface vibration coherence spectrum (Fig.4.44d) illustrating the value of the quantity for source identification especially of tonal sources.

Without detailed measurements with the enclosure removed further source location is not possible.

5.2.2.2 **Overhung excitation systems**

The overhung excitation system is appreciably more compact than the traditional excitation system as illustrated in Fig.4.47. The overall exciter sound power level was 104.0 dB(A), which relates to a free field S.P.L. of 88.7 dB(A) at 1m and actual site

level of 93.2 dB(A). From the various acoustic spectra much can be deduced about the principal noise generating mechanisms.

The sound power spectra for the complete exciter and its constitute parts (Fig.4.50), and the intensity at the cooler flanges with the cooler unconnected (Figs.4.54a and 4.54b) all exhibit components at 800 Hz and harmonics thereof due to the pilot exciter siren tones.

The sound power and pressure spectra have a strong tone at 3.5 kHz, which contributed 40% of the overall power level. This tone is due to magnetic forcing on the exciter as is evident from the R.E. endcover sound power unexcited and full load spectra in Figs.4.52a and 4.52b.

The forcing mechanism is similar to the main noise problem of D.C. machines[66,67]. There is radial and circumferential pole ripple forcing at the rotor slot passing frequency, which for 70 armature slots is 3.5 kHz. The magnitude of the force may be 10^4 times less than the constant force, but still is sufficient to induce large vibration and noise. It is complex to predict the forcing magnitude due to the high levels of accuracy necessary to calculate these small forces. A finite element mesh solution at different rotor angular positions in time can be Fourier decomposed to give ripple forces[67].

This forcing can be minimised by optimising the pole arc in terms of armature slot pitch. For example if the pole is an integral + 1/2 number of armature slots per pole pitch a 180° phase rotation between adjacent poles could be established and therefore limiting particular vibration modes. Skewing the armature by one armature slot pitch

levels are 98.2 dB(A) and 92.4 dB(A) respectively, which closely resembles the measured level of 97.0 dB(A) and 91.8 dB(A).

Broadband aerodynamic noise constitutes approximately half the overall level. The rotating rectifier is more compact and the diode module diameter is 2.3 times less for the overhung exciter than the 660MW unit. For vortex shedding the sound power varies as a 6th power of peripheral speed implying that noise output is 20 dB less for the overhung construction.

It is therefore expected that vortex shedding on the exciter armature will be the main source of broadband noise. The overhung exciter is 5 times shorter and the rotor diameter is 1.15 times greater, which relates to 3.4 dB less than the 660MW unit using Hübner's[20] proportionalities of length of armature and 6th power of peripheral speed.

5.2.3 Rear end generator coupling

The uncovered R.E. generator coupling for a 985MW unit was a strong noise source emitting 112.4 dB(A) sound power. The spectrum, illustrated in Fig.4.8c, contains pure tones at 100 Hz and harmonics thereof. This is due to the fluctuating pressure distribution on the surface of the 2 upshaft connections consisting of copper stalks and copper straps, which pass generator field current over the coupling interface from the exciter. The broadband noise, due to vortex shedding from the highly irregular protrusions rotating at a high peripheral velocity of $125ms^{-1}$, contributes 83% of the overall level.

The sound power level measured from the coupling with a conventional 5mm steel

unlined cover was 103.5 dB(A) with the spectrum noticeably altered, Fig.4.23c. The sound transmission loss yielded by the cover is 9 dB. The reason for the low reduction for the 5mm cover and the subsequent significant noise levels, 93.1 dB(A) free field S.P.L. and 94.6 dB(A) site S.P.L., was due to a number of standing waves being set up between the different upshaft connections geometries and the tight fitting enclosures. These resulted in the tonal components between 2.5 kHz and 4 kHz. The transmission loss is further reduced by 1.5 dB, because of the 2.5cm clearance gap from the cover to the exciter for ventilation.

To reduce R.E. generator coupling noise new acoustic covers were designed (Fig.4.56). The sound power emission from the modified cover was 98.6 dB(A) with the temporary wooden F.E. baffle connected. The reason for an improvement of 4.9 dB is apparent by comparing the sound power for the modified and original cover plotted in Figs.4.57b and 4.23c. The acoustic absorption has been effective in "damping" the predominant pure tones in the frequency range 2.5 kHz - 4 kHz. The spectrum is more characteristic of the uncovered R.E. generator coupling, Fig.4.8c, with broadband noise superimposed with pure tones at 100 Hz and harmonics thereof due to radial stalks. The extra tone at 800 Hz is due to 14 exposed bolt heads spaced as 16. This will be less pronounced for the countersunk site bolt holes. As explained in section 4.4.3 the sound power emission is raised 2.4 dB by the temporary wooden F.E. baffle implying a total reduction of 7.3 dB. The site output power of 96.2 dB(A) relates to a free field pressure of 85.8 dB(A) and an actual site level of 87.3 dB(A).

The sound pressure surface vibration coherence was effective in identifying the influence of the R.E. coupling cover on the high sound pressure levels despite the high levels of reverberant background noise for the site 660MW investigation. The

coherence tends to 1 for the standing waves components in the frequency range 2.5 kHz - 4 kHz. The spectral similarity between cover vibration velocity squared and unweighted sound pressure 1m from the exciter F.E. was also strong as is evident by comparing Fig.4.44f and 4.44g.

5.2.4 **Pilot exciter**

The pilot exciter was the major noise source for the complete 660MW unit emitting 106.7 dB(A) sound power creating a S.P.L. of 102 dB(A) at 1m. The majority of the sound power, 105.6 dB(A), exits directly out through the cover ventilation openings. The sound power and sound pressure spectra, Figs.4.23d and 4.43d, have strong tonal components at 800 Hz and harmonics thereof, which contribute the major part of the overall level. The remainder of noise generation is broadband. These tones are also evident for the overhung exciter and 350MW exciter enclosure, which contains the pilot exciter, sound power spectra Figs.4.50 and 4.11c respectively.

To reduce the noise emission from the 660MW pilot exciter new acoustic covers were designed (Fig.4.55). The sound power emission from the modified cover was 95.3 dB(A), which relates to a free field S.P.L. of 88.9 dB(A) at 1m from the pilot exciter and an actual site S.PL. of 90.9 dB(A). The sound power spectrum, Fig.4.57a, is reduced in level, but retains a similar composition.

The 800 Hz and harmonics thereof tonal components are created by the pilot exciter's siren mechanism. The air centrifugally thrust outwards from the 16 permanent magnet shoes encounters very different airflow impedances dependant upon the rotor position relative to the stator windings and vent openings. This creates a volume pulsation of air through the stator vents used to cool the machine.

The stator ducts produce an interference pattern and radiate noise to the far field. This monopole volume pulsation is the most effective means of noise generation, which explains how a relatively small machine can generate such predominant noise levels. It is a problem frequently encountered in electrical machines with small air gaps[68,69].

The remainder of the noise generation is due to vortex shedding effects and unsteady flow effects through the stator vent channels. The noise generation of this component will be considered in detail in chapters 6 and 7.

6. PILOT EXCITER SIREN TONE CALCULATIONS

6.1 GENERAL THEORY OF SIREN TONE CALCULATIONS

6.1.1 Introduction

The pilot exciter has been identified as the major noise source for the complete 660MW unit emitting 106.7 dB(A) sound power creating a sound pressure level of 102 dB(A) at 1m. The spectra contain strong tonal components at 800 Hz and harmonics thereof, which contribute the major part of the overall level. The tonal components are generated by the volume pulsation of air through the stator vent ducts due to a periodic variation of airflow resistance with rotor position. As well as this siren effect broadband aerodynamic noise is created by unsteady flow effects and vortex shedding.

A prerequisite of implementing design changes to reduce these noise levels at source is to produce a theoretical model, which can relate the siren tone noise levels to the machine geometries and aerodynamic behaviour that create them. To quantitively relate the cause with the effect is the objective of the foregoing analysis. To explain the siren mechanism further and present the physical structures being modelled the construction of the 660MW pilot exciter is outlined initially. The theoretical modelling process is discussed in this section. The detailed duct acoustic behaviour, airflow modelling, solution for volume pulsation and radiation characteristics of the pilot exciter are outlined in the remainder of this chapter. A full scale test rig was designed to accurately simulate airflow and acoustic behaviour. This provided parameters which could not be predicted accurately enough, verified the modelling process not only with the final sound power emission levels but also in intermediate steps and facilitated comparison of the dynamic behaviour with the quasi-static model adopted. This is presented in the following chapter.

6.1.2 660MW pilot exciter construction

The general arrangement of a 660MW pilot exciter is illustrated in Fig. 6.1 and more detailed axial and radial cross-sections are illustrated in Figs. 6.2 and 6.3 respectively. The solid steel rotor has sixteen magnetic poles, which consist of permanent magnets restrained by magnet pole shoes. The laminated stator consists of five packets of core plate. The stator is cooled by air passing radially through the vents which provide a 6.35mm thick gap. The vent plate profile and two pole magnets are illustrated in Fig. 6.3. The shaded parts of the stator are windings, which pass axially through the machine. The maximum duct length is 63.5mm. The core is built on eight axial support bars. The machine ventilates by using the self generated head of the magnet poles. Air enters axially between the magnet poles and exhausts through the ventplate. The pole shoes are slightly skewed, but the pilot exciter rotor still acts as an inefficient radial blower. To indicate the dimensions of the pilot exciter the outer diameter of the magnet pole shoes are 465mm, the outer diameter of the stator is 597mm and the length of the stator core is 362mm.

6.1.3 Theoretical model

The prediction of sound power level due to the volume pulsation of air through stator ventilation ducts has been published by one author, Talaat[68], for an induction motor. The basic approach adopted for this model is similar, but a number of the underlying assumptions and techniques used by Talaat have been found to be incorrect. This model incorporates a number of significant improvements, which have been experimentally vindicated using the full scale test rig.

The source of the volume pulsation of air through the stator vents, the variation in airflow resistance can be further explained by considering Fig. 6.3. When the rotor

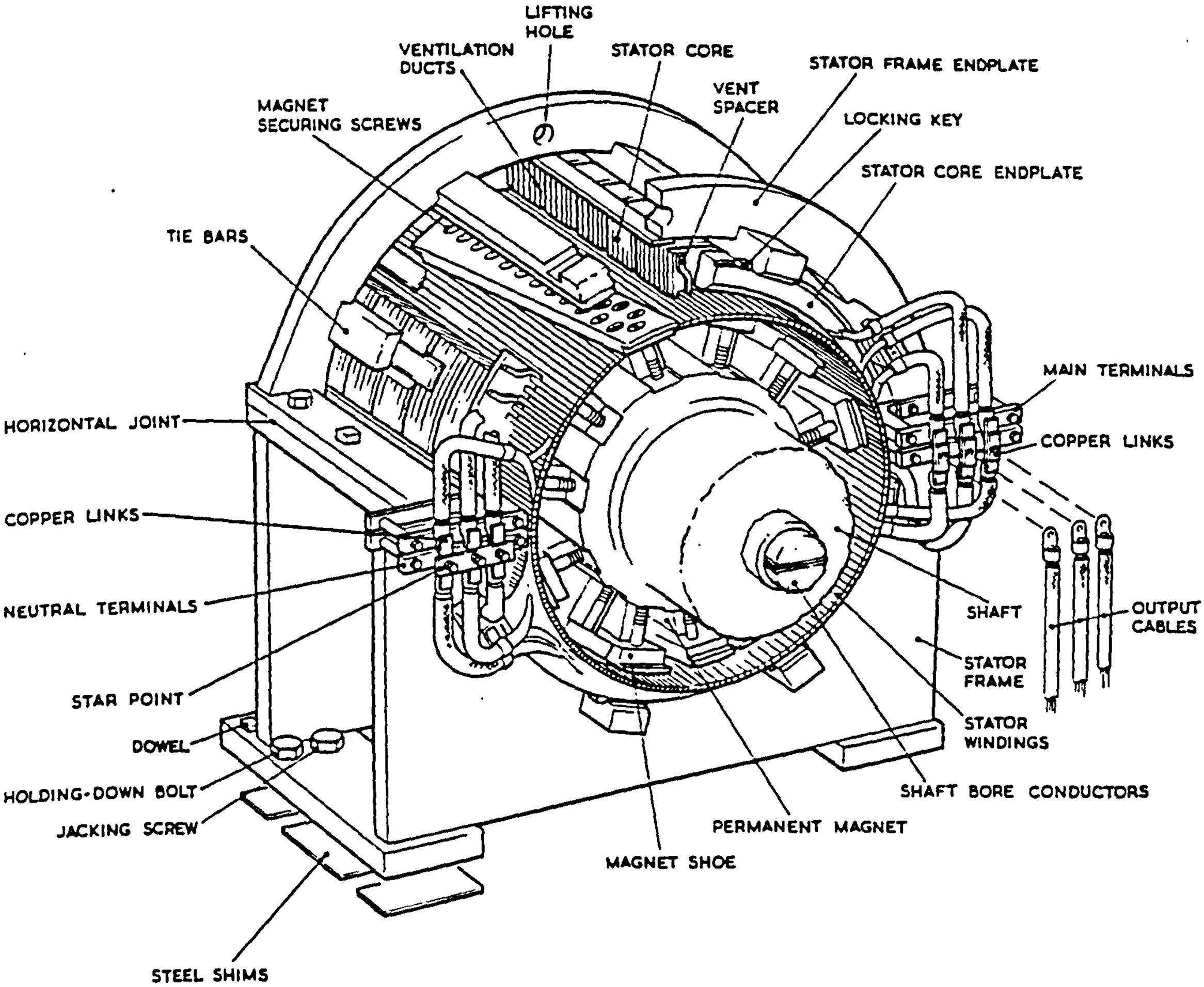

Fig.6.1 General arrangement of 660MW pilot exciter.

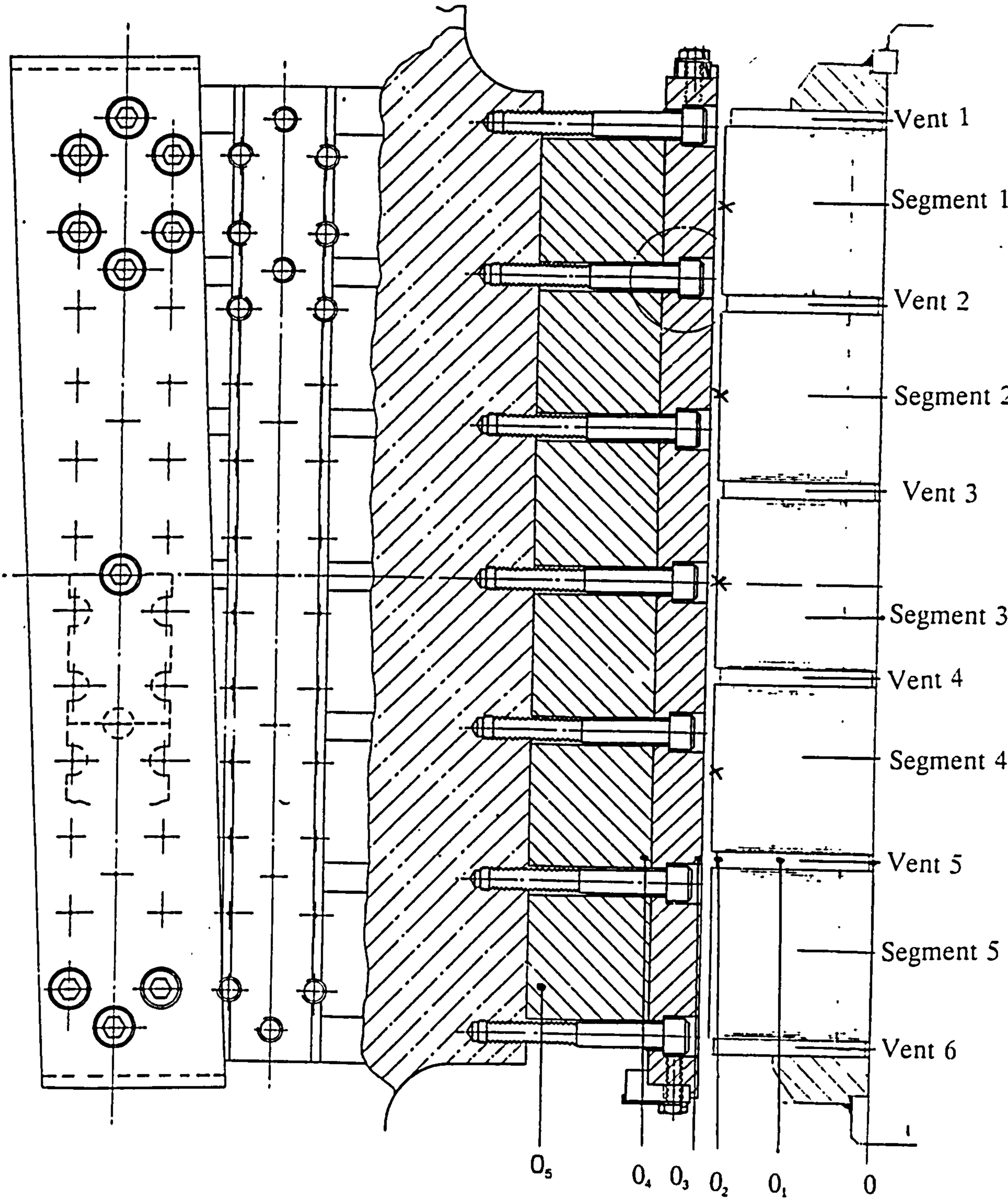

Fig.6.2 Axial cross-section of 660MW pilot exciter.

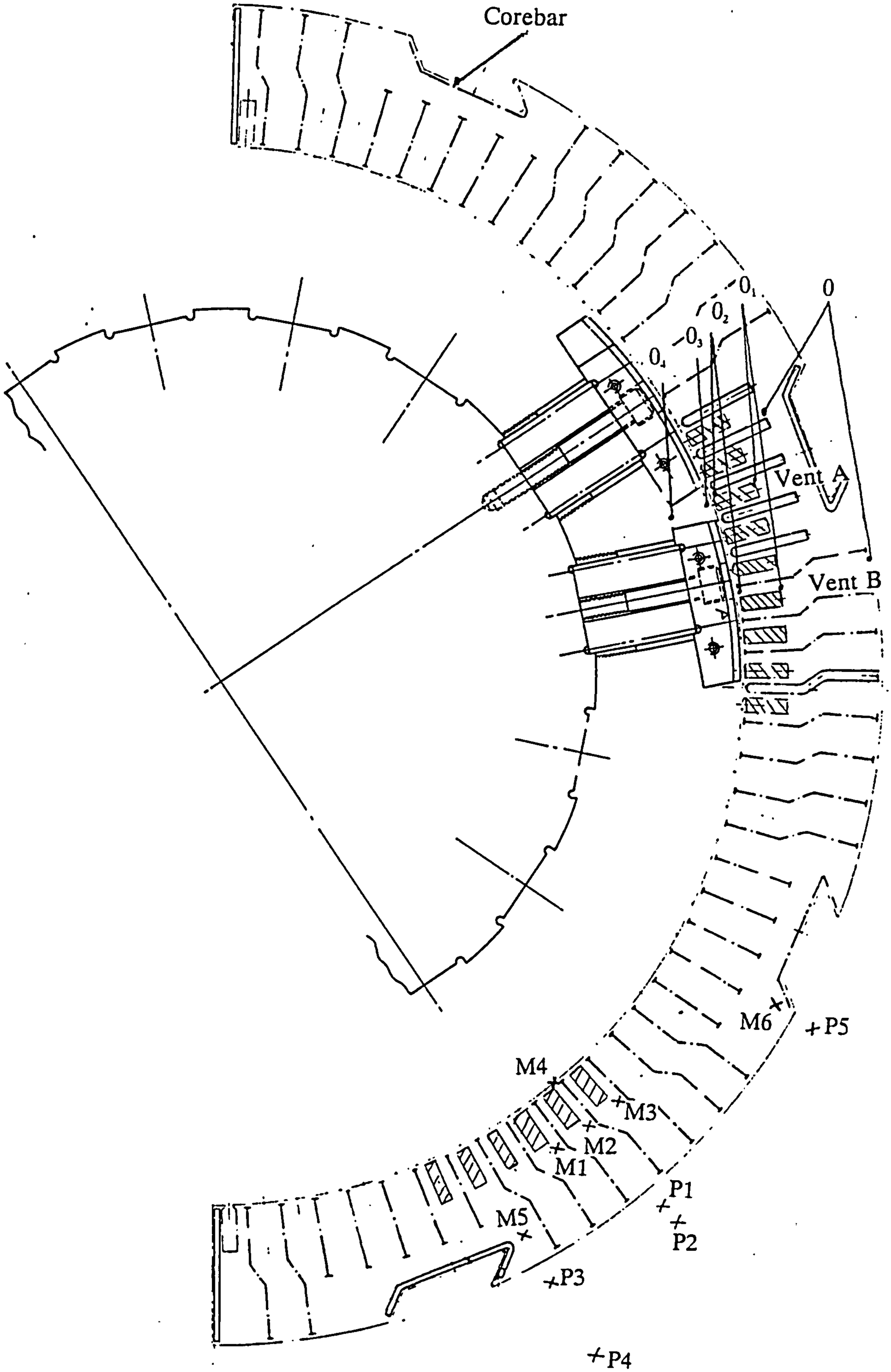

Fig.6.3 Radial cross-section of 660MW pilot exciter.

position aligns the gap between two poles with vent A, for example, the resistance to airflow is at a minimum. The resistance to air flow is at a maximum, when the centre of the pole aligns with a vent, such as vent B in Fig. 6.3. The cyclic variation in airflow resistance occurs at a fundamental frequency equal to the speed in revolutions per second times the number of pilot exciter magnet poles. This cyclic variation in resistance, in conjunction with the self generated pressure cause the generation of alternating volume pulsations at the fundamental and high order harmonic frequencies plus the steady cooling flow.

Quasi-static behaviour is assumed to enable standard fluid mechanics to be used to calculate the maximum and minimum airflow resistances. The real transient airflow behaviour is complex and the quasi-static assumption is investigated with time domain pressure measurements on the test rig. Talaat[68] assumed that the volume pulsation was sinusoidal plus a steady flow. Analysis of the time variation of the resistance indicates this is incorrect and also excludes modelling higher order harmonics, which as in the pilot exciter case under consideration, may be important.

A stator duct acts as an acoustically driven system, which picks up and radiates sound. It is assumed that the influence of energy reflected back to the driving system is negligible due to its greater store of energy, the correctiveness of which is assessed experimentally. The relationship between the volume pulsation, assumed to occur in or close to the air gap, and the outlet pulsation is calculated by considering an equivalent acoustic circuit for the duct.

The radiated sound power is predicted by summating the contribution of each duct to the sound pressure level at a large number of positions. The radiation characteristics

of any machine are highly dependant on the phase relationship between the various contributions.

Talaat's model did not incorporate this incurring large potential errors. This model accounted for radial phase lag between vents due to the time delay of adjacent vents experiencing the pressure pulses. There is a similar effect also for vents in an axial plane, because of the magnetic pole skew.

6.2 EQUIVALENT CIRCUIT

An acoustic equivalent circuit is used to model the acoustic behaviour of the stator duct as outlined in [63, 70]. The equivalent acoustic circuit is given in Fig. 6.4 and the equations for the various impedance terms are presented in Appendix B. The radiation impedance of the duct opening is considered as that of an baffled cylinder[63,70]. The constriction in the vent duct can be represented by a lumped acoustic inductance term obtained by Karal[71], who used a high order mode hypothesis. This approach yields good agreement with experiment[72] and better results than the entropy fluctuation hypothesis. Prediction of the source impedance is a very difficult problem, so it is commonly measured when required[70]. This is also difficult, but it is believed that the source impedance in this case will prevent backward pressure waves and have negligible influence on emitted sound power. This will be examined further from measurements made in the test rig air gap.

For the fundamental frequency of 800 Hz and higher order harmonics the length of the vent duct channel is greater than one eighth of a wavelength. The acoustic impedance of each vent duct channel is analoguous to that of the long ideal transmission line. The area of each vent duct varies linearly with the radius of the machine, which can be

solved for using the 1 dimensional wave equation. This solution makes it possible to represent each vent duct section by its equivalent T-network. Each acoustic impedance is transformed to be that seen from the air gap, as the excitation is assumed to take place at the air gap. The equations used to calculate the equivalent acoustic circuit are given in Appendix B.

The model assumes that the centrifugal pressure head generated by the pole shoes exists behind the variable non-linear airflow resistance r. This resistance regulates the volume flow of air through the stator vent duct channel. The periodic variation in resistance with rotor position has been previously illustrated. It is expected that lumping all the nonlinear resistances into one single resistance located at the stator inlet will introduce little error as the majority of the resistance takes place at the entrance to and before the stator vent duct channel. This has been verified by considering the influence of each term in eqn. (C.10) on the total resistance. The concept of the nonlinear resistance term is used to model rotating disk sirens, for example by Jones[73]. Acoustic resistance due to viscosity is negligible.

The resistance r is derived using standard duct fluid mechanics[74] as outlined in Appendix C. The main modelling difficulty is predicting the pressure drop from the magnet pole outlet (0_3 in Fig.6.3) to stator vent inlet (0_2 in Fig.6.3). The minimum resistance was considered as an expansion term from the pole shoes and a contraction at the stator duct. The constriction coefficient is 0.37 from the area ratio, which is less than the coefficient of 0.5 for a sharp edged entry. For this condition the maximum equivalent area using eqn. (C.10) is 1.5×10^{-5} m². As expected this value is less than the minimum constriction in the air circuit of 2.48×10^{-5} m² at the stator inlet (0_3 in Fig. 6.3). The major resistance occurs at the constriction of the pole magnets (0_4 in Fig. 6.3)

and the inlet to the stator duct (0_2 in Fig.6.3). The maximum resistance cannot be accuracy predicted. As the airgap is small (2.5mm) compared with the pole shoe width (74mm) the resistance to airflow for the ventilation path through vent B relative to that through vent A is appreciably greater (Fig. 6.3). For a large value of resistance, which will be at least 10 times that of the minimum resistance, the equivalent area will be less than 4.5×10^{-6} m². The value of 4.5×10^{-6} m² was used for the curve fitting solution in section 6.3 for ease of convergence but the influence of the minimum area within the range 0-4.5×10^{-6} on volume velocity is less than 20%.

The actual behaviour at the stator inlet will be further complicated by the rotational action of the magnet poles increasing the angle of air exhaust from the magnet poles. This effect tends to increase the airgap pressure drop[75], but analytical expressions to calculate this influence are seldom adequate to characterise the true behaviour. As the main objective of the analysis is to calculate the pulsation of air through the stator ducts the relative influence of airflow angle should be reasonably minimal on the fluctuating component. This influence and that of "swirling" air entering the stator duct result in a larger underestimation of the mean velocity component.

The prediction of static pressure head centrifugally generated by the rotation of the magnet poles is not possible from simple analysis as it's behaviour is very different from known components such as radial fans. It may be predicted using a computational fluid dynamics package, but even this will have large uncertainty. The simple approach adopted in [68] to estimate the centrifugal head as the difference between peripheral velocities squared at the pole tips and shaft body times $\rho/2$ may incur less errors for the rotor duct arrangement on an induction motor. The error is however significant for a structure as complex and inefficient as the pilot exciter magnet poles. The pressure

head will also vary significantly with axial length as the impedance seen by the poles decreases markedly for the outermost ducts. It was therefore necessary to measure the head directly.

6.3 VOLUME PULSATION CALCULATION

To determine the radiated sound power it is necessary to calculate the volume velocity emitted from each stator duct. The solution calculates the individual volume velocity of the fundamental and higher order harmonics through the outlet radiation resistance of each of these frequency components. The outlet volume velocity harmonics, $V(\omega_n)$, are calculated by relating them to the volume velocity, $V_2(\omega_n)$, through the nonlinear variable resistance r using the alternating volume velocity equivalent circuit in Fig. 6.4b. The alternating pressure drop acting on the equivalent circuit is $P_D(\omega_n)$. From Fig. 6.4b.

$$V_2(\omega_n) = [a(\omega_n) + jb(\omega_n)]\, V(\omega_n) \qquad 6.1$$

$$P_D(\omega_n) = [R(\omega_n) + jX(\omega_n)]\, V(\omega_n) \qquad 6.2$$

The instantaneous volume velocity through r, $V_r(t)$, is the summation of the average volume velocity, V_o, and the alternating volume velocity components $V_2(\omega_n)$.

$$V_r(t) = V_o + \sum_{n=1}^{\infty} K(\omega_n)\, V(\omega_n) \cos(n\omega t + \emptyset(\omega_n)) \qquad 6.3a$$

where $K(\omega_n) = (a(\omega_n)^2 + b(\omega_n)^2)^{1/2}$, $\emptyset(\omega_n) = \tan^{-1}(b(\omega_n)/a(\omega_n))$ 6.3b,c

The instantaneous pressure drop across r, $P_r(t)$, is the static pressure P minus the

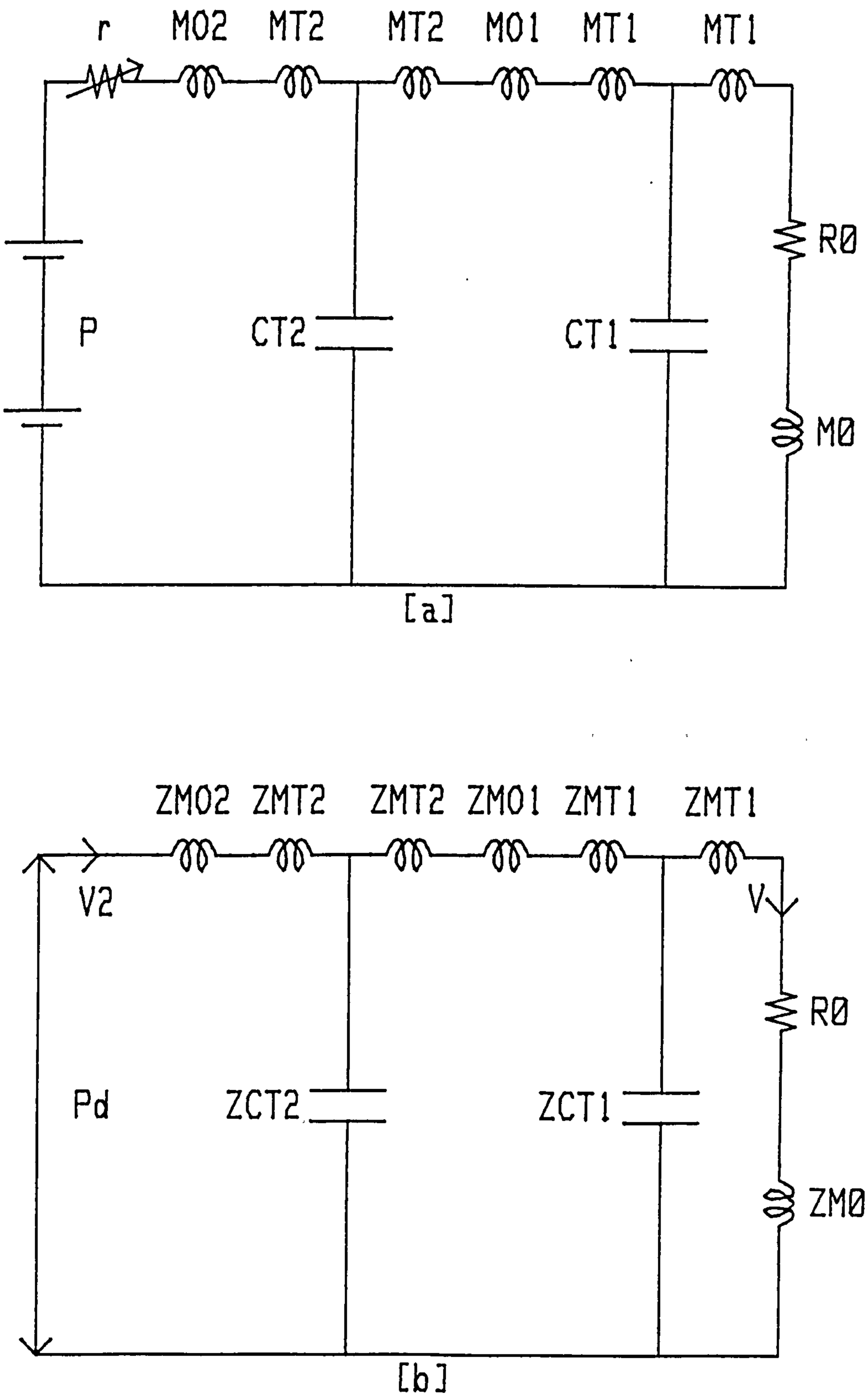

Fig.6.4 The equivalent circuit used in the calculation
a) with total instantaneous quantities
b) with alternating rms components

equivalent circuit alternating pressure drop components $P_D(\omega_n)$ from Fig. 6.4b.

$$P_r(t) = P - \sum_{n=1}^{\infty} Z(\omega_n)\, V(\omega_n) \cos(n\omega t + \theta(\omega_n)) \qquad 6.4a$$

where $Z(\omega_n) = (R(\omega_n)^2 + X(\omega_n)^2)^{1/2}$, $\theta(\omega_n) = \tan^{-1}(X(\omega_n)/R(\omega_n))$ 6.4b,c

By definition the nonlinear resistance r is

$$r = P_r/V_r = (\rho/2)\, V_r/S^2 \text{ where S is the equivalent area} \qquad 6.5a$$

therefore

$$S^2 = (\rho/2)\, V_r^2/P_r \qquad 6.5b$$

or

$$S(t) = (\rho/2)^{0.5}[V_o + \sum_{n=1}^{\infty} K(\omega_n)\, V(\omega_n) \cos(n\omega t + \emptyset(\omega_n))]/[P - \sum_{n=1}^{\infty} Z(\omega_n)\, V(\omega_n) \cos(n\omega t + \theta(\omega_n)]^{0.5} \qquad 6.6$$

By considering eqn. (6.6) it is apparent that the resonant behaviour of the duct will have a significant influence on the higher order harmonic volume velocity components. The magnitude and phase for $Z(\omega)$ and $K(\omega)$ are plotted in Figs. 6.5a-d and for the 2 duct lengths in the vent, Fig. 6.3. The impedance function Z has a major resonance at 2.18 kHz for the long duct. This is the most important resonance as the majority of the ducts, which contribute to the sound radiation are of this length.

The calculation of the maximum and minimum equivalent airflow areas was given in the preceding section. To solve eqn. (6.6) for the mean velocity and the significant alternating volume velocity frequency components it is necessary to estimate how the equivalent area varies between the maximum and minimum. The area variation was considered as the rotor passes the stator duct with reference to Fig. 6.6. The air flow area increases linearly as the trailing tip of pole 1 (T1) moves from P1 to P2. The

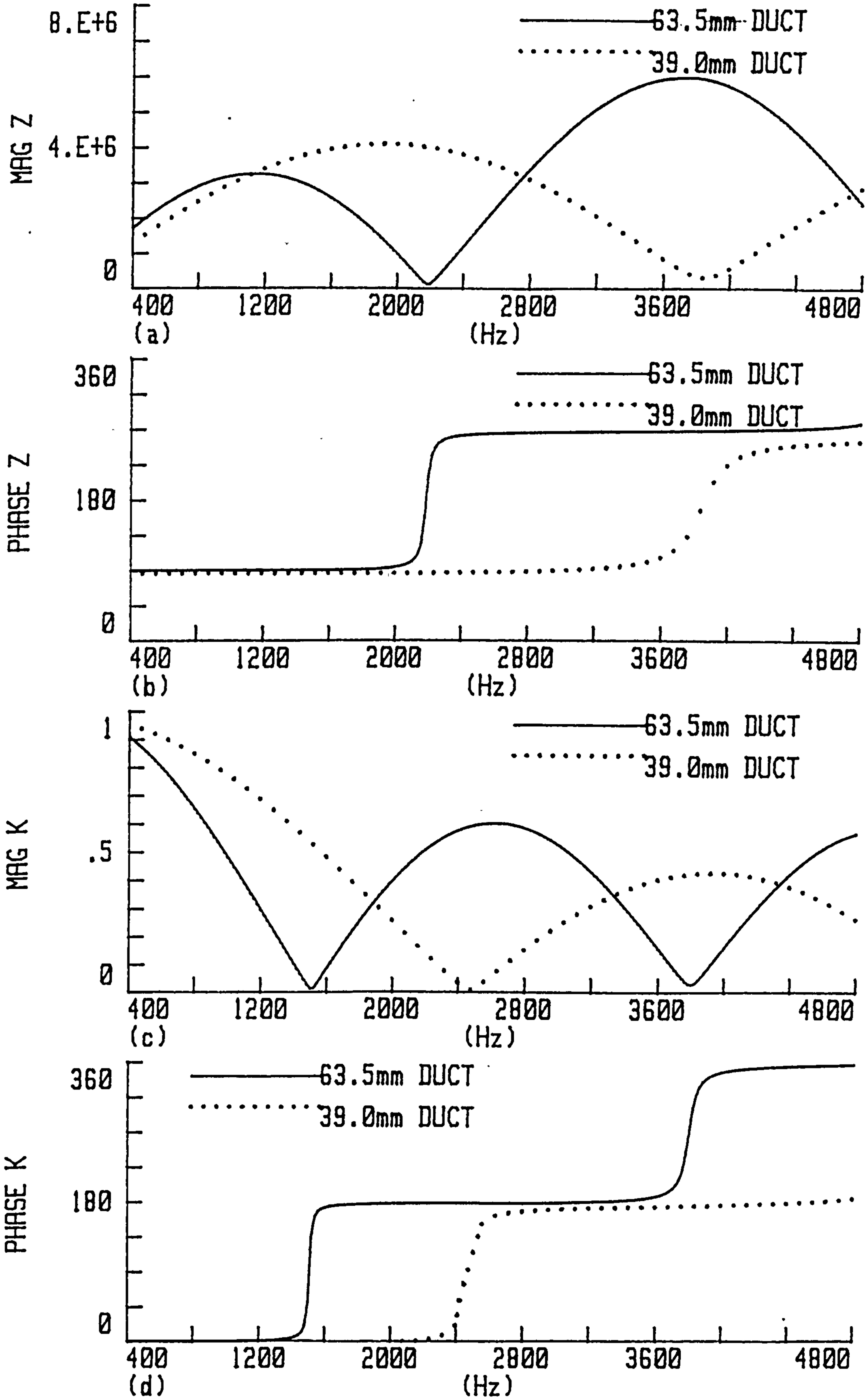

Fig.6.5 **Acoustic constants for Z a) magnitude & b) phase and K c) magnitude & d) phase.**

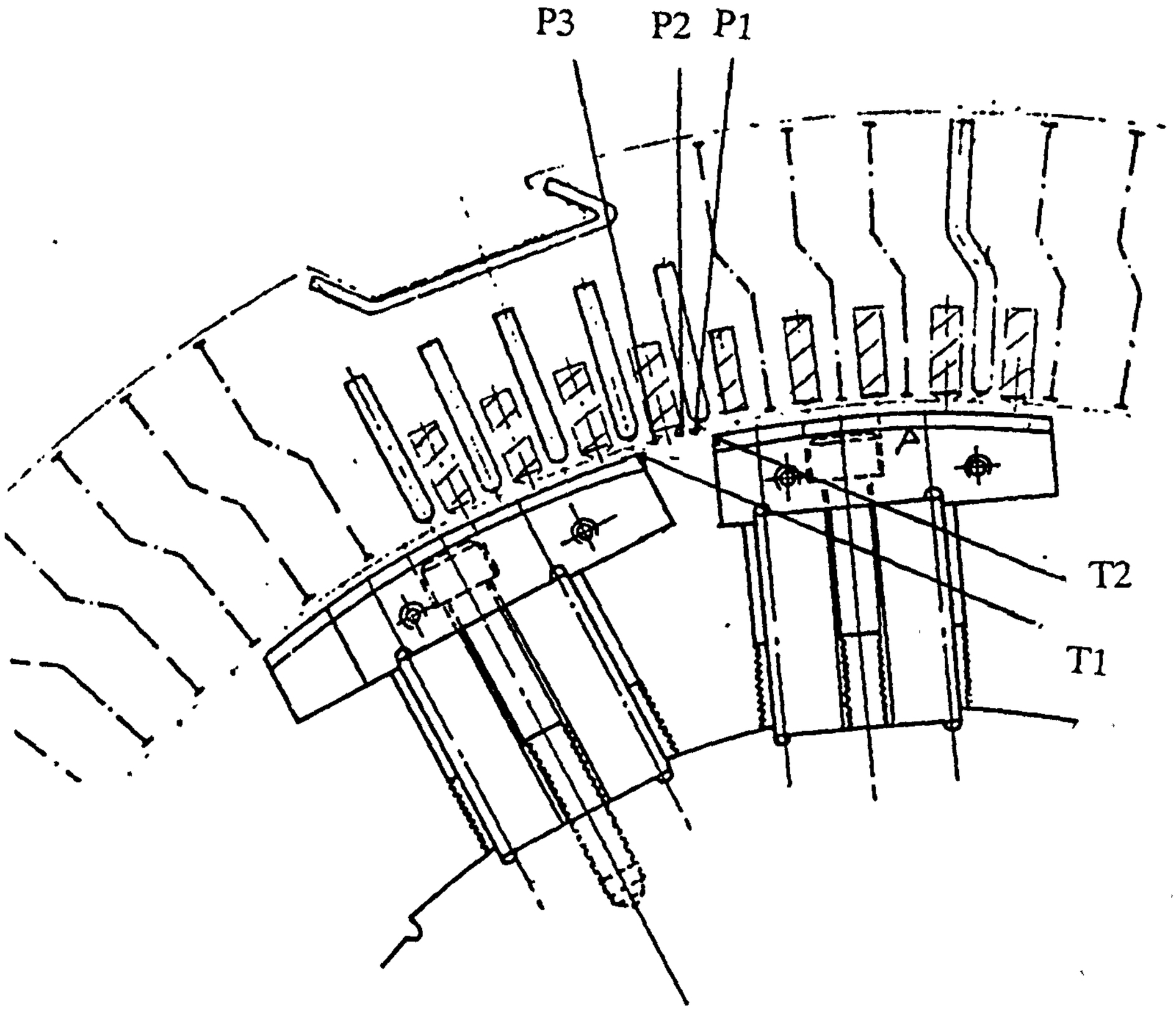

Fig.6.6 Expanded radial cross-section of 660MW pilot exciter.

area remains constant until T1 reaches P3 after which it increases to a maximum value. This is maintained until the leading tip of pole 2 (T2) reaches P1 and the pole starts "closing" the duct. The decrease in area is symmetrical with the increase. The approximate time variation in area is plotted in Fig. 6.7.

Eqn. (6.6) was solved for the volume velocity harmonics using a curve fitting program, which employed a least squares curve fitting method[76]. The program solved for the average volume velocity and the first six harmonics of the pole passing frequency using the magnitude and phase constants for Z and K and a phase curve fitting parameter for each volume velocity pulsation term. The average measured static air gap pressure, P, was used. This was 375 Pa for 3000 r.p.m. operation. The solution averaged to a mean r.m.s. error of 10.8% for the impedances of the long duct. The waveform accurately simulates the original area variation, Fig. 6.7 for the passing of 1 pole pitch. This could be further improved by incorporating more harmonics. The magnitude of the first four harmonics are given in Table R. The 2500 r.p.m. volume velocity harmonics were also calculated using the mean static pressure of 296 Pa. The levels are given from the longer duct (63.5mm) and the shorter duct (39mm).

	Volume velocity frequency components (m^3/s)			
	1st harmonic	2nd harmonic	3rd harmonic	4th harmonic
3000 r.p.m. long duct	6.2 E-5	8.3 E-5	1.4 E-5	1.1 E-5
short duct	5.6 E-5	4.8 E-5	2.2 E-5	2.2 E-5
2500 r.p.m. long duct	6.3 E-5	8.4 E-5	7.6 E-5	3.2 E-5
short duct	5.1 E-5	3.7 E-5	1.6 E-5	9.5 E-6

Table R: Volume velocity predictions for 1st 4 harmonics at 3000 r.p.m. and 2500 r.p.m. for the long and short duct lengths

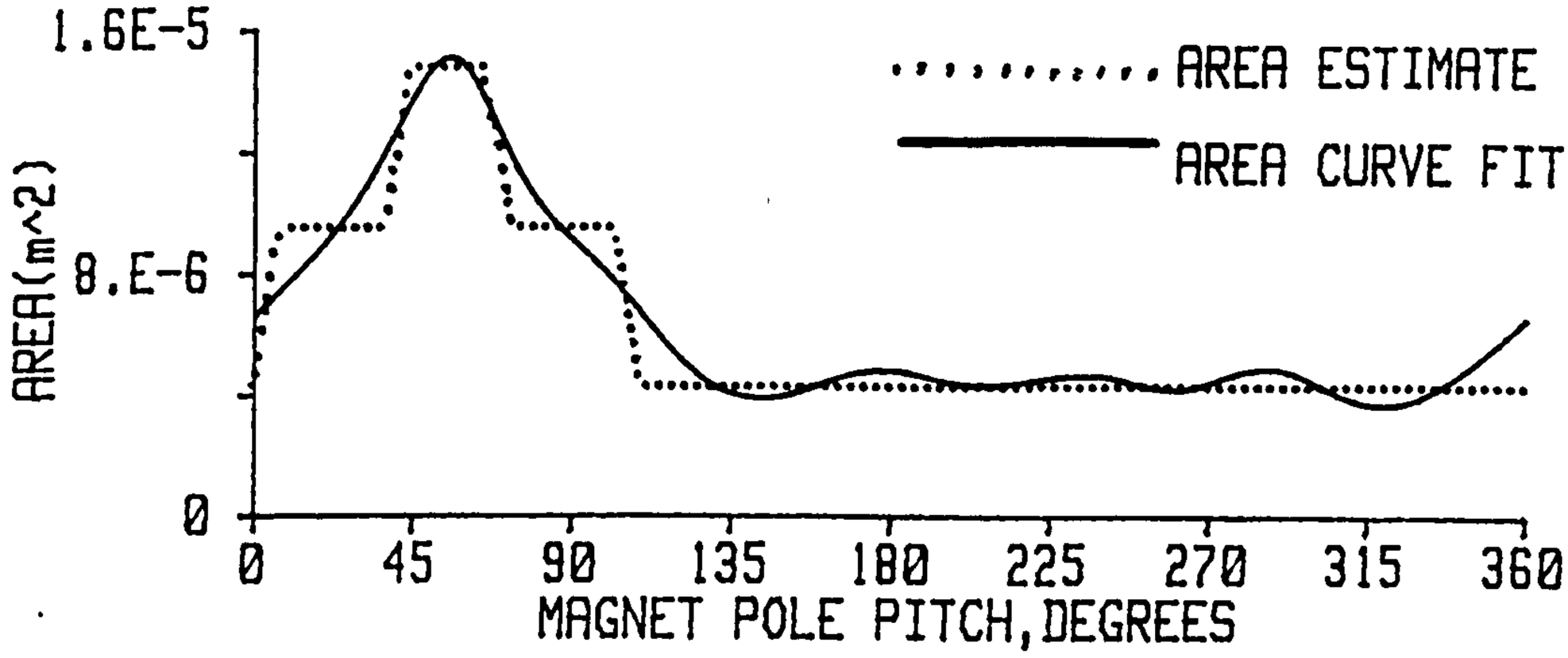

Fig.6.7 Estimated area variation and curve fit of this using eqn. (6.6) as the rotor passes 1 magnet pole pitch.

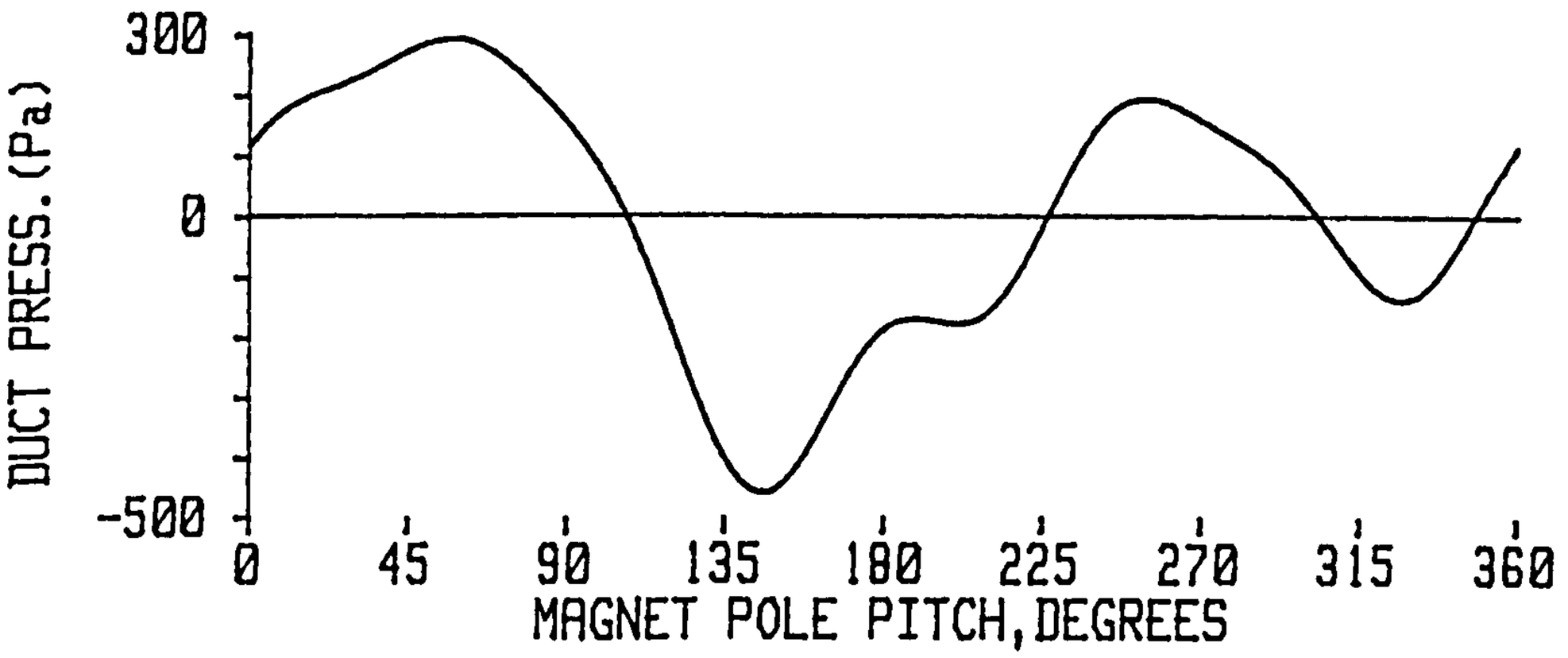

Fig.6.8 Predicted variation of duct inlet pressure.

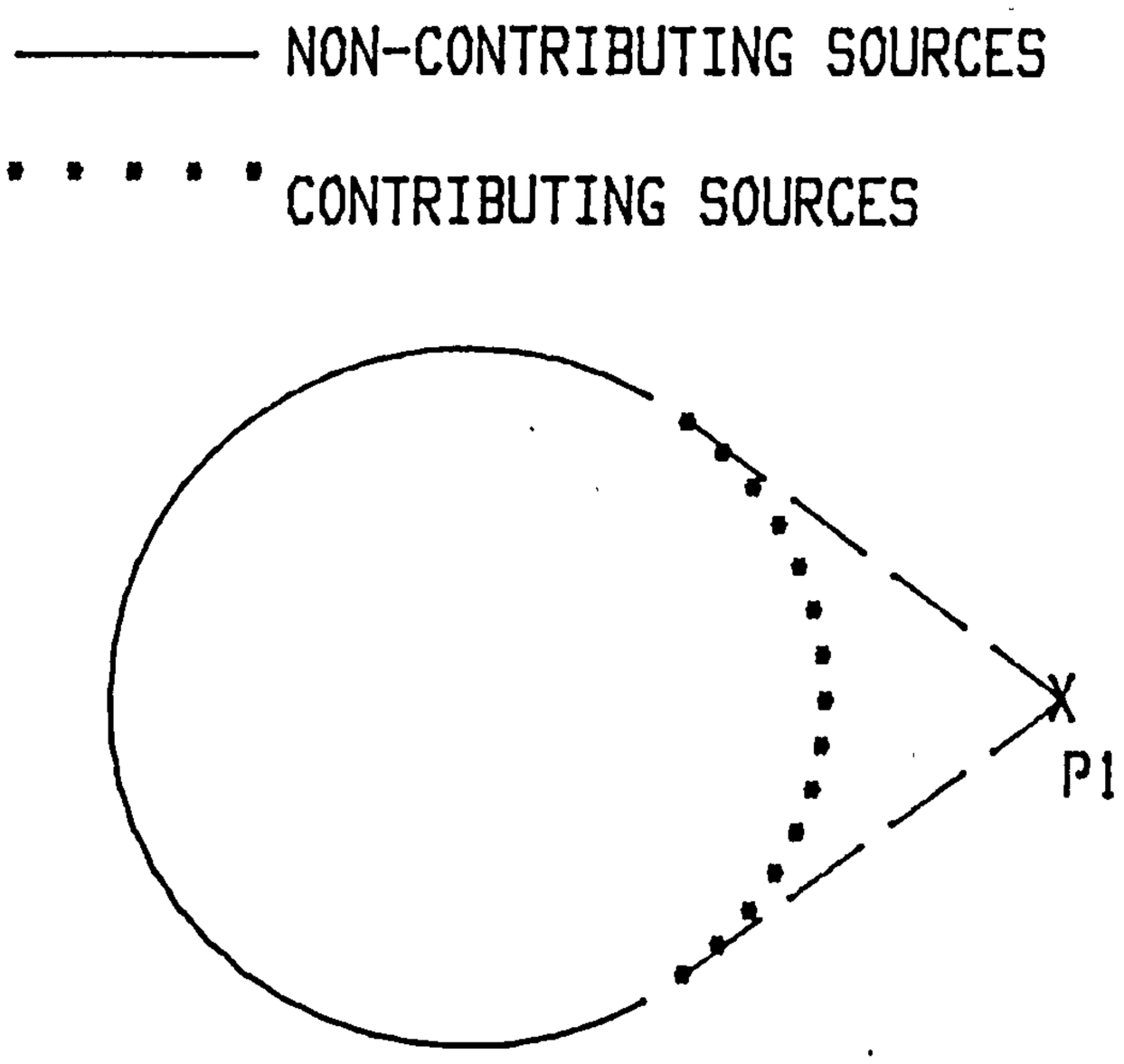

Fig.6.9 Baffled source distribution illustrating sources which contribute to pressure at P1.

For comparison with the measurements in section 7.3.4 the air gap pressure fluctuation at the duct inlet was predicted for 3000 r.p.m. operation. The alternating pressure components P_D were summated using eqn. (6.4a) rearranged with $P_D(t) = P - P_r(t)$. The resultant waveform, plotted in Fig. 6.8, exhibits a large negative pressure pulse.

6.4 RADIATION MODEL

The sound power radiated and sound pressure at any location is highly dependent not only on the magnitude of the volume pulsation, the source strength, but also on the interference pattern created by the pilot exciter as a whole. This radiation efficiency is dependent upon the phase relationship between the volume pulsation of each duct. A spatial configuration of discrete simple sources, each with its own complex source strength, can be used to represent the more complicated source the pilot exciter constitutes with 6 axially separated rings each of 96 sources (Figs. 6.1 to 6.3). The pressure at a point in the sound field is the summation of the pressure produced by each of the individual sources. Each duct is considered as a simple baffled source. A baffled source can be imagined as a simple source mounted on or close to a rigid plane boundary termed a baffle. The sound pressure at a distance r from each source is

$$p(r,t) = \{j\ \rho c\ Vk/(2\pi r)\}\ e^{j(\omega t - kr)} \qquad 6.7$$

where V is the volume velocity (m^3s^{-1}) and k is wavenumber.

The distance from the source to the field point of interest was calculated exactly in each case as a geometric approximation, such as that employed by Embleton[77], can result in significant inaccuracies.

For a baffled source pattern the sources on a ring, which contribute to the sound pressure at a position P1, lie on an arc between two chords from that position to the ring. This is illustrated in Fig. 6.9.

From the ratio of 16 magnet poles to 96 vents each 6th vent experiences the same pulsation at the same instant in time. The phase lag between adjacent vents is 60°. Due to skew of the rotor each axial vent is displaced by 3.1mm, which for a pole pitch of 91.3mm corresponds to an angular distance of 12.3° of 1 magnet pole pitch.

The radiation model calculates the appropriate magnitude for the volume pulsation using the r.m.s. volume pulsations calculated in section 6.3 accounting for axial and radial phase variation. The volume velocity for short and long ducts were incorporated in the model. The corebar regions were complex and it was assumed that the 2 ducts coinciding with the centre of the core bar will have the pressure waves reflected directly back therefore not contributing to the radiation pattern. The volume velocity for these vents was therefore considered as zero.

The volume pulsation for each vent varies along the length of the machine due to the axial variation in air gap static pressure. This is illustrated in 7.2.1. The volume pulsation for each axial plane is weighted for this variation. To ensure sufficient accuracy to characterise the sound pressure distribution and subsequently the sound power level, which equals the mean sound pressures times the enclosing area, a large number of points were considered (6237).

The variation of radial sound pressure level for the 800 Hz tone in two planes, at the centre and F.E. of the test rig is plotted in Figs.6.10a and b respectively. The

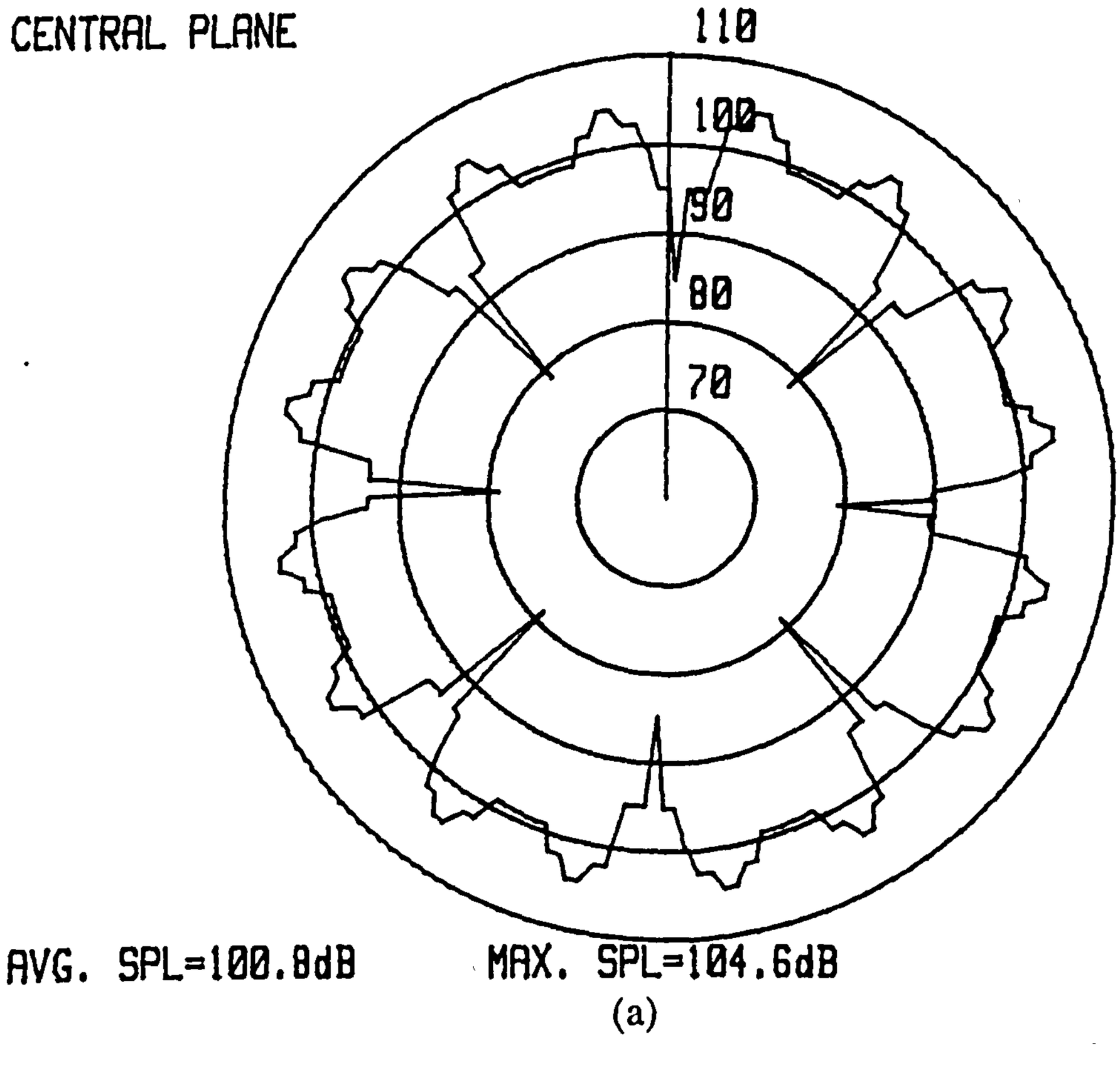

(a)

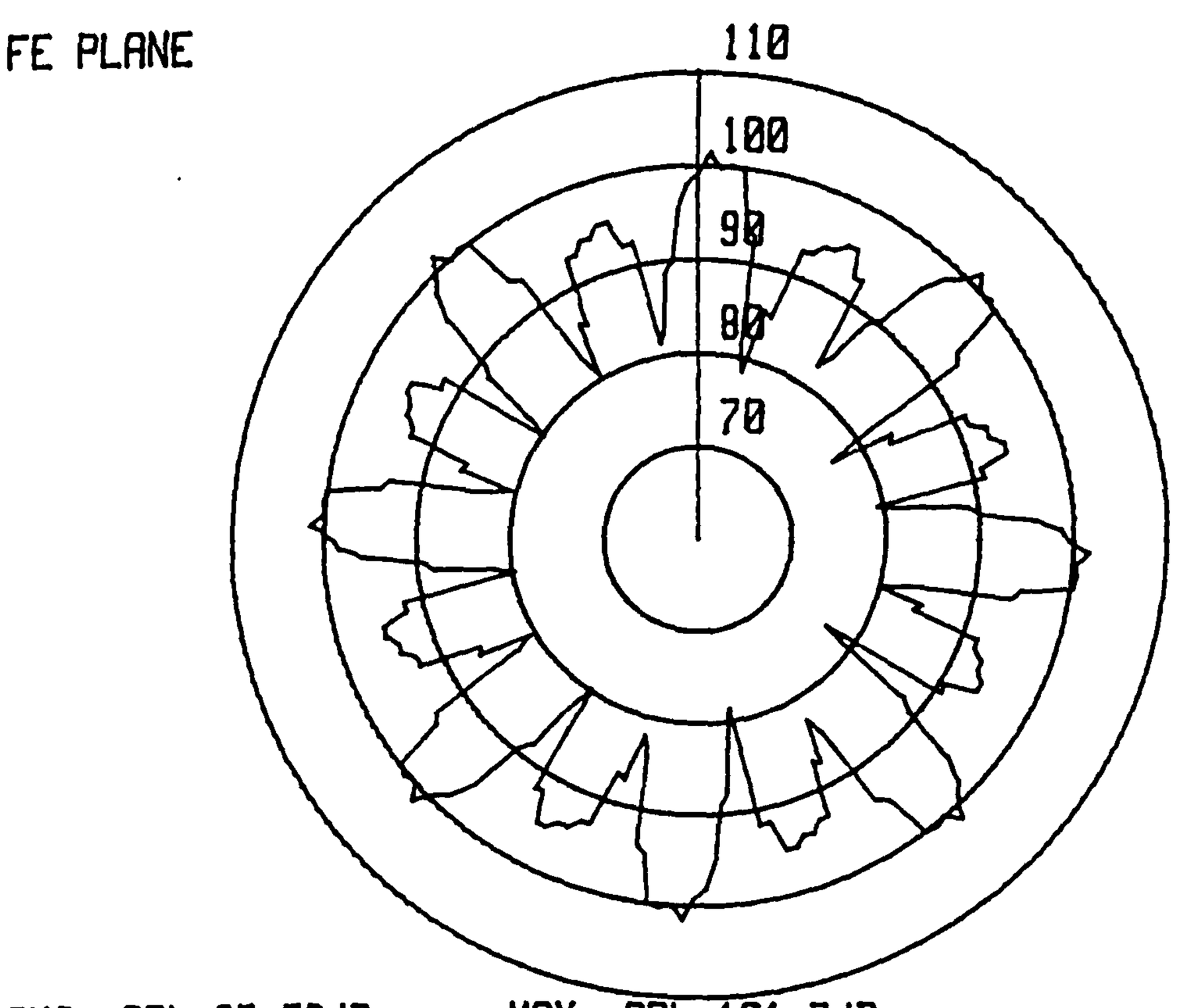

(b)

Fig.6.10 Predicted sound pressure level (dB(lin)) radiation pattern for pilot exciter 800 Hz siren tone for planes at the a) centre and b) F.E.

radiation pattern is complex due to the radial and axial phase relationship, different duct lengths and no radiation from the corebar ducts. For the F.E. plane, Fig.6.10b, the predominant influence is that of the adjacent vent 6, Fig.6.2, and the effect of the corebars is readily apparent creating major nulls. For the central plane the corebars do not create similar nulls due to the equal influence of vents 3 and 4. The nulls at 45° intervals are created by the axial phase difference, which causes the volume pulsation at these positions to have small values with different signs causing a large degree of cancellation.

The predicted sound power for the 3000 r.p.m. and 2500 r.p.m. operation is given in tables S and T respectively.

Frequency (Hz)	Predicted sound power level dB(lin)	Measured sound power level dB(lin)
800	99.3	101.0
1600	97.8	102.8
2400	88.1	101.2
3200	95.2	92.4

Table S Predicted and measured sound power levels for 1st 4 harmonics at 3000 r.p.m.

Frequency (Hz)	Predicted sound power level dB(lin)	Measured sound power level dB(lin)
667	100.3	96.7
1333	95.8	97.4
2000	92.9	95.1
2667	91.1	89.7

Table T Predicted and measured sound power levels for 1st 4 harmonics at 2500 r.p.m.

In general the agreement between the predicted and measured sound power, with the exception of the 2.4 kHz tone at 3000 r.p.m., is good for both operational speeds. Most harmonics are predicted to within 3 dB. The 2.4 kHz tone is underestimated for two reasons. Firstly the duct impedance resonance at 2.18 kHz for the longer duct is very sharp. At 200 Hz above and below this resonance the impedance is a factor of 5 higher, Fig.6.5a, and consequently the volume velocity is a factor 5 lower than that at the resonance.

The duct impedance calculation is liable to some error because of dimensional tolerances and modelling assumptions, which could culmimate in significant underestimation of the volume velocity prediction if the actual resonance coincides with 2.4 kHz. Secondly for the 3rd harmomic the radial phase lag is 180° between adjacent vents causing the volume velocity to alternate between positive and negative values significantly reducing the radiation to the far field. In practice due to random effects the actual radial phase difference will vary from the predicted value of 180°, section 7.3.7. This means that the reduction in radiated sound power may be less than the ideal case.

It is probable as the 3rd harmonic for the 2500 r.p.m. operational speed at 2 kHz is only underestimated by 2.2 dB the influence of phase difference deviating from the predicted value of 180° is of secondary importance. A potential underestimation of the 1st resonance predicted as 2.18 kHz by 10% would result in a significant increase in the volume velocity for the 3rd harmonic at 3000 r.p.m., but not 2500 r.p.m., explaining the underestimation in sound power prediction.

7. EXPERIMENTAL RESULTS FROM PILOT EXCITER TEST RIG

7.1 PILOT EXCITER TEST RIG

7.1.1 Objectives

A full scale test rig was designed to accurately simulate the airflow and acoustic behaviour of the pilot exciter. The detailed description of the test rig construction is given in 7.1.2 and the ability of the test rig to accurately simulate the acoustic emission of the pilot exciter is illustrated in section 7.3. It has previously been deduced from the 660MW pilot exciter site investigation that the predominant source mechanisms are siren tones and broadband aerodynamic noise. The test rig confirmed these deductions.

The test rig has the following principal objectives.

i) To obtain parameters which cannot be predicted

ii) To verify the theoretical modelling process

iii) To investigate the quasi-static airflow modelling assumption

iv) To incorporate further detailed noise source identification measurements

The self generated head of the pole shoes is very difficult to predict as conventional fan theory is not applicable for the irregularly shaped pole shoe configuration. The complexity of this prediction and the significant variation of air gap pressure with axial length means that the static pressure head must be measured.

The test rig has been used to verify the theoretical model outlined in chapter 6 not only by measuring the overall sound power, but also in intermediate steps comparing other measurable parameters such as airgap pressure variation with predictions. The

resonant behaviour of the duct, calculated as the duct impedance Z, can be investigated by comparing the variation of sound pressure in the airgap, vents and externally with rotational speed. The phase relationship between the volume pulsations from different ducts can be investigated experimentally.

The major modelling assumption was that of quasi-static airflow behaviour. The correctness of the assumption that the fluid mechanics behaviour can be considered as a series of separate time instants can be vindicated if the pressure variation with time at the duct inlet is similar to that predicted from the variation of equivalent area as the pole passes (Fig. 6.8).

The test rig was also used for noise source identification by conducting detailed nearfield sound pressure and vector sound intensity measurements. The variation of these quantities with rotational speed can yield important insight into source mechanisms with a 6th and 8th power of velocity relationship implying unsteady flow and turbulent effects respectively. The coherence technique was extensively employed to relate nearfield localised sound pressure levels in potentially high source regions such as the core bar, winding spacer outlet and pole shoe tip regions to the far field sound pressure in positions of interest. This facilitated some correlation of cause and effect.

7.1.2 Test rig construction

A purpose built test rig was necessary due to general practical testing difficulties for an actual machine as well as specific limitations with fitting instrumentation in the air gap. The overall test rig assembly is illustrated in Figs. 7.1a and b with each component described in detail as follows.

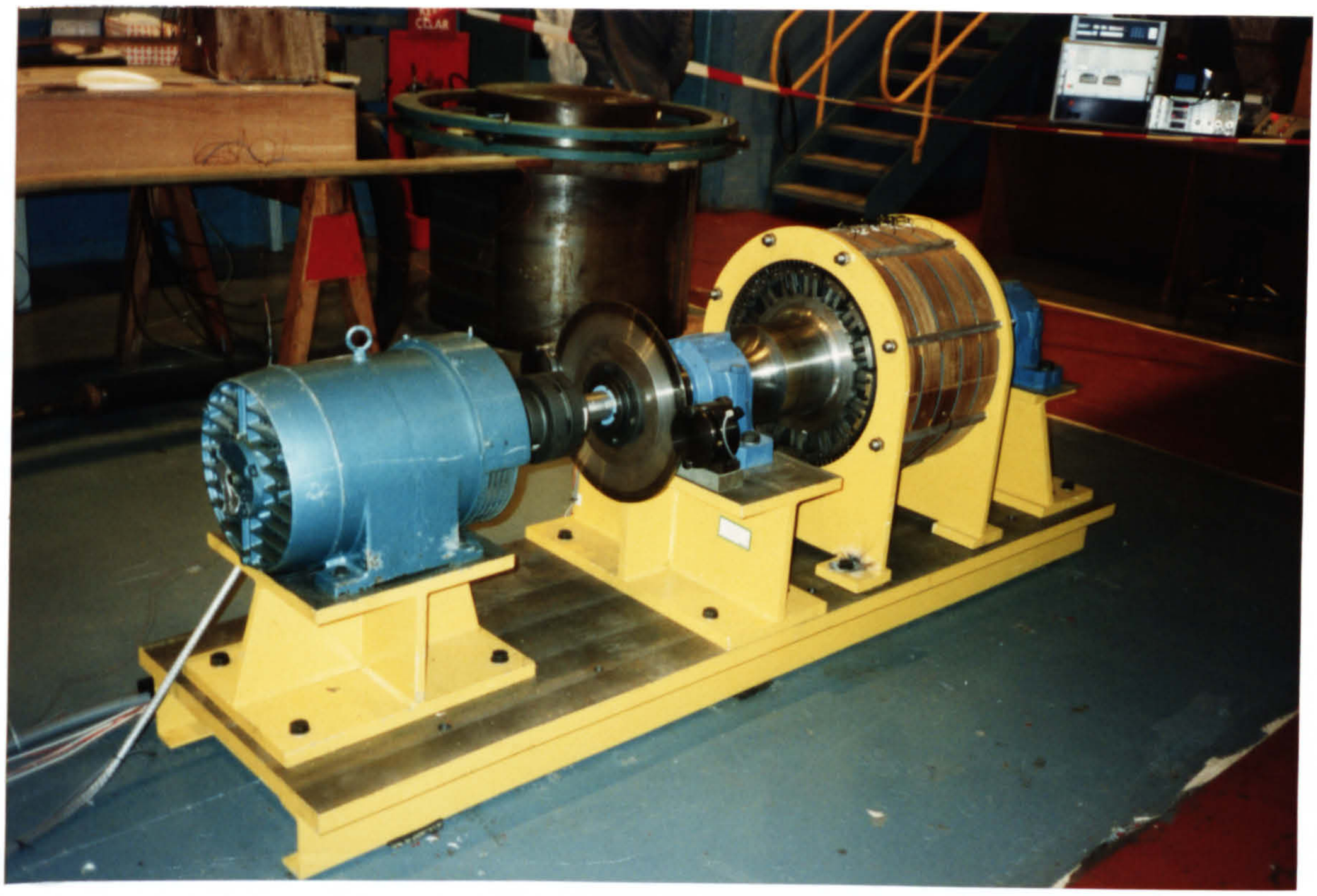

(a)

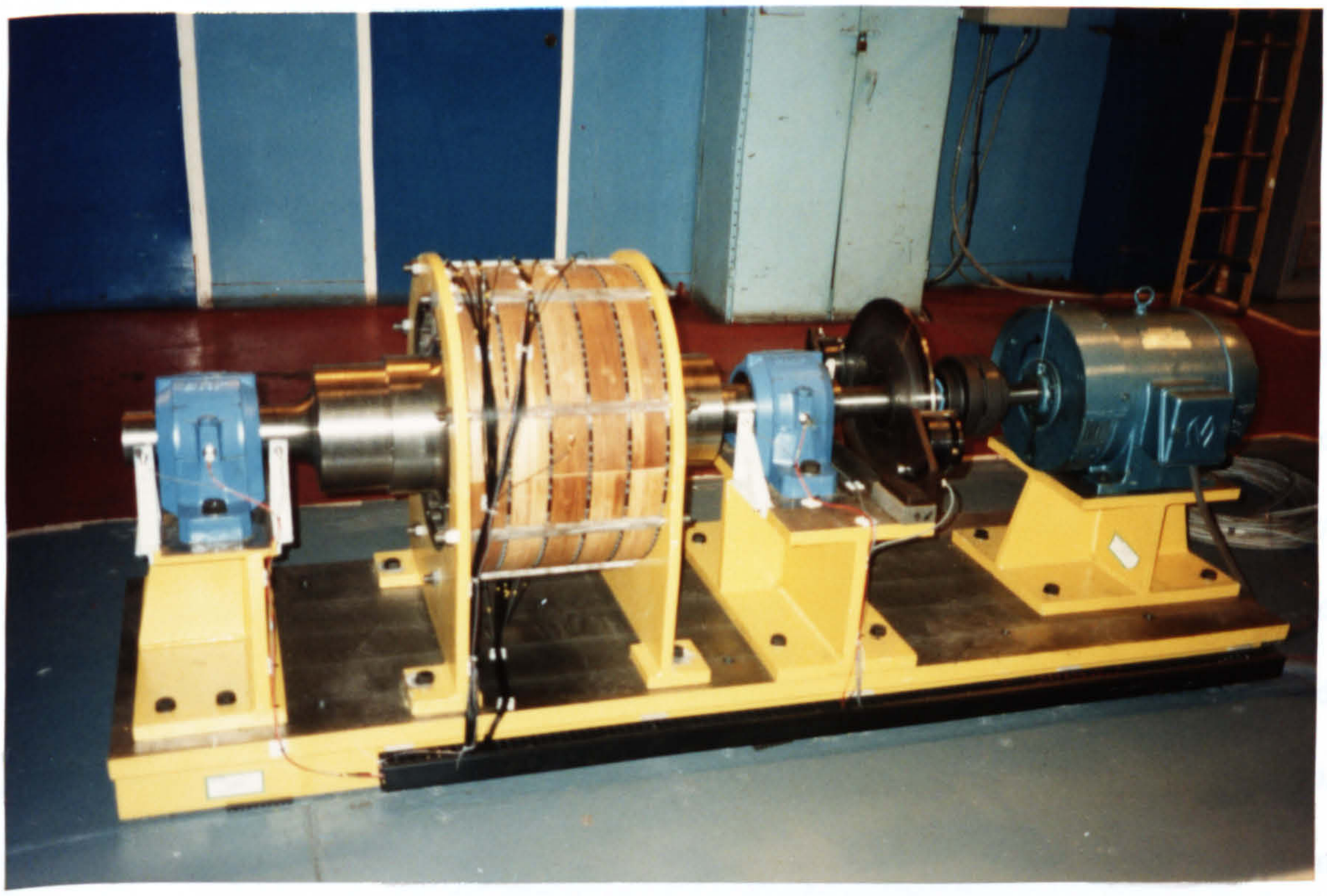

(b)

Fig.7.1 General arrangement of assembled test rig.

7.1.2.1 **Rotor**

A mild steel shaft was machined to the same dimensions of an actual pilot exciter. The correct dimensions were maintained 20 cm outboard of the magnet poles ensuring correct air inlet conditions. The 6 permanent magnets comprising the pole were replaced with 1 steel bar. The carbon steel pole shoes were identical to the actual machine. The same number and type of retaining bolts were employed. Aerodynamically the rotor is identical, Fig. 7.2a, to an actual machine, Fig. 6.1.

The bearings were standard self aligning ball bearings mounted in plummer blocks supported on fabricated stools. The rotor was balanced with the addition of brass weights to the pole tips to within 14μm peak-peak bearing vibration displacement at 3000 r.p.m. The test rig was overspeed at 10% above 3000 r.p.m. for 5 minutes to verify safe operation.

7.1.2.2 **Stator**

To enable insertion of instrumentation and for ease of assembly the stator comprised of wooden segments to simulate the packets of steel core plate. The 6 vent plates were steel and identical to the vent plate in an actual machine. The winding passes axially along the machine, Fig. 6.1. This was simulated using paxolin blocks of the same dimensions and surface finish as the actual winding. Vent plate, paxolin spacers and a wooden segment used to simulate the top half of 1 core packet is given in Fig. 7.2b. The endwindings are not simulated, but this is believed to have a negligible effect on the siren tone generation and otherwise the airflow paths are very similar to the actual pilot exciter.

The clamping arrangement differs, but the only influence of this on the airflow, the

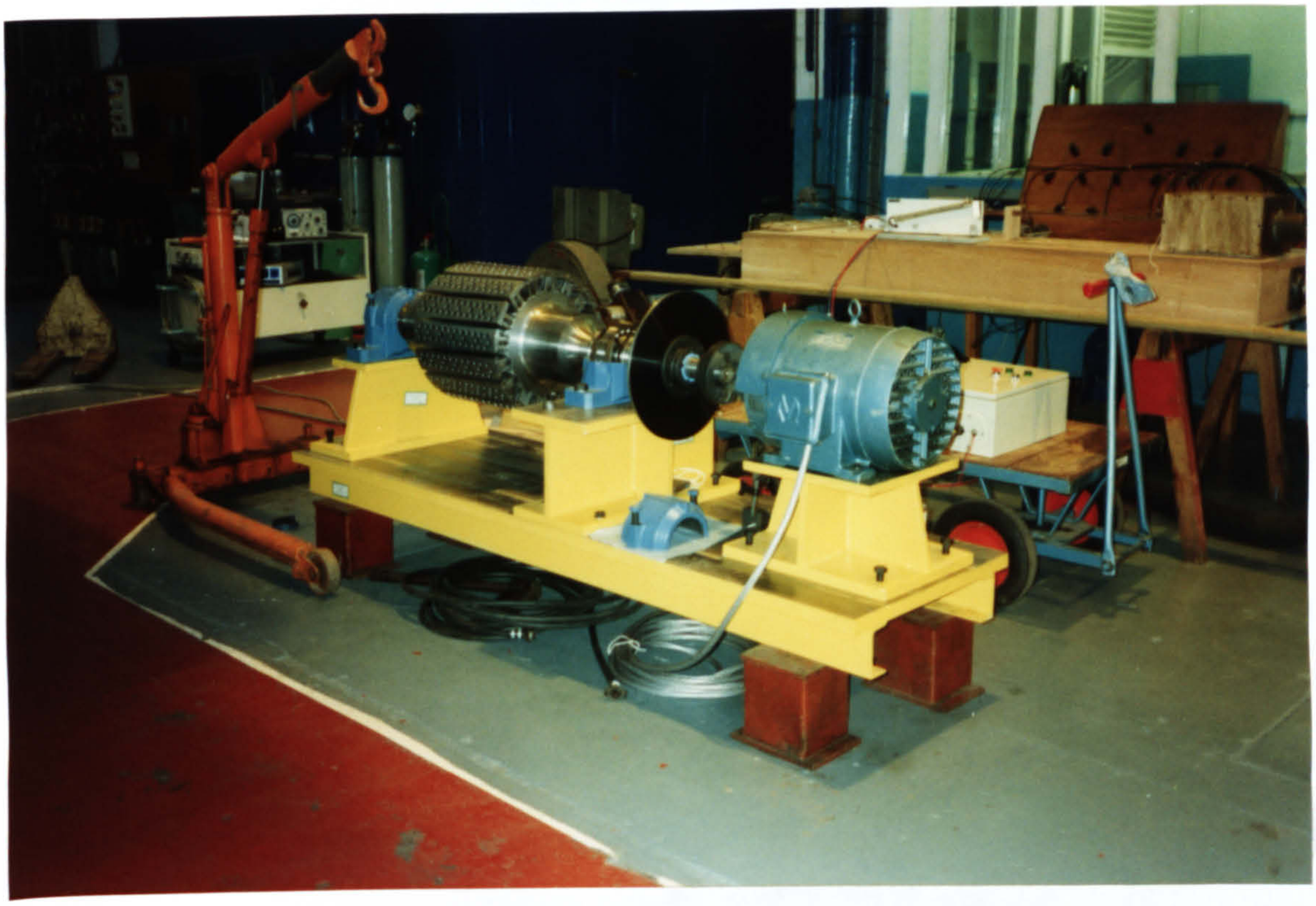

(a)

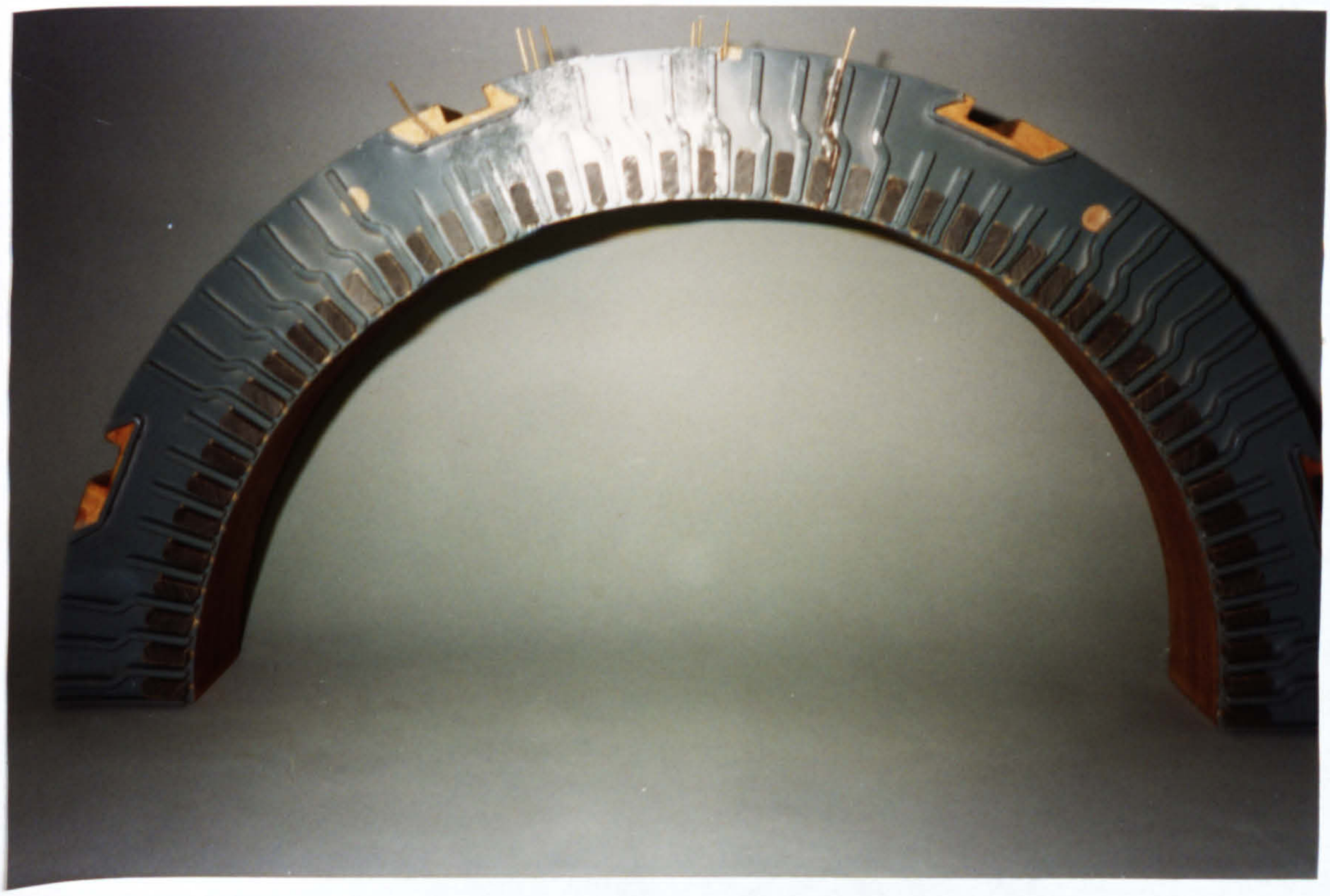

(b)

Fig.7.2 General arrangement of a) rotor assembly b) stator assembly.

dovetail core support bars, are exactly reproduced by the dovetail spacers welded onto the ventplate, Fig. 7.2b. The overall core construction is illustrated in Figs. 7.1a and b.

7.1.2.3 **Drive and control systems**

The drive system consisted of a 15kW Mawdsley induction motor supplied from a 3 phase Brentford invertor to provide a variable frequency drive. Detailed testing was conducted at 3000 r.p.m., the normal running speed, and 2500 r.p.m. with limited measurements on other speeds. A flexible coupling allowed some angular misalignment and damping. Mechanical braking was applied using two Matrix Engineering caliper disk brakes each of which supplied a braking torque of 144 Nm. The rig braked from 3000 r.p.m. to rest in 15-20s.

The shaft absolute and bearing vibration levels were similar, so the bearing vibration levels measured with piezoelectric accelerometers were used to ensure acceptable vibration levels. A trip level was set as 200μm peak-peak vibration displacement. The remainder of the control circuitry consisted of an interlock contactor with stop, start and emergency stop push buttons and a power supply for the disk brakes.

7.1.3 **Instrumentation**

7.1.3.1 **Aerodynamic**

The mean static pressure was measured using a 2mm bore pressure tapping mounted flush with the centre of the wooden stator segment, numbers 1 to 4 in Fig. 6.2. The pressure tappings are top dead centre with segment 3 having 4 tappings each separated by 90°. The pressures were recorded with a digital manometer.

The mean velocity was measured from each vent duct using 8-10 measurements at the outlet with a small pitot tube and digital manometer.

7.1.3.2 **Acoustic**

The performance characteristics of the sound pressure and intensity measurement equipment has been outlined in section 3.3.2. This equipment was supplemented with small electret microphones, type EK3024, produced by Knowles Electronics. The dimensions (2.3 x 4 x 5.6mm) enabled measurements to be taken at all locations in the vent ducts. When connected in the source follower mode the maximum level before saturation was 140 dB S.P.L., 200 Pa. The mechanically robust and small microphones have a high sensitivity, typically 22mV/Pa at 1 kHz. The sensitivity and phase varied with frequency. Each microphone was calibrated using a ½" Brüel and Kjaer 4155 microphone as reference in the direct free field of a loudspeaker excited with broadband noise. The amplitude and phase response, illustrated in Fig. 7.3 for one microphone, was stable. Each measurement was corrected with its own amplitude and phase characteristics.

7.2 AERODYNAMIC RESULTS

7.2.1 Static airgap pressure

The static airgap pressures at 3000 r.p.m. are tabulated below for measurement positions as indicated in Fig.6.2.

Segment				Average
1	2	3	4	
201	365	435	499	375

Table U: Static air gap pressure (Pa) at 3000 r.p.m.

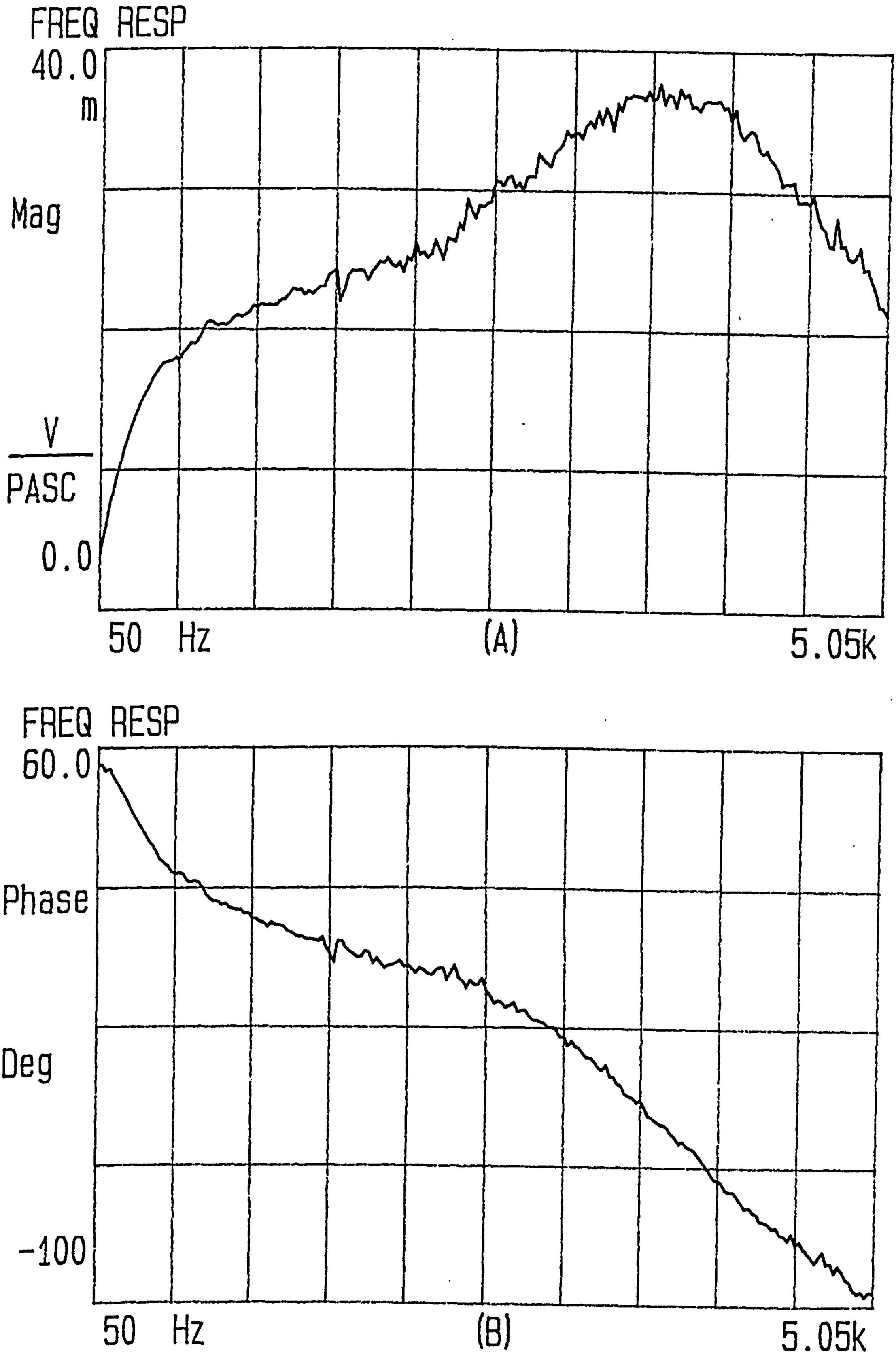

Fig.7.3 **Typical EK3024 electret microphone a) magnitude and b) phase responses.**

The variation in air gap pressure with operational speed is illustrated in Fig. 7.4. There is a 1.85th power relationship between air gap pressure and rotational speed, which is similar to the 2nd power law for fans. At 3000 r.p.m. the mean pressure at vents 1, 2 and 3 is 100 Pa, 283 Pa and 400 Pa respectively. These pressures were used to calculate the volume velocity pulsations in chapter 6.

7.2.2 Average outlet volume velocity

The mean velocity for each vent duct was obtained using between 8-10 pitot tube measurements. These 25 vent duct averages were then averaged to obtain a mean velocity of each of the 6 axial planes illustrated in Fig.6.2. The results are given in table V.

	Vent plane						Total 1-6
	1	2	3	4	5	6	
average velocity (m/s)	4.9	9.8	13.5	12.6	10.5	3.8	-
total volume velocity (m^3/s)	0.037	0.075	0.10	0.096	0.080	0.029	0.417

Table V: Average outlet velocity and total volume velocity for each of the 6 axial planes at 3000 r.p.m.

7.3 ACOUSTIC RESULTS

7.3.1 Sound power determination

The sound power level was determined for the pilot exciter test rig by completely enclosing it with 19 sound intensity scan measurements. The enclosed area was between both the bearing pedestals (Fig. 7.1).

The overall sound power level at 3000 r.p.m. was 110.3 dB(A). The narrowband sound power spectrum illustrated in Fig. 7.5a has the characteristic components at 800

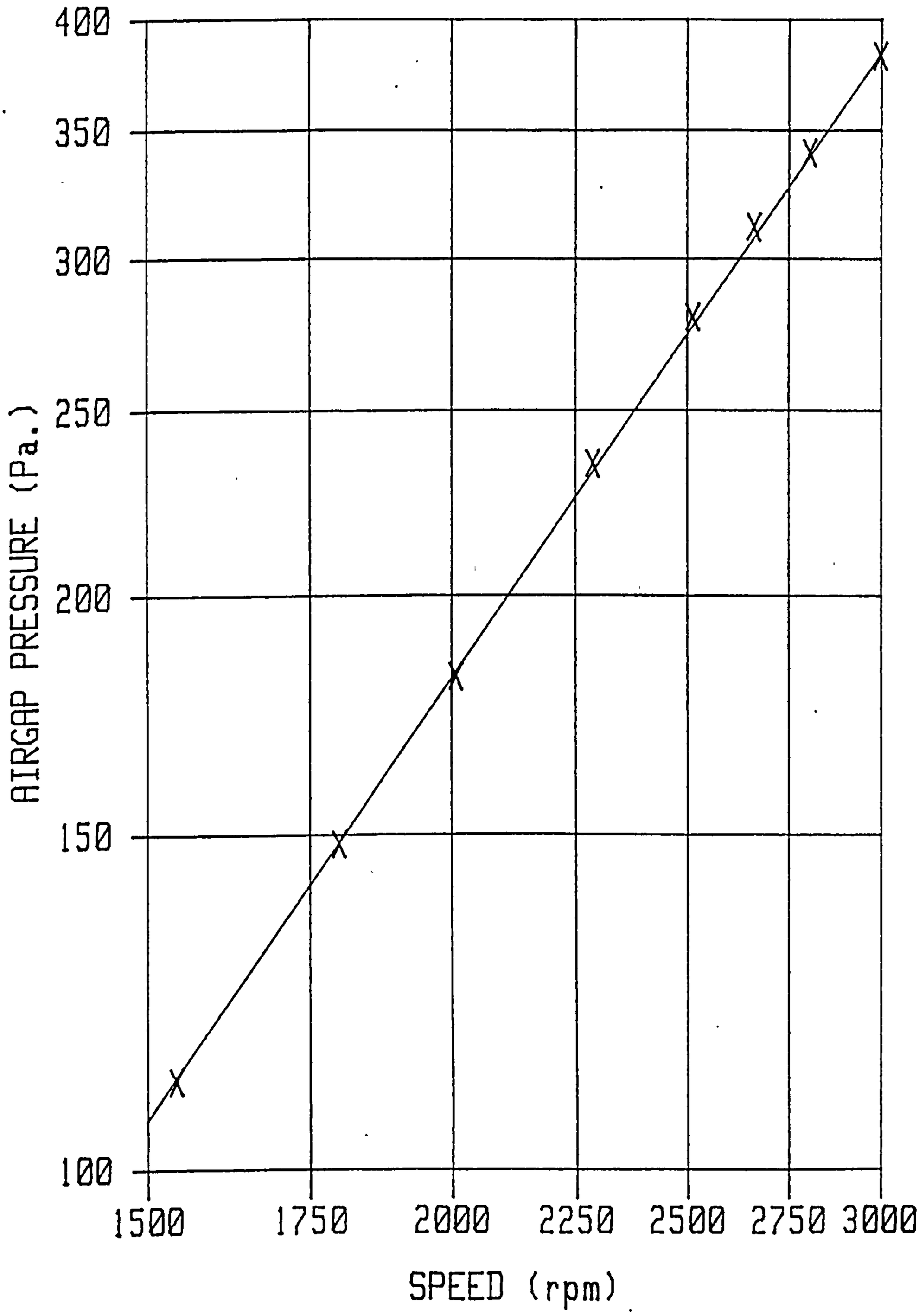

Fig.7.4 **Variation of average air gap pressure (Pa) with operational speed.**

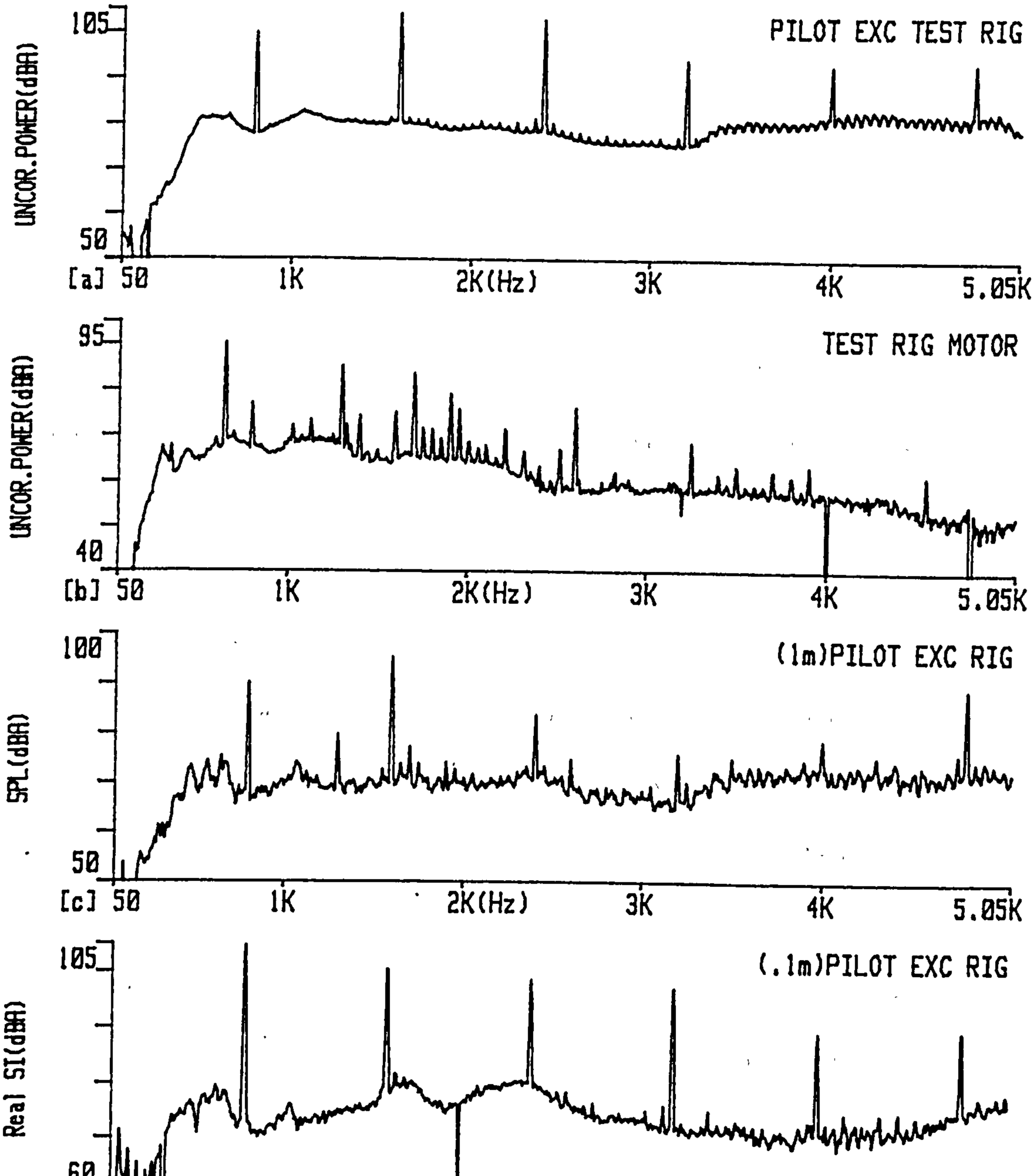

Fig.7.5 Narrowband a) test rig sound power b) drive motor sound power c) sound pressure level at 1m from test rig & sound intensity at 0.1m from d) the centre of test rig and e) R.E. test rig pole tips.

Hz and harmonics thereof discussed in chapters 4 and 5. The harmonic components are given in table W.

	800 Hz	1600 Hz	2400 Hz	3200 Hz	4000 Hz	4800 Hz
Sound power level dB(lin)	101.0	102.8	101.2	92.4	91.5	92.4

Table W: Pilot exciter test rig sound power tonal levels at 3000 r.p.m.

The measurement accuracy of the sound power determination has been discussed in section 5.1. The value of F_3 was 2.1 dB, which relates to a negligible phase mismatch. For the scanned measurement the spatial sampling error for F_4 equal to 0.56 was 0.9 dB. As the complete measurement survey was repeated 4 times with different scan patterns to within 0.1 dB the error predicted from F_4 is overestimated. This is consistent with the belief expressed in 5.1 that the scanning technique more closely represents the continuous surface integral and application of F_4 is not strictly valid. The very good measurement accuracy was due to the pilot exciter emitting strong, uniform noise levels in a low reverberation region in the absence of significant background noise. The drive motor emitted only 94.9 dB(A) sound power with a spectrum illustrated in Fig. 7.5b.

The overall test sound power level of 110.3 dB(A) was close to the 106.7 dB(A) measured at site. The spectra, Figs. 7.5a and 4.23d, are very similar in nature. The slight differences in level and spectral composition is principally due to the cover employed at site. The cover contained large ventilation grills, which radiated noise strongly. In general the internal reverberant build up, which increased the sound pressure levels at the main transmission counterbalanced the smaller radiation area. Therefore the overall level is similar, but due to the different directivity pattern of

each tone the absence of the cover has altered the relative magnitude of the tonal components.

The sound power simulation is therefore good confirming that the main source mechanisms were aerodynamic and not magnetic. To further validate the theoretical model the sound power level was determined at 2500 r.p.m. yielding an overall level of 105.1 dB(A) with harmonic components given in table X.

	667 Hz	1333 Hz	2000 Hz	2667 Hz	3333 Hz	4000 Hz
Sound power level dB(lin)	96.7	97.4	95.1	89.7	87.7	88.4

Table X: Pilot exciter test rig sound power tonal levels at 2500 r.p.m.

7.3.2 Point sound intensity vector measurements

The sound pressure level 1m from the side of the pilot exciter was 102 dB(A) with spectrum given in Fig. 7.5c. The level is nominally identical to that at site, but the spectral composition has some differences with that measured at site as illustrated in Fig. 4.43d, due to different background noise, reverberation characteristics and in particular the influence of the site cover on directivity.

The sound intensity distribution is illustrated in Fig. 7.6. The highest levels occur along the side of the pilot exciter body with an approximately uniform distribution. The intensity at the centre of the body increases slightly from 5 to 20cm due to the interference pattern reaching a maximum of 110.1 dB(A). The levels then decrease with an increase square law to 99.3 dB(A) at 1m. The radial sound intensity, Fig. 7.5d, at 0.1m from the centre exhibits strong tonal components similar to the overall sound power, Fig. 7.5a. The sound intensity level is also high at the ends of the

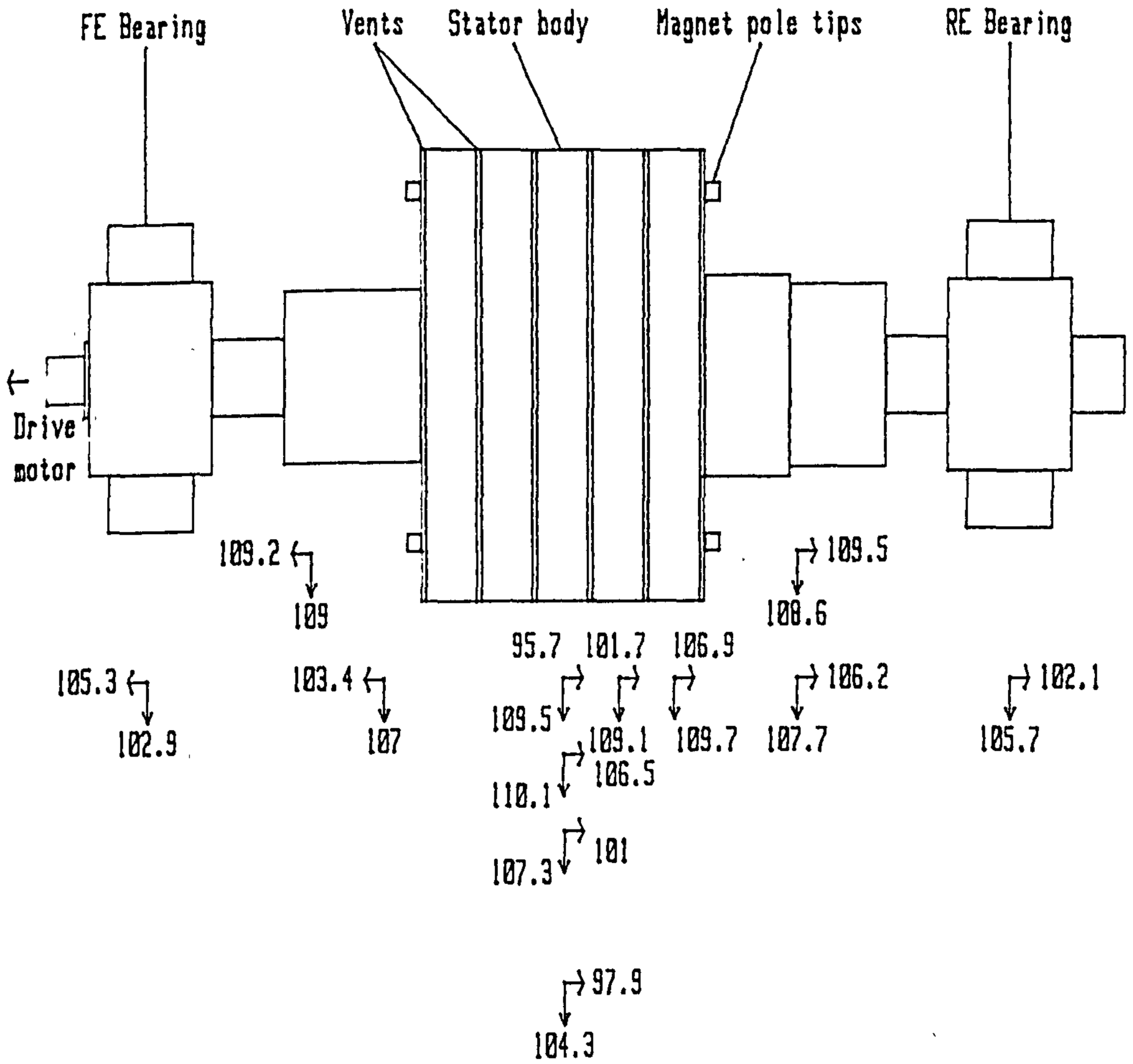

Fig.7.6 Sound intensity distribution around pilot exciter test rig (dB(A)).

machine with 109.5 dB(A) axial flow 0.1m from the R.E. pole tips. The spectral composition is different in nature being mainly broadband in nature, Fig. 7.5e indicating the influence of the vortex shedding off the high velocity pole tips. The absence of tonal components is expected as that the siren tones emanate from the vents on the side of the machine.

7.3.3 Variation of external S.P.L. with rotational speed

The variation of external S.P.L. and the spectral content with rotational speed was investigated to obtain insight into the source mechanisms. The sound pressure spectra 5cm from the centre of the pilot exciter at 1500, 2000, 2500 and 3000 r.p.m. are plotted in Figs. 7.7a-d respectively. The siren tones are significant in all these spectra, but their relative magnitudes vary with speed. The resonant behaviour of the duct is clearly illustrated as the largest harmonic always coincides with the 1st resonant frequency of 2.18 kHz, Fig. 6.5a.

The variation of overall sound pressure level and that of the first 3 harmonics with operational speed is plotted in Fig. 7.8. The overall level exhibits a gradual, smooth increase with rotational speed with a 4.9th power law. This is similar to the 5th power law found by Hübner[20] for induction motors. Source mechanisms, due to fluctuating forces being exerted on the fluid, follow a 6th power law. Unsteady flow effects and vortex shedding source mechanisms are included in this category. The relationship for the first 3 harmonic components is more complex due to the resonant behaviour of the duct. A monopole source, due to volume pulsation of fluid, has a 4th power law with speed. The radiation resistance also alters with frequency contributing to the 6-7th power relationship. But due to duct resonance behaviour no general relationship can be stated.

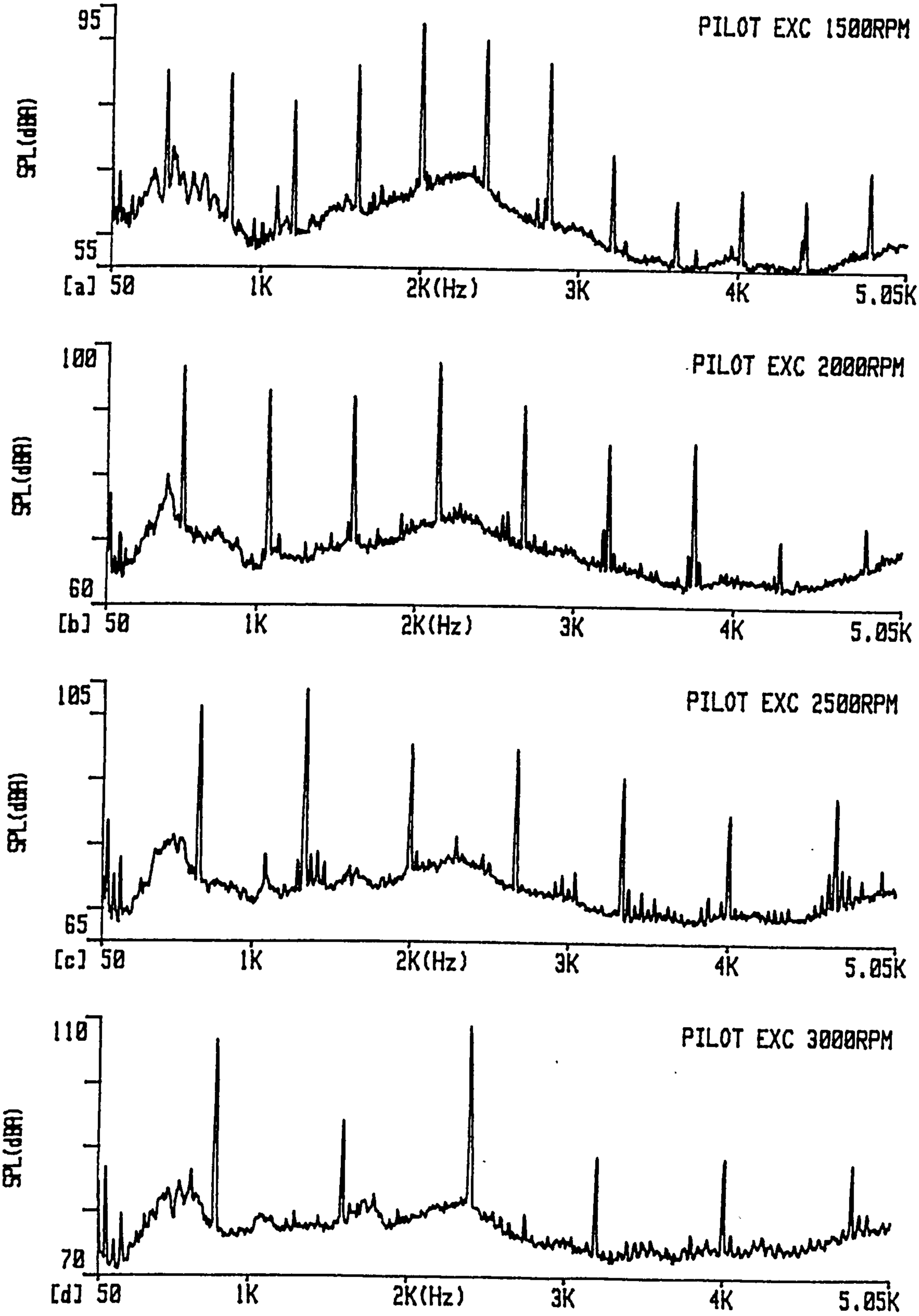

Fig.7.7 Sound pressure level 0.05m from centre of test rig at a) 1500 r.p.m. b) 2000 r.p.m. c) 2500 r.p.m. d) 3000 r.p.m.

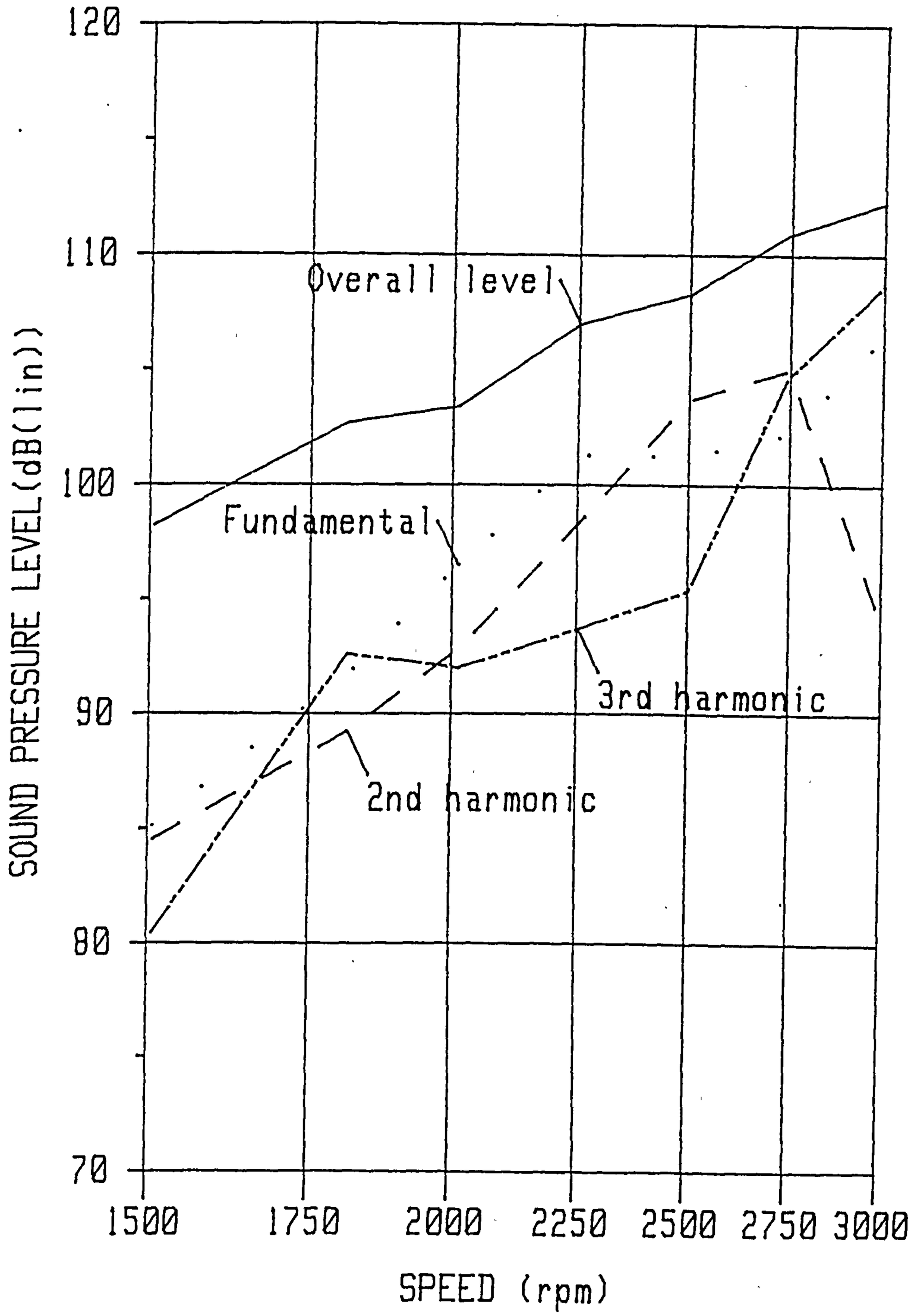

Fig.7.8 **Variation of sound pressure level with rotational speed at 5cm from centre of test rig.**

7.3.4 Airgap pressure fluctuation

The airgap pressure fluctuation was measured using small electret microphones inserted in the cooling duct between a spacer bar in the vent plate and a paxolin block simulating the winding. The microphones were positioned flush with the stator bore 2mm inside the duct. The pressure fluctuations are large especially at higher speeds and in the centre of the machine, section 7.2.1. The microphones saturate at a S.P.L. of 140 dB, which is exceeded by the central vents. The pressure waveforms were similar irrespective of axial position in shape, but not magnitude. To illustrate the pressure fluctuation a measurement in vent 1 at the R.E. of the pilot exciter was deemed representative and easier to interpret in the absence of saturation.

The time variation of pressure and the corresponding frequency spectrum for vent 1 at 1000 r.p.m., 2000 r.p.m. and 3000 r.p.m. are illustrated in Fig. 7.9. The time variation is similar at all speeds exhibiting a sharp pulse of pressure at the pole passing frequency. The frequency spectra therefore have a similar composition irrespective of the rotational speed with the fundamental the largest component and harmonics decreasing with frequency. This is in contrast to the outlet pressure presented in the previous section due to the strong influence of the duct resonance. One cycle of pressure variation at 3000 r.p.m., Fig. 7.9e, indicated by dotted lines, is similar to the predicted variation at the duct inlet, Fig. 6.8. The relatively minor differences are created by random effects and some degree of high order ripple. This ripple is due to reflected pressure waves amplified by the duct resonance. The reflections are of minor importance, confirming that the source impedance will limit this influence. The quasi-static assumption, despite the complexity of the true aerodynamic behaviour, therefore appears a good approximation of the real conditions.

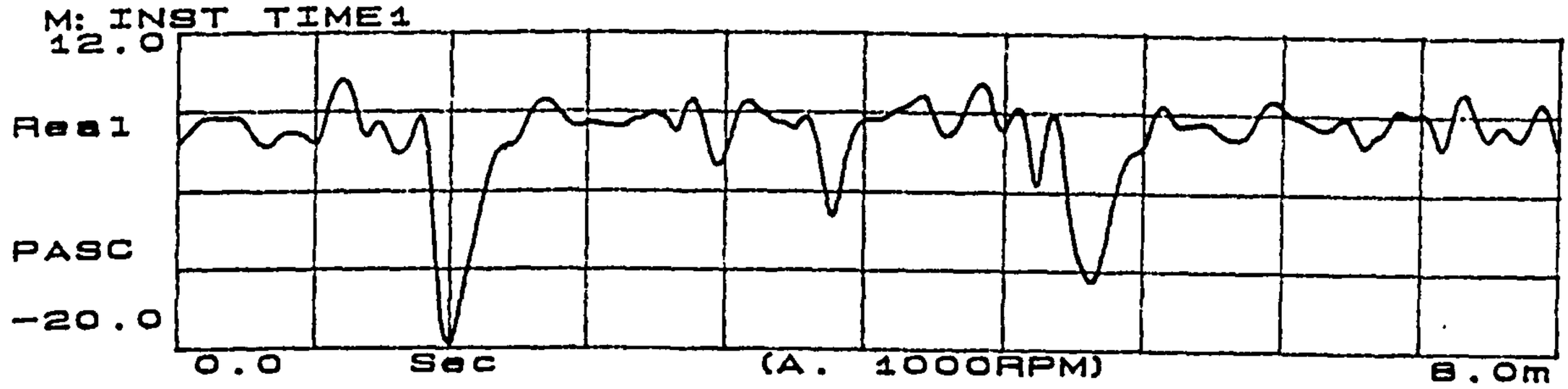

Fig.7.9 Sound pressure measured in vent 1 air gap a) & b) 1000 r.p.m., c) & d) 2000 r.p.m., e) & f) 3000 r.p.m.

The variation of the first 4 pressure harmonics, measured in vent 2, with operational speed is given in Fig. 7.10. Above 2000 r.p.m. saturation due to the microphone characteristics becomes prevalent. Despite this there is a clear basic trend that all harmonics increase in the same proportion to each other with increase in rotational speed. This illustrates that the "forcing" mechanism for the siren tones is solely due to rotor geometries and invariant of duct resonance behaviour.

The harmonics all follow a 1.65th power law with rotational speed, which is similar to the 1.85th power law measured with static pressure. The overall sound power level follows a 3.3th power law relationship, which tends to the 4th power expected for a monopole source of this nature. The 6-7th power law observed for external S.P.L. harmonics is due to the variation of duct impedance with frequency as illustrated in Fig.6.5.

7.3.5 Vent pressure fluctuation

To investigate the significant resonant behaviour evident in the external sound pressure, measurements were conducted in the duct at the outlet of the winding spacer, for positions similar to M1 in Fig.6.3. The variation of the pressure and the corresponding frequency spectra in vent 3 at 1000, 2000 and 3000 r.p.m. are given in Fig. 7.11. The influence of the duct resonant behaviour is very clear causing pronounced difference between the waveform in Figs. 7.9 and 7.11. At 1000 r.p.m. a significant pulse is still evident at the pole passing frequency, Fig. 7.11. There is also superposition of an 8th harmonic (2133 Hz), which was only of minor importance in the airgap waveform, Fig. 7.9b. This is due to the duct resonance of 2.18 kHz, Fig. 6.5a. The influence is more prominent at 2000 and 3000 r.p.m., when the 4th (2133 Hz) and 3rd (2400 Hz) harmonics respectively dominating the pressure amplitude,

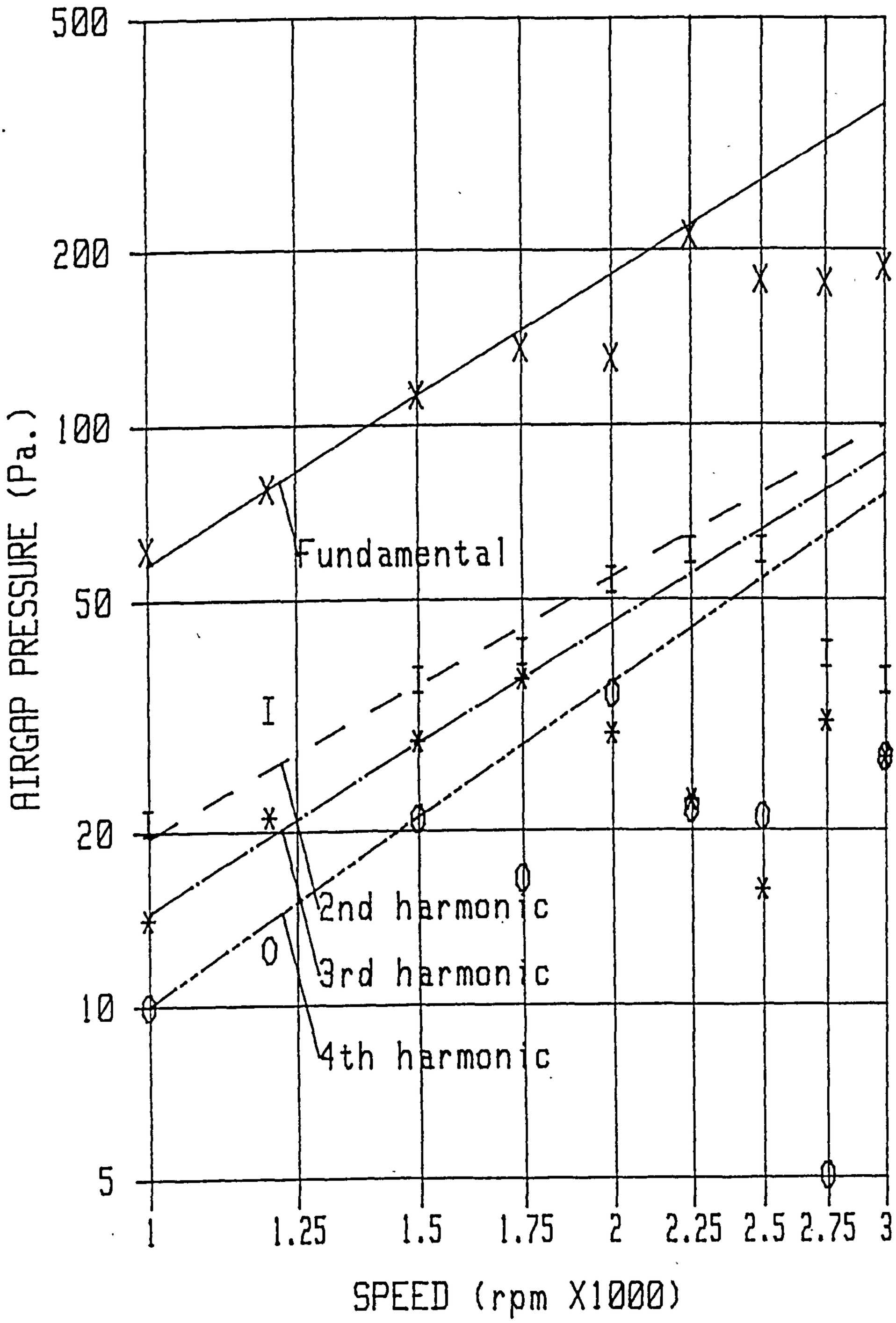

Fig.7.10 Variation of 1st 4 sound pressure harmonics with rotational speed.

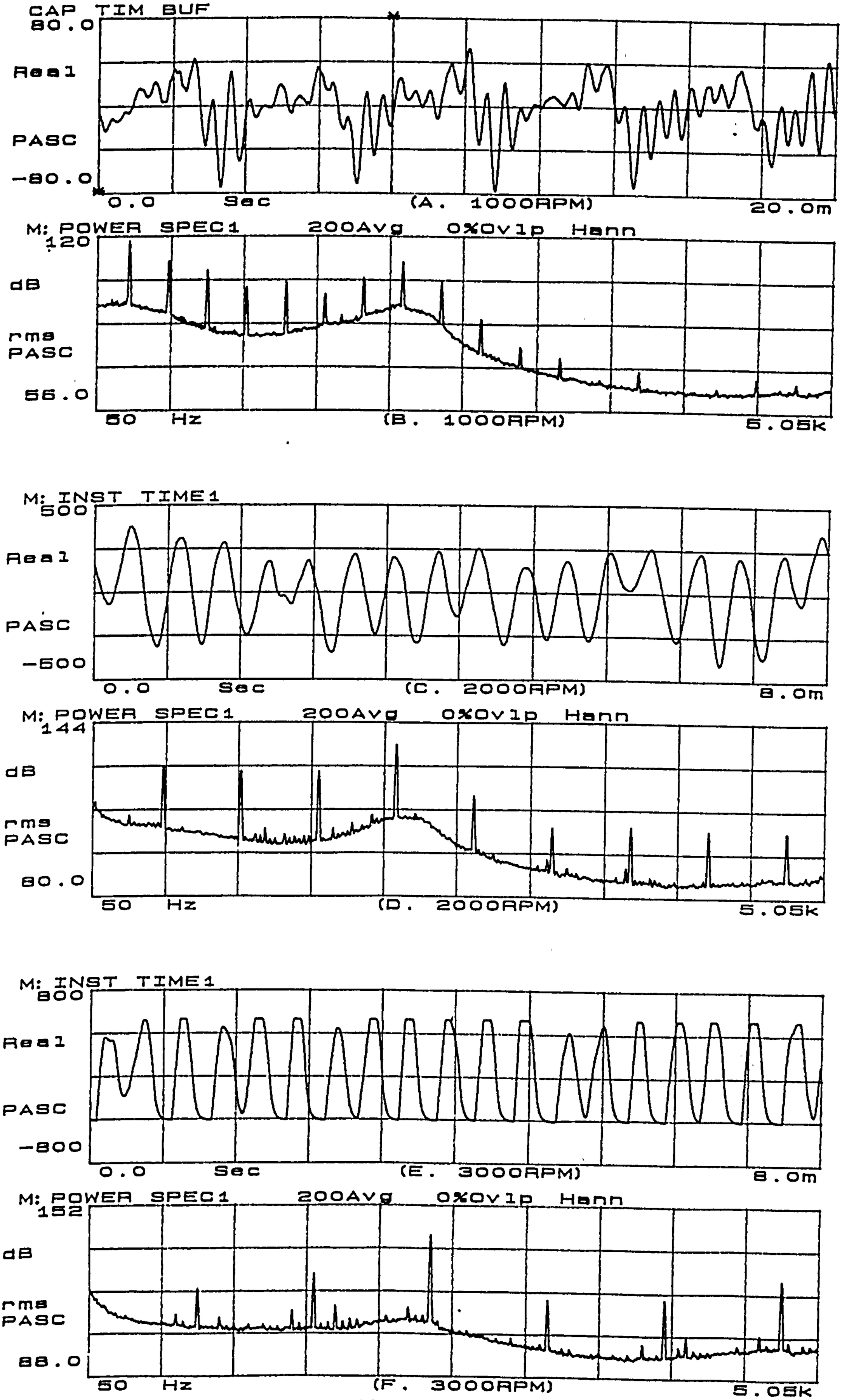

Fig.7.11 Sound pressure measured in vent 3 at the outlet of the winding spacer a) & b) 1000 r.p.m., c) & d) 2000 r.p.m., e) & f) 3000 r.p.m.

Figs. 7.11c-f. Duct design has therefore a significant influence on noise levels.

7.3.6 **Sound pressure coherence**

The application of the coherence function to relate noise sources characterised by nearfield sound pressure to farfield emission also measured with sound pressure has been illustrated in 4.2.4. Sound pressure within the duct was measured using the electret microphones and external measurements were performed using ½" condenser microphones. The "source" regions considered included the R.E. pole tips, the winding spacer outlet, the airgap and the corebars.

The coherence between a microphone 5cm from the R.E. pole tip and a further 10cm radial outwards is high tending to 1 (Fig. 7.12a). Even at 1m radially outwards there is some coherence tending to 0.5 (Fig. 7.12b) especially in the high frequency band above 3.4 kHz. This is also prevalent in the axial sound intensity spectrum at 10cm (Fig. 7.5e). The influence of high frequency vortex shedding on noise emission is readily apparent.

The vortex shedding region at the expansion resulting at the outlet of the winding spacer was investigated using 3 microphones M1, M2 and M3 as illustrated in Fig. 6.3. The coherence between each of these and a microphone at variable distance from the central duct (M2) was measured. At 1cm from the outlet of the vent, P1, (5cm from the internal microphones) the coherence was high only for the microphone in the central duct (Fig. 7.13b), whereas tending to zero for the two adjacent measurements (Figs. 7.13a and c). This is true for frequencies excluding the siren tones, which exhibit strong coherence for all measurement positions due to nature of the siren mechanism. The bands of strong coherence correspond with the duct resonances at 2.18 kHz and 5.2

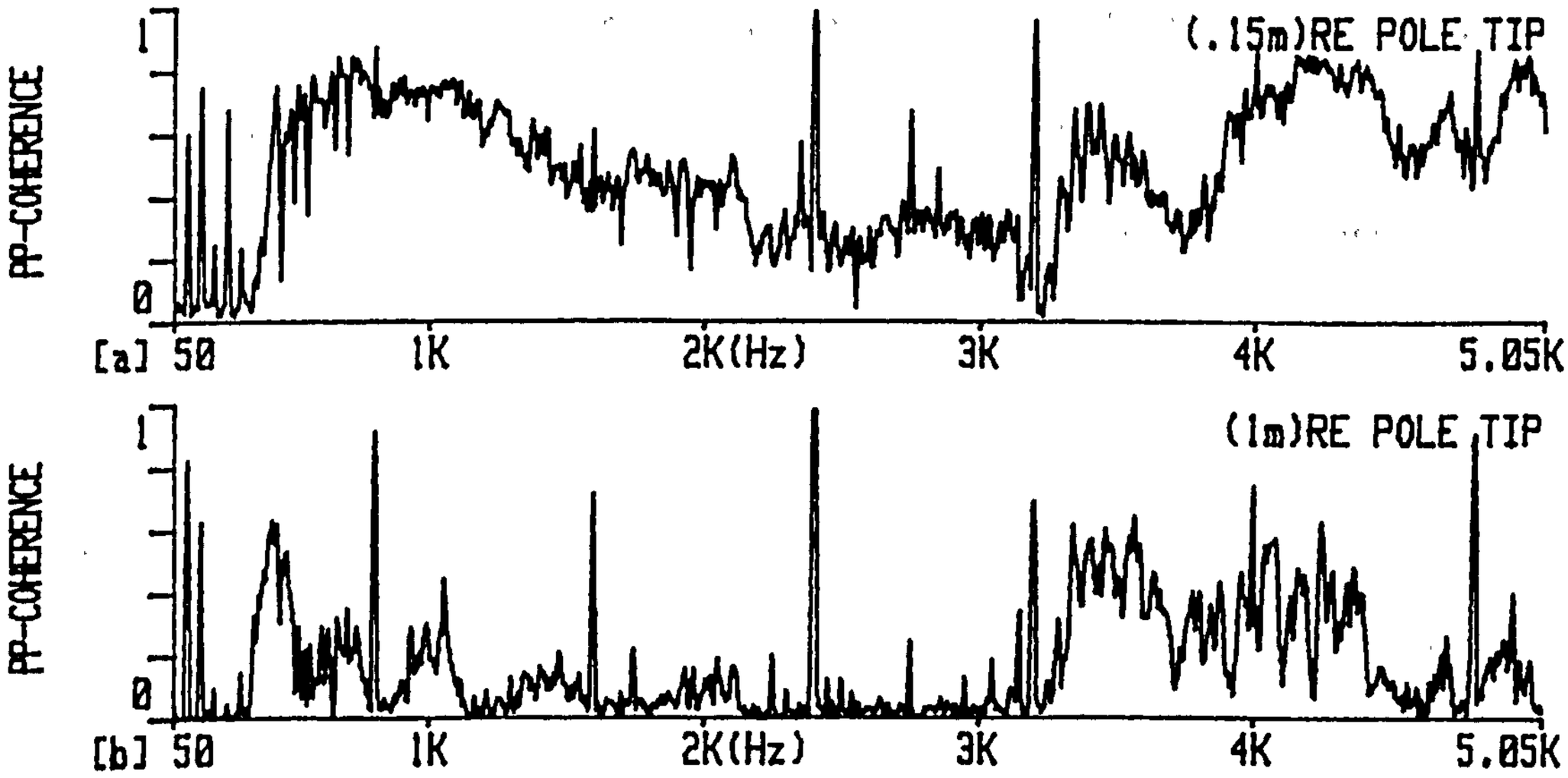

Fig.7.12 Sound pressure coherence between 0.05m from R.E. pole tip and a) 0.15m b) 1m from R.E. pole tip.

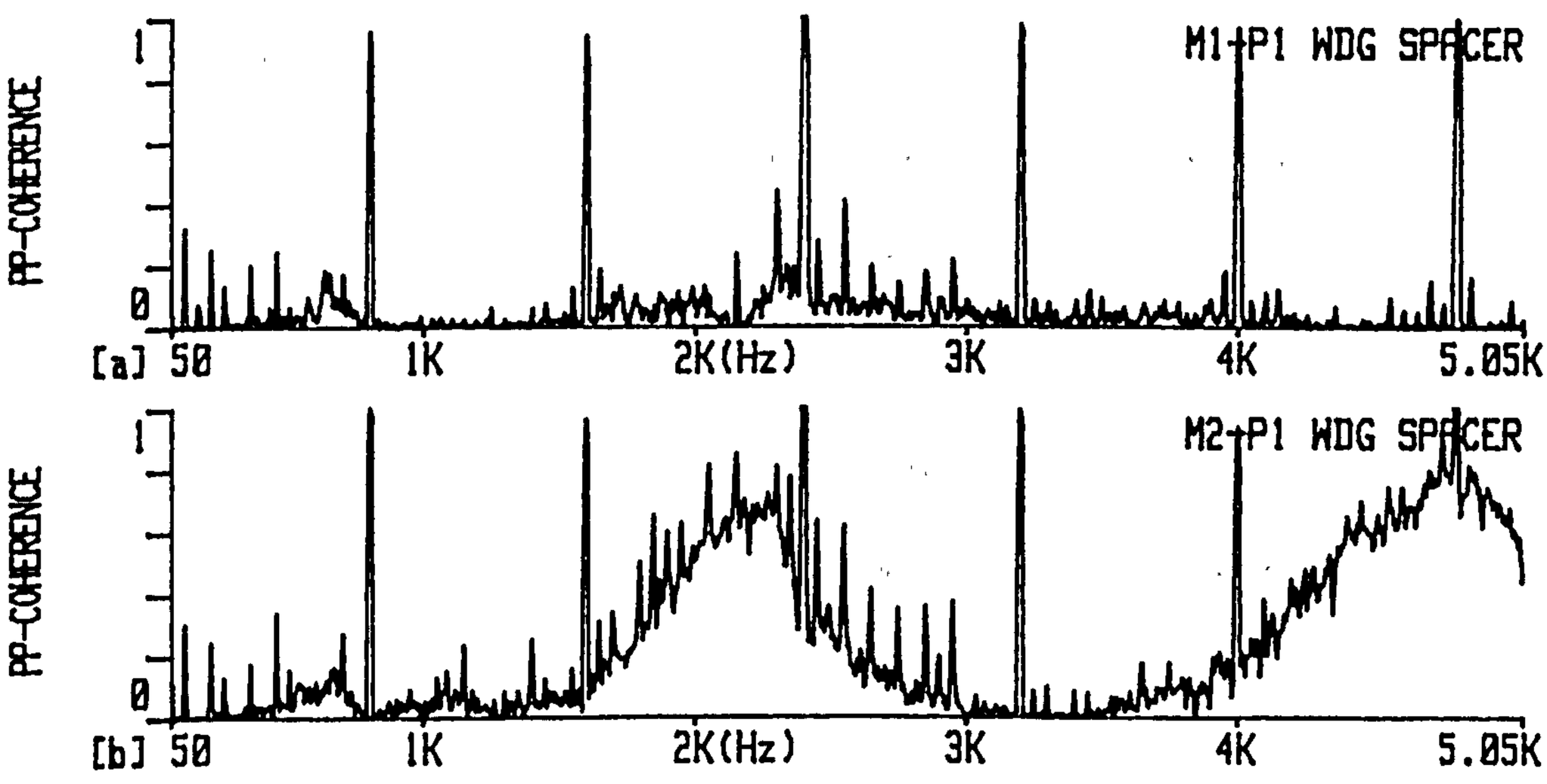

Fig.7.13 Sound pressure coherence between winding spacer outlet and duct outlet a) M1-P1 b) M2-P1 c) M3-P1 d) M2-P2.

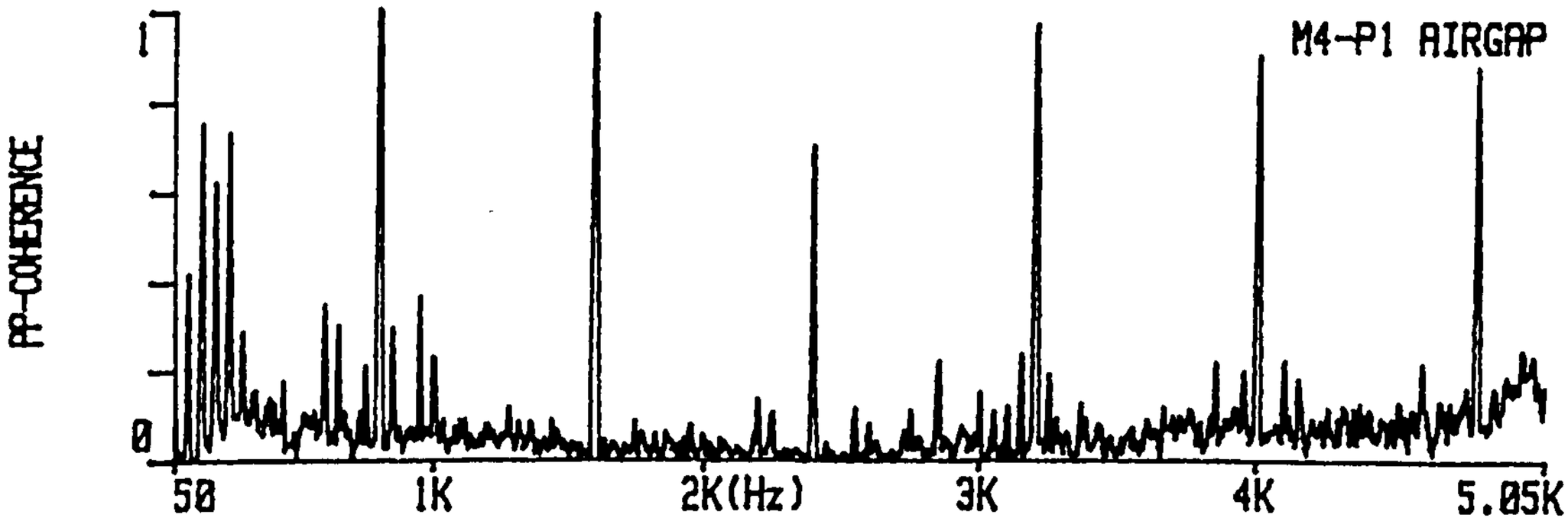

Fig.7.14 Sound pressure coherence between air gap M4 and outlet P1.

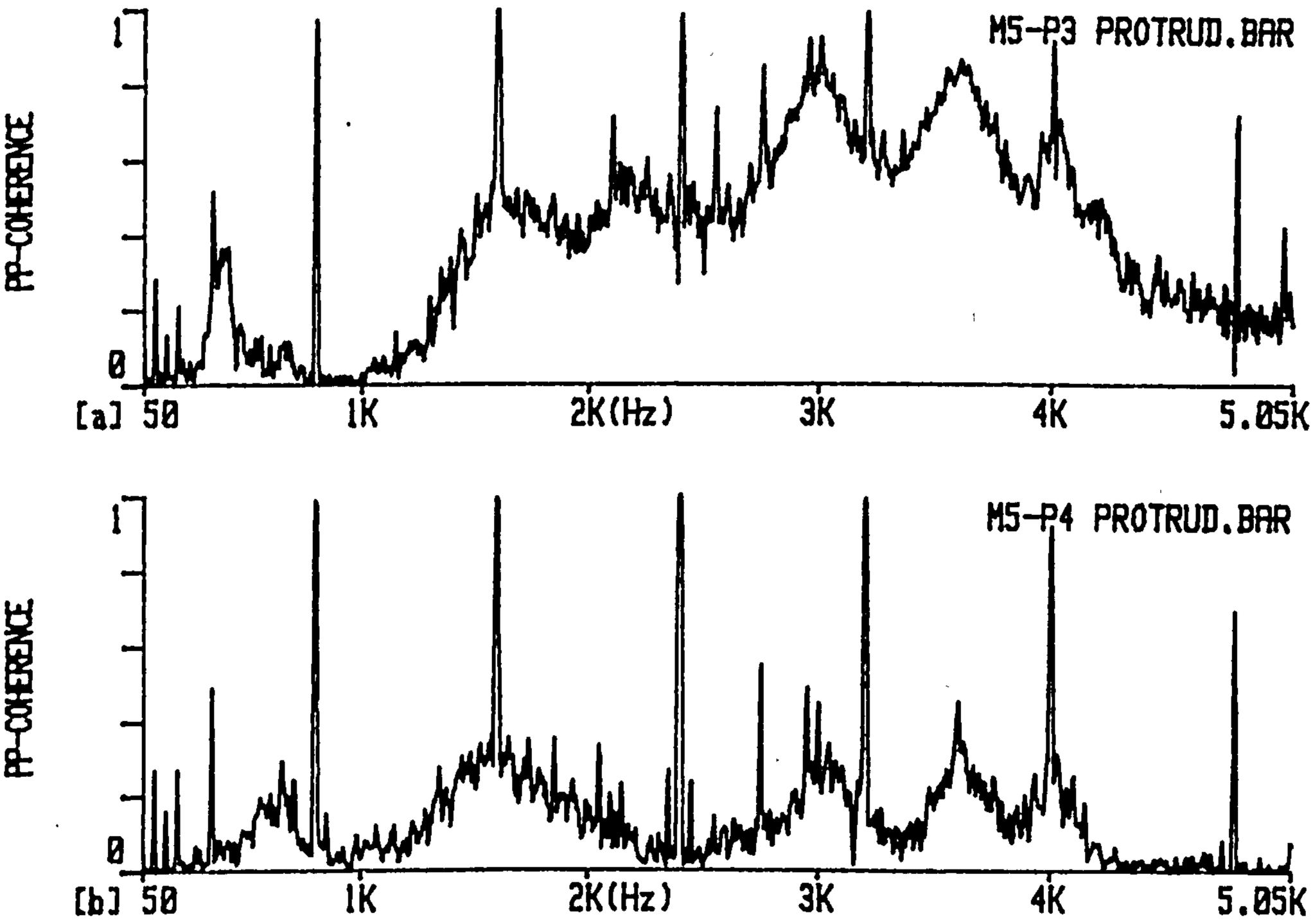

Fig.7.15 Sound pressure coherence between core bar and duct outlet

a) M5-P3 b) M5-P4 c) M6-P5.

The fundamental (800 Hz) phase difference between 5 pairs of adjacent ducts in a radial plane was assessed by averaging. This was repeated for each of the 6 axial planes. The phase lag was as predicted from the direction of rotation.

Vents						Average 1-6
1	2	3	4	5	6	
70.1°	57.4°	45.6°	47.8°	58.3°	50.0°	54.9°

Table Y: Average radial phase difference between adjacent ducts for fundamental siren tone (800 Hz)

There is a variation of ±15° around an overall average of 54.9°, which is close to the predicted 60°. The variance can be explained in terms of the random behaviour superimposed on the periodic waveform, which is reflected in Figs. 7.9 and 7.11. This should be minimised by 200 averages per measurement. Slight practical errors in positioning of the microphones will also contribute to the discrepancy. The higher order harmonics for the central vent planes, 3 and 4, were averaged from 4 pairs of measurements.

	2F (1600 Hz)	3F (2400 Hz)	4F (3200 Hz)
vent 3	155°	190.6°	224°
vent 4	122.8°	190.8°	147°

Table Z: Average radial phase difference between adjacent ducts for 2nd to 4th harmonics

The basic trend is towards a radial phase difference for each harmonic of n60°, where

n is the harmonic number. The variance within each set of 4 measurements was larger still and was commonly ±50% of the mean. This variance explains, why the radiation efficiency of the 2.4 kHz tone was greater than that predicted in chapter 6.

The pole shoe skew angle introduced a phase lag of a predicted 12.3° between axially adjacent vents. The phase angle was measured between 4 pairs of axially adjacent vents yielding the following result. These levels more closely resemble the 12.3°, 24.6°, 36.9° and 49.2° predicted

1F (800 Hz)	2F (1600 Hz)	3F (2400 Hz)	4F (3200 Hz)
15°	27°	22°	32°

Table AA: Average axial phase difference between adjacent ducts for first 4 harmonics

7.4 SUMMARY

The test rig has been proven to accurately simulate the noise and aerodynamic behaviour of an actual 660MW pilot exciter. This has confirmed that the predominate mechanisms were aerodynamic, with siren tones at pole passing frequencies and harmonics thereof and broadband noise due to vortex shedding and unsteady flow effects.

There has been close agreement between the theoretical modelling and the measured sound power for two operational speeds, 3000 r.p.m. and 2500 r.p.m., for the 1st 4 harmonic siren tones. The levels have commonly been predicted to within ±3 dB. The modelling process has also been further validated in intermediate steps. The

inlet duct pressure fluctuation was measured and there was close correlation with the predicted value. This illustrated that despite the complexity of the true airflow behaviour, the quasi-static assumption is a close approximation of the real conditions. The influence of backward pressure waves are not significant. The largest discrepancy was with the 3rd harmonic due to the resonant behaviour of the duct making exact modelling more difficult which is reflected in the sound power underestimation at this frequency. The phase relationship between the ducts have some variance, but converge to the predicted values.

This analysis has highlighted that the radiated noise levels are dependant upon the forcing pressure waves, dictated by the detailed pole geometries, the duct resonant behaviour, defined by the precise stator duct geometries, and the phase relationship of the consequent volume pulsations. Detailed noise reduction has not been attempted at this stage, but the tools to enact this have been presented. Reduction of higher order forcing pressure harmonics by making the transition of a pole passing less abrupt will result in only one prominent pressure pulsation harmonic. The stator design should then aim to ensure no coincidence close to this frequency. The interaction of phase relationship is dependant upon the number of stator and rotor ducts and should be chosen to produce a radiation pattern with a large degree of cancellation.

The main sources of broadband noise are the pole tips and the corebars. A streamline tip profile will reduce noise levels. The use of semi-circular corebars will reduce the generation of broadband noise, as illustrated by the pressure coherence measurements and also reduced radiation efficiency of the siren tones.

8. CONCLUSIONS AND SUGGESTIONS FOR FURTHER INVESTIGATION

A variety of powerful, new measurement and analysis techniques have been applied to generators and their excitation system components. Extensive investigations have been conducted on a variety of units at site and during factory testing. These techniques have provided a clear, correlated new level of insight into the noise emission from generator units.

i) Generator unit noise level quantification

The noise emission from each component has been quantified in a manner not possible from traditional techniques. Sound intensity measurements have enabled sound power determination within acceptable, quantifiable accuracy limits despite the presence of strong background noise and high levels of reverberation. For the 660MW unit at site the major sources of sound power in rank order were the pilot exciter, R.E. generator coupling, generator and main exciter. The site sound pressure level was accurately explained in terms of contribution from the adjacent plant, the reverberant background noise and the direct background noise. Substantial noise reduction for this unit can be accomplished by treating the physically small pilot exciter and R.E. generator coupling, which has since been implemented and verified experimentally. Acoustically enclosing the generator and main exciter will yield little reduction in sound pressure levels and represents unproductive expenditure. The general reverberation levels are not predominated by the generator unit, but by the boiler fed pumps, stop and throttle valves and the turbines.

Sound power emission was determined from traditional, distributed exciters and overhung exciters within the factory, but this was not possible for the generator. Even after correction for phase mismatch errors the residual pressure intensity index

was exceeded by the F_3 indicator. Sound power determination with acceptable accuracy requires substantial action to reduce the direct background noise.

ii) **Sound field indicators**

Despite the considerable advantages afforded by the sound intensity measurement technique error assessment is complex. Sound power determination using the scanning sound intensity technique is currently at the standardisation stage. As the field indicators are inextricably related to the measurement a "true" reference level would have been ideal when assessing measurement accuracy. Despite this as these measurements have been applied under a diversified range of conditions and as there was a wide range of supplementary measurement data it is still possible to make valid observations on the best means to assess accuracy. The standard sound field indicators F_2, F_3 and F_3-F_2 have proven reliable for characterising the measurement environment and indicating refinement of measurement procedure for both scanning and point techniques. F_3 and not F_2 determines the bias error introduced by phase mismatch and should be adopted for the point standard as well. The F_4 indicator clearly overestimates the spatial sampling error for scanned measurements and also point measurements, when certain regions contribute strongly to the total level. For scanned measurements spatial sampling error may be better assessed using repeated measurements with different patterns, although this may be too time consuming. Point sampling should employ a partial variance approach to weight regions, which contribute strongly to the overall level.

iii) **Sound pressure particle velocity coherence**

The sound pressure particle velocity coherence and the relationship between real and reactive intensity have been used in an industrial application to classify sound fields

including a weak source in a multi-source diffuse field, a strong direct source and a strong source in a reverberant region. This correlates closely with relative sound power levels, point vector sound intensity and sound pressure level of the plant items, supplementing information from the standard indicators.

iv) **Noise generation mechanisms**

Much previously unpublished information about the main noise source mechanisms for each component has been presented. For a hydrogen cooled generator magnetically induced vibration and aerodynamic source each contribute about 50% of the total level with mechanical sources relatively unimportant. The radial magnetic forcing is dominated by the twice supply component with harmonics greater than a 3rd order of this relatively unimportant. The large generator casing transmission loss has been shown to limit the aerodynamic noise. For the air cooled generator the aerodynamic noise represents the major contribution to it's overall level. The main source mechanisms for the traditional exciter arrangement are aerodynamic due to vortex shedding from the rotating rectifier and armature. The more compact overhung exciter emitted less broadband aerodynamic noise, but exhibited a significant contribution to the overall level due to magnetic forcing induced by flux ripple at the rotor slot passing frequency. Ventilation holes in the exciter hub created resonant tones. The R.E. generator coupling upshaft connections are source of broadband aerodynamic noise and discrete tone at upshaft passing frequencies. The coupling cover induced many standing waves reducing the cover attenuation. The pilot exciter was the major noise source, creating siren tones at magnet pole passing frequencies and broadband aerodynamic noise.

v) **Pilot exciter noise level calculation**

The pilot exciter was investigated further and a theoretical model produced, which relates the siren tone levels to the machine geometries and aerodynamic behaviour that creates them. In general the agreement between predicted and measured sound power levels is good for two operational speeds and the 1st 4 harmonics, commonly to within 3 dB. Previous models have only considered the fundamental siren tones neglecting higher order harmonics, however this model necessarily incorporated the 2nd and 3rd harmonics, which had magnitudes greater than the fundamental. A full scale test rig was used in conjunction with the theoretical formulation, which accurately simulated the acoustic and aerodynamic behaviour of an actual machine. The test rig provided parameters, which could not be predicted accurately enough, validated the theoretical modelling process, not only in terms of the sound power prediction, but also in intermediate steps and vindicated the quasi-static modelling assumption. The later point was of particular importance as it constituted the main modelling difficulty. A new technique of measuring pressure fluctuations in the airgap and in the vent ducts with miniature microphones yielded unique insight into the noise generation mechanisms. The parameter dependence afforded by this approach will be a vital tool at the design stage to control noise at source, which is applicable to other small air gap electrical machines.

The pressure coherence measurements, and detailed sound intensity vector measurements have identified the main sources of broadband noise to be the magnet pole tips at the ends of the machine and the corebars. A more streamline tip profile will reduce noise levels. The use of a semi-circular corebar profile will also significantly reduce the generation of broadband noise and the radiation efficiency of the siren tones.

vi) **Suggestions for further investigation**

Further work to ascertain the best spatial sampling error indicator is necessary especially for the scanning technique. A comparison of rapid scanning of complex fields, in source nearfields, with F.F.T. and digital filter analysers would be particularly useful.

The theoretical model of the pilot exciter siren tones has suggested means to reduce this level. The airgap pressure frequency composition is dictated by the magnet pole geometries. The shoe edges should be tapered to make the airflow resistance transition less abrupt reducing higher order harmonics. Stator duct resonance has a critical influence on noise radiation and the design should avoid coincidence with the main "forcing" pressure frequency. The interaction of phase relationship is dependent upon the number of stator and rotor ducts and should be chosen to produce a radiation pattern with net cancellation. It is suggested that these design changes should be investigated on the test rig. Accurate prediction of airgap airflow behaviour was particularly difficult to model. Computational fluid dynamics could be used to investigate the variation of airflow resistance and the influence of a peripheral velocity component on these calculations.

After the pilot exciter and R.E. generator coupling modifications the main contribution to the sound pressure levels around a generator unit is the reverberant background noise. It is therefore essential to assess the principal contribution to these levels such as valves, boiler feed pumps and turbines and the propogation of this noise. In recent years considerable advancements have been made into the propogation of noise in factory spaces and this could be applied very beneficially to power stations.

Richard Williams

Richard Williams

APPENDIX A : PHASE MISMATCH CORRECTION

Jacobsen[33] presented a simple, but effective means to compensate for phase mis-match between microphones. The theory behind the adjustment is as follows. The sound intensity at a point in space is proportional to the mean square pressure and the phase gradient of the pressure $\nabla\emptyset$

$$\mathbf{I} = - (p^2/\rho_o c)\ (\nabla\emptyset/k) \qquad \text{A.1}$$

where $\rho_o c$ is the characteristic impedance of air and k is the wavenumber. This is approximated using the two microphone technique in terms of the phase shift $\Delta\emptyset$

$$I_r \approx - (\Delta\emptyset/k\Delta r)\ (p^2/\rho_o c) \qquad \text{A.2}$$

The estimated intensity is subject to the bias error due to phase error $\emptyset_e$

$$\hat{i}_r \approx - ((\Delta\emptyset+\emptyset_e)/k\Delta r)\ (p^2/\rho_o c) = I_r - (\emptyset_e/k\Delta r)\ (p^2/\rho_o c) \qquad \text{A.3a,b}$$

The residual intensity I_o is measured due to system phase mismatch error even when both microphones are subjected to the same pressure p_o. The intensity due to the phase error from eqn. (A3a) is

$$I_o \approx - (\emptyset_e/k\Delta r)\ (p_0^2/\rho c) \qquad \text{A.4}$$

The estimated intensity can be expressed in terms of the residual intensity and pressure by substituting eqn. (A.4) into eqn. (A.3).

$$\hat{i}_r/I_r = 1+(p^2/I_r)(I_o/p_o^2),\ I_r/\hat{i}_r = 1-(p^2/\hat{i}_r)(I_o/p_o^2) \qquad \text{A.5a,b}$$

The true sound power is

$$W = \int_s I_r.\ dS \qquad \text{A.6}$$

Rearranging eqn. (A.5) and substituting into eqn. (A.6) yields

$$W = \int_s \hat{i}_r\ dS - (I_o\rho_o c/p_o^2) \int_s (p^2/\rho_o c).\ dS \qquad \text{A.7}$$

The error in sound power determination can therefore be expressed as

$$\hat{W}/W = 1 + (\int_s p^2.dS/\int_s I_r\ dS)\ (I_o/p_o^2) \qquad \text{A.8}$$

$$W/\hat{W} = 1 - (\int_s p^2\ dS/\int_s \hat{i}_r\ dS)\ (I_o/p_o^2) \qquad \text{A.9}$$

In logarithmic form the error is

$$L_E(\omega) = 10 \log (\hat{W}/W) \qquad \text{A.10}$$

$$= 10 \log \{1 + \text{sgn}(WI_o) 10^{0.1(\Delta pI - \delta po|Io|)}\} \qquad \text{A.11}$$

$$= -10 \log \{1 - \text{sgn}(\hat{W}I_o) 10^{0.1(\Delta p\hat{I} - \delta po|Io|)}\} \qquad \text{A.12}$$

where sgn denotes the sign of the product in brackets and

$$\Delta_{pI} = F_3 = 10 \log \left| \int_s p^2 . ds/(\rho c \int_s I_r ds) \right| \qquad \text{A.13}$$

is the well-known global pressure-intensity index identified in terms of the integral of the true, signed intensity and

$$\Delta_{pi} = 10 \log \left| \int_s p^2 ds/(\rho c \int_s \hat{i}_r ds) \right| \qquad \text{A.14}$$

is another global pressure-intensity index based on the integral of the measured, signed intensity. This differs from the literature [21, 24, 27] which claim that the phase error should be related to the indicator.

$$\Delta_{p|I|} = F_2 = 10 \log [\int_s p^2 . ds/(\rho c \int_s |I_r| ds)] \qquad \text{A.15}$$

It is important to assess the influence of phase correction, because error assessment using eqn. (A.11) can be misleading as the pressure-intensity index depends on intensity, which is subject to an phase error itself. Jacobsen has applied this correction very effectively to unmatched microphones in a variety of testing conditions using the scanning technique. Tolerable agreement was even obtained for the global pressure-intensity index of 15 dB, some 10 dB greater than the residual pressure-intensity index of the unmatched microphones. Correction was possible even when the phase error exceeded the phase being measured. The correction is dependant on a number of assumptions:-

i) The phase error, $\emptyset_e$, must vary slowly with frequency.

ii) The residual pressure-intensity index must be accurately determinable.

iii) The phase error, $\emptyset_e$, is independent of the sound field.

Measurements outlined in section 3.3.4 indicate that the phase error does vary slowly with frequency for both microphones. As repeatable results were obtained in a good quality special purpose cavity calibrator it can be assumed the second condition has been met. The third condition can only be assessed experimentally and Jacobsen's[33], ability to correct for phase error in a variety of different sound fields suggests that the actual sound field is not problematic. As these conditions are met it is believed that some improvement will be achieved for well-matched microphones even with this simple procedure.

APPENDIX B : ACOUSTIC EQUIVALENT IMPEDANCE OF A STATOR VENT CHANNEL

The equivalent acoustic circuit impedance terms in Fig. 6.4 were derived using the existing equations for circular openings[63,70] and constrictions[71] replacing the radius of the circle in these equations by $(S/\pi)^{0.5}$. These equations are based upon the assumption that $(S/\pi)^{0.5} < \lambda/2$, which is satisfied as the effective radius is 0.0056m compared with a wavelength (λ) of 0.427m for 800 Hz. All impedances are transformed to be as seen from the air gap. The area at a transition denoted in Fig. 6.3 is denoted by S subscript the appropriate transition. Upper case S denotes the larger area and lower case s the smaller area at the transition.

The radiation impedance of the stator vent duct channel, expressed for a series resistance and inductance term, was considered to be that for a baffled cylinder.

$$R_o = (1/2\pi)\ \rho c\ k^2\ (S_o/S_1)\ (s_1/S_2),\ X_o = \omega\rho\ (0.479/S_o^{0.5})\ (S_o/S_1)\ (s_1/S_2) \qquad \text{B1a,b}$$

The transmission line equivalent T-network parameters for the channel section $0\text{-}0_1$ of length $= h_1$ are given by

$$R_{c1} = (\rho c/S_1)\ (s_1/S_2),\ kh_1 = n\ \pi \pm \gamma_1 \qquad \text{B2a,b}$$

$$Z_{MT1} = \pm j\ R_{c1}\ \tan\ (\gamma_1/2)\ ,\ Z_{CT1} = \mp\ j\ R_{c1}/\sin\ \gamma_1 \qquad \text{B2c,d}$$

Two parallel contribution at 0_1, each of area 0.5s, are

$$X_{01} = \omega\rho\ 0.479(H_{01}/(2s_1)^{0.5})\ (s_1/S_2) \qquad \text{B3}$$

where the discontinuity inductance correction factor H_{01} is a function of $(s_1/S_1)^{0.5}$ as given in [70].

The transmission line equivalent T network parameters for two parallel channels, each of length h_2 are

$$R_{c2} = \rho c/S_2 \ , \ kh_2 = n\,\pi \pm \gamma_2 \qquad \text{B4a,b}$$

$$Z_{MT2} = \pm\, j\, R_{c2} \tan(\gamma_2/2) \ , \ Z_{CT2} = \mp\, j\, R_{c2}/\sin(\gamma_2) \qquad \text{B4c,d}$$

Two parallel constrictions at 0_2, each of area $0.5s_2$ are

$$X_{02} = \omega\rho\ 0.479\ H_{02}/(2s_2)^{0.5} \qquad \text{B5}$$

where the discontinuity inductance correction factor H_{02} is a function of $(s_2/S_2)^{0.5}$ as given in [70].

APPENDIX C CALCULATION OF EQUIVALENT MAXIMUM AND MINIMUM AIRFLOW AREAS FOR STATOR VENT DUCT CHANNEL

The pressure drop at each point in the airflow circuit in Figs. 6.2 and 6.3 is given by the following equation. Upper case S denotes the larger area and lower case s the smaller area at the transition. Upper case P denotes the pressure at the larger area side of a transition and lower case p the pressure on the smaller area side. V subscript large S denotes the velocity on the large area side of a transition and v subscript small s denotes the velocity on the small area side.

The pressure drop caused by a contraction at a sharp edged entry to the pole shoes is given by:

$$P_a - p_5 = (\rho/2)\ (v_{s5}^2 - v_a^2 + 0.5\ v_{s5}^2) \qquad C1$$

where v_a is the air velocity before entering the pole shoes, usually considered to equal zero and P_a is ambient pressure.

The pressure drop caused by diffusion between 0_5 and 0_4 is given by

$$p_5 - P_4 = (\rho/2)\ (v_{S4}^2 - v_{s5}^2) \qquad C2$$

The pressure drop caused by contraction at 0_4 is given by [74] with a contraction coefficient K_{c4} as

$$P_4 - p_4 = (\rho/2)\ (v_{s4}^2 - v_{S4}^2 + K_{c4}\ v_{s4}^2) \qquad C3$$

The pressure drop caused by diffusion between 0_4 and 0_3 is given by

$$p_4 - p_3 = (\rho/2)\ (v_{s3}^2 - v_{s4}^2) \qquad C4$$

There is an extra pressure drop, $P_{c5,3}$, due to centrifugal action from pole shoe inlet to outlet. The pressure drop between 0_3 and 0_2 for minimum resistance will contain an expansion term at the outlet of pole shoes and a constriction term at the inlet of the stator vent with a contraction coefficient of K_{c2}.

$$p_3 - p_2 = (\rho/2)\ [v_{S3}^2 - v_{s3}^2 + (v_{s3} - v_{S3})^2] + (\rho/2)\ [v_{s2}^2 - v_{S2}^2 + K_{c2}\ v_{s2}] \qquad C5$$

The pressure drop caused by diffusion between 0_2 and 0_1 is given by

$$p_2 - p_1 = (\rho/2)\ (v_{s1}^2 - v_{s2}^2) \qquad C6$$

The pressure drop caused by sudden expansion at 0_1 is given by

$$p_1 - P_1 = (\rho/2)\ [v_{S1}^2 - v_{s1}^2 + (v_{s1} - v_{S1})^2] \qquad C7$$

The pressure drop caused by diffusion between 0_1 and 0 is given by

$$P_1 - P_0 = (\rho/2)\ (v_{S0}^2 - v_{S1}^2) \qquad C8$$

The pressure drop caused discharge at 0 is given by

$$P_0 - P_d = (\rho/2)\ [v_d^2 - v_{S0}^2 + (v_{S0} - v_d)^2] \qquad C9$$

Based on the principle of continuity of flow and using the definition that the resistance to air flow is equal to the pressure drop divided by the volume flow velocity, the minimum resistance to air flow is given by

$$\text{minimum resistance} = (\rho/2)\ V_{rmin}\ \{(Q1/Q2)^2\ [0.5s_5^2 + K_{c4}/s_4^2 + (1 - s_3/S_3)^2 /s_3^2 + 1/S_3^2] - 1/S_2^2 + K_{c2}/s_2^2 + (1 - s_1/S_1)^2\ /s_1^2 + 1/S_o^2\}$$

$$= (\rho/2)\ V_{rmin}\ (1/S_{max}^2) \qquad C10$$

Where Q_1 and Q_2 equal the number of stator and rotor slots respectively.

APPENDIX D : SOUND FIELD INDICATORS

The sound field indicators used in ISO 9614-1[5] are defined as follows.

F_2, the Surface Pressure - Intensity Indicator :

$$F_2 = \bar{L_p} - 10 \lg [(1/N) \sum_{i=1}^{N} |I_{ri}| / I_o] \qquad D1$$

where L_p is the sound pressure level corresponding to the sample average mean square pressure, N is the total number of measurement points, I_{ri} is a sample normal intensity and I_o is 1×10^{-12} Wm^{-2}.

F_3, the Negative Partial Power Indicator :

$$F_3 = L_p - 10 \lg [(1/N) \sum_{i=1}^{N} I_{ri}/I_o] \qquad D2$$

F_4, the Field Non-Uniformity Indicator :

$$F_4 = [1/\bar{I_r}] [(1/N-1)) \sum_{i=1}^{N} [I_{ri} - \bar{I_r}]^2]^{1/2} \qquad D3$$

value $\bar{I}_r$ is the sample average normal intensity.

F_5, the Sound Field Temporal Variability Indicator :

$$F_5 = [1/I_r] [1/(M-1) \sum_{k=1}^{M} [I_{r,k} - \bar{I_r}]^2]1^{1/2} \qquad D4$$

where $\bar{I_r}$ is the mean of M short time average samples $I_{r,k}$. M will normally take a value of 10. A recommended short averaging time is 8 to 12 seconds.

The spatial sampling error, E_r, for given confidence limits can be calculated in terms of the variance coefficient, $F_4 = S_n/I_r$ using the equation

$$E_r = 10 \log \{1 + F_4 t_s/1\sqrt{(N-1)}\} \text{ dB} \qquad D5$$

where t_s is the statistical parameter, the student t, for a certain confidence limit, N is the number of measurement positions, S_n is the standard deviation of the N measurements and I_r is the average intensity.

REFERENCES

1. Say, M.G., "Alternating Current Machines", Longman Scientific & Technical, 1983.

2. Fahy, F.J., "Sound Intensity", Elsevier Applied Science, London, 1989.

3. Van Zyl, B.G. and Anderson, F., Evaluation of the intensity method of sound power determination, J. Acoust. Soc. Amer., **57**, 1975, 682-686.

4. Fahy, F.J., Measurement of acoustic intensity using the cross-spectral density of two microphone signals, J. Acoust. Soc. Amer., **62(4)**, 1977, 1057-1059.

5. ISO International Standard 9614-1 1990. Acoustics - determination of sound power levels of noise sources using sound intensity - part 1 : measurement at discrete points.

6. Schwarzenbach, A., Noise in steam power stations, Brown Boveri Rev,**2**, 1972, 30-35.

7. Bannister, R.L. and Niskodé, P.M., Analysis and control of steam turbine-generator noise, Noise Control Engineering, **2(1)**, 1974, 6-13.

8. Pailly, C., Bruit des groupes turbo-alternateurs, Report No. HJ.41-4360, Electricite de France, Département Acoustique et Vibrations, 92140 Clamart, France, 1974.

9. Grabkowski, S.E. and Van Schaick, T.E., Sound power level determination for large steam turbine-generators, IEEE Transactions on Power Apparatus and Systems, **PAS-94(1)**, 1975, 31-36.

10. Grabkowski, S.E., Sirota, S.R., Jenkins, S. and, Buechler, J.P., Controlling noise in a large steam turbine-generator room, IEEE Transactions on Power Apparatus and Systems, **PAS-97(2)**, 1978, 504-512.

11. Pleeck, D. and Petersen, E.C., Real time sound intensity measurements performed with an analog and portable instrument, In Proceedings of Recent Developments in Acoustic Intensity Measurements; ed. M. Bockhoff. Centre Technique des Industries Mécaniques, Senlis, France, 1981.

12. Reiniche, W.L., Intensimetrische Schalleistungsermittlung bei Dampfturbozatzen, VGB Kraftwerktech, **66(7)**, 1986, 610-615.

13. Taillifet, D., Tamalet, J.C., Wegner, M. and Vuillerod, G., Characterisation of the main sources in hydro power plants, In Proceedings of Inter-Noise 88, ed. M. Bockhoff. Centre Technique des Industries Mécaniques, Senlis, France, 1988, 1143-1146.

14. Hong, Z., Lulu, F., and Meirong, W., Fuzzy Classification of Noise Level of 300MW Turboset Produced in China, Proceedings of CSEE, **8(4)**, 1988, 61-66.

15. Goldfracht, E., and Segal, A., Prediction of sound level due to long sound sources in industrial halls, In Proceedings of Inter-Noise 88, ed. M. Bockhoff. Centre Technique des Industries Mécaniques, Senlis, France, 1988, 1659-1662.

16. Yang, S.J., "Low noise electric motors", Oxford University Press, 1981.

17. Electric motor noise and vibration, Proceedings of the Institute of Acoustics, **12(6)**, 1990.

18. Tampion, A.A., Stoll, R.L. and Sykulski, J.K., Variation of turbogenerator stator core vibration with load, IEE Proceedings-C, **138(5)**, 1991, 389-400.

19. Barton, S.C., Massingill, J.A. and Taylor, H.D., Design Features and characteristics of large steam turbine generators, Trans. A.I.E.E., **77(3)**, 1959, 1335-1348.

20. Hübner, G., Aerodynamische Geraüsche umlaufender Maschinenteile, VDI Berlin, **48**, 1961, 113-117.

21. Francois, P., The generation of noise and the response of the structures in asynchronous motors, particularly as far as the flow is concerned, Applied Acoustics, **3**, 1970, 23-45.

22. Szechenyi, E., Sound transmission through cylinder walls using statistical considerations, J. Sound Vib., **19(1)**, 1971, 83-94.

23. Crocker, M.J., Experimental methods of identifying sound sources on a machine, Archives of Acoustics, **8(4)**, 1983, 293-316.

24. Xinzhao, C., Dengxiao, L., Jian, C. and Zhengshi, L., A study on identifying the sources of dominant frequency components of electric motor noise, Noise Control Engineering, **33(1)**, 1989, 11-15.

25. Macadam, J.A., The measurement of sound radiation from room surfaces in lightweight buildings, Applied Acoustics **9(2)**, 1976, 103-118.

26. McGary, M. and Crocker, Surface intensity measurements on a diesel engine, Noise Control Engineering, **16(1)**, 1981, 26-36.

27. Brüel & Kjaer, Application package for Spatial Transformation of Sound Fields, BZ7007, Naerum, Danemark.

28. Gan, W.S., Application of acoustic holography to acoustic intensity for the characterisation of composite sound sources. In Proceedings of the Sound International Congress in Acoustic Intensity, ed. M. Bockhoff, Centre Technique des Industries Mécaniques, Senlis, France, 1985, 413-420.

29. Nielsen, T.G., Analysers for intensity measurements. Proc. Symposium on Acoustic Intensity, Tokyo, 1987, 22-36.

30. Tichy, J., and Kihlman, T., Sound intensity field in front of plates with and without damping, In Proceedings of Inter-Noise 88, ed. M. Bockhoff. Centre Technique des Industries Mécaniques, Senlis, France, 1988, 111-114.

31. Jacobsen, F. and Nielsen, T., Spatial correlation and coherence in a reverberant sound field, J. Sound Vib., **118(1)**, 1987, 175-180.

32. Hübner, G., Sound intensity measurement method - errors in determining the sound power level of machines - correlation with sound field indicators. In Proceedings of Inter-Noise 87, ed. Li Peizi. Acoustical Society of China, P.O. Box 2712, Beijing, People's Republic of China, 1987, 1227-1230.

33. Jacobsen, F., A simple and effective correction for phase mis-match in intensity probes. Applied Acoustics., **33(3)**, 1991, 165-180.

34. Ren, M. and Jacobsen, F., Phase mismatch errors and related indicators in sound intensity measurement, J. Sound Vib., **149(3)**, 1991.

35. Pascal, J.C., Analytical expressions for random errors of acoustic intensity. In Proceedings of Inter-noise 86, ed. Robert Lotz. Noise Control Foundation, New York, 1986, 1073-1076.

36. Jacobsen, F., Random errors in intensity estimation, J. Sound Vib., **128(2)**, 1989, 247-257.

37. Johns, W.D. and Porter, R.H., Ranking of compressor station noise sources using sound intensity techniques., Noise and Vibration Control Worldwide, **19**, 1988, 70-75.

38. Reinhart, T.E. and Crocker, M.J., Source identification on a diesel engine using acoustic intensity measurements, Noise Control Engineering, **18(3)**, 1982, 84-92.

39. Stirnemann, A., Bolleter, U. and Rathe, E.J., Possibilities and limits of sound power measurements with a real-time intensity analyser. J. Sound Vib., **98**, 1985, 403-413.

40. Bockhoff, M., Sound power determination in the presence of background noise. In Proceedings of the Second International Congress on Acoustic Intensity, ed. M. Bockhoff Centre Technique des Industries Mécaniques, Senlis, France, 1985, 275-288.

41. Pettersen, O.K.O. and Newman, M.J., The determination of radiated sound power using sound intensity measurements. Report No. STF44A86166, ELAB, Elektronikklaboratoriet ved NTH, N-7034, Trondheim, Norway, 1986.

42. Pepin, H., Localisation des sources de bruit sur une machine industrielle. In Proceedings of the Second International Congress on Acoustic Intensity, ed. M. Bockhoff. Centre Technique des Industries Mécaniques, Senlis, France, 1985, 413-420.

43. Astrup, T., Noise emission from chain saws. In Proceedings of the Second International Congress on Acoustic Intensity, ed. M. Bockhoff, Centre Technique des Industries Mécaniques, Senlis, France, 1985, 253-258.

44. Fuller, C.R., Structural influence of the cabin floor on sound transmission into aircraft - analytical investigations. J. Aircraft, **24**, 1987, 731-736.

45. Tretheway, M.W., Application of the selective two-microphone acoustic intensity method for noise source identification, Noise Control Engineering, **30(1)**, 1988, 22-29.

46. Ying, S.P. and Dennison, E.E., Application of coherence techniques for noise in power plants, Noise Control Engineering, **15(2)**, 1980, 81-87.

47. Pettersen, O.K.O. and Newman, M.J., Is our confidence in scanned intensity measurements justified?, In Proceeding of Inter-Noise 89, Newport Beach, CA, USA, 1989, 979-984.

48. Hübner, G., Sound power determination of machines using sound intensity measurements - reduction of number of measurement positions in cases of "hot areas", In Proceedings of Inter Noise 88, 1988, 1113-1116.

49. Hübner, G., Sound intensity measurement technique - discussion of some actual problems, In Proceedings of Inter-Noise 90, 1990, 655-660.

50. Gade, S., Temporal variability of intensity measurements, In Proceedings of Inter - Noise 89, 1989, 991-994.

51. Jacobsen, F., Random errors in sound power determination based upon intensity measurement. J. Sound Vib., **131(3)**, 1989, 475-487.

52. Entek Scientific Corporation, Acoustic intensity analysis software, ESIM, 4480 Lake Forest Drive, Cincinnati, Ohio, U.S.A.

53. Brüel & Kjaer, Sound intensity program, WT9378, Naerum, Denmark.

54. Villot, M., Uncertainties in the cross-spectral method for acoustic intensity under semi-reverberant conditions. J. Acoust Soc. Amer., **78**, 1986, 691-701.

55. Frederiksen, E., and Schultz, O., Pressure microphones for intensity measurements with significantly improved phase properties, In Brüel & Kjaer Technical Review No 4-1986. Brüel & Kjaer, Naerum, Denmark, 11-23.

56. Probst, W., Determination of the combined correction for room reflection and angle error, when measuring the sound power level of large size machines, In Proceedings of Inter-Noise 90, 1990, 669-672.

57. Kinsler, L.E., Frey, A.R., Coppens, A.B. and Sanders, J.V., "Fundamentals of Acoustics", 3rd edn. John Wiley, New York, 1982.

58. Tandon, N., The effect of background noise on noise source location by the sound intensity technique, Applied Acoustics, **26**, 1989, 193-198.

59. Jacobsen, F., Active and reactive, coherent and reverberant sound fields, J. Sound Vib., **130(3)**, 1989, 493-507.

60. Bendat, J.S. and Piersol, A.G., "Engineering applications of correlation and spectral analysis", John Wiley & Sons, New York, 1980.

61. Bühlmann, E.T. and Stirnemann, A., Suppression of external noise in sound intensity measurements in reverberant rooms and in the near field of the external source. In proceedings of the Second International Congress on Acoustic Intensity, ed. M. Bockhoff. Centre Technique des Industries Mécaniques, Senlis, France, 1985, 283-288.

62. Auguztinoviz, F., Some problems of noise source localisation in industrial plants using the coherence method, In Proceedings of Inter-Noise 87, 1987, 1451-1454.

63. Beranek, L.L., "Acoustics", American Institute of Physics, New York, 1987, 330.

64. Hübner, G., The use of sound field indicators for the measurement of the sound intensity determined sound power, In Proceedings of Inter-Noise 89, 1989, 1015-1020.

65. Jacobsen, F., Sound field indicators: useful tools, Noise Control Engineering, **35**, 1989, 37-46.

66. Hamata, V., Magnetic noise of d.c. machines, ACTA Tech. C.S.A.V., **2**, 1966, 202-226.

67. Wignall, A.N., "Analysis and prediction of electromagnetic vibration forces on the main pole of a d.c. machine", Ph.D. Thesis, Heriot Watt University, 1989.

68. Talaat, M.E., Calculation of windage-noise power level in large induction motors, Trans. Am. Inst. electr. Engrs., **76**, 1957, 46-55.

69. Ploner, B., Aerodynamic noise in medium-sized asynchronous motors, Brown Boveri rev, **63**, 1976, 493-499.

70. Munjal, M.L., "Acoustics of ducts and mufflers", John Wiley, New York, 1987.

71. Karal, F.C., The analoguous impedance for discontinuities and constrictions of circular cross section, J. Acous. Soc. Am., **25(2)**, 1953, 327-334.

72. Lung, T.Y. and Doige G.A., A time-averaging testing method for acoustic properties of piping systems and mufflers with flow", J. Acous. Soc. Am., **73(3)**, 1983, 867-876.

73. Clark Jones, R., A fifty horsepower siren, J. Acous. Soc. Am., **18**, 1946, 371-387.

74. Ward-Smith, A.J., "Internal fluid flow : the fluid dynamics of flow in pipes and ducts", Oxford University Press, 1986.

75. Kotbra, V., Flow and heat transfer in radial channels of electric machines, Res & Dev. Inst. for Rotating Electr. Machines Brno, Czechoslovakia, **18(1)**, 1990, 83-96.

76. Adby, P.R. and Dempster, M.A.H., "Introduction to optimisation methods", Chapman and Hall, London, 1974, 66-72.

77. Embleton, T.F.W. and Thiessen, G.J., Efficiency of circular sources and circular arrays of point sources with linear phase variation, J. Acous. Soc. Am., **34(6)**, 1962, 788-795.

IEEE Transactions on Energy Conversion, Vol. 8, No. 1, March 1993

ADVANCED TECHNIQUES FOR NOISE SOURCE IDENTIFICATION ON A LARGE GENERATOR UNIT

R.G.D. Williams
GEC Alsthom Turbine Generator Ltd.,
P.O. Box 25,
Lichfield Road,
Stafford,
ST17 4LN,
England, U.K.

S.J. Yang, Senior Member
Dept. Electrical and Electronic Engineering,
Heriot-Watt University,
31-35 Grassmarket,
Edinburgh,
EH1 2HT,
Scotland, U.K.

Abstract - Power station acoustic noise assessment, which has experienced increased environmental awareness and subsequently more stringent legislation for a number of years, has received an added stimulus due to the recent advent of powerful measurement and analysis techniques including sound intensity and coherence. These experimental techniques are explained and results, for a generator unit, illustrate their value in providing a unique, correlated insight into noise problems. This includes noise quantification, full explanation of site sound pressure level in terms of the various influences and major noise source identification. These techniques are widely applicable and an invaluable aid to any industrial noise problem.

Keywords - sound intensity, coherence, turbogenerators, electric machinery, noise, vibration, source identification.

INTRODUCTION

Considerable interest has been directed to the assessment and control of airborne noise in modern power plants for a number of years. This is as a result of increased awareness of the environment and subsequently more stringent legislation. Noise assessment has received added stimulus due to the advent of a number of new, powerful measurement and analysis techniques

As a first step to reduce the noise emission it is necessary to identify the part of the plant which causes the high noise output. The measurement of S.P.L. (sound pressure level) has been found to be inadequate in analysing noise sources from large turbine generator units. Sound power cannot be determined for large machines such as turbine generators in situ by sound pressure measurements [1]. In some instances major noise problems can be indicated from the sound pressure [2], although the sound pressure is seldom simply related to adjacent machinery in industrial spaces such as a turbine hall. More commonly the sound pressure is created by a complex interaction of plant radiation characteristics, reverberation and interference fields from many items of co-functioning equipment as can be seen from fig. 1.

The innovation of digital signal processing and subsequent sophisticated measurement techniques have enabled even complex sound fields to be characterised. A detailed study was conducted into the noise output from a modern 660 MW generator and its excitation system consisting of the main exciter, the rotating rectifier, the pilot exciter and associated couplings with a layout given in fig. 2. The techniques outlined in this paper are applicable to many other industrial noise problems.

A variety of different measurement techniques were utilised to investigate the difficult reverberant, multi source acoustical environment found in power stations. Sound pressure was measured to investigate environmental considerations. Sound intensity was measured to determine the sound power from the different items comprising a generator unit and its vector properties were utilised to indicate directional flow of acoustic energy. Fahy [3] fully explains the sound intensity technique and illustrates its application with many examples and references. Reiniche [4] uses the sound intensity technique on a turbine generator unit to determine sound power. The factors which cause a difference between sound pressure and the average sound intensity are discussed by Reiniche, but specific source localisation is limited. The coherence between structural vibration and sound pressure was investigated to assist with source location. This approach has proven successful on power plant [5].

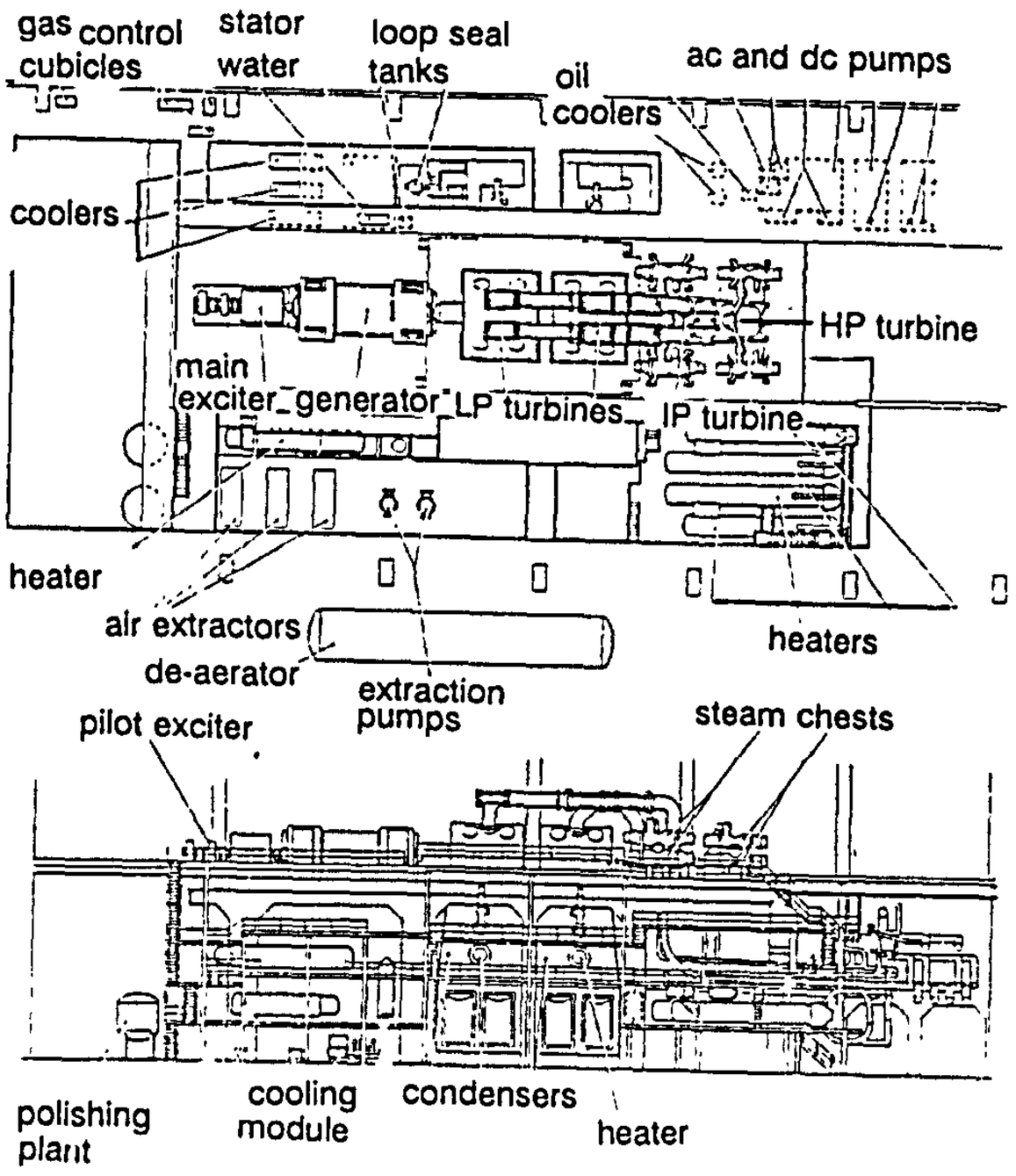

Fig. 1 Typical power plant in turbine hall.

This paper aims to provide a unified explanation of the noise problem by fulfilling the following objectives:

1. To quantify site sound pressure levels.
2. To determine the sound power from the constituent items comprising the generator unit enabling ranking of noise sources.
3. To predict the S.P.L. due to the generator unit component alone.
4. To fully explain the S.P.L. beside the generator unit.
5. To investigate the nature of the sound fields.

92 WM 063-8 EC A paper recommended and approved by the IEEE Electric Machinery Committee of the IEEE Power Engineering Society for presentation at the IEEE/PES 1992 Winter Meeting, New York, New York, January 26-30, 1992. Manuscript submitted July 11, 1991; made available for printing December 23, 1991.

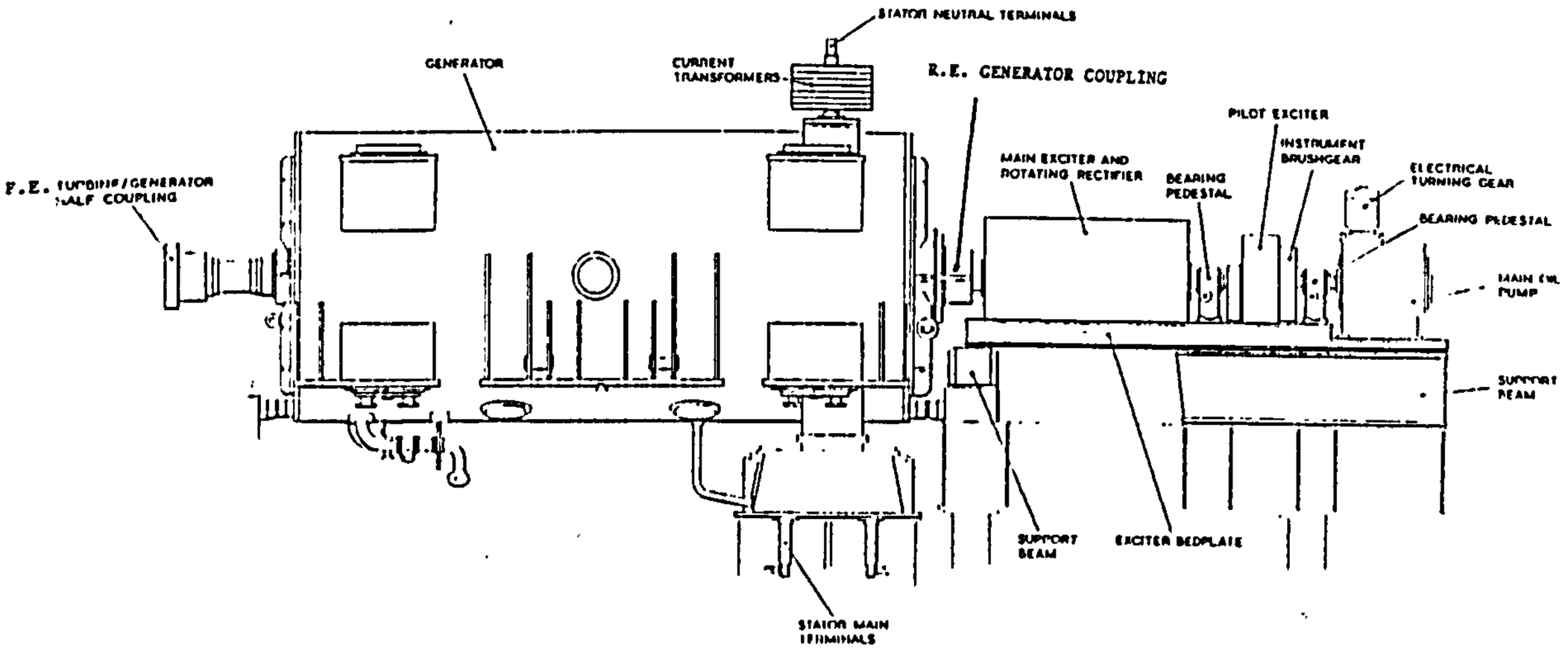

Fig. 2 660 MW generator unit layout.

EXPERIMENTAL TECHNIQUES AND BACKGROUND THEORY

Sound Pressure Level

To enable environmental assessment the sound pressure levels were measured at 1 m from the generator unit at a height of 1.2 m above the solid floor at locations illustrated in fig. 3. A Bruel and Kjaer integrating sound level meter with A weighting filter supported on a tripod was used in compliance with BS.5969.

Sound Power Determination by Sound Intensity Measurement

Sound power radiated from a machine is the principal measure of source strength, which is not very sensitive to the acoustic environment. Sound pressure, however, is dependent upon measurement position and environment. The sound power is therefore of critical importance in plant accredition and noise reduction work, quantifying noise emission, evaluating design changes and ranking noise sources. Before the advent of sound intensity measurement sound power determination was based upon sound pressure measurement under specified acoustic conditions using procedures outlined in ISO 3740-3747. It is not possible to measure noise from a turbine generator component using these procedures as one part of the system cannot operate in isolation and noise from other components contaminate the pressure measurements. It is impractical to transport and operate a generator, for example, in a special purpose test facility such as anechoic and reverberation chambers.

In recent years the availability of accurate, reliable instrumentation for the measurement of sound intensity allows identification and quantification of noise sources in their normal operating environments. In principle, the sound intensity technique may be applied under any ambient conditions provided the source noise and background noise remains reasonably constant.

Sound intensity is defined as the rate at which sound energy is transmitted through a unit area in a direction normal to that area. The net mean sound power from a machine is therefore the surface integral of the sound intensity normal to an enclosing area. The average sound intensity is computed as a vector quantity equal to the time averaged product of the instantaneous sound pressure and its corresponding instantaneous particle velocity. The component of intensity in the r direction is given by

$$I_r = \langle p(t)\, v_r(t) \rangle \qquad (1)$$

where $p(t)$ = sound pressure
$v_r(t)$ = particle velocity
I_r = sound intensity in the r direction

the symbol <> implies a time average.

Measurement of sound intensity has been attempted unsuccessfully in the past due to difficulty in measuring the particle velocity. The theoretical formulation provided in recent years [6] and the advent of digital signal processing techniques and special microphones have now made sound intensity measurements possible. The particle velocity can be synthesised from Euler's momentum equation which relates particle velocity to the pressure gradient at a point

$$\rho \frac{\partial v_r}{\partial t} + \frac{\partial p}{\partial r} = 0 \qquad (2)$$

where ρ is the fluid mass density. The particle velocity can be synthesised from the integral of the pressure gradient, which can be estimated as the pressure difference between two closely spaced microphones. It can be shown [6] that in the frequency domain the intensity spectrum, $I_r(\omega)$, can be expressed in terms of the imaginary part of the cross-spectrum of the two microphone signals, $\mathrm{Im}(G_{12})$, and the microphone separation Δr

$$I_r(\omega) = \frac{-\mathrm{Im}(G_{12})}{(\omega \rho \Delta r)} \qquad (3)$$

The cross-spectrum can be easily evaluated using dual-channel Fast Fourier Transform (F.F.T.) analysis.

To determine the sound power from each component of the generator unit the continuous surface integral of sound intensity was approximated using the scanning technique, in which the intensity probe is transversed normal to the measurement surface. The alternative sampling technique of measuring the sound intensity at discrete points requires a prohibitive number of measurement points to suppress high levels of background noise for a structure such as a large generator. The scanning technique was therefore preferable for this application. Surfaces were divided into individual areas less than 1 m^2 and the probe was scanned over the surface in a set of parallel straight lines joined by semicircles. A scan rate of 0.25 ms^{-1} was used with a line density of 12 cm. A measurement distance of 10 cm was employed to minimise the influence of background noise. For the scanning technique the probe signals are non-time stationary and random errors cannot be strictly predicted. However it is believed that provided the probe is scanned slowly enough for reasonable 'space' overlapping of time-sampled signal segments to occur, then the random errors of estimates are comparable to those from the same number of independent segments.

The sound intensity technique can be employed even in the presence of strong extraneous noise. The suppression of background noise employs Gauss's Integral Theorem by which the volume integral of the divergence of any field vector, in this case sound intensity, may be expressed in terms of the integral over the enclosing surface of the component normal to the surface.

$$\int_{VOL} \nabla . I dV = \int_s I . dS = \int_s I_n . dS = W_s \qquad (4)$$

where W_s is the net mean sound power generated by source mechanism with the enveloping surface. Noise sources external to the surface do not contribute to the surface integral and hence not to W_s.

Since 1984 the working group ISO/TC43 have been developing a draft standard ISO DIS/9614-1 "The determination of the sound power levels of sources

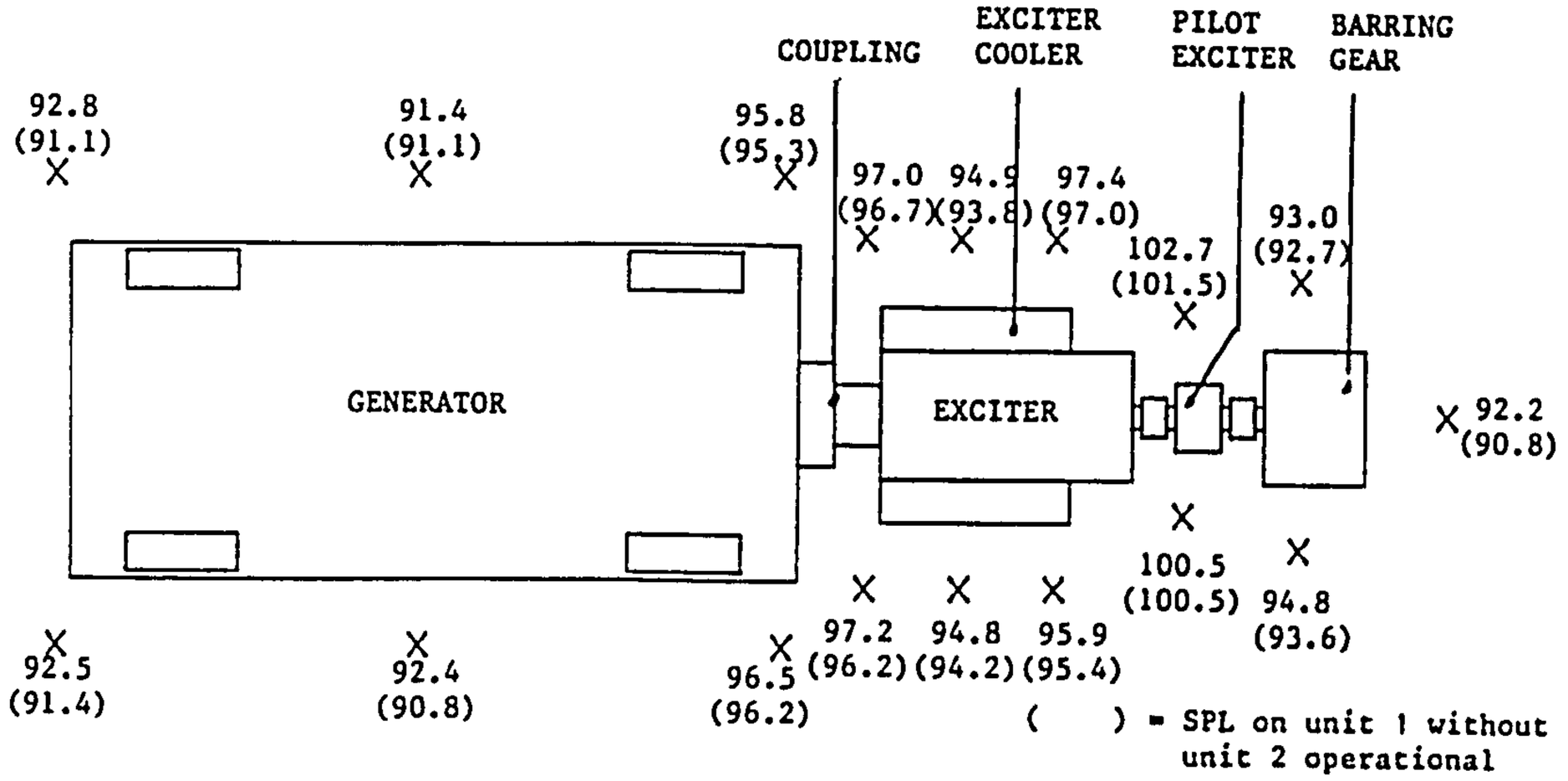

Fig. 3 S.P.L. at 1 m from the generator unit (dBA).

by sound intensity measurement at discrete points". At the time of writing this document is at the final acceptance stage to become a full standard. Due to the extra difficulty associated with non-time stationary signals from the scanning technique further investigation is necessary to develop a companion standard. It is commonly believed that this will prove successful and both techniques will result in similar accuracy.

It is necessary to carefully assess the error limits associated with the sound power determination for each component arising due to the following schematic and random errors.

(i) The finite difference error associated with approximating the pressure gradient at a point as the difference between two sound pressures divided by their separation.

(ii) The phase mismatch of the two microphones and measurement system.

(iii) The time averaged sampling associated with any measurement, which are related to averaging time, bandwidth etc.

(iv) The spacial averaging associated with approximising the Gaussian integral to a summation of partial sound powers.

The sound intensity was determined by means of an intensity probe (Bruel & Kjaer 3519) provided with two ½" phase matched condenser microphones with a 12 mm spacer and a dual channel frequency analyser (Hewlett Packard 3562) combined with a Hewlett Packard 9816 computer for post processing of data.

As the generator is symmetrical it's sound power emission was determined by scanning one third of the generator from floor level to top dead centre and appropriate scaling of area ratios to obtain a total figure. The exciter, R.E. generator coupling cover and pilot exciter were each completely scanned, when measuring their sound power. Measurement repeatability was investigated.

Discrete Point Sound Intensity Vector Measurement

To pinpoint major noise sources and indicate the flow of acoustic energy in the region of the generator unit point 2D sound intensity vector measurements were used. The magnitude of sound intensity from background sources, for example axial flow beside the generator from the turbines, can be investigated to assess its influence on S.P.L.

Surface Vibration Sound Pressure Coherence Measurement

The coherence function is a measure of statistical similarity between two signals. These signals may be related by cause and effect or they may only be similar due to the fact that they arise from a common phenomenon. In general the relationship between sound power radiation and surface vibration is complex. It is dependent not only upon the vibration velocity distribution on the surface, but also on the radiation efficiency of the structure, which is determined by the interference pattern created by an infinite number of mass injection elements in the radiating surface.

The relationship between sound pressure and surface vibration on various plant items was investigated in two methods. The coherence function was calculated between surface vibration measured with a piezo-electric accelerometer supported on a magnetic base in the frequency range 50 to 5050 Hz and sound pressure measured using a ½" condenser microphone supported on a tripod. The coherence varies between 0 and 1 dependent upon the relationship between source and sound pressure. The vibration velocity squared composition was also compared to the sound pressure spectrum for a variety of distances from 5 cm to 1 m.

RESULTS

Sound Pressure Level

The overall A-weighted sound pressure levels and their measurement locations 1 m from the generator unit are illustrated in fig. 3. For comparison purposes to assess the influence of background reverberant noise the S.P.L. measured on unit 1 without unit 2 in operation is quoted in brackets. Both units are identical on parallel axes 80 m apart.

Sound Power Determination

The sound power emission for the generator unit constituent components are given in table 1. The measured sound power levels were in rank order 106.7±1 dBA from the pilot exciter, 103.5±1 dBA from the R.E. generator coupling cover, 97.3±2 dBA from the generator and 96.8±2.5 dBA from the exciter. The quoted error limits were based upon instrument errors and statistical considerations. The A-weighted narrowband sound power levels are plotted in fig. 4a-d and the A-weighted $\frac{1}{3}$-octave sound power level are given in fig. 5.

The sound power of one third of the generator from floor level to top dead centre was 92.5 dBA, which scales up to 97.3 dBA for the total machine. The sound power is mainly related to low radial intensities of typically 75-76 dBA, which are reasonably uniformly distributed over the side of the machine. The A-weighted narrowband generator sound power

Component	Net Sound Power Level in dBA
Generator	97.3
R.E. Coupling Cover	103.5
Exciter	96.8
Pilot Exciter	106.7

Table 1 - Net sound power levels for generator unit constituent components

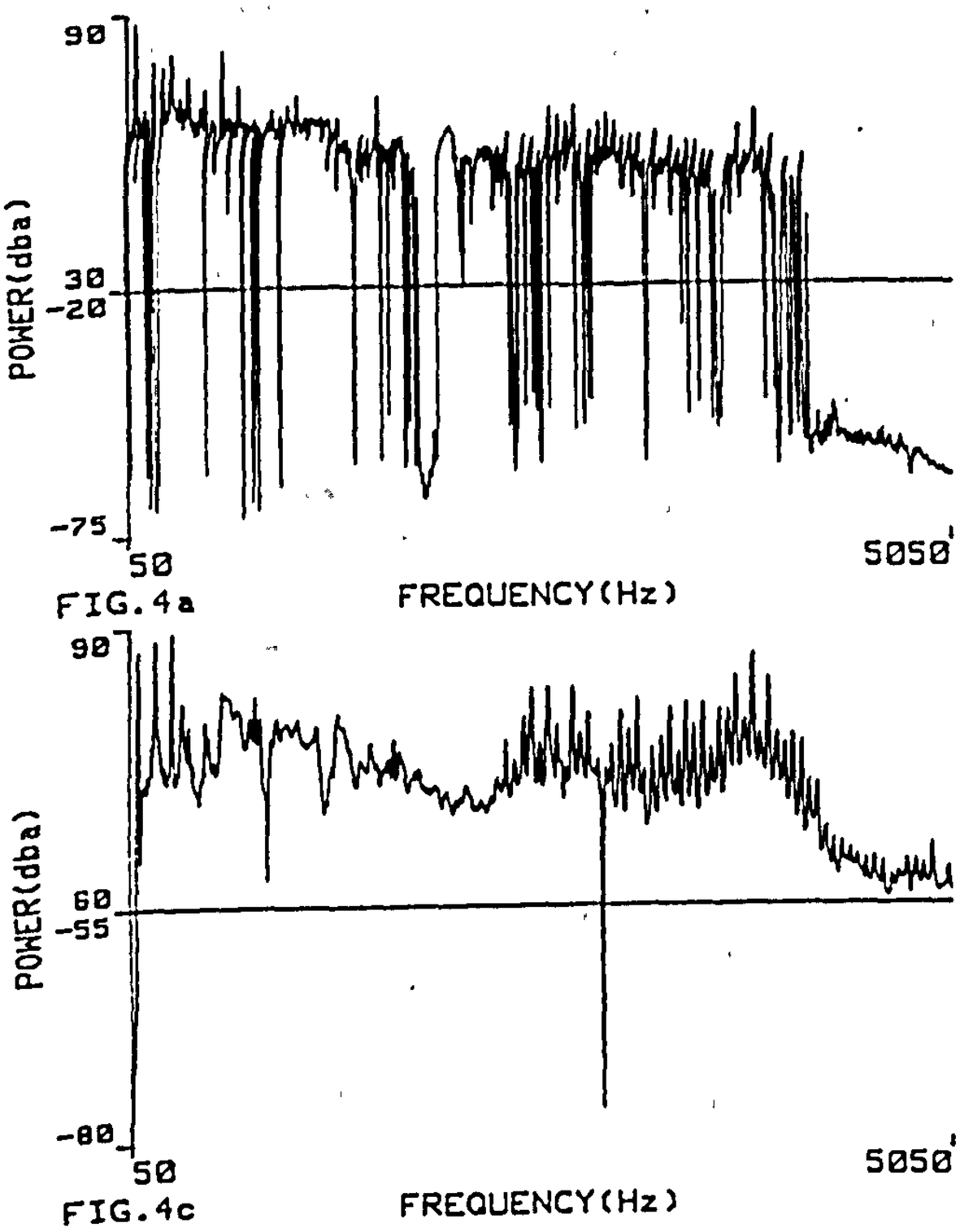

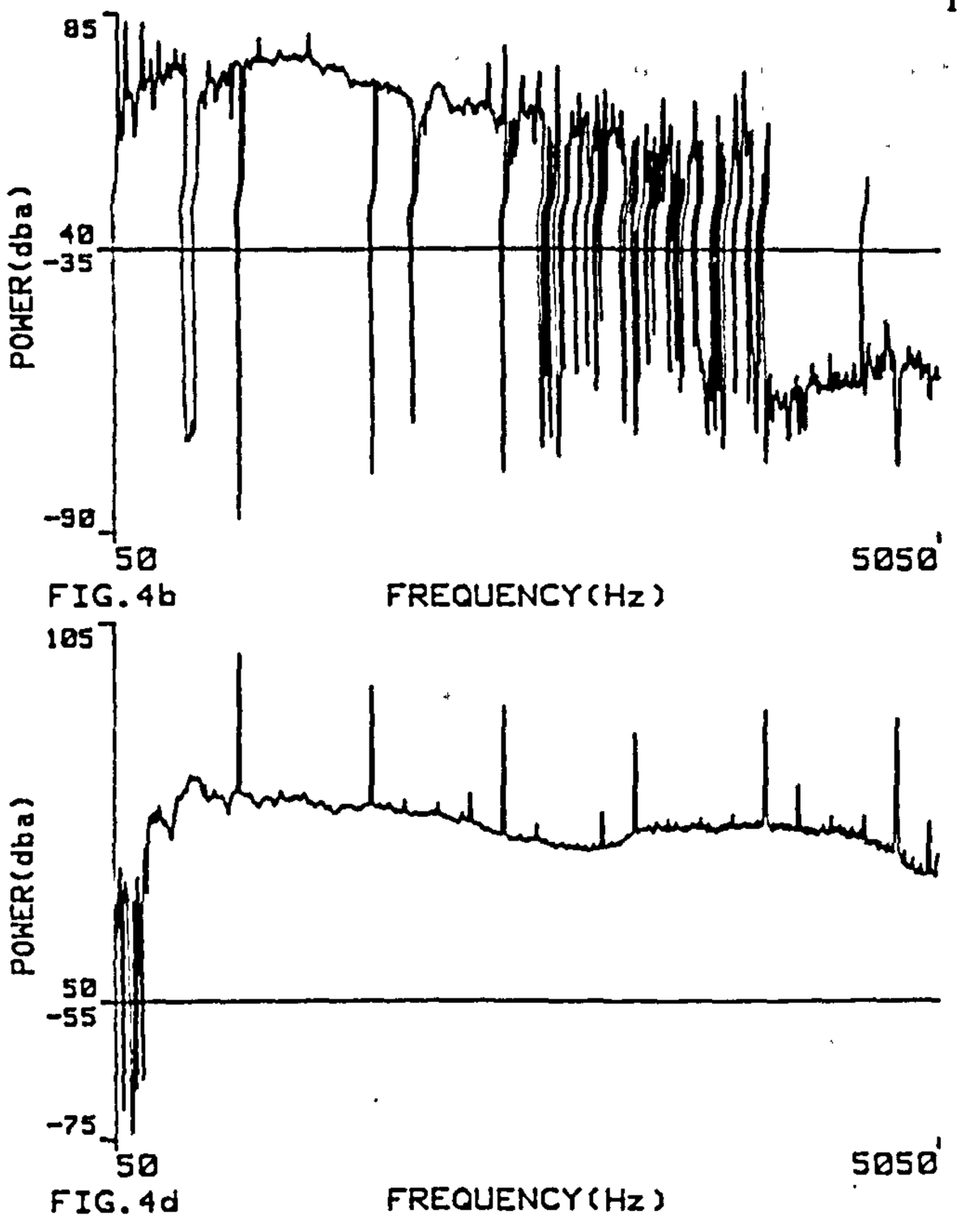

Fig. 4 Narrowband sound power levels for (a) generator, (b) exciter, (c) R.E. generator coupling (d) pilot exciter.

spectrum is illustrated in fig. 4a. The spectrum contains some negative tones up to 4 kHz, but the spectrum is predominantly broadband noise output with predominant peaks at 100 Hz and harmonics thereof. Above 4 kHz the spectrum denotes low levels of power absorption. Power absorption is discussed in a later section.

The main measurement problem for low levels of generator sound power determination was due to a diffuse multi source sound field created mainly by other sources. Due to the plant configuration the generator casing shielded much of the direct background noise. The inter-channel phase mismatch error can be calculated [3] from the residual sound pressure intensity index and the reactivity, which is the difference between sound pressure and sound intensity levels for any given measurement. For this system the residual index was greater than 22 dB in all 1/3 octave bands. The reactivity was commonly 16 dB, which although high is measurable to within ±1 dB. Random error due to spacial sampling was assessed by repeating every 4th measurement 4 times to obtain 4 spaced averaged intensities. The random error of the sound power determination can then be assessed for normally distributed measurements using the variation coefficient $V_n = \frac{S_n}{I_{avg}}$ in the following equation:

$$e_r = 10 \log \left(\frac{1 + V_n t_s}{\sqrt{n-1}}\right) \text{dB} \qquad (5)$$

where t_s is the statistical parameter, the student t, for a certain confidence limit, n is the number of repeated measurements, S_n is the standard deviation of the average intensity values and I_{avg} is the average of the repeated averages. For the degree of freedom = 3 and 90% confidence limits the student t is 2.35 and the random error was less than 1 dB for most of the frequency bands. This coincides with measurement repeatability for each area of commonly 1 dB. The resultant error limits are the sum of phase mismatch and random errors, which is ±2 dB.

The measured exciter sound power of 96.8 dBA was further complicated by stronger directional noise from the pilot exciter and the rear end generator coupling. It was imperative for such a difficult measurement to completely enclose the exciter optimising the use of the Gaussian Integral Theorem to suppress the background noise. The value of cancelling energy fringing can be illustrated by considering the rear end measurements. The rear end face of the exciter was measured as an input of 93.3 dBA due to energy from the pilot exciter. However when adjacent measurement areas of the side and roof are included the net sound power became an output of 93.2 dBA. The sound spectrum as illustrated in fig. 4b contains negative power above 3 kHz due to low level absorption and insufficient suppression of background noise.

The average measured reactivity was 13 dB in most 1/3 octave bands implying similar phase mismatch error to those for the generator of

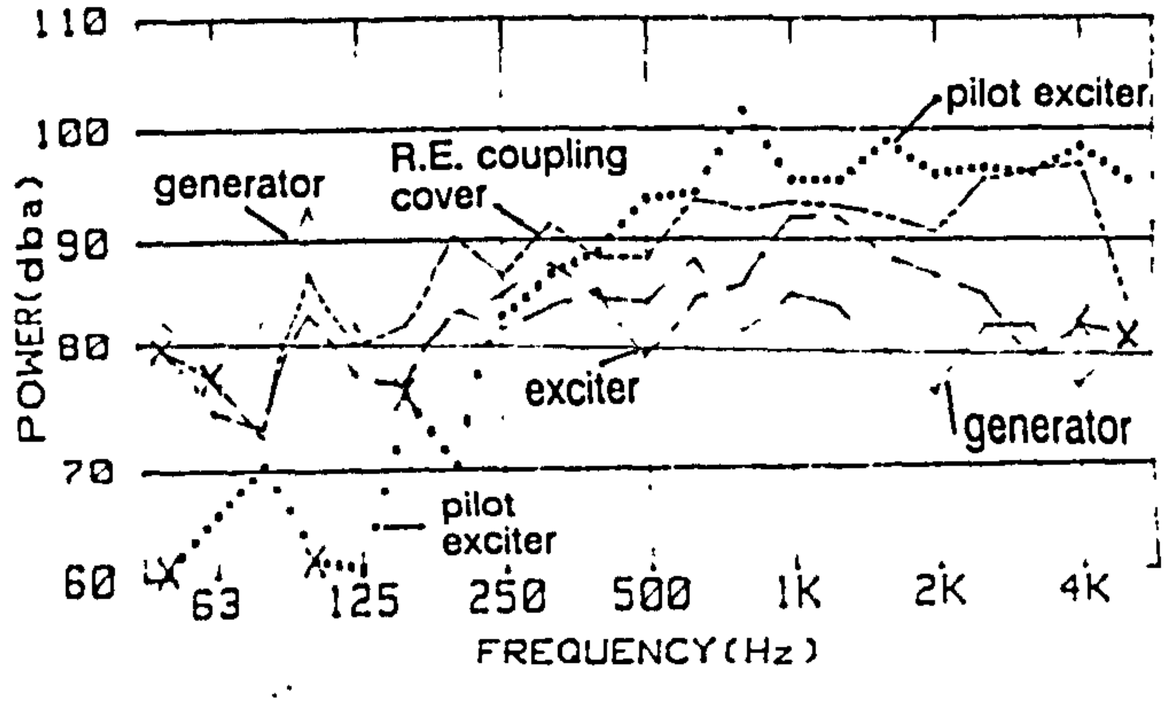

Fig. 5 A-weighted $\frac{1}{3}$-octave sound power levels for generator unit components.

– – – – R.E. Coupling Cover ——— Generator

· · · · · · · Pilot Exciter – – – Exciter

× Negative Sound Power Level

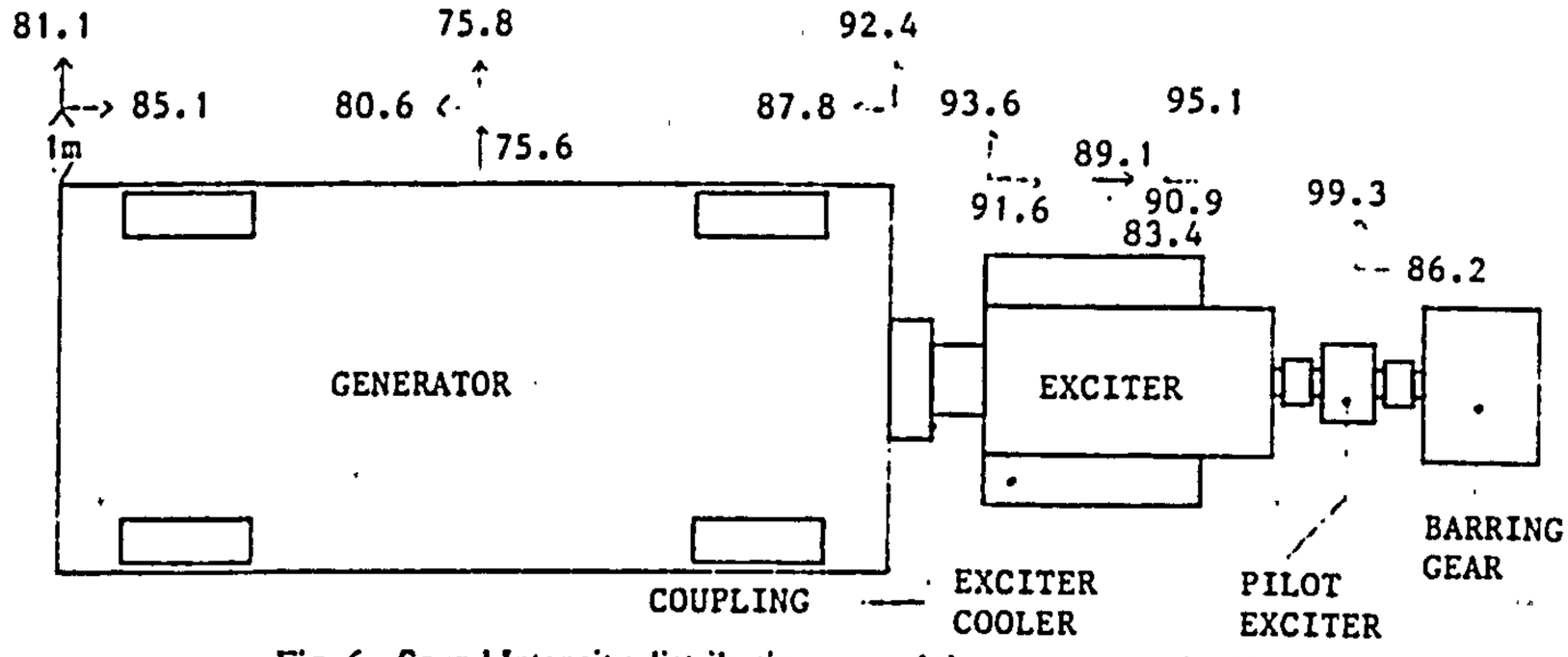

Fig. 6 Sound Intensity distribution around the generator unit (dBA).

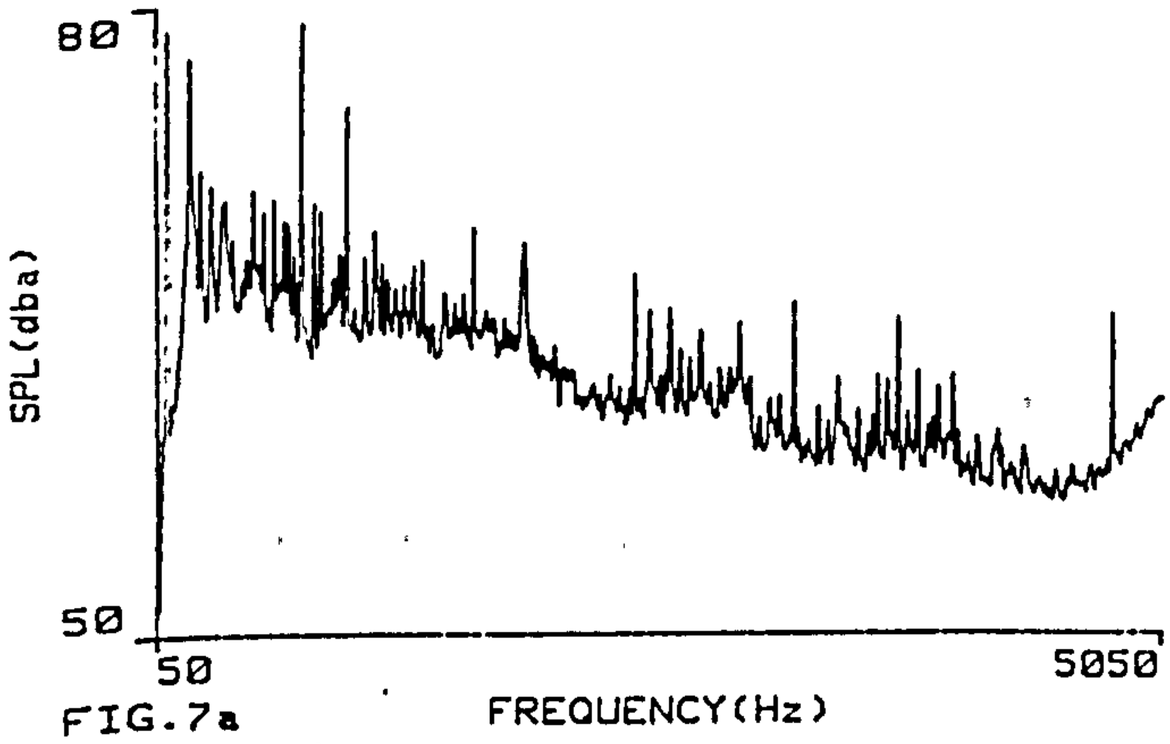

FIG.7a

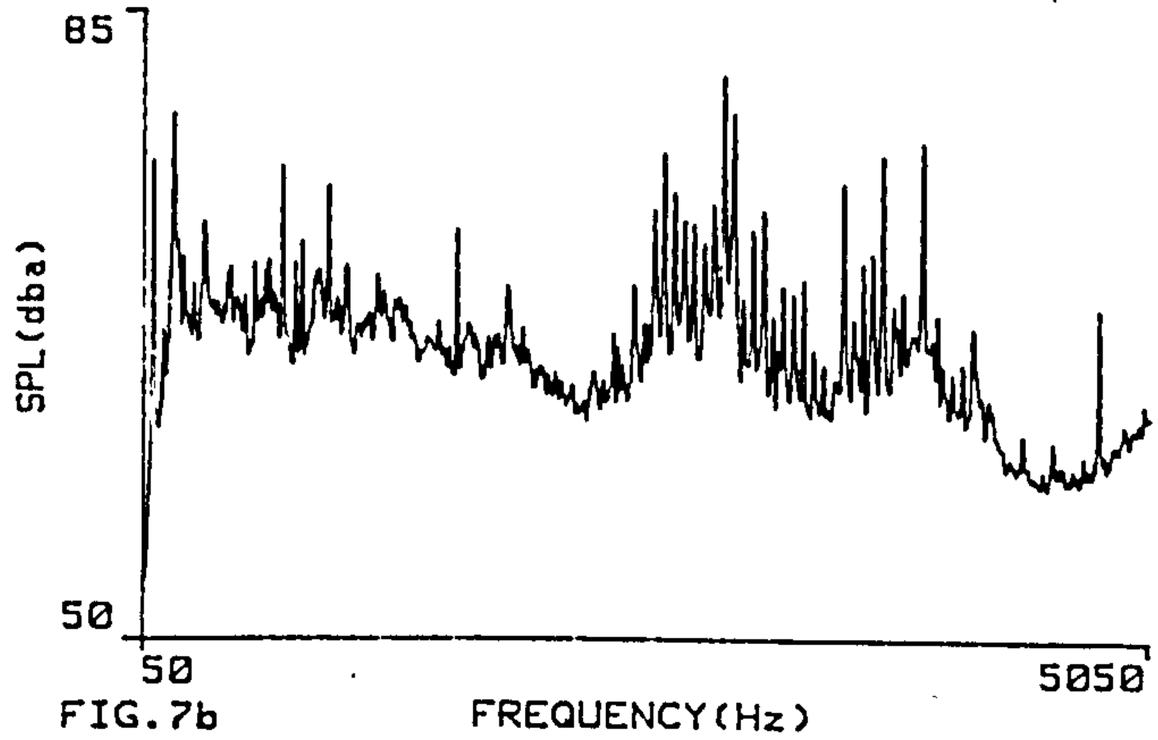

FIG.7b

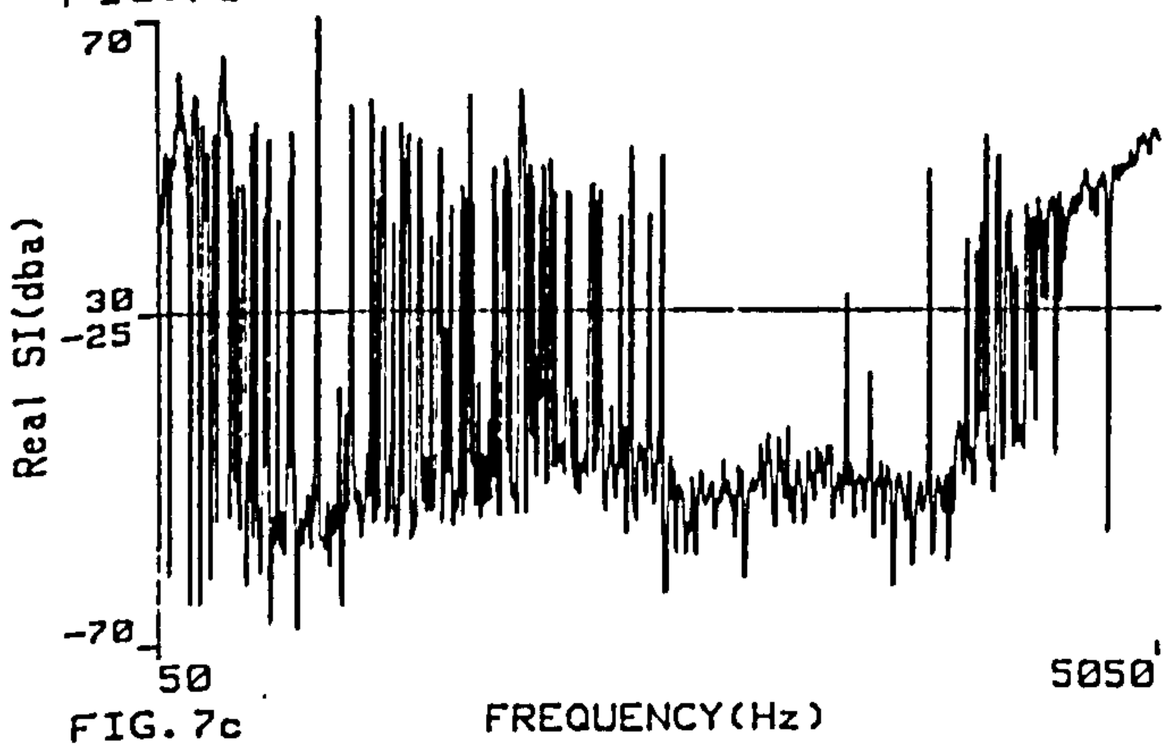

FIG.7c

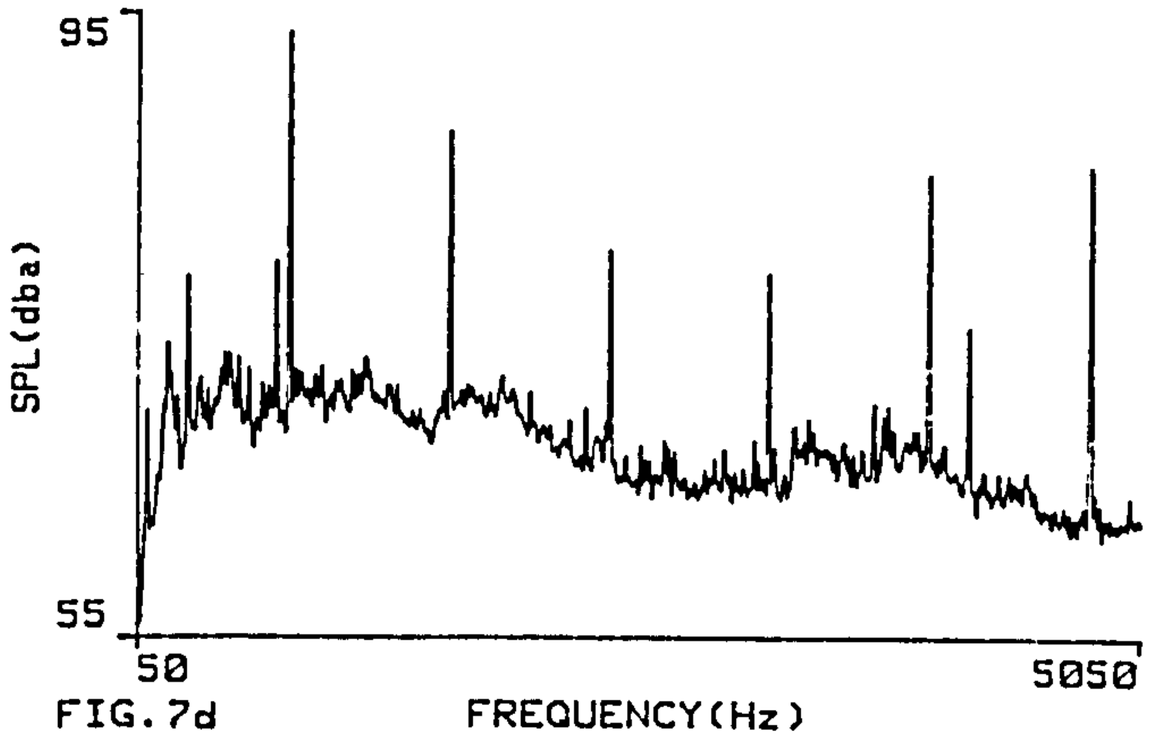

FIG.7d

Fig. 7 (a) Narrowband sound pressure level 1 m from the generator F.E.
(b) Narrowband sound pressure level 1 m from the generator R.E.
(c) Narrowband axial sound intensity 1 m from the generator centre.
(d) Narrowband sound pressure level 1 m from the exciter R.E.

pressure at 1 m has increased due to a number of tonal components in the range 2.5 kHz to 4 kHz, as illustrated in fig. 7b. The resultant sound intensity is 93.9 dBA from the rear end generator coupling. This value and the spectral similarity between R.E. coupling sound power fig. 4c and sound pressure fig. 7b indicate a significant influence of the coupling on S.P.L. beside the generator. At the generator centre the overall intensity is from the turbine in the 4 kHz-5 kHz frequency range, from the rear end coupling in the range 2.5 kHz-4 kHz and bidirectional at lower frequencies, as indicated in fig. 7c. The resultant sound intensity levels of 86.5 dBA and 93.9 dBA at the front and rear ends are an order of magnitude greater than the typical generator near field output intensities of 75-76 dBA therefore clearly illustrating the influence of background noise on the sound pressure level beside the generator.

Beside the exciter F.E. the sound pressure spectrum and level are similar to those at the generator R.E. with 94.2 dBA direct intensity flow from the coupling at 1 m. 1 m from the exciter rear end the S.P.L. of 98.5 dBA is significantly contributed to by the 96.5 dBA sound intensity from the pilot exciter. The sound pressure spectrum shown in fig. 7d is markedly different to that at the F.E. with tones at 800 Hz and harmonics thereof emanating from the pilot exciter (fig. 4d). At 1 m from the exciter centre sound pressure spectrum shows the contribution from the R.E. coupling and the pilot exciter. The radial sound intensity 10 cm from the exciter was 83.4 dBA. The low levels of intensity relative to the direct components from the coupling and the pilot exciter further indicate the main source of noise emission in the region.

Surface Vibration Sound Pressure Coherence

The coherence between sound pressure at 10 cm and surface vibration at the generator centre is low commonly tending to 0 except for a few tones in range 50 Hz to 1 kHz as shown by fig. 8a. The vibration velocity squared spectrum (fig. 8b) and the unweighted sound pressure spectrum (fig. 8c) are not comparable except for a limited number of tones at 100 Hz and harmonics thereof.

The sound pressure vibration coherence is similarly low beside the exciter, as shown by fig. 8d, except for tones at 2281 Hz, 2400 Hz and

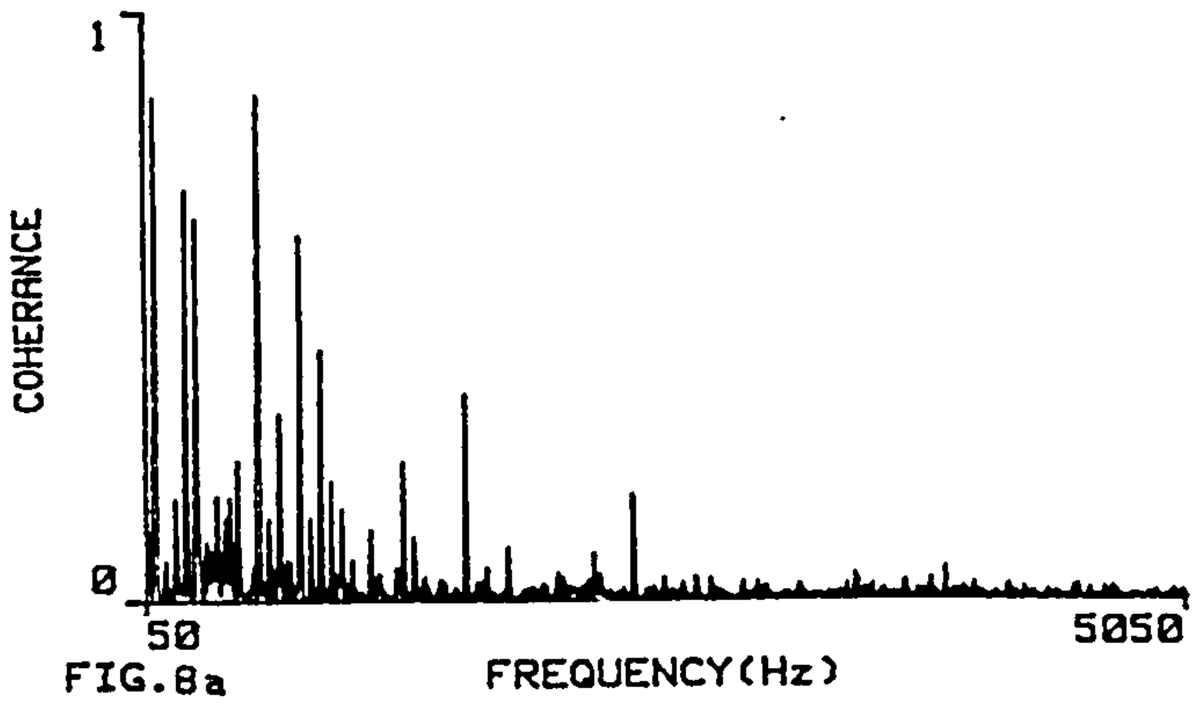

FIG.8a

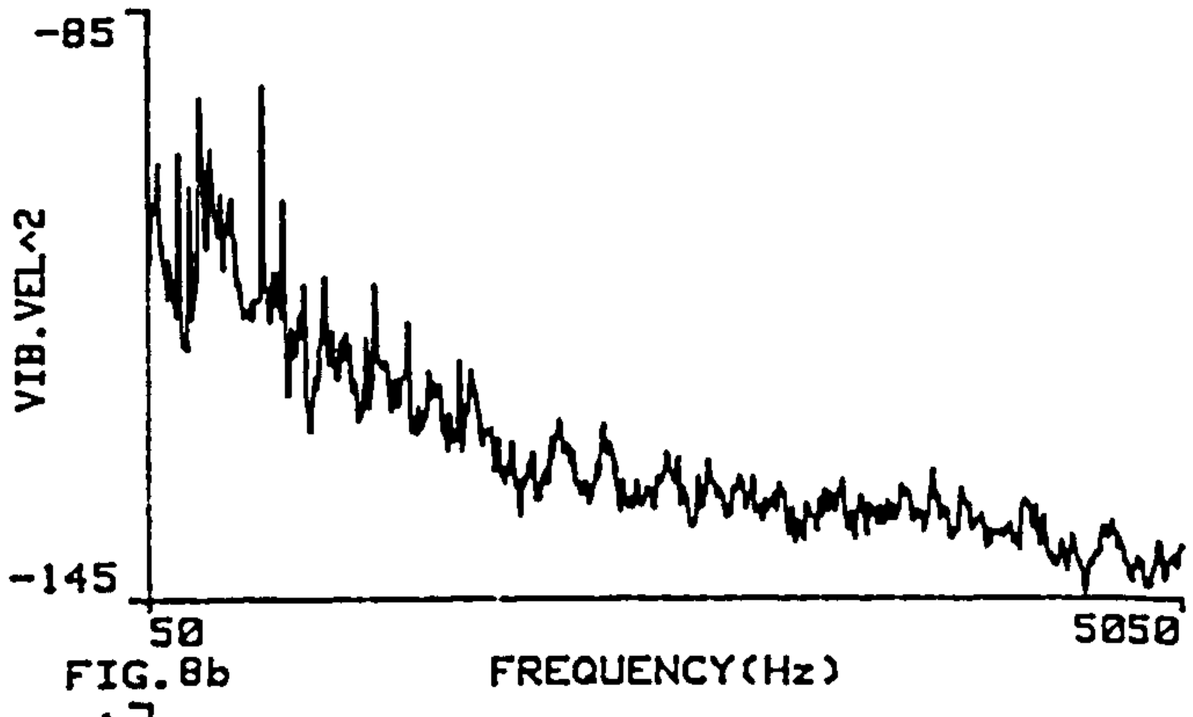

FIG.8b

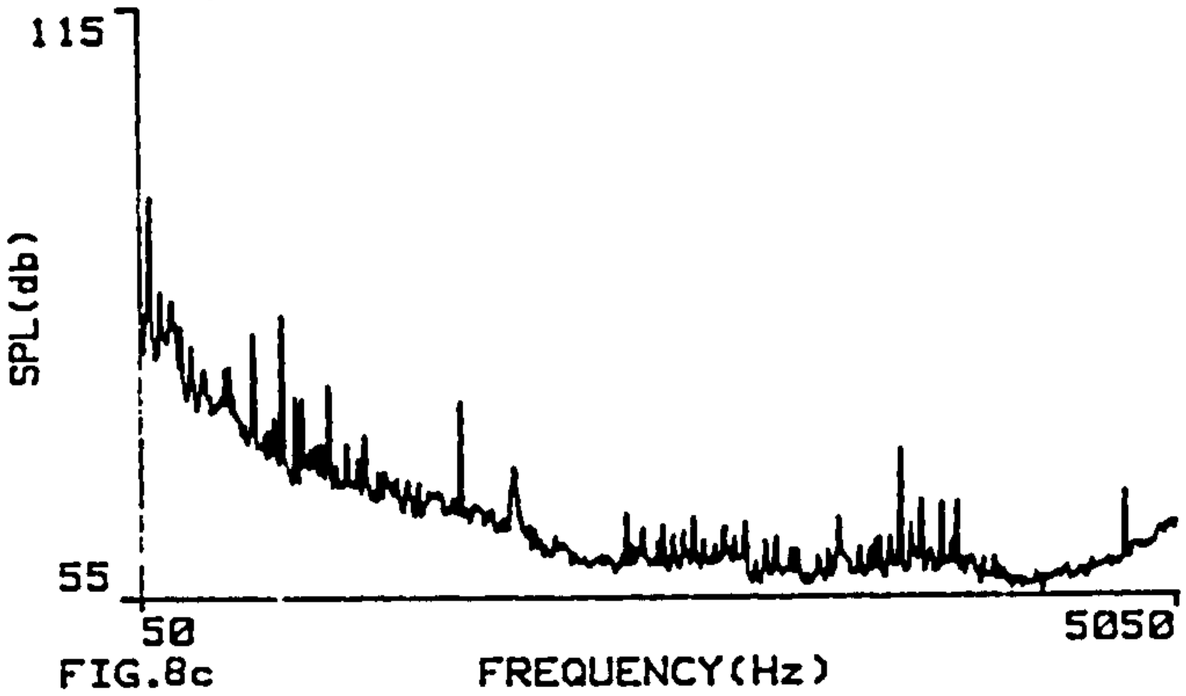

FIG.8c

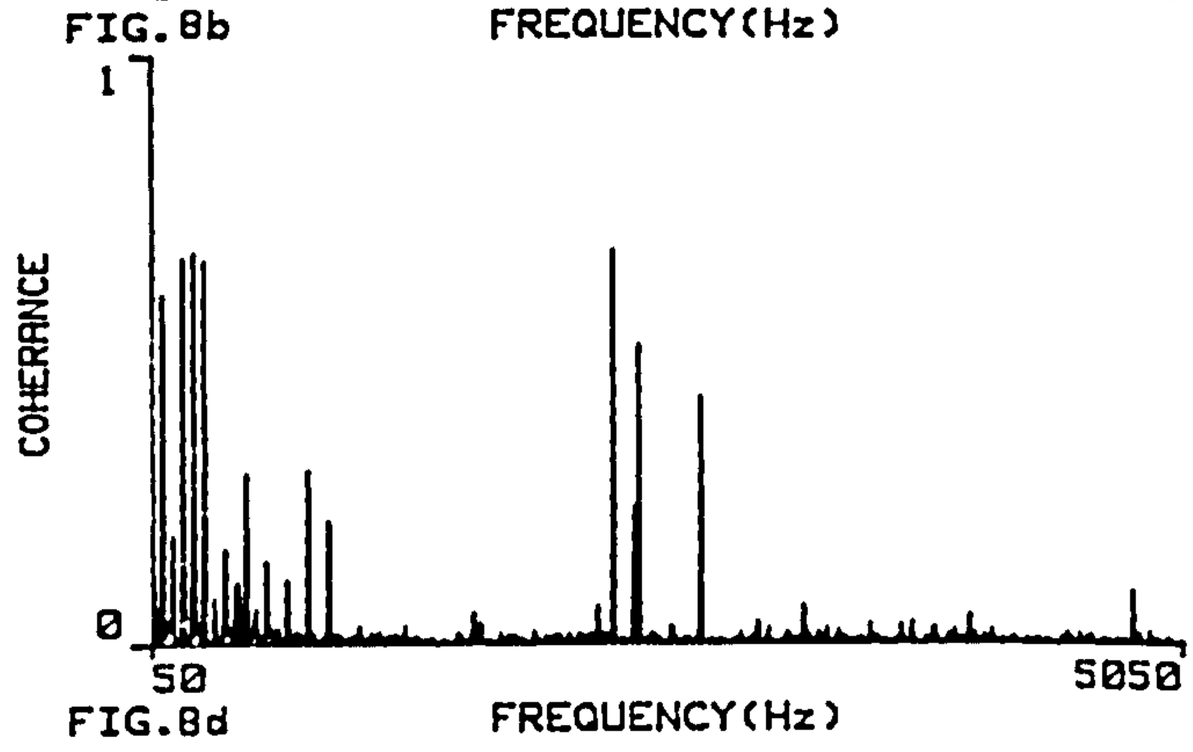

FIG.8d

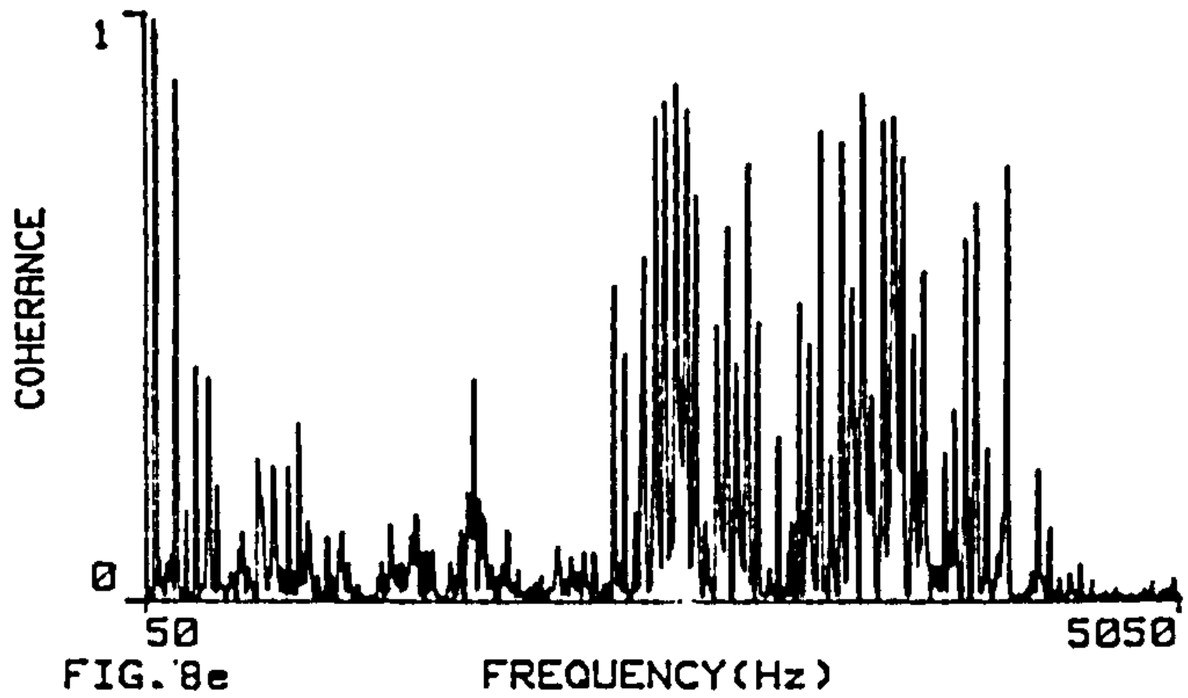

FIG.8e

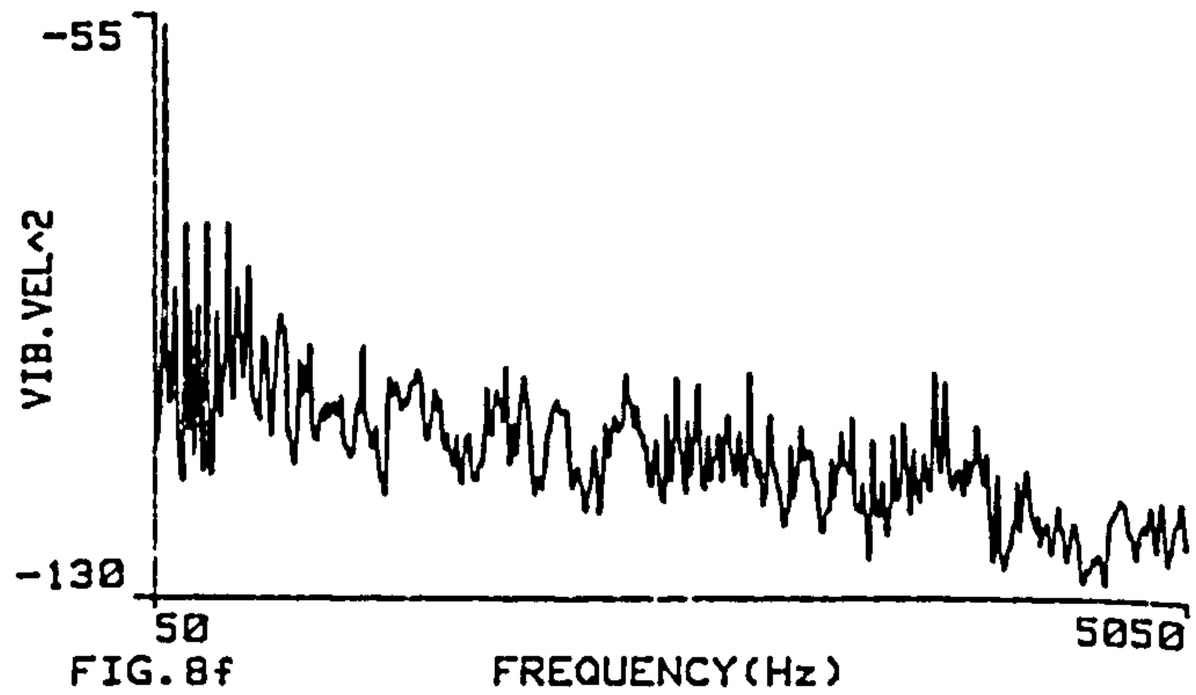

FIG.8f

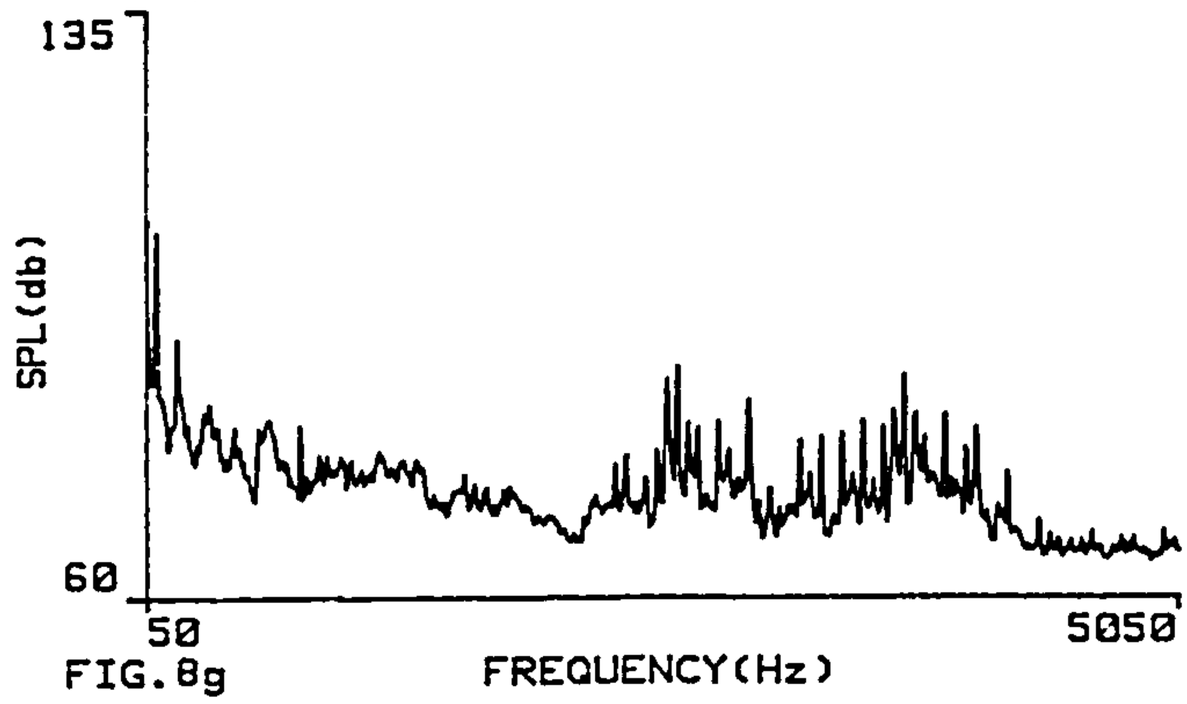

FIG.8g

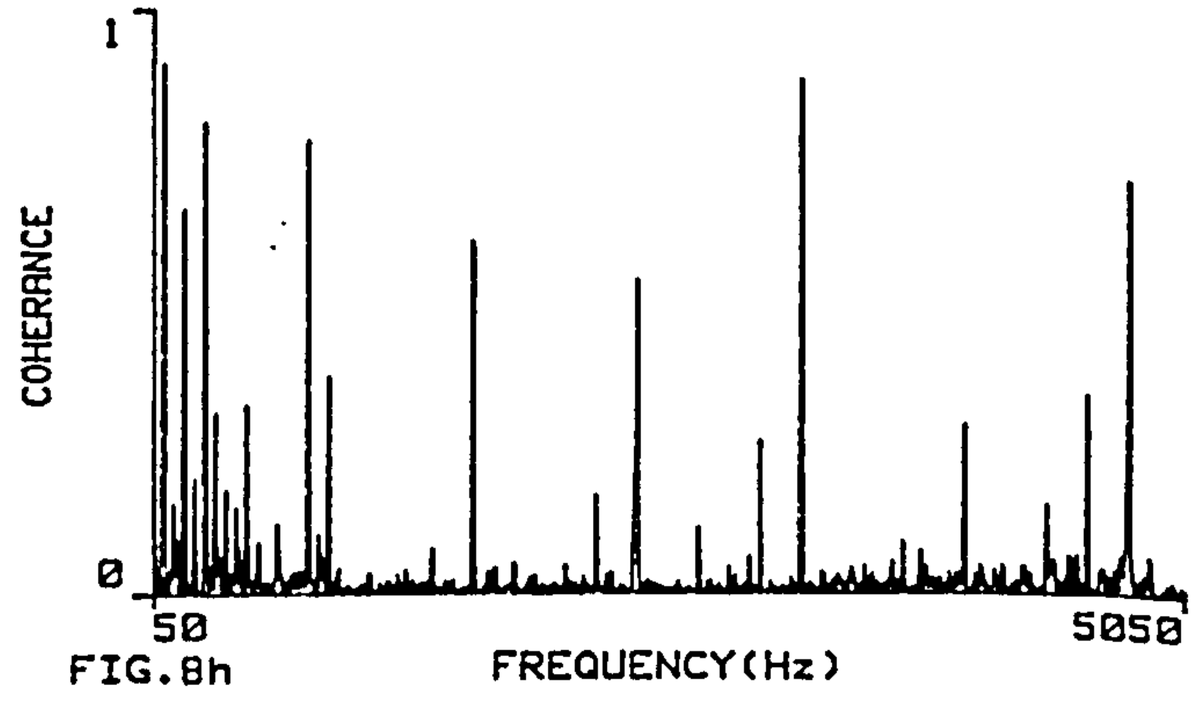

FIG.8h

Fig. 8
(a) Narrowband coherence between surface vibration and sound pressure 10 cm from generator centre.
(b) Narrowband vibration velocity squared on generator centre (plotted in dB ref 1 ms^{-1}).
(c) Narrowband sound pressure at 10 cm from generator centre.
(d) Narrowband coherence between surface vibration and sound pressure 0.1 m from exciter centre.
(e) Narrowband coherence between surface vibration and sound pressure 1 m from R.E. coupling.
(f) Narrowband vibration velocity squared on R.E. coupling cover.
(g) Narrowband sound pressure level at 1 m from R.E. coupling cover.
(h) Narrowband coherence between pilot exciter cover vibration and sound pressure 1 m from exciter R.E

Equipment	Generator			Exciter			Pilot Exciter
Location	F.E.	Centre	R.E.	F.E.	Centre	R.E.	
Reverberant S.P.L.	90.5	90.5	90.5	90.5	90.5	90.5	90.5
Predicted S.P.L. due to equipment	82.4	82.4	82.4	86.0	86.0	86.0	99.7
Direct background intensity component	86.5	80.6	93.9	94.2	89.1	96.6	-
Total predicted S.P.L. at 1 m	92.4	91.5	95.7	96.2	93.7	97.8	100.2
Measured S.P.L. at 1 m	92.8	91.4	95.8	97.0	94.9	98.5	101.5

Table 3 - Comparison of predicted S.P.L. due to reverberation, direct background noise and predicted plant level with measured levels (all levels are in dBA)

2700 Hz. By contrast the coherence between sound pressure at 1 m from the exciter centre and coupling cover vibration is clear for the coupling cover tones at 100 Hz and harmonics thereof and in the range 2.5 kHz to 4 kHz. This is illustrated in fig. 8e. The spectral similarity between cover vibration velocity squared and unweighted sound pressure 1 m from the exciter front end can be seen by comparing fig. 8f and 8g. Similarly between pilot exciter cover vibration and the sound pressure a 1 m from the exciter rear end there is strong coherence between tones at 800 Hz and harmonics as can be seen from fig. 8h.

The coherence measurements therefore correlate with the sound intensity point measurements indicating the value of this alternative technique for source location.

DISCUSSION

1. Reverberation

The S.P.L. beside unit 2 generator with only unit 1 in operation was 87.5 dBA. As the generator shielded this point from direct noise flow this level represents the general reverberation level of 1 unit. The general reverberation level for the station due to 2 units is hence doubled to 90.5 dBA. This reverberant level contribution is reflected in the difference between S.P.L. measured beside unit 1 with and without unit 2 in operation. For example at the generator F.E. the S.P.L. was increased from 91.1 dBA by 87.9 dBA to 92.8 dBA. The S.P.L. increase from 93.8 dBA to 94.9 dBA at the exciter centre relates to an extra 88.4 dBA. Both these increases due to unit 2 approximise to the 87.5 dBA reverberant S.P.L. due to 1 unit.

2. Composition of Sound Pressure Level at 1 m

It is important when assessing sound pressure level to decompose the level into its contributing influences rather than assume it is due to equipment directly. The preceding analysis has decomposed the level into 3 influences, namely, the general reverberant sound field, direct sound intensity from other background noise sources and the predicted sound pressure due to equipment directly. This analysis can be compared to the measured levels by summating the 3 factors. The results are summarised in table 3. These explain the site S.P.L. to within 1 dB at all locations and more commonly to within 0.5 dBA. This clearly illustrates the influence of general reverberation and direct background noise on S.P.L. beside the exciter and the generator. It is apparent that the exciter and generator do not set the S.P.L. beside them.

3. Noise Generation Mechanisms

(i) Generator Noise

It is evident from the foregoing analysis that the generator emits low levels of noise and does not determine the S.P.L. beside it.

From the measured narrowband spectra a number of deductions can be made about the major sources of generator noise. The sound power and vibration spectra indicate a prominent 100 Hz component due to magnetically induced vibration transmitted directly from the core to wrapper. This tone and its harmonics were added and this constituted half of the total power. The remainder of the noise is due to broadband aerodynamic generation. The S.P.L. inside an air cooled generator was measured as 112.5 dBA and hence for a hydrogen cooled generator with lower internal absorption and larger diameters will be closer to 120 dBA. Despite the high level the 22 mm thick steel wrapper provides a large transmission loss. This was calculated using statistical energy analysis techniques as ranging from 31 dB at 100 Hz to 57 dB at 4 kHz. This provides the key to low generator noise emission.

(ii) Exciter Noise

The exciter noise emission is clearly less important than that of the adjacent pilot exciter and R.E. coupling cover. Detailed source accreditation is not possible because of the limitations associated with taking measurements external to a reverberant enclosure in regions of high background noise.

However from the measured spectra it was apparent that the major noise sources were broadband aerodynamic. This noise is created by vortex shedding effects from the exciter rotor periphery, the fans and the rotating rectifier with diodes, fuses, attaching bolts and electrical connections. Tones exist, but these are of lesser importance. Tones at 1200 Hz and 2400 Hz are due to the number of fan blades and diode modules, at 100 Hz they are due to the rectifier field connections and at 2700 Hz they are created by the exciter armature slot siren effect or radial magnetic pole ripple forcing.

(iii) Rear End Generator Coupling Cover Noise

The rear end generator coupling as a large diameter and the upshaft electrical connections are a source of broadband and discrete tone aerodynamic noise. For the measurement survey it was apparent that the protective coupling cover is acoustically ineffective. This sound transmission loss yielded by the cover is only 9 dB. The reason for the low reduction for the 5 mm cover and subsequent significant noise levels was due to a number of standing waves being set up between the different upshaft connections geometries and the tight fitting enclosures. These resulted in the tonal components between 2.5 kHz and 4 kHz. The transmission loss is further reduced by the 2.5 cm clearance gap from the cover to the exciter for ventilation. The upshaft connections are radial copper stalks and copper straps, which pass generator field current over the coupling interface from the exciter.

(iv) Pilot Exciter Noise

The pilot exciter creates siren tones at 800 Hz and harmonics thereof due to the volume pulsation of air through the stator ducts. This arises because the air centrifugally thrust outwards from the 16 permanent magnet shoes encounters different air flow impedance dependent upon the rotor position relative to stator windings and core bars. Broadband noise is also generated due to unsteady flow effects and vortex shedding from the pole shoes.

Much of the acoustic energy exits directly outwards through the inlet and outlet open ventilation grills.

CONCLUSIONS

1. The techniques employed were successful in bringing a new level of insight into the noise emission from generator units. The four measurement techniques, sound pressure, sound intensity to determine sound power, sound intensity to indicate directional flow of acoustical energy and sound pressure surface vibration coherence, have provided a clear, correlated insight into noise problems. This has enabled quantification of the noise problem, full explanation of the site S.P.L. at 1 m in terms of the various influences and identification of the major noise sources.

2. The major sources of sound power in rank order were the pilot exciter (106.7 dBA), the R.E. generator coupling cover (103.5 dBA), the generator (97.3 dBA) and the exciter (96.8 dBA). The predicted site S.P.L. due to these components were 99.7 dBA from the pilot exciter, 95.8 dBA from the R.E. generator coupling cover, 86.0 dBA from the exciter and 82.4 dBA from the generator.

3. The accurate explanation of site S.P.L. in terms of reverberation, adjacent plant emission and background noise and information yielded from the coherence technique have strengthened confidence in the sound power levels and rank order. It is apparent that substantial noise reduction for this unit can be accomplished by treating the physically small pilot exciter and R.E. generator coupling. This work has indicated that acoustically enclosing the generator and exciter will yield little reduction in sound pressure levels and represents unproductive expenditure.

4. The pilot exciter and R.E. coupling cover will have acoustically lined seal enclosures reducing the maximum noise levels from future sets to 86 dBA.

5. General reverberation levels are not predominated by the generator unit, but by the boiler feed pumps, stop and throttle valves and turbines. Improvements are being made with these components in parallel with the generator unit study and the noise emission of this equipment is also being enacted. In recent years general station noise levels have been reduced by 6 dB and the trend will continue as greater insight is produced by these techniques. The experimental approach outlined in this paper is an essential tool for analysing all industrial noise problems as a first step towards finding optimal cost effective reduction.

6. These results have indicated the main source mechanism for each component. For the generator this was 50% magnetically induced vibrations and 50% aerodynamic noise. The large generator casing transmission loss limits the latter. The exciter generated aerodynamic noise from the rotating rectifier and the armature. The R.E. generator coupling cover created many standing waves, which reduced cover attenuation. The pilot exciter created siren tones and also broadband aerodynamic noise.

7. Even these powerful techniques have limitations and cannot discriminate between the intensity from one source and the contribution to the intensity from other sources present. The probe only measures net intensity and only the implementation of the surface integral nullifies other sources. For this reason detailed vector characterisation of plant is not possible with so many background sources. The technique also cannot provide detailed further source identification or different components inside a reverberant enclosure, such as the exciter cover unless it is removed. The sound power determination by sound intensity measurement is not standardised at the time of writing, but this will follow in the near future.

RECOMMENDATIONS

The following relatively simple unit modifications should be made:

(i) Large coupling covers should be acoustically lined with absorption material and sealed to ensure maximum attenuation.

(ii) The pilot exciter should have a closed ventilation circuit or inlet and outlet air mufflers. Covers should be lined with sound absorbent material.

REFERENCES

1. Grabkowski, S.E., and Van Schaick, T.E., "Sound power level determination for large steam turbine-generators", IEEE Transactions on Power Apparatus and Systems, Vol. PAS-94, No. 1, 1975, p. 31-36.

2. Grabkowski, S.E., Sirota, S.R., Jenkins, S., Buechler, J.P., "Controlling noise in a large steam turbine-generator room", IEEE Transactions on Power Apparatus and Systems, Vol. PAS-97, No. 2, 1978, p. 504-512.

3. Fahy, F.J., "Sound intensity", Elsevier Applied Science, London, 1989.

4. Reiniche, W.L., "Intensimetrische schalleistungsermitlung bei dampfturbosatzen", VGB Kraftwerkstech, Vol. 66, Part 7, 1986, p. 610-615.

5. Ying, S.P., Dennison, E.E., "Application of coherence techniques for noise in power plants", Noise Control Engineering, Vol. 15, Part 2, 1980, p. 81-87.

6. Fahy, F.J., "Measurement of acoustic intensity using the cross-spectral density of two microphone signals", J. Acoust. Soc. Am., 62(4) 1977, p. 1057-1059.

ACKNOWLEDGEMENTS

The authors wish to express their indebtedness to GEC Alsthom Large Generators for their support of this noise control study and publication of findings. The work was also supported by the Science and Engineering Research Council of the United Kingdom. Personal gratitude is extended to colleagues especially Mr. S.G. Houldcroft and Mr. R.M. Booth for guidance and Mr. S.D.R. Cameron for assistance with measurements.

Richard G.D. Williams was born in Northern Ireland on 16th August 1966. He received the B.Eng. Degree in Electrical and Electronic Engineering from Heriot-Watt University, Edinburgh in 1988. In 1988 he joined GEC Alsthom Large Generations Ltd. in England. He is conducting research into noise source identification on large generator sets as part of an Industrial Ph.D. Studentship between GEC Alsthom and Heriot-Watt University. He is an Associate Member of the Institution of Electrical Engineers (U.K.).

S.J. Yang (M '65 SM '79) received the B.Sc Degree in Electrical and Electronic Engineering from the University of Hong Kong in 1964 and the Ph.D. Degree from the University of London in 1970. From 1970 to 1972, he was a Senior Scientific Officer with the British Rail Research Department in Derby, England. Since 1972, he has been with Heriot-Watt University, Edinburgh. His areas of interest include noise and vibration of electrical machines and micro electro mechanical systems. He is a Fellow of the Institution of Electrical Engineers (U.K.) and the Institute of Acoustics (U.K.).

Applied Acoustics 35 (1992) 311–323

Sound-Field Characterisation and Implications for Industrial Sound-Intensity Measurements

R. G. D. Williams

GEC Alsthom Turbine Generators Ltd, PO Box 25, Lichfield Road, Stafford, ST17 4LN, UK

&

S. J. Yang

Department of Electrical and Electronic Engineering, Heriot–Watt University, 31–35 Grassmarket, Edinburgh, EH1 2HT, UK

(Received 4 September 1991; revised version received 18 October 1991; accepted 22 October 1991)

ABSTRACT

Sound-field characterisation is of vital importance in evaluating and improving the reliability of sound-intensity measurements. This paper examines indicators of the sound-field characteristics and the consequent implications for sound-intensity measurements. Results illustrate how the coherence between sound pressure and particle velocity can classify sound fields as diffuse multi-source, direct, or direct-plus-reverberant from one source. The measurements were conducted in a power station, which is typical of many commonly encountered multi-source, reverberant environments confronting the noise-control engineer. The value of sound-pressure/particle-velocity coherence is consistent with the form of acoustic field implied by the sound-power, vector-sound-intensity, and sound-pressure measurements. Some practical difficulties of sound-intensity measurement in complex environments are discussed, as is the identification of these by coherence and the standard sound-field indicators.

1 INTRODUCTION

The development of the sound-intensity technique during the 1980s has made the task of noise-source identification easier, since it provides a useful

Applied Acoustics 0003-682X/92/$05.00

tool for the noise-control engineer. Noise-source identification can be accomplished by ranking sources of sound power[1] and by using vector-intensity mapping of sources.[2] Sound power can, in principle, be determined *in situ*, even in the presence of stationary background noise, with practical limits of suppression in the range 14–18 dB.[3] This represents an upper limit to suppression, defined as the logarithmic difference between the sound pressure integrated over a closed surface and the intensity integrated over the same surface. For commercially available phase-matched microphone pairs with a nominal residual pressure-intensity index of 18 dB, the suppression limit is more typically 12 dB.

Despite the well-documented advantages of the intensity technique, caution should be exercised when conducting measurements in, and analysing data from, many practical industrial environments. Commonly, there is a complex interaction of plant-radiation characteristics, reverberation, and interference fields from many items of cofunctioning equipment. Under some conditions, significant measurement errors can accrue. In the nearfield of a source, measurement inaccuracy can arise because the instrument capability is exceeded by the highly reactive fields close to vibrating plant. These fields can be difficult to interpret with many positive and negative frequency components.[4] Measurements in reverberant regions inside enclosures also pose severe demands on the instrumentation. Background noise is suppressed by application of the Gauss Integral Theorem, but correct and optimal suppression increases the range of measurement acceptability.[5,6] Low levels of sound power can be absorbed by a source, causing an underestimation in sound-power level,[7] which may be insignificant when the source is operating in a region containing stronger sources.

Owing to these above-mentioned difficulties, it is essential when conducting intensity measurements to understand the structure of the source sound field, that of other sources in the region, and the acoustical environment of the measurement site in order to refine the measurement procedure. The international standard ISO 9614 'The determination of the sound-power levels of sources by sound-intensity measurement at discrete points', proposes the calculation of a number of indicators. These define accuracy, classify the measurement environment broadly, and suggest refinement of the measurement procedure. These are discussed in detail by Hübner.[6] A sound-power-level standard based upon the scanning techniques is currently being developed. For scanned measurements, the random error of the scanned estimate of L_p and L_{In} at any point on a segment is unknown. It is therefore unclear if $F_2 = L(P) - L(|I|)$, the surface pressure-intensity indicator, and $F_3 = L(P) - L(I)$, the negative partial-power indicator, are still valid. These symbols are as defined in ISO 9614. The

parameter F_4, the field non-uniformity indicator, denotes if sufficient points have been measured to estimate the true integral of normal intensity accurately. However, since the scanned probe covers the complete surface, this indicator is unlikely to be applied to manual measurements.

A supplementary approach adopted to investigate the nature of sound fields is the measurement of sound-pressure/particle-velocity coherence and its variation with measurement bandwidth. This approach has been successfully used by Jacobsen[8,9] under controlled conditions to classify direct and multi-source diffuse sound fields, as well as direct-plus-reverberant sound fields from one source.

The purpose of the paper is to present results used for sound-field classification and discuss the implications for sound-intensity measurement. The results include sound-pressure/particle-velocity coherence and the standard indicators calculated from a survey of sound-power intensity. The measurements were conducted in the complex environment of a power station with strong reverberant-noise fields and many sources of background noise from cofunctioning plant.

2 FUNDAMENTAL RELATIONSHIPS

2.1 Sound intensity

The instantaneous sound intensity is defined as the rate of flow of sound energy per surface area, the elemental area being so orientated that it lies perpendicular to the instantaneous particle-velocity vector. The time-average sound intensity is computed as a vector quantity equal to the time-averaged product of the instantaneous sound pressure and its corresponding instantaneous particle velocity. The component of intensity in the r direction is given by:

$$I_r = \langle p(t)v_r(t) \rangle \tag{1}$$

where $p(t)$ = sound pressure, $v_r(t)$ = particle velocity, I_r = sound intensity in the r direction, and the symbol $\langle\ \rangle$ implies a time average.

The theoretical formulation provided in recent years[10] and the advent of digital-signal-processing techniques and special microphones have made sound-intensity measurements possible. Arguably the most popular method of sound-intensity measurement is to use the imaginary part of the cross-spectrum between two closely spaced microphones when a dual-channel FFT analyser is employed. The intensity in the r direction in this case is calculated as:

$$I_r(\omega) = -\mathrm{Im}\,(S_{12})/(\omega\rho\,\Delta r) \tag{2}$$

where ω is the angular frequency, Δr is the microphone separation, and $\mathrm{Im}(S_{12})$ is the imaginary part of the single-sided cross-spectrum between two microphone signals.

2.2 Sound-pressure/particle-velocity coherence

The coherence between sound pressure and particle velocity indicates whether the sound field is produced by one or more sound sources. The coherence between the sound pressure and the particle velocity, u, in the measurement direction is by definition:

$$\gamma^2_{pu}(\omega) = (|S_{pu}(\omega)|^2)/(S_{pp}(\omega)S_{uu}(\omega)) \tag{3}$$

where $S_{pu}(\omega)$ is the cross-power spectrum of sound pressure and particle velocity and $S_{pp}(\omega)$ and $S_{uu}(\omega)$ are the power spectra of sound pressure and particle velocity, respectively.

Another useful, closely related quantity is the frequency-band coherence defined in eqn (4). In cases where the intensity spectrum changes in sign within the frequency band, the frequency-band coherence can be small even where the coherence tends to unity. The influence of bandwidth on the frequency-band coherence can yield further information about the nature of the sound field:

$$\gamma^2_{pu}(\omega_0, \Delta\omega) = \left|\int_{\omega_a}^{\omega_b} S_{pu}(\omega)\,\mathrm{d}\omega\right|^2 \Big/ \left[\int_{\omega_a}^{\omega_b} S_{pp}(\omega)\,\mathrm{d}\omega \int_{\omega_a}^{\omega_b} S_{uu}(\omega)\,\mathrm{d}\omega\right] \tag{4}$$

The sound-pressure/particle-velocity coherence can be derived from the signals of two closely spaced pressure microphones in conjunction with intensity measurements by using the following expression:[8]

$$S_{pp}(\omega) = \{S_{11}(\omega) + S_{22}(\omega) + 2C_{12}(\omega)\}/4 \tag{5}$$

$$S_{uu}(\omega) = \{S_{11}(\omega) + S_{22}(\omega) - 2C_{12}(\omega)\}/(\omega\rho\,\Delta r)^2 \tag{6}$$

$$S_{pu}(\omega) = [-2Q_{12}(\omega) + \mathrm{j}\{S_{22}(\omega) - S_{11}(\omega)\}]/(2\omega\rho\,\Delta r) \tag{7}$$

where S_{11} and S_{22} are the power spectra of each pressure signal, C_{12} is the real part and Q_{12} the imaginary part of the cross-spectrum of the two pressure signals, and Δr is the microphone-separation distance. The coherence function can be calculated by substituting eqns (5)–(7) into eqn (3).

The potential value of the coherence indicator can be demonstrated as follows. The parameter L_p could be significantly greater than L_I owing to a diffuse field generated by the source, or a diffuse field from extraneous sources, or owing to near-field effects. If L_p exceeds L_I because of near-field effects, the coherence is high irrespective of spectral resolution, provided that measurements are not made too close to a thin plate. Tichy & Kihlman[11]

illustrated that, for a 10-mm-thick undamped steel plate, the percentage of negative intensity in each third octave ranged from 25% at 200 Hz to 5% at 1 kHz for a measurement distance of 100 mm. In a diffuse field generated by one source, the coherence is high only for a very narrow measurement bandwidth.[8] This is due to the bias error introduced by inadequately fine frequency resolution. In a reverberant field containing a single coherent source, the coherence between pressure and particle velocity should tend to unity. However, the bias error introduced by reflections delayed longer than the individual record lengths can be significant in reducing the measured coherence. For multiple uncorrelated sources, coherence will always be low.

3 EXPERIMENT

The measurement system consisted of a Brüel & Kjaer 3519 sound-intensity probe provided with two $\frac{1}{2}$-in phase-matched condenser microphones separated by a 12-mm spacer and a dual-channel frequency analyser (Hewlett Packard 3562), combined with a Hewlett Packard 9816 computer for post-processing of data. The system was calibrated by using a Brüel & Kjaer 3541 intensity cavity. The pressure-residual-intensity index was >22 dB above 100 Hz.

The measurement survey was conducted in a power station containing two 660-MW steam-turbine generator units. The station contains a multitude of cofunctioning equipment with four turbines driving each generator and many auxiliary pumps, valves, steam lines, and condensers. The turbine hall has dimensions of 58 m × 144 m × 31 m, and the turbine generator units were the only plant on the top level of three floors. The turbine-hall reverberation time was approximately 3 s from 125 Hz to 4 kHz. The investigation concentrated upon the generator unit, its excitation system consisting of a main exciter and pilot exciter and the rear-end (R.E.) generator coupling as illustrated in Fig. 1.

The number of discrete measurement points is prohibitive for a structure such as a large generator (10 m long, 4·8 m in diameter) when suppression of high levels of background noise is required. The scanning technique was therefore preferable for this application. Surfaces were divided into individual areas of less than 1 m^2, and the probe was scanned over the surface in a set of parallel straight lines joined by semicircles. A scan rate of $<0{\cdot}25\ ms^{-1}$ was used with a line separation of 12 cm. A measurement distance of 10 cm was employed to minimise the influence of background noise. This practice follows the recommendations of Petterson and Newman.[12] The sound-power emission from the generator was determined by scanning one-third of the generator from floor level to top dead centre

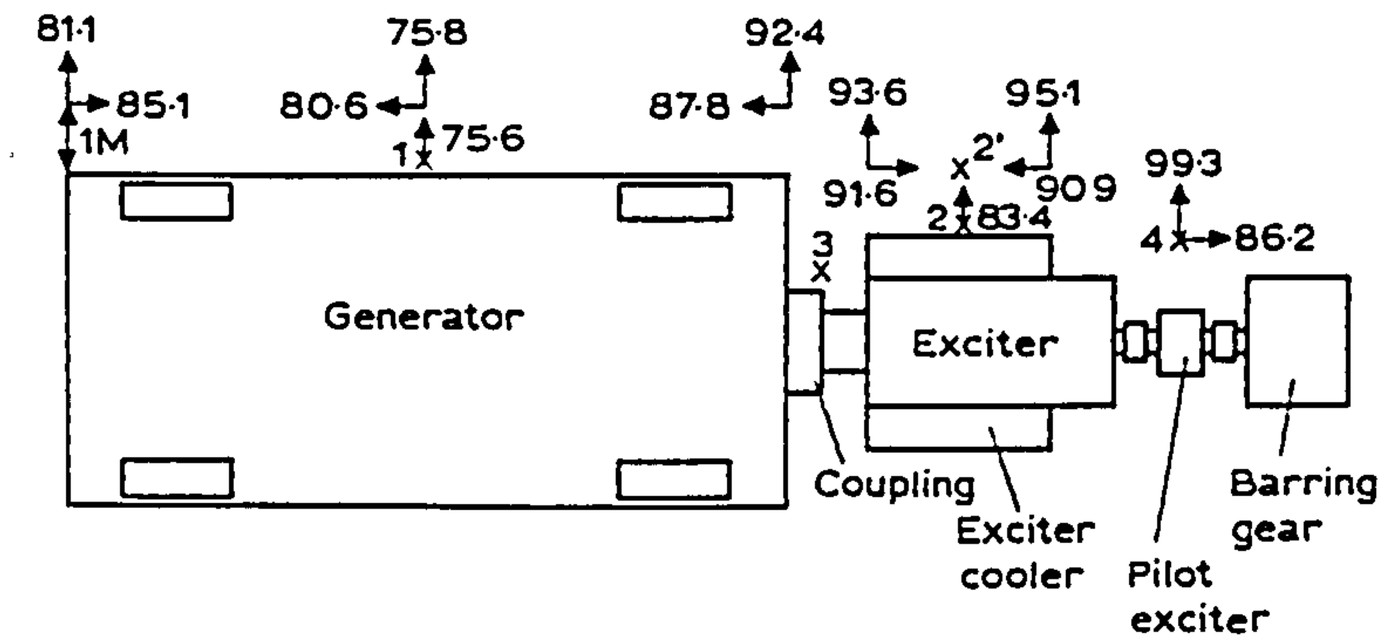

Fig. 1. Sound-intensity distribution around the generator unit and measurement locations of sound-pressure/particle-velocity coherence (denoted by X).

and appropriate scaling to obtain a total figure. The exciter, R.E. generator-coupling cover, and pilot exciter were each completely scanned.

To assist with accrediting the measurement environment and to indicate the main flow of acoustic energy in the region of the generator unit, point 2D sound-intensity vector measurements were used.

The sound-pressure/particle-velocity coherence function was measured at a number of locations denoted by X in Fig. 1. The locations were:

(i) 0·1 m from the generator centre;
(ii) 0·1 m and 1 m from the exciter centre:
(iii) 0·1 m from the R.E. generator coupling; this region is enclosed on both sides by the generator and exciter steel casings;
(iv) 1 m from the open ventilation grill on the pilot-exciter side.

Measurements were conducted with frequency resolutions of 1·25 and 6·25 Hz.

4 RESULTS

4.1 Sound-pressure level

The sound-pressure level (S.P.L.) was on average 92·5 dBA beside the generator except towards the rear end, where the level increased to 96·5 dBA. At a distance of 1 m from the exciter, levels approached 97 dBA at the front end, decreased to 94·9 dBA in the centre, and increased to 97·4 dBA at the rear end. At 1 m from the pilot exciter, S.P.L. was 102 dBA.

4.2 Sound-power determination

The measured sound-power levels were, in rank order, 106·7 $\pm$ 1 dBA from the pilot exciter, 103·5 $\pm$ 1 dBA from the R.E. generator coupling,

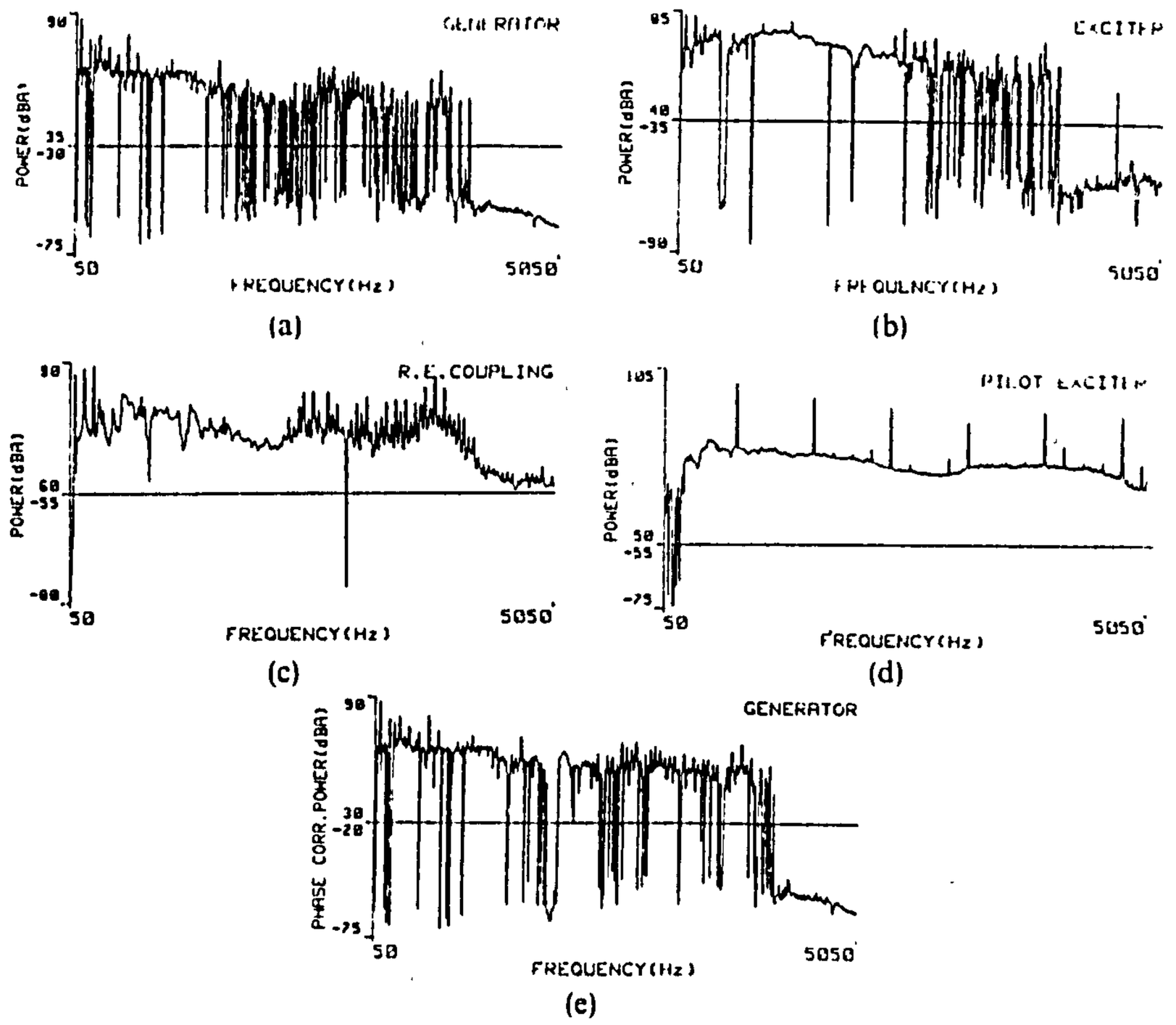

Fig. 2. A-weighted narrowband sound-power levels for (a) generator, (b) exciter, (c) R.E. generator coupling, (d) pilot exciter, (e) generator with a phase-mismatch correction.

$97{\cdot}3 \pm 2$ dBA from the generator, and $96{\cdot}8 \pm 1$ dBA from the exciter. The quoted error limits were based upon instrument errors and statistical considerations, which are discussed later. The A-weighted narrowband sound-power levels are plotted in Figs 2(a)–(d) and the A-weighted $\frac{1}{3}$-octave sound-power levels are plotted in Fig. 3(a).

The generator sound power is associated with low radial intensities of typically 75–76 dBA, which are reasonably uniformly distributed over the side of the machine. The narrowband generator sound-power spectrum is illustrated in Fig. 2(a). The spectrum contains some negative power tones between 2 and 4 kHz but is mainly broadband, with predominant peaks at 100 Hz and harmonics thereof. Many of the negative powers are due to the influence of phase mismatch because of the low-intensity emission. This can be illustrated by using the phase-mismatch correction to the sound power outlined by Jacobsen[13] in eqn (8), which is:

$$P_a = P_m - (I_0 \rho c / p_0^2) \int_s (p^2/\rho c)\, dS \tag{8}$$

where P_a = adjusted sound power, P_m = measured sound power, ρc = specific acoustic impedance of the air, p = r.m.s. sound pressure, I_0 is the residual intensity measured when both microphones are subjected to the same pressure p_0, in a small calibration chamber, for example. The adjusted sound power illustrated in Fig. 2(e) has considerably less negative intensity, except above 4 kHz, where it is largely unaltered, perhaps implying the presence of low levels of power absorption, as suggested by Reiniche.[7]

The main measurement problem in determining the low levels of generator sound power was the diffuse multi-source sound field created by other sources. Owing to the plant configuration, the generator casing shielded much of the direct background noise. The negative partial-power indicator, which is the indicator $F_3 = L(P) - L(I)$ for the generator, was typically 18 dB for most third octaves as illustrated in Fig. 3(b), implying a phase-mismatch error for microphones with a pressure-residual-intensity index of 22 dB +1·5, −2 dB.

The spatial sampling random error was assessed by repeating every fourth measurement four times to obtain four space-averaged intensities. The random error of the sound-power determination can then be assessed for normally distributed measurements by using the variation coefficient $V_n = S_n/I_{avg}$ in the following equation:

$$e_r = 10 \log \{(1 + V_n t_s)/\sqrt{(n-1)}\} \tag{9}$$

where t_s is the statistical parameter, Student's t, for a certain confidence limit (90% in this case), n is the number of repeated measurements, S_n is the standard deviation of the average-intensity values, and I_{avg} is the average of the repeated average. The random error was less than 1 dB for most of the frequency bands.

The measurement of exciter sound power was complicated by the stronger directional noise from the pilot exciter and rear-end generator coupling. The cancellation of the background noise can be illustrated by considering the rear-end measurements. The partial sound power of the exciter rear-end face was measured as a negative 93·3 dBA owing to energy from the pilot exciter. However, when adjacent measurement areas of the side and roof are included, the net sound power became a positive 93·2 dBA. The sound-power spectrum as illustrated in Fig. 2(b) contains negative power above 3 kHz owing to low-level energy absorption and insufficient suppression of background noise. The value of F_3 was less than 14 dB, implying a phase-mismatch error of ±1 dB. The spatial random error of ±1·5 dB was higher owing to many areas of negative intensity at the ends. The sound-power levels from the R.E. coupling and pilot exciter were higher, these being 103·5 dBA and 106·7 dBA, respectively, with spectra illustrated in Figs 2(c) and 2(d), respectively. These measurements were comparatively simple, since

both were concentrated strong sound sources. Care was taken to measure high regions from vents, etc., as separate areas. The average pressure-intensity index was less than 5 dB for all third octaves above 200 Hz, which are the bands that constitute the majority of the A-weighted level, causing limited phase-mismatch errors. The random error of ± 1 dB is therefore the total error limit in both cases.

4.3 Standard indicators

The value of the surface-pressure-intensity indicator, F_2, the negative partial-power indicator F_3, and the difference between these can indicate the form of the acoustic environment. The indicators F_3, F_2, and $F_3 - F_2$ are illustrated in Figs 3(b), 3(c), and 3(d). The high value of F_2 for the generator of 16 dB, and the intermediate value of $F_3 - F_2$ of between 1 and 3 dB for all $\frac{1}{3}$ octaves except one below 1·6 kHz, indicate low levels of source-noise emission compared with the diffuse multi-source sound field. Above 1·6 kHz, $F_3 - F_2$ tends to 5 dB, or greater, implying an inaccurate measurement, which is reflected in the negative tonal components between 2 and 4 kHz in Fig. 2(a).

For the exciter, $F_3 - F_2 > 3$ dB for the $\frac{1}{3}$ octaves at 500 Hz and above 3 kHz, coinciding with regions of negative power measurement and again implying inaccurate results in these bands. The value of F_2 is less for the

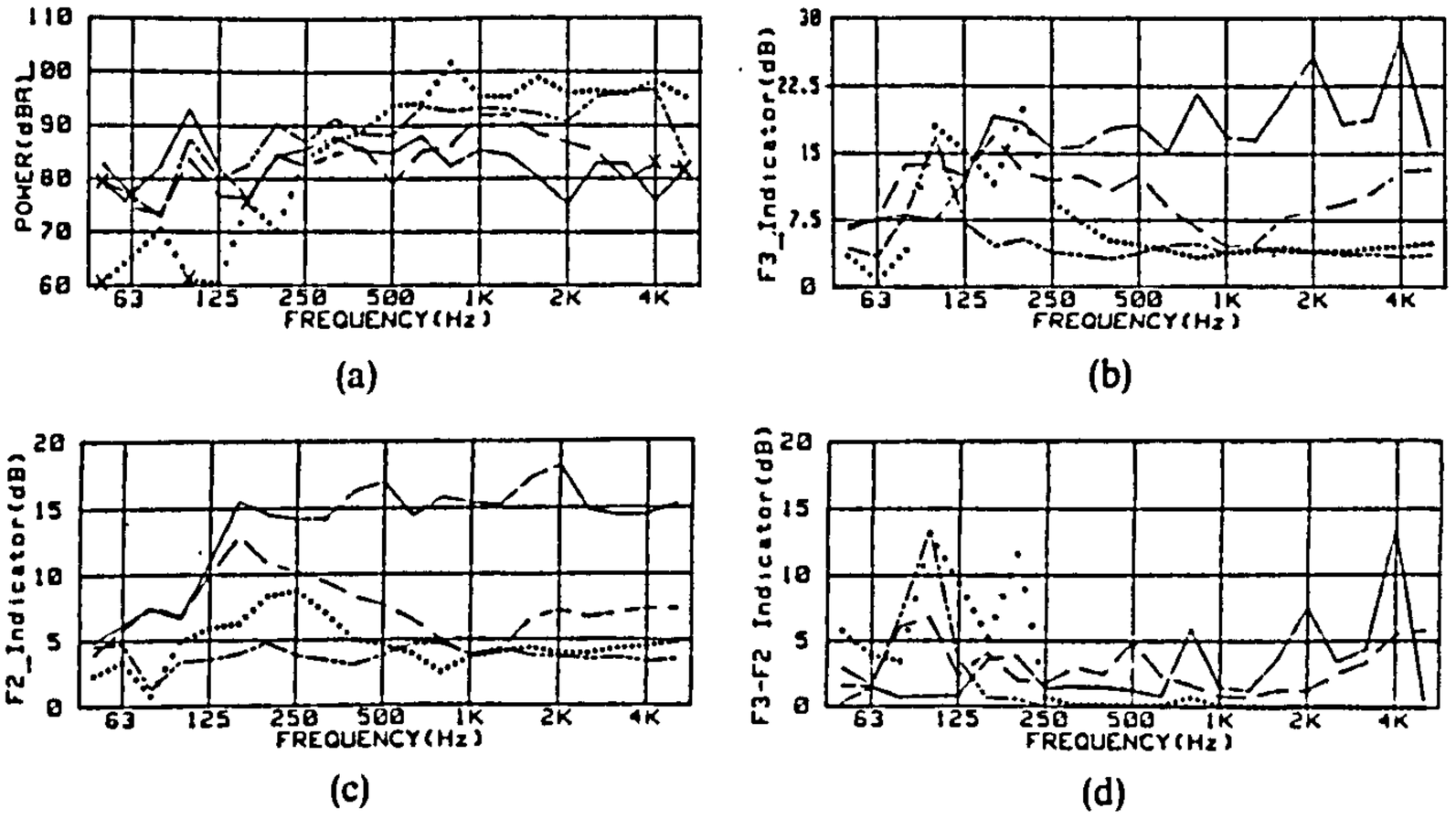

Fig. 3. (a) A-weighted $\frac{1}{3}$-octave sound-power levels for generator unit components; (b) $\frac{1}{3}$-Octave F_3 indicator for generator measurements; (c) $\frac{1}{3}$-Octave F_2 indicator for generator measurements; (d) $\frac{1}{3}$-Octave $F_3 - F_2$ indicator for generator measurements; -·-·- R.E. coupling cover; —— generator; ..... pilot exciter; --- exciter; X negative sound-power level.

exciter owing to the strong direct sound fields. The significant sound-power emission for the R.E. coupling and pilot exciter is above 250 Hz, for which the indicator $F_3 - F_2$ tends to zero. This, in conjunction with the low F_2 indicator, clearly shows a strong noise source.

4.4 Point-sound-intensity measurements

The sound-intensity-vector distribution in Fig. 1 clearly shows that the predominant flow of acoustical energy was not from the generator and exciter but from adjacent plant. This correlates with the predicted low levels of generator and exciter sound power. At the generator front (turbine) end, there was an axial flow of 86·5-dBA sound intensity from the turbines. At the rear end, the resultant sound intensity was 93·9 dBA from the rear-end generator coupling. These intensities are much greater than those for the typical generator near field intensities of 75–76 dBA. At the exciter rear end, there is a 96·5-dBA sound intensity from the pilot exciter. At 10 cm from the exciter, the radial sound intensity was 83·4 dBA, illustrating the low levels of exciter sound intensity compared with that from the pilot exciter and R.E. coupling cover.

4.5 Sound-pressure/particle-velocity coherence

The sound-pressure/particle-velocity coherence measured at fixed points 1 m from the generator centre is plotted for the frequency ranges 50–5050 Hz and 50–1050 Hz in Figs 4(a) and 4(b) for a line bandwidth of 6·25 Hz. For comparison purposes, the measurement was repeated with the finer spectral resolution of 1·25 Hz as illustrated in Fig. 4(c). It is apparent that, for all frequencies above 1 kHz, the coherence is very low ($<0{\cdot}1$) and only at a few discrete frequencies lower than 1 kHz does the coherence approach unity. Since the coherence is low in general, especially above 1 kHz, and independent of spectral resolution, as is evident from comparing Figs 4(b) and 4(c), the field beside the generator is due to multi-source diffuse fields, with the generator making a relatively weak contribution. This is consistent with the low sound-power and radial-intensity measurements.

The coherence measured at 0·1 m from the exciter centre was higher than that for the generator, but still generally low. The value is commonly between 0·15 and 0·5 for a number of tones throughout the frequency range 50–5050 Hz, as illustrated in Fig. 4(d). The coherence is invariant with spectral resolution. At 1 m from the exciter, the stronger direct background noise is not shielded by the exciter to the same extent. The coherence, which is greater than 0·8 for the coupling-cover and pilot-exciter tones, as

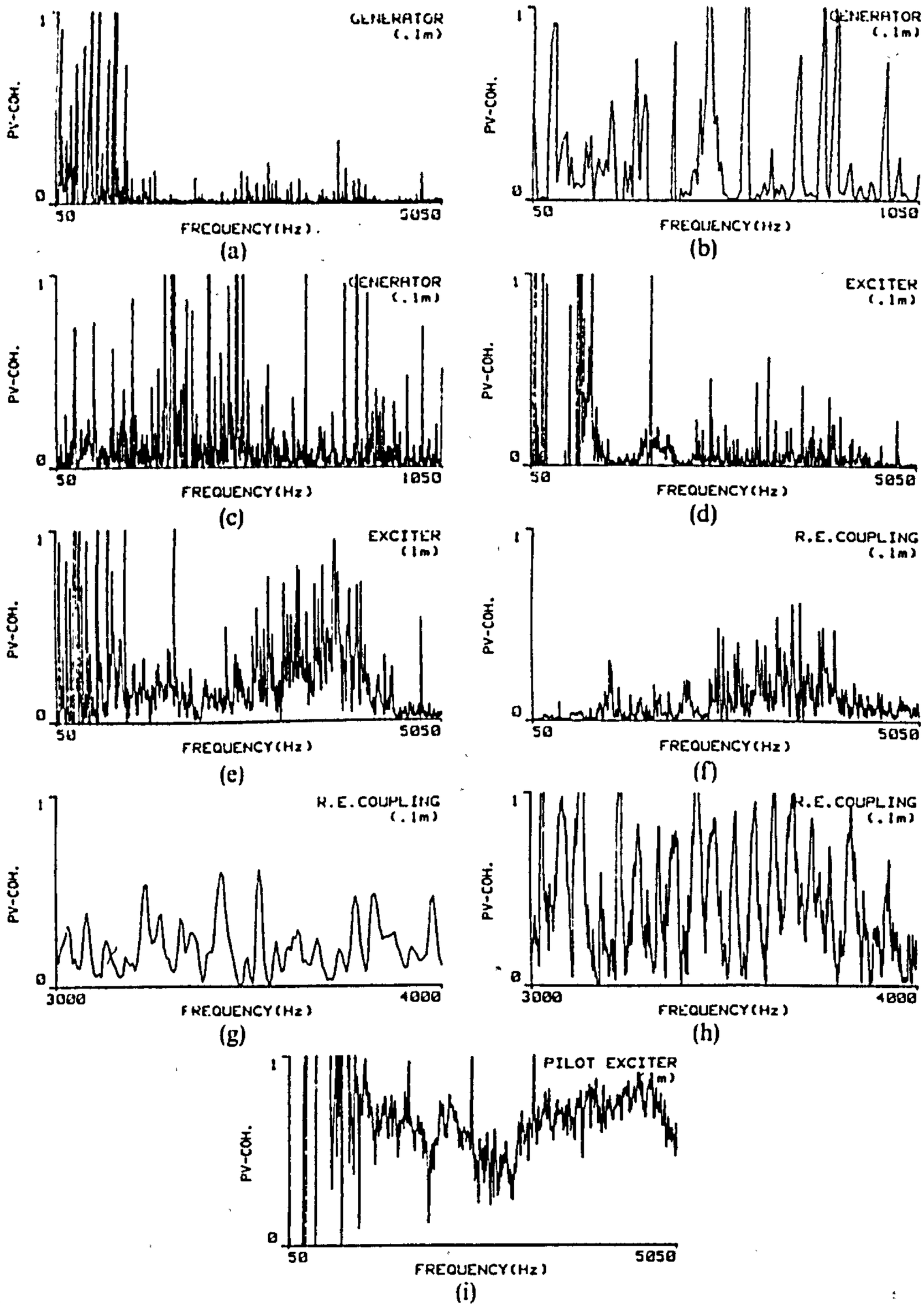

Fig. 4. Sound-pressure/particle-velocity coherence: (a) with 6·25-Hz bandwidth 0·1 m from generator centre; (b) with 6·25-Hz bandwidth 0·1 m from generator centre; (c) with 1·25-Hz bandwidth 0·1 m from generator centre; (d) with 6·25-Hz bandwidth 0·1 m from exciter centre; (e) with 6·25-Hz bandwidth 1 m from exciter centre; (f) with 6·25-Hz bandwidth 0·1 m from R.E. coupling; (g) with 6·25-Hz bandwidth 0·1 m from R.E. coupling; (h) with 1·25-Hz bandwidth 0·1 m from R.E. coupling; (i) with 6·25-Hz bandwidth 1 m from pilot exciter.

illustrated in Fig. 4(e), indicates that, at 1 m from the exciter, there is a strong direct field, which will significantly raise the sound-pressure level.

At a distance of 0·1 m from the rear-end generator coupling, the coherence has a value of 0·5 at frequencies coinciding with the sound-power tones (Fig. 2(c)) for the 6·25-Hz measurement-line bandwidth as seen in Figs 4(f) and 4(g). For the finer spectral resolution of 1·25 Hz, the coherence has increased to unity for the tones in the range from 3 to 4 kHz (Fig. 4(h)). The increase in coherence with decrease in spectral resolution is due to a bias error. This indicates that the coupling region between the generator and exciter bodies contains a reverberant field generated by one main source.

The coherence 1 m from the pilot-exciter side for this range of 50–5050 Hz with a 6·25-Hz bandwidth is high, commonly greater than 0·7. This is illustrated in Fig. 4(i). The coherence is invariant of spectral resolution, indicating that the field beside the pilot exciter is the strong direct field from one source. This is consistent with the high sound-power and radial-intensity measurements.

5 CONCLUSIONS

The sound-pressure/particle-velocity coherence has been shown to reflect the nature of the sound field. Measurements conducted in an industrial environment have identified a weak source in a multi-source diffuse field, a strong direct source, and a strong source in a reverberant region. This information clearly correlates with relative sound-power levels, point-vector sound-intensity levels, and sound-pressure levels of the plant items. The coherence has identified difficulty with sound-power determination in a manner similar to the $F_3 - F_2$ indicator. Measurement difficulties in the presence of high background noise have been illustrated.

The coherence function can be derived simply in conjunction with sound-intensity measurement. It is suggested that coherence could be measured at the start of a sound-power survey to assist with sound-field classification and allow optimal measurement procedures to be adopted. Alternatively, the function could be measured after a survey to add further credence to sound-power levels when a component is deemed to contribute weakly to the surrounding noise fields.

ACKNOWLEDGEMENTS

The authors wish to express their indebtedness to GEC Alsthom Large Generators for their support of the noise-control study and publication of

findings. The work was supported by the Science and Engineering Research Council of the United Kingdom. Personal gratitude is extended to Professor F. J. Fahy, of the Institute of Sound and Vibration Research, for vigilant proof-reading of the manuscript and many stimulating discussions.

REFERENCES

1. Johns, W. D. & Porter, R. H., Ranking of compressor station noise sources using sound-intensity techniques. *Noise & Vibration Control*, **19** (1988) 70–5.
2. Pepin, H., Localisation des sources de bruit sur une machine industrielle. In *Proceedings of the Sound International Congress on Acoustic Intensity, France*, 1985, pp. 413–20.
3. Stirnemann, A., Bolleter, U. & Rathe, E. J., Possibilities and limits of sound-power measurements with a real-time intensity analyzer. *J. Sound Vib.*, **98** (1985) 403–13.
4. Kihlman, T. & Tichy, J., Studies of sound-intensity measurements on a steel panel. In *Proceedings of Inter-Noise 87, China*, 1987, pp. 1231–4.
5. Fahy, F. J., *Sound Intensity*. Elsevier Applied Science, London, 1989, Chapter 8.
6. Hübner, G., Recent development of requirements for an intensity-measurement code determining sound-power levels of machines. In *Proceedings of the Second International Congress on Acoustic Intensity, France*, 1985, pp. 307–18.
7. Reiniche, W. L., Experience with industrial applications on intensimetry. In *Proceedings of the Second International Congress on Acoustic Intensity, France*, 1985, pp. 361–8.
8. Jacobsen, F., Active and reactive, coherent and incoherent sound fields. *J. Sound Vib.*, **150** (1989) 493–507.
9. Jacobsen, F., Sound-field indicators: useful tools. *Noise Control Engng*, **35** (1989) 37–46.
10. Fahy, F. J., Measurement of acoustic intensity using the cross-spectral density of two microphone signals. *J. Acoust. Soc. Am.*, **62** (1977) 1057–9.
11. Tichy, J. & Kihlman, T., Sound-intensity field in front of plates with and without damping. *Proceedings of Inter-Noise 88, France*, 1988, pp. 111–14.
12. Petterson, O. K. O. and Newman, M. J., The determination of radiated sound power using sound-intensity measurements. Report No. STF44 A86166, ELAB, Elektronikklaboratioriet ved NTH, N-7034, Trondheim, Norway, 1986.
13. Jacobsen, F., A simple and effective correction for phase mis-match in intensity probes. *Appl. Acoust.*, **33** (1991) 165–80.